

university
of south africa



UNISA

**EVALUATION OF MICROEXTRACTION METHODS FOLLOWED BY
INDUCTIVELY COUPLED PLASMA OPTICAL-EMISSION
SPECTROSCOPY FOR THE QUANTITATIVE DETERMINATION OF
MERCURY FROM SELECTIVE FOSSIL FUELS AND THEIR
DERIVATIVES**

by

Mxolisi Junior Kiwanuka (11741635)

submitted in accordance with the requirements
for the degree of

Masters

in

Chemistry

at the

UNIVERSITY OF SOUTH AFRICA

Prof N Mketi

Prof N.P Nomngongo

February 2024

DECLARATION

Name: Mxolisi Junior Kiwanuka
Student number: 11741635
Degree: Master of Science in Chemistry

Exact wording of the title of the dissertation as appearing on the electronic copy submitted for examination:

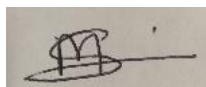
EVALUATION OF MICROEXTRACTION METHODS FOLLOWED BY INDUCTIVELY COUPLED SPECTROSCOPY FOR THE QUANTITATIVE DETERMINATION OF MERCURY FROM SELECTED FOSSIL FUELS AND THEIR DERIVATIVES

I declare that the above dissertation is my own work and that all the sources that I have used or quoted have been indicated and acknowledged by means of complete references.

I further declare that I submitted the dissertation to originality checking software and that it falls within the accepted requirements for originality.

I further declare that I have not previously submitted this work, or part of it, for examination at Unisa for another qualification or at any other higher education institution.

(The dissertation will not be examined unless this statement has been submitted.)



SIGNATURE

DATE: 29/02/2024

UNIVERSITY OF SOUTH AFRICA

KEY TERMS DESCRIBING THE TOPIC OF A DISSERTATION/THESIS

The Executive Committee of Senate decided that in order to assist the library with retrieval of information, master's and doctoral students must list approximately ten key terms which describe the topic of the dissertation/thesis at the end of the summary of the dissertation/thesis.

If the dissertation/thesis is not written in English, the key terms in English must be listed at the end of the English summary.

The following is an example of key terms used for a thesis/dissertation:

Title of thesis/dissertation:

EVALUATION OF MICROEXTRACTION METHODS FOLLOWED BY INDUCTIVELY COUPLED PLASMA OPTICAL-EMISSION SPECTROSCOPY FOR THE QUANTITATIVE DETERMINATION OF MERCURY FROM SELECTIVE FOSSIL FUELS AND THEIR DERIVATIVES.

KEY TERMS:

Inductively coupled plasma-optical emission spectrometry (ICP-OES); methionine; hydrogen peroxide (H₂O₂); microwave assisted-hydrogen peroxide digestion (MWAHPD); deep eutectic solven; vortex-assisted dispersive liquid-liquid microextraction; choline chloride; ethylene glycol; levulinic acid; betaine and mercury; magnetic solid phase microextraction; graphene oxide; Fe₃O₄-GO-Au; mercury; fuel oils

DEDICATION

This dissertation is dedicated to my grandmother, Mrs Esselina Mathe, my mothers, Ms Nana Gladys Ndlangamandla and Ms Thobile Ndlangamandla, my late father, Dr Abdul Kiwanuka, my siblings (Mr Ndumiso Sithole, Mr Man Sithole, Ms Xoliswa Simelane) and the entire Ndlangamandla family for their prayers, support and motivation.

ACKNOWLEDGEMENTS

I would like to thank my Lord Jesus Christ for providing me with courage, direction, and safety throughout my M.Sc. research study.

I also take this opportunity to offer my sincere gratitude and acknowledgement to my research mentor, Prof Nomvano Mketi and my co-supervisor Prof Philiswa Nosizo Nomngongo, for their exceptional advice, support, encouragement, and inspiration for the past three years of my study. Their extensive scientific knowledge, and analytical approach have created safe working environment for me. I learned to think logically and advance my scientific knowledge because of the several discussions we had throughout this journey. I am thankful that they took time out of their hectic schedule to assist me, and I appreciate their patience. This project would not have been successful without their scientific expertise and guidance.

I would also like to extend my acknowledgement to the University of South Africa (UNISA) for offering me the opportunity to pursue my M.Sc. studies. I also thank the UNISA Chemistry Department for providing all the facilities for my research. My special thanks also go to NRF-THUTHUKA and UNISA-Women in Research for their financial assistance. I would also like to thank the UNISA Food and Environmental Analytical Chemistry Research Group laboratory mates (Mr Njabulo Mdluli, Mr Kgomotso Mabena, Mr Mceliseni Zuma, Mr Basil Munjanja, Mr Divin Mkendi, Mr Damilare Babatunde, Mr Samuel Mgiba, Mr Oluseyi Salami, Ms Musiiwa Sengane, Ms Thabang Kgoedi, Ms Nomatter Ncube, Ms Amanda Ngema, Ms Celiwe Dlangalala, Mrs Louisah Mahlaule Glory, and Ms Nomonde Ndlovu) for their motivation and continued support during the period of my study.

I also extend my sincere gratitude to Dr Siyasanga Mpelane from University of Johannesburg (UJ) for his assistance with TEM and SEM-EDS analysis and Dr Ishmael Nkoana Mongalo from UNISA, College of Agricultural and Environmental Sciences (CAES) for giving me access to the microwave digester. I would also like to thank Mr

Siyabonga Mhlongo from Institute for Nanotechnology and Water Sustainability for assistance with BET, FT-IR, TGA and UV-Vis. Lastly, my gratitude is extended to Ms Tshegofatso Modungwe from Physics department for assisting us with P-XRD.

Lastly but not least, I would like to thank my parents, my girlfriend and siblings for their love, support, and their prayers. I am truly grateful to God for having such an awesome family in my life.

PUBLICATIONS AND BOOK CHAPTERS

This dissertation consists of three manuscripts, one under review, two in preparation, one review in preparation and one book chapter published.

1. M. Kiwanuka^a, P.N Nomngongo^b, N Mketo^a. *Novel microwave assisted-hydrogen peroxide digestion of fuel oils using methionine as a capping reagent for the determination of mercury by inductively coupled plasma-optical emission spectrometry (UNDER REVIEW).*
2. M. Kiwanuka^a, P.N Nomngongo^b, N Mketo^a. *Vortex assisted deep eutectic solvent based dispersive liquid-liquid microextraction (VA-DES-LLME) for spectroscopic determination of Hg in fuel samples (IN PREPARATION).*
3. M. Kiwanuka^a, P.N Nomngongo^b, N Mketo^a. *Ultrasound-assisted magnetic dispersive solid phase microextraction based on Fe₃O₄-GO-Au for the preconcentration of mercury in fuel oils followed by ICP-OES determination (IN PREPARATION).*
4. M. Kiwanuka^a, P.N Nomngongo^b, N Mketo^a. *Recent trends in sample preparation methods for total determination of mercury in non-aqueous matrices (IN PREPARATION).*
5. M. Kiwanuka^a, P.N Nomngongo^b, N Mketo^a. *Biogenic nanomaterials as adsorbent for mercury remediation.* In book: *Biogenic Nanomaterials for Environmental Sustainability: Principles, Practices, and Opportunities* (pp.455-472). DOI: [10.1007/978-3-031-45956-6-18](https://doi.org/10.1007/978-3-031-45956-6-18) **(PUBLISHED).**

CONFERENCE PRESENTATIONS

1. University of South Africa Florida campus CAES-CSET Innovation week **30 November 2022** poster presentation, Mxolisi J. Kiwanuka, Nomvano Mketi, & Philiswa N. Nomngongo, “*Novel microwave assisted-hydrogen peroxide digestion of fuel oils using methionine as a capping reagent for the determination of mercury by inductively coupled plasma-optical emission spectrometry*”.
2. South African Chemical Institute (SACI) conference held in Stellenbosch, Cape Town, South Africa from **8-14 January 2023**, oral presentation, Mxolisi J. Kiwanuka, Nomvano Mketi & Philiswa N. Nomngongo “*Novel microwave assisted hydrogen peroxide digestion of fuel oils using methionine as a capping reagent for the determination of mercury by inductively coupled plasma-optical emission spectrometry*”.

ABSTRACT

Microextraction sample preparation methods are miniaturized formats which contributes to green approaches in Analytical Chemistry. They are mainly characterized by the minimum use of organic solvents.

The aim of this research work was to develop environmentally friendly sample preparation methods followed by inductively coupled plasma optical emission spectroscopy for the determination of mercury in fossil fuels and their selected derivatives. Three different sample preparation methods were developed and applied for this purpose. These three different sample preparation methods were microwave-assisted hydrogen peroxide digestion, vortex assisted deep eutectic solvent based dispersive liquid-liquid microextraction and ultrasound-assisted magnetic dispersive solid phase microextraction.

Multivariate optimization tools were employed for the optimization of the most influential parameters for the three different sample preparation methods. For microwave-assisted hydrogen peroxide digestion, the optimized parameters were sample mass, digestion time, temperature, hydrogen peroxide concentration and methionine concentration. The vortex-assisted deep eutectic solvent based dispersive liquid-liquid microextraction optimized parameters were sample pH, extraction time, extractant volume, disperser solvent volume and centrifugation time. Finally for ultrasound-assisted magnetic dispersive solid phase microextraction, the optimized conditions were adsorbent mass, sonication time, pH, eluent concentration and elution time. The analyses were conducted using inductively coupled plasma-optical emission spectroscopy.

The three methods were validated by analyzing NIST SRM 2778 with certified mercury concentration levels of $38.98 \mu\text{g}/\text{kg} \pm 1.10 \mu\text{g}/\text{kg}$. The recoveries obtained were 93-107 %, 99.9 % and 105 % for microwave-assisted hydrogen peroxide digestion, vortex-assisted deep eutectic solvent based dispersive liquid-liquid microextraction and ultrasound-assisted magnetic dispersive solid phase microextraction, respectively. The limits of detection and limits of quantification obtained were $0.25 \mu\text{g}/\text{L}$ and $0.80 \mu\text{g}/\text{L}$ for microwave-assisted hydrogen peroxide digestion respectively. For vortex-assisted deep

eutectic solvent based dispersive liquid-liquid microextraction, they were 0.025 µg/L and 0.083 µg/L and for ultrasound-assisted magnetic dispersive solid phase microextraction were 0.035 µg/L and 0.119 µg/L, respectively. A good precision of less than 5 % was achieved for all the three different sample preparation methods.

The validated sample preparation methods were applied in real fossil fuels which were coal and crude oil. The methods were also applied in real crude oil derivatives which were gasoline, diesel oil and kerosene. Coal samples were obtained in triplicates from a coal mine in Mpumalanga, South Africa, while crude oil samples were obtained in triplicates from a petrochemical company in Johannesburg, South Africa. Crude oil derivatives were obtained from three local filling stations around Johannesburg, South Africa. The concentrations obtained were 0.876±0.023-0.975±0.025 µg/g in coal samples, 0.383±0.043-0.510±0.09 µg/g for crude oil samples, 0.306±0.010-0.390±0.035 µg/g for gasoline samples, 0.360±0.003-0.434±0.050 µg/g for diesel oil samples and 0.09±0.09-0.098±0.02 µg/g for kerosene samples.

The three different microextraction sample preparation methods were successfully developed and applied in fossil fuels and their selected derivatives prior to quantification of mercury using inductively coupled-plasma optical emission spectroscopy.

CONTENTS

DECLARATION	i
DEDICATION	iii
ACKNOWLEDGEMENTS	iv
PUBLICATIONS AND BOOK CHAPTERS	vi
CONFERENCE PRESENTATIONS	vii
ABSTRACT	viii
LIST OF FIGURES	xiv
LIST OF TABLES	xviii
LIST OF EQUATIONS	xxi
LIST OF ABBREVIATIONS AND ACRONYMS	xxii
CHAPTER I: INTRODUCTION	1
PREAMBLE	1
1.1 Background information	1
1.1.1 Coal	1
1.1.2 Crude oil	5
1.1.3 Mercury	8
1.2 Problem statement	11
1.3 AIMS AND OBJECTIVES	12
1.3.1 Aim	12
1.3.2 Specific objectives	12
1.4 JUSTIFICATION	13
1.5 HYPOTHESIS	14
1.6 RESEARCH QUESTIONS	14
1.7 DISSERTATION OUTLINE	14
REFERENCES	17
CHAPTER II: LITERATURE REVIEW	22
PREAMBLE	22
2.1 Background information	22
2.1.1 Physical and chemical properties of mercury	23
2.1.2 Species of mercury	24
2.1.3 Occurrence of mercury in non-aqueous matrices	24

2.2	Sample preparation methods for total determination of Hg in nonaqueous matrices.....	25
2.2.1	Mineralization sample preparation methods	26
2.2.2	Combustion sample preparation methods	36
2.2.3	Extraction sample preparation methods	40
2.3	Optimization of sample preparation methods (Univariate or multivariate)	66
2.3.1.	Univariate optimization strategy	66
2.3.2.	Multivariate optimization strategies	67
2.4	Characterization techniques	71
2.5	Summary of Recently Published Work 2013-2023	73
2.6	Conclusion.....	78
	REFERENCES.....	80
	CHAPTER III	88
3.1.	Introduction	89
3.2.	Experimental methods.....	91
3.2.1.	Samples, reagents, standard solutions, and glassware	91
3.2.2.	Instrumentation	92
3.2.3.	Microwave-assisted hydrogen peroxide digestion (MW-AHPD)	93
3.2.4.	Multivariate optimization	94
3.3.	Results and discussion	95
3.3.1.	Thermal stability of methionine.....	95
3.3.2.	Two level half factorial design	96
3.3.3.	Response surface methodology (RSM)	97
3.3.4.	Validation of the proposed MW-AHPD method	99
3.3.5.	Greenness assessment of MW-AHPD method	101
3.3.6.	Comparison of the proposed MW-AHPD with other literature reports	103
3.3.7.	Application of MW-AHPD in real coal and fuel samples.....	107
3.4.	Conclusion	108
	REFERENCES.....	110
	CHAPTER IV	113
	ABSTRACT	113
4.1.	Introduction	113
4.2.	Materials and methods	116

4.2.1.	Reagents and solutions	116
4.2.2.	Instrumentation	117
4.2.3.	Characterization techniques	118
4.2.4.	Preparation of deep eutectic solvents.....	119
4.2.5.	Vortex-assisted-natural deep eutectic solvent-based dispersive liquid-liquid microextraction (VA-DES-DLLME) procedure.....	119
4.2.6.	Optimization of the VA-DES-DLLME procedure	120
4.3.	Results and discussion	121
4.3.1.	Characterization of synthesized deep eutectic solvents (DESS)	121
4.3.2.	Selection of deep eutectic solvents (DESS)	129
4.3.3.	Multivariate optimization of deep eutectic solvent based dispersive liquid-liquid microextraction parameters.....	130
4.3.4.	Validation studies.....	134
4.3.5.	Greenness assement of VA-DLLME procedure	134
4.3.6.	Comparison of the proposed method with other literature reports.....	136
4.3.7.	Application of VA-DES-DLLME in real fuel samples	138
4.4.	Conclusion.....	139
	REFERENCES.....	141
	CHAPTER V	145
	ABSTRACT	145
5.1	Introduction	145
5.2	Experimental section	147
5.2.1.	Chemicals and reagents	147
5.2.2.	Instrumentation	148
5.2.3.	Characterization techniques	149
5.2.4.	Synthesis of nanoparticles	151
5.2.5.	Ultrasound assisted magnetic dispersive solid phase microextraction (UA-m-DSPME) procedure	152
5.2.6.	Optimization of UA-D-m-SPME procedure	153
5.2.7.	Application of the MGO-Au nanocomposite to real fuel samples.....	154
5.2.8.	Reusability studies	154
5.3	Results and discussion	155
5.3.1.	Characterization methods for the prepared nanoparticles.....	155

5.3.2. Choice of eluent.....	165
5.3.3. Multivariate optimization	166
5.3.4. Validation of the proposed method	169
5.3.5. Comparison of the developed method with other literature reports.....	170
5.3.6. Greenness assessment of the newly developed m-SPME procedure	173
5.3.7. Interference studies.....	174
5.3.8. Reusability studies	174
5.4 Conclusion.....	176
REFERENCES.....	178
CHAPTER VI.....	181
(OVERALL CONCLUSION & FUTURE RECOMMENDATIONS)	181
PREAMBLE.....	181
6.1 Overall conclusion.....	181
6.2 Future recommendations	184
APPENDIX.....	185
PREAMBLE.....	185

LIST OF FIGURES

FIGURE 1. 1: COAL GENESIS [11].	29
FIGURE 1. 2: SCHEMATIC REPRESENTATION OF THE FISCHER-TROPSCH PROCESS [18].	30
FIGURE 1. 3: ELECTRICITY GENERATION FROM COAL [20]	31
FIGURE 1. 4: SCHEMATIC DIAGRAM FOR CRUDE OIL FORMATION PROCESS [24].	32
FIGURE 1. 5: SCHEMATIC REPRESENTATION FOR CRUDE OIL PROCESSING [28].	33
FIGURE 1. 6: GENERAL MERCURY LIFE CYCLE [35].	35
FIGURE 1. 7: HUMAN ORGANS WHICH ARE AFFECTED BY MERCURY.	36
FIGURE 1. 8: TYPES OF HUMAN EXPOSURE TO MERCURY [35].	37
FIGURE 2. 1: DIFFERENT SAMPLE PREPARATION METHODS FOR THE SPECTROMETRIC DETERMINATION OF TOTAL MERCURY IN NON-AQUEOUS MATRICES.	53
FIGURE 2. 2: VARIOUS TECHNIQUES FOR THE PREPARATION OF MINERALIZATION SAMPLES BEFORE SPECTROMETRIC MEASUREMENT OF TOTAL MERCURY IN NON- AQUEOUS MATRICES.	54
FIGURE 2. 3: VARIOUS COMBUSTION TECHNIQUES USED BEFORE TOTAL MERCURY IN NONAQUEOUS MATRICES IS DETERMINED SPECTROSCOPICALLY.	64
FIGURE 2. 4: DIFFERENT EXTRACTION TECHNIQUES USED BEFORE THE TOTAL MERCURY IN NON-AQUEOUS MATRICES WAS DETERMINED USING SPECTROMETRY. .	69
FIGURE 2. 5: SCHEMATIC REPRESENTATION OF D-LLME [86].	71
FIGURE 2. 6: SCHEMATIC PRESENTATION OF CP-DLLME [92].	72
FIGURE 2. 7: TYPES OF SINGLE DROP MICROEXTRACTION (SDME).	74
FIGURE 2. 8: HOLLOW FIBER LIQUID-LIQUID MICROEXTRACTION (HF-LLME) [99].	75
FIGURE 2. 9: EXTRACTION INDUCED BY EMULSION BREAKING (EIEB) [102].	76
FIGURE 2. 10: SCHEMATIC DIAGRAM FOR SOLID PHASE EXTRACTION (SPE) [129]	84
FIGURE 2. 11: SCHEMATIC REPRESENTATION OF MAGNETIC SOLID PHASE MICROEXTRACTION (M-SPME) [134].	86
FIGURE 2.12: MODES OF SPME. (A) DI-SPME, (B) HS-SPME AND (C) MEMBRANE-	

PROTECTED SPME [137].	87
FIGURE 2. 13: SCHEMATIC REPRESENTATION OF DISPERSIVE SOLID PHASE MICROEXTRACTION (DSPME) [24].	88
FIGURE 2.14: ULTRASOUND -ASSISTED EXTRACTION (UAE) [161].	94
FIGURE 2. 15: MICROWAVE-ASSISTED EXTRACTION (MAE) [163].	96
FIGURE 2. 16: THE QUANTITY OF PUBLICATIONS DETAILING VARIOUS SAMPLE PREPARATION TECHNIQUES BEFORE SPECTROMETRIC MEASUREMENT OF TOTAL MERCURY IN NON-AQUEOUS MATRICES.	102
FIGURE 2. 17: NUMBER OF PUBLICATIONS REPORTED FOR DIFFERENT EXTRACTION METHODS FOR TOTAL DETERMINATION OF MERCURY IN NON-AQUEOUS MATRICES.	103
FIGURE 2. 18: NUMBER OF PUBLICATIONS FOR DIFFERENT NON-AQUEOUS MATRICES.	104
FIGURE 2. 19: ANALYTICAL TECHNIQUES THAT HAVE BEEN REPORTED FOR THE SPECTROMETRIC DETERMINATION OF TOTAL MERCURY IN NON-AQUEOUS MATRICES AFTER SAMPLE PREPARATION.	105
FIGURE 2. 20: OPTIMIZATION STRATEGIES FOR SAMPLE PREPARATION METHODS.	106
FIGURE 3. 1: KEY STEPS OF A MW-AHPD PROCEDURE.	126
FIGURE 3. 2: THERMOGRAM FOR METHIONINE.	128
FIGURE 3. 3: PARETO GRAPHIC FOR TOTAL HG AT 95% CONFIDENCE LEVEL FOR TWO LEVEL HALF FACTORIAL DESIGN (2^{5-1}) FOR SAMPLE MASS, TIME, TEMPERATURE, [H ₂ O ₂], AND [METHIONINE] OPTIMIZATION (N=3).	129
FIGURE 3. 4: TOTAL MERCURY RESPONSE SURFACES OF TOTAL HG VS [H ₂ O ₂]. TIME, [H ₂ O ₂]. TEMPERATURE, [H ₂ O ₂]. [METHIONINE], [METHIONINE]. TEMPERATURE, [METHIONINE]. TIME AND TIME. TEMPERATURE MEASURED WITH A CCD. 0.1 G OF SAMPLE MASS, 5 M [H ₂ O ₂], 5.95 M [METHIONINE], AND 200 °C WERE THE EXPERIMENTAL PARAMETERS.	131
FIGURE 3. 5: COMPARISON OF PERCENTAGE RECOVERIES OF TOTAL MERCURY UNDER	

OPTIMUM CONDITIONS WHEN DIGESTING (A) NO METHIONINE, (B) METHIONINE AND (C) STANDARD METHOD.	132
FIGURE 3. 6: PICTOGRAM VISUALISING THE GREENNESS OF THE PROPOSED PROCEDURE FROM AGREEPREP. SOFTWARE.	135
FIGURE 4. 1: VORTEX ASSISTED-NATURAL DEEP EUTECTIC SOLVENTS BASED DISPERSIVE LIQUID-LIQUID MICROEXTRACTION (VA-DES-DLLME) PROCEDURE.	150
FIGURE 4. 2: FT-IR SPECTRA FOR A) DES 1 AND ITS PURE COMPOUNDS, B) DES 2 AND ITS COMPOUNDS AND C) DES 3 AND ITS PURE COMPOUNDS.	154
FIGURE 4. 3: THERMOGRAPHS FOR A) DES 1 AND ITS PURE COMPOUNDS, B) DES2 AND ITS PURE COMPOUNDS AND C) DES 3 AND ITS PURE COMPOUNDS.	156
FIGURE 4. 4: ¹³ C NMR FOR DES 1.	158
FIGURE 4. 5: ¹³ C NMR FOR DES 2.	159
FIGURE 4. 6: ¹³ C NMR FOR DES 3.	160
FIGURE 4. 7: RECOVERIES FOR DES1, DES2 & DES3 AFTER A DES-DLLME PROCEDURE	161
FIGURE 4. 8: PARETO CHART SHOWING THE OVERALL MERCURY CONTENT OF FUEL OILS USING A TWO-LEVEL HALF FACTORIAL DESIGN (2 ⁵⁻¹).	162
FIGURE 4. 9: RESPONSE SURFACES VS PH. EXTRACTANT VOLUME, PH. DISPERSER SOLVENT VOLUME, PH. VORTEX TIME, EXTRACTANT VOLUME. DISPERSER SOLVENT VOLUME OBTAINED FROM BOX BEHNKEN DESIGN. EXPERIMENTAL CONDITIONS: 5 ML SAMPLE MASS, 4.5 PH, 164 µL EXTRACTANT VOLUME AND 665 µL DISPERSER SOLVENT VOLUME.	164
FIGURE 4. 10: PICTOGRAM FOR AGREEPREP FOR VA-DES-DLLME METHOD... ..	166
FIGURE 5. 1: CRUCIAL STEPS FOR ULTRASOUND ASSISTED-DISPERSIVE MAGNETIC SOLID PHASE MICROEXTRACTION PROCEDURE (UA-M-DSPME).	184
FIGURE 5. 2: FT-IR SPECTRA FOR (A) GO, (B) MGO AND (C) MGO-AU.	187
FIGURE 5. 3: UV-VIS SPECTRA FOR (A) GO, (B) MGO, AND (C) MGO-AU.	188

FIGURE 5. 4: POWDER X-RAY DIFFRACTION PATTERNS FOR (A) GO, (B) MGO, AND (C) MGO-AU.	190
FIGURE 5. 5: THERMOGRAPHS FOR (A) GO, (B) MGO, AND (C) MGO-AU.	191
FIGURE 5. 6: SCANNING ELECTRON MICROSCOPY FOR (A) GO, (B) MGO, (C) MGO-AU. AND (D) EDS FOR MGO-AU.	192
FIGURE 5. 7: TRANSMISSION ELECTRON MICROSCOPY FOR (A) GO, (B) MGO, AND (C) MGO-AU.	194
FIGURE 5. 8: THE NITROGEN ADSORPTION ISOTHERM CURVE OF MGO-AU CORE SHELL NANOCOMPOSITE.	195
FIGURE 5. 9: THE PORE SIZE DISTRIBUTION OF MGO-AU CORE SHELL NANOCOMPOSITE.	196
FIGURE 5. 10: RECOVERIES (%) FOR (A) HCL, (B) HCL+ AU, AND (C) HCL+ THIOUREA.	197
FIGURE 5. 11: TWO-LEVEL HALF FACTORIAL DESIGN.	198
FIGURE 5. 12: SURFACE RESPONSES TOTAL HG VERSUS PH. SORBENT MASS, SORBENT MASS. SONICATION TIME, SONICATION TIME. ELUENT CONCENTRATION AND SORBENT MASS. ELUENT CONCENTRATION.	199
FIGURE 5. 13: COMPARATIVE ANALYSIS OF THE ADSORBENTS GO, MGO, AND MGO-AU FOR THE TOTAL MERCURY MEASUREMENT IN FUEL OILS.....	200
FIGURE 5. 14: PICTOGRAM FOR UA-M-SPME PROCEDURE.	204
FIGURE 5. 15: REUSABILITY OF THE MGO-AU CORE-SHELL NANO- COMPOSITE FOR ADSORPTION OF HG IN FUEL MATRICES.....	206

LIST OF TABLES

TABLE 2. 1: DIFFERENT WET DIGESTION METHODS APPLIED TO NON-AQUEOUS MATRICES PRIOR TO QUANTIFICATION OF HG.	57
TABLE 2. 2: DETERMINATION OF HG FROM DIFFERENT MATRICES USING COMBUSTION METHOD.	67
TABLE 2. 3: LIQUID-LIQUID EXTRACTION METHODS FOR DETERMINING HG FROM DIFFERENT NON-AQUEOUS SAMPLES.	78
TABLE 2. 4: SOLID PHASE EXTRACTION METHODS FOR THE DETERMINATION OF HG FROM DIFFERENT NON-AQUEOUS SAMPLES.	90
TABLE 3. 1: REAL SAMPLES AND THEIR ABBREVIATIONS.	124
TABLE 3. 2: OPERATING PARAMETERS OF ICP-OES FOR MERCURY ANALYSIS.	125
TABLE 3. 3: VARIABLES THAT WERE INVESTIGATED AND THEIR LEVELS FOR HALF FRACTIONAL DESIGN.	126
TABLE 3. 4: VARIABLES INVESTIGATED AND THEIR LEVELS IN CENTRAL COMPOSITE DESIGN.	127
TABLE 3. 5: ANALYTICAL PERFORMANCES OF THE NEWLY DEVELOPED MW-HPD.	133
TABLE 3. 6: DEFAULT WEIGHTS USED IN AGREEPREP.	134
TABLE 3. 7: COMPARING THE NEWLY ESTABLISHED MW-AHPD'S MERIT FIGURES WITH THOSE FROM OTHER SOURCES REPORTS ON MW-AD IN FUEL OILS.	137
TABLE 3. 8: TOTAL MERCURY CONCENTRATION LEVELS, REPORTED IN $\mu\text{G/G}$, WERE MEASURED AFTER DIGESTION USING MW-AHPD AND ICP-OES IN ACTUAL COAL, CRUDE OIL, GASOLINE, DIESEL OIL, AND KEROSENE (1, 2, AND 3).	139
TABLE 4. 1: THE COMPONENTS OF DESs AND THEIR CHEMICAL STRUCTURAL INFORMATION	148
TABLE 4. 2: DIFFERENT TYPES OF FUEL SAMPLES.	148
TABLE 4. 3: TWO-LEVEL HALF FACTORIAL (2^{5-1}) EXPERIMENTAL DESIGN.	151
TABLE 4. 4: RESPONSE METHODOLOGY BASED ON BBD EXPERIMENT DESIGN.	152
TABLE 4. 5: ^{13}C NMR DATA FOR DES1.	157
TABLE 4. 6: ^{13}C NMR DATA FOR DES2.	157

TABLE 4. 8: ¹³ C NMR DATA FOR DES3.	158
TABLE 4. 9: COMPARING THE SUGGESTED METHOD'S FIGURES OF MERIT WITH OTHER LLE FIGURES OF MERIT THAT HAVE BEEN PUBLISHED.	168
TABLE 5. 1: DIFFERENT TYPES OF FUEL OILS AND THEIR ABBREVIATIONS.	179
TABLE 5. 2: SYNTHESISED NANOCOMPOSITES AND THEIR ABBREVIATIONS.	179
TABLE 5. 3: TWO-LEVEL HALF FACTORIAL (2 ⁵⁻¹) EXPERIMENTAL DESIGN.	185
TABLE 5. 4: RESPONSE METHODOLOGY BASED ON BBD EXPERIMENT DESIGN.	185
TABLE 5. 5: THE BET RESULTS OF THE GO, MGO AND MGO-AU CORE SHELL NANOCOMPOSITE.....	195
TABLE 5. 6: COMPARISON OF THE FIGURES OF MERITS BETWEEN NEWLY DEVELOPED M-SPE WITH OTHER SPE REPORT ON FUEL MATRICES.	202
TABLE 5. 7: EFFECT OF VARIOUS INTERFERING CATIONS ON THE PRECONCENTRATION AND DETERMINATION OF TOTAL Hg USING ONLINE UA-M-DSPME METHOD: CONCENTRATION OF INTERFERING ION = 100 µG L ⁻¹	205
TABLE 5. 8: TOTAL MERCURY CONCENTRATION LEVELS (µG/G) IN REAL CRUDE OIL, GASOLINE, DIESEL OIL AND KEROSENE.	207
TABLE S 1: THE EFFECT OF VARYING SAMPLE MASS, HYDROGEN PEROXIDE CONCENTRATION, METHIONINE CONCENTRATION, DIGESTION TIME AND TEMPERATURE ON THE DIGESTION OF REAL CRUDE OIL SAMPLE TO ACHIEVE HIGH PERCENTAGE RECOVERIES OF TOTAL Hg. REPLICATES (N=3).	215
TABLE S 2: ANALYSIS OF VARIANCE (ANOVA) FOR TWO-LEVEL HALF FACTORIAL DESIGN FOR MW-AHPD.	216
TABLE S 3: THE EFFECT OF VARYING DIGESTION TIME, TEMPERATURE, [H ₂ O ₂], [METHIONINE] WHILE KEEPING SAMPLE MASS CONSTANT IN FURTHER OPTIMIZATION USING ON THE DIGESTION OF CENTRAL COMPOSITE DESIGN. EXPERIMENTAL CONDITIONS: 0.1G (N =3).	217
TABLE S 4: ANALYSIS OF VARIANCE FOR CCD FOR MW-AHPD	218
TABLE S 5: THE EFFECT OF VARYING SAMPLE PH, VOLUME OF DISPERSER SOLVENT, VOLUME OF	

EXTRACTING SOLVENT, EXTRACTION TIME AND CENTRIFUGATION TIME, ON THE VA-DES-DLLME OF REAL CRUDE OIL SAMPLE TO ACHIEVE HIGH PERCENTAGE RECOVERIES OF TOTAL Hg. REPLICATES (N=3).	219
TABLE S 6: ANALYSIS OF VARIANCE FOR TWO-LEVEL HALF FACTORIAL DESIGN FOR VA-DES-DLLME.	220
TABLE S 7: THE EFFECT OF VARYING pH, VORTEX TIME, DISPERSER SOLVENT, EXTRACTANT VOLUME, WHILE KEEPING CENTRIFUGATION TIME CONSTANT IN FURTHER OPTIMIZATION USING BBD. EXPERIMENTAL CONDITIONS: 5 MINUTES CENTRIFUGATION TIME (N =3)	221
TABLE S 8: ANALYSIS OF VARIANCE FOR CCD FOR VA-DES-DLLME.	222
TABLE S 9: THE EFFECT OF VARYING SORBENT MASS, SAMPLE PH, SONICATION, ELUENT CONCENTRATION, AND ELUTION TIME AND CENTRIFUGATION TIME, ON THE UA-M-DSPME OF REAL CRUDE OIL SAMPLE TO ACHIEVE HIGH PERCENTAGE RECOVERIES OF TOTAL Hg. REPLICATES (N=3)	223
TABLE S 10: ANALYSIS OF VARIANCE OF HALF FACTORIAL DESIGN FOR UA-M-DSPME.	223
TABLE S 11: THE EFFECT OF VARYING PH, SONICATION TIME, SORBENT MASS, AND ELUENT CONCENTRATION, WHILE KEEPING ELUTION TIME CONSTANT IN FURTHER OPTIMIZATION USING BBD. EXPERIMENTAL CONDITIONS: 5 MINUTES ELUTION TIME (N =3).	225
TABLE S 12: ANALYSIS OF VARIANCE OF BBD FOR UA-M-DSPME.	225

LIST OF EQUATIONS

$$CaHbOc + O_2 \rightarrow CO_2 + H_2O \quad \text{Eq. 2. 1. 63}$$

$$y = a_0n = 1kaixi + A \quad \text{Eq. 2. 2. 98}$$

$$Y = a_0 + i = 1kaixi + 1 \leq i \leq jkaijxixj + i = 1kaiixi^2 \quad \text{Eq. 2. 3. 98}$$

$$2k + 2k + n_0 \quad \text{Eq. 2. 4. 99}$$

$$k^2 + k + n_0 \quad \text{Eq. 2. 5. 99}$$

$$N = k^2 + k + c_0 \quad \text{Eq. 2. 6. 99}$$

$$\% \text{Recoveries} = \frac{\text{Spiked conc.} - \text{obtained conc.}}{\text{Spiked value}} \times 100 \quad \text{Eq. 3. 1 126}$$

$$\% \text{Recoveries} = 18.4A + 9.16B + 4.92C + 1.83D - 1.52A^2 - 0.448B^2 - 0.022C^2 - 0.01299CD - 280 \quad \text{EQ. 3. 2 127}$$

$$0.00207D^2 + 0.018AB - 0.057AC - 0.0193AD - 0.0083BC - 0.0155BD -$$

$$\% \text{Recoveries} = 11.86 - 2.0746A^2 - 0.1474B^2 - 32.93C^2 - 58.6D^2 - 0.0776AB - 1.800AC - 0.64AD - 1.333BC - 3.478BD - 10.7CD \quad \text{Eq. 4. 1 164}$$

LIST OF ABBREVIATIONS AND ACRONYMS

ANOVA	Analysis of variance
BJH	Barrett-Joyner-Halenda
BBD	Box-Behken design.
BET	Brunauer-Emmett-Teller
CNTs	Carbon nanotubes
CCD	Central composite design
CPE	Cloud point extraction
CV-AAS	Cold vapor atomic absorption spectroscopy
DESS	Deep eutectic solvents
DI-SDME	Direct immersion- single drop microextraction
DLLME	Dispersive liquid-liquid microextraction
DSPME	Dispersive solid phase microextraction
DTz	Dithizone
DD	Doehlert design
ET-AAS	Electro-thermal atomic absorption spectroscopy
EF	Enrichment factor
EIEB	Extraction induced by emulsion breaking
FFD	Full factorial design
FAAS	Flame atomic absorption spectroscopy
FT-IR	Fourier Transformed Infrared spectroscopy
GO	Graphene oxide
GFAAS	Graphite atomic absorption spectroscopy
GAC	Green Analytical Chemistry
HF-LPME	Hallow fiber-liquid phase microextraction
HS-SDME	Head space-single drop microextraction
HB-AD	Heating block-assisted digestion
HP-AD	Hot Plate-assisted digestion
HG-AAS	Hydride-atomic absorption spectroscopy
HF	Hydroflouric acid
HBA	Hydrogen bond acceptor
HBD	Hydrogen bond donor
H ₂ O ₂	Hydrogen peroxide

ICP-MS	Inductively coupled plasma-mass spectrometry
ICP-OES	Inductively coupled plasma-optical emission spectroscopy
LOD	Limit of detection
LOQ	Limit of quantification
LLE	Liquid-liquid extraction
LLME	Liquid-liquid microextraction
Fe ₃ O ₄ -GO-Au	Magnetic graphene oxide coated with gold
Fe ₃ O ₄ @GO@ ILs	Magnetic graphene oxide coated with ionic liquids
m-SPE	Magnetic solid phase extraction
Hg	Mercury
MOF	Metal organic framework
MLOD	Method limit of detection
MLOQ	Method limit of quantification
MW-AAD	Microwave-assisted acid digestion
MAE	Microwave-assisted extraction
MW-AHPD	Microwave-assisted hydrogen peroxide digestion
MIC	Microwave-induced combustion
MF-AA	Muffle furnace assisted ashing
HNO ₃	Nitric acid
NR	Not reported
P-B	Plackett-Burman
PTFE	Polytetrafluoroethylene
PVDF	Polyvinylidene Fluoride
KMnO ₄	Potassium permanganate
P-XRD	Powder-X-ray diffraction
RSM	Response surface methodology
SEM-EDS	Scanning electron microscopy-energy dispersive spectroscopy
SAED	Selected area electron diffraction
SDME	Single drop microextraction
NaBH ₄	Sodium tetraborohydride
NaOH	Sodium hydroxide
SPE	Solid phase extraction
SPME	Soildi phase microextraction
SRM	Standard reference material
SnCl ₂	Stannous chloride
H ₂ SO ₄	Sulphuric acid
HAuCl ₄	Tetrachlouric acid
TGA	Thermal gravimetric analysis
TLFD	Three level factorial design
TEM	Transmission electron microscopy

FrFD	Fractional factorial design
UAE	Ultrasound-assisted extraction
UA-m-DSPME	Ultrasound assisted-magnetic dispersive solid phase microextraction
UV-Vis	Ultraviolet visible spectroscopy
EPA	Environmental protection agency
VA-DES-DLLME	Vortex-assisted deep eutectic solvent-dispersive liquid-liquid microextraction

CHAPTER I: INTRODUCTION

PREAMBLE

This chapter provides an overview of the history of crude oil and coal. It goes into detail about its origins, make-up, and utilization of these energy sources. This chapter also discusses how mercury can be found in various energy sources and how it poses danger to the ecology. We highlighted some of the chosen mineralization and extraction sample preparation techniques along with their advantages and disadvantages. The current research project's problem statement and justification are presented in this chapter as well. Ultimately, the study's purpose and particular goals are elucidated, and then the dissertation's overall scope is discussed.

1.1 Background information

Mankind has been utilizing fossil fuels as a source of energy since the start of the first industrial revolution. During the First Industrial Revolution, coal was the most dominant fossil fuel for energy source utilized during the First Industrial Revolution [1,2]. For nearly a millennium, people have utilized coal as a fuel source for cooking, heating, and hot metal forging in their homes. Coal is still used as a source of energy in nations including South Africa, the United States of America, China, Russia, and India [3]. The former had a golden age until the 20th century before being overtaken as a major energy source by crude oil, natural gas, and nuclear power among other energy sources [4]. Fossil fuels are fossil fuels play a vital role in global economic prosperity and are regarded as the cornerstone for the survival of humanity [5]. In the following sections, we discuss coal, crude oil and derivatives such as gasoline, diesel oil, and kerosene genesis, composition, processing, occurrence, and negative effects of mercury in these energy sources in greater depth.

1.1.1 Coal

Coal is a remarkably complex combination of macerals and minerals and inorganic elements in organic associations plus liquids, gases, and semi-solid organics, all overprinted by coal metamorphism. Coal is a remarkably complex (primarily) biologic rock. Coal is a function of three fundamental aspects, each a reflection of the origin and

diagenesis/metamorphism of the coal: organic petrological and geochemical parameters, inorganic petrological and geochemical parameters, and coal rank. In simple terms, coal is the product of macerals, minerals, and the degree of metamorphism.

Coal is a sedimentary deposit composed predominantly of readily combustible carbon. The former is found beneath the earth's surface and was formed naturally over a million years ago because of the burial of ancient plants and animals that were exposed to extreme heat and pressure (**Fig. 1.1**) [6]. This process generally happens in locations that are swampy and have groundwater close to the topsoil. The initial step in coal formation is peatification. The latter involves the partial breakdown of dead mosses, leaves, twigs, and other tree pieces to generate peat [7].

When a river floods or the sea level rises, the marsh may occasionally be covered in sand and muck. With these sediments bearing down on it, the peat may eventually lose some of its water and gas content and transform into lignite, a soft brown coal [8]. The most prevalent bituminous family of coals is formed as temperatures and pressures rise and more water and gases are lost [8]. Finally, high temperatures and pressures cause bituminous coal to turn into a black matured coal called anthracite. These types of coal are called ranks, and they depend more on the depth of burial than time. Hence, an increase in rank represents an increase in the proportion of carbon within the coal [9,10].

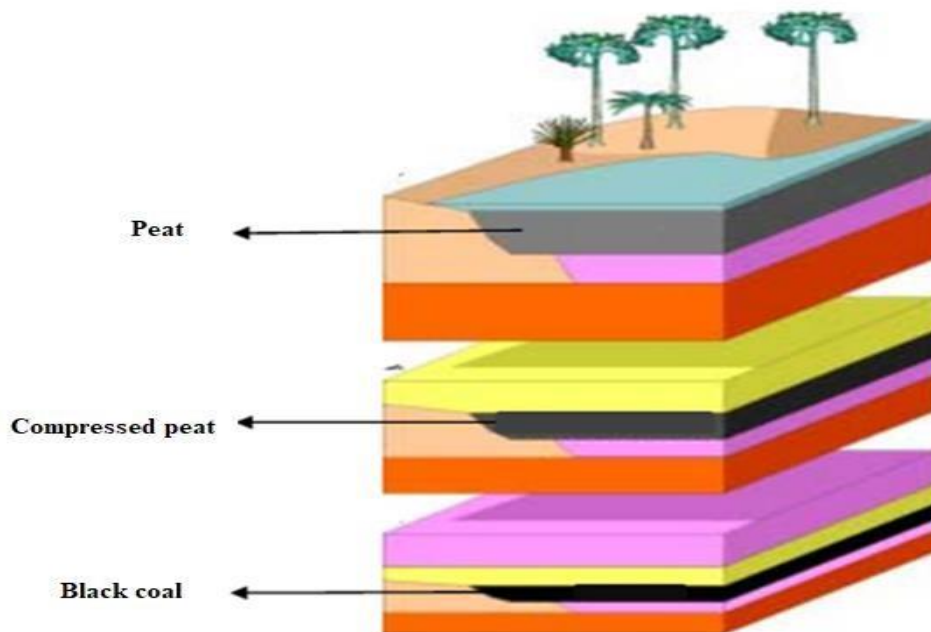


Figure 1. 1: Coal genesis [11].

1.1.1.1 Coal composition

Coal is a mixture of solid, liquid, and gaseous phases with allothigenic or authigenic origin [12]. Coal composition depends on coal rank. However, all forms of coal have fixed carbon, varied moisture levels, ash, volatile matter, and mineral stuff. Low-rank coals are rich in ash, moisture, volatile matter, hydrogen, nitrogen, oxygen, and sulphur. This kind of coal has high MgO, CaO, and SO₃ concentrations [13]. High coal ranks show higher concentrations of SiO₂, Al₂O₃, Fe₂O₃, K₂O, Na₂O, and TiO₂. The coal rank also affects mineral matter. High coal ranks are richer in quartz, Fe oxyhydroxides, illite, mica, chlorite, spinel, dolomite, and hexahydrides. While low-rank coal is abundant in gypsum, calcite, pyrite, montmorillonite, feldspars, zeolite, Al oxyhydroxides, and Fe, Al, and Ba sulphates [14] Another pollutant found in coal, albeit in trace quantities, is mercury, a target analyte in this study. Accurate quantitative mercury assessment in coal remains difficult to perform because of the former's low abundance and volatile nature [15].

1.1.1.3 Processing of coal

Coal is usually processed using an industrial technology called Fischer-Tropsch to produce ultraclean syngas such as gasoline, diesel oil, and kerosine (**Fig. 1.2**). First, coal, biomass, waste, and natural gas are converted using steam conversion technology into syngas which is CO and H₂ [16]. After that, the syngas is prepared as a feed for Fischer Tropsch technology, which turns it into syncrude, which can be refined further to produce commercial products [17].

Fischer-Tropsch reactor

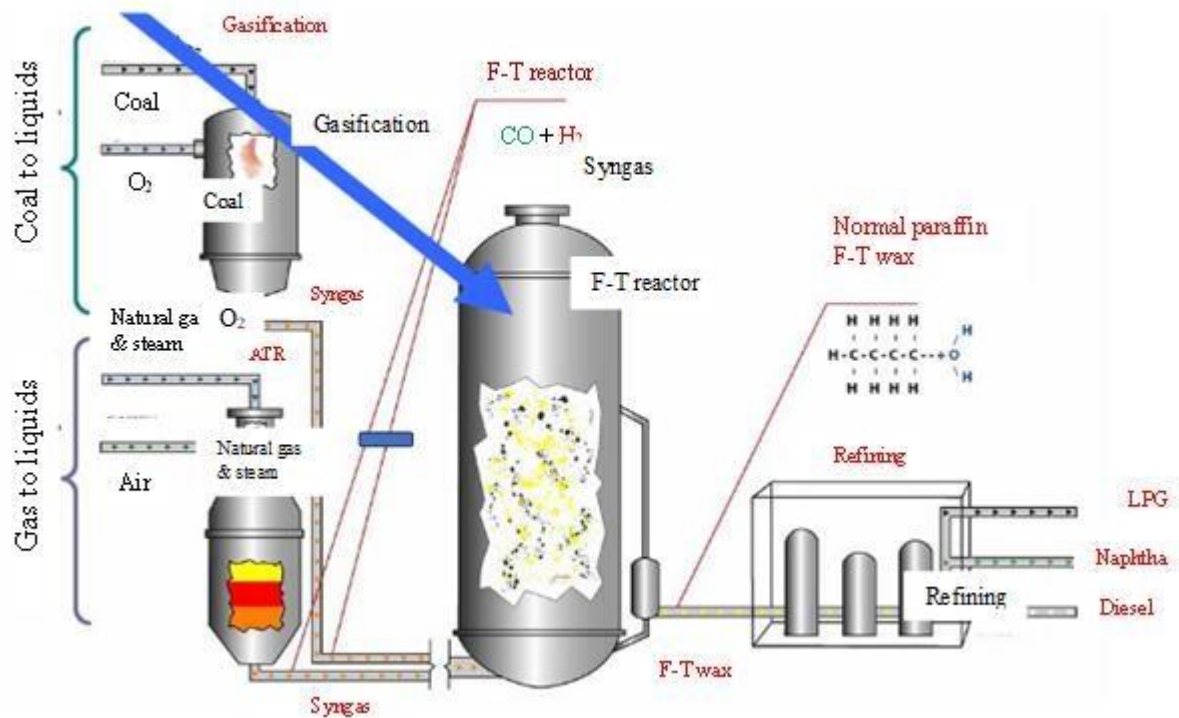


Figure 1. 2: Schematic representation of the Fischer-Tropsch process [18].

Moreover, power plants use coal to produce electricity (**Fig. 1.3**). To increase its surface area and speed of burning, coal is first ground into a fine powder. The powdered coal is subsequently added to the combustion chamber of a boiler and heated to extremely high temperatures. The heated gasses and heat energy they produce converts the water in the boiler's tubes from liquid into steam. The turbines that generate energy are turned by the steam that is created [19].

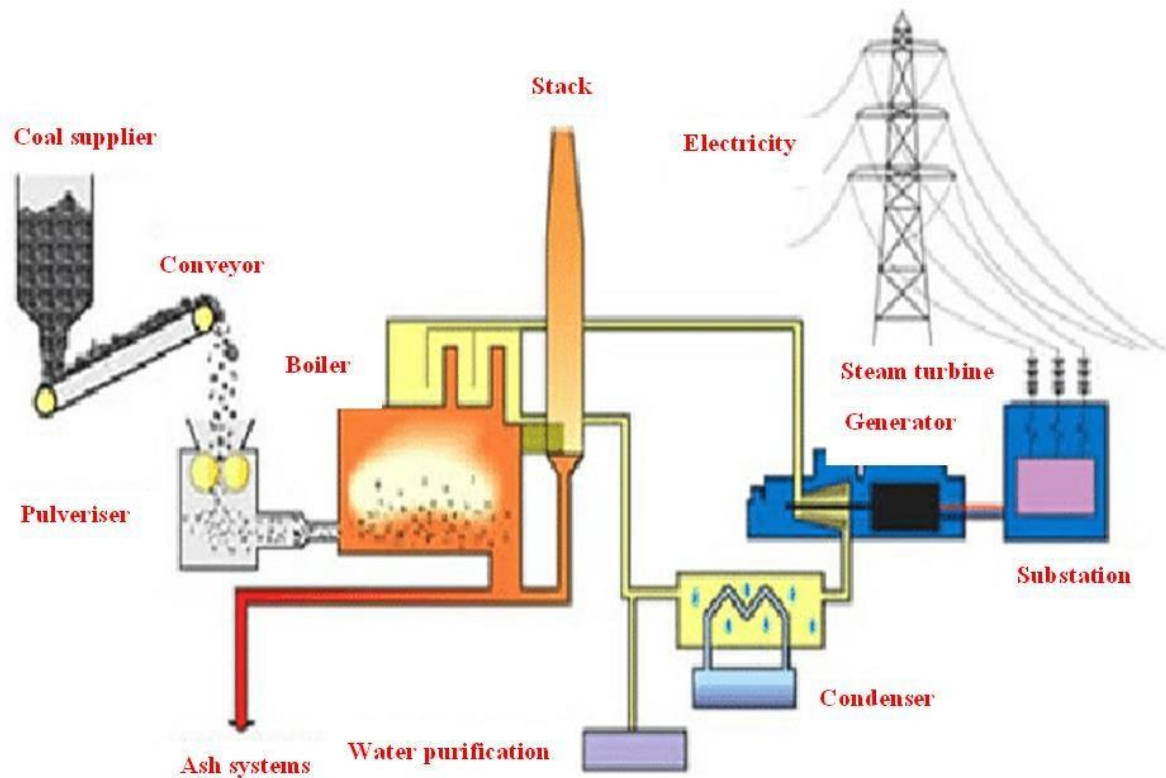


Figure 1. 3: Electricity generation from coal [20].

1.1.2 Crude oil

Crude oil is a complex, oily, flammable liquid that occurs spontaneously and is mostly found in deep geological locations beneath the surface of the earth (**Fig. 1.4**). Crude oil is formed when vast quantities of dead marine animals, often zooplankton and algae, are buried beneath sedimentary rocks and subjected to extreme heat and pressure [21]. Crude oil is also formed in phases. Marine life dies and is buried on the sea floor during the first step of the creation of crude oil. It then eventually gets covered by mud, a site of some bacterial degradation. These buried marine creatures also mix with inorganic materials that enter the ocean by rivers [22]. Over many years, high heat and pressure from the earth's sediments eventually form crude oil, migrating through the rocks' pores, cracks, and fissures, forming oil fields [23].

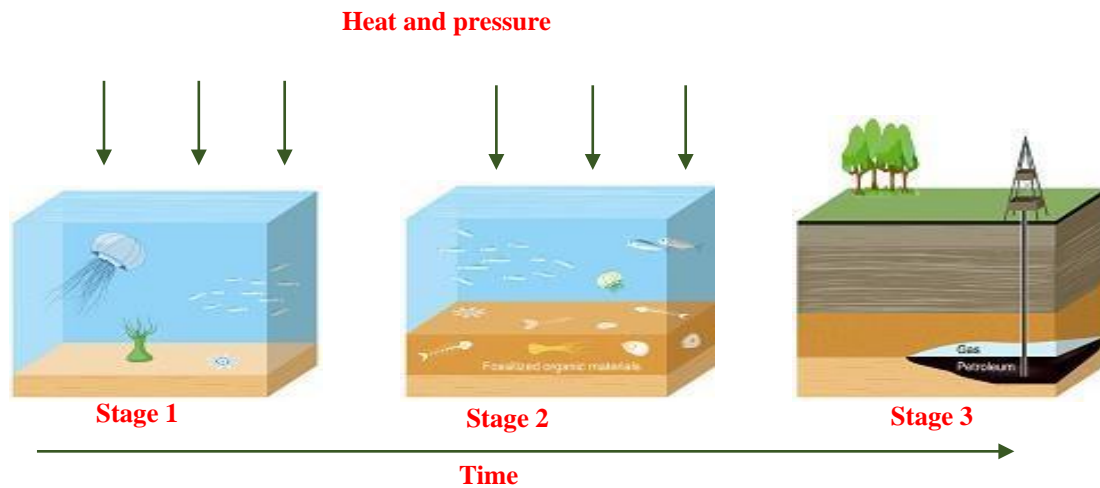


Figure 1. 4: Schematic diagram for crude oil formation process [24].

There are two common types of crude oil: light and heavy. There are more saturated hydrocarbons and fewer aromatic compounds in light crude oil. For instance, fewer than 40 % of paraffinic hydrocarbons and more than 50 % of saturated hydrocarbons are present in naphtheno-paraffinic oil [25]. Conversely, any oil that is difficult to flow is considered heavy crude oil. It differs from natural bitumen in that it contains a significant amount of C15+ [26]. Furthermore, depending on the amount of sulfur it contains, crude oil might be classified as sweet or sour. Sweet crude oil has a comparatively low sulfur concentration compared to sour crude oil's high sulfur content [27].

1.1.2.1 Crude oil composition

Crude oil is a homogenous mixture of asphaltenes, resins, hydrocarbons, aromatic hydrocarbons, and hetero-functionalized organic molecules with oxygen, sulfur, and nitrogen [28]. The primary components of all forms of crude oil are carbon and hydrogen, with smaller amounts of sulfur, nitrogen, and oxygen present. The elemental composition of crude oils depends on the type and origin of the crude [29]. The additional elements exist naturally in crude oil, during the formation of crude oil. The elemental composition of crude oil is shown in **Table 1.1**.

Table 1. 1: Crude oil elemental composition [30,31].

Element	% weight
Carbon	80-87
Hydrogen	10-15
Oxygen	0-5
Nitrogen	0-1
Metals	<1

1.1.2.2 Crude oil processing

Fractional distillation is an industrial method used to separate crude oil into its fractional component's fuels (**Fig. 1.5**). The fundamental idea behind this procedure is that various compounds boil at various temperatures [32]. The first step in this process is to infuse the necessary heat through a fired tube for fractionation. Different components of crude oil with different boiling points are combined and heated to higher temperatures. After then, as the mixture boils, creating vapor different compounds are separated, and the vapor seeps into the lengthy column's bottom [32]. Column interiors are applied using a variety of trays or decks. The draw-off products are collected, and the entering goods are distributed using specially made trays. The vapor cools as it travels through the trays and climbs through the column. A material in the vapor condenses to form a liquid when it reaches a height where the temperature in the column equals the boiling point of the material. Higher boiling point compounds condense toward the bottom of the column, while the substance with the lowest boiling point condenses at the top [33].

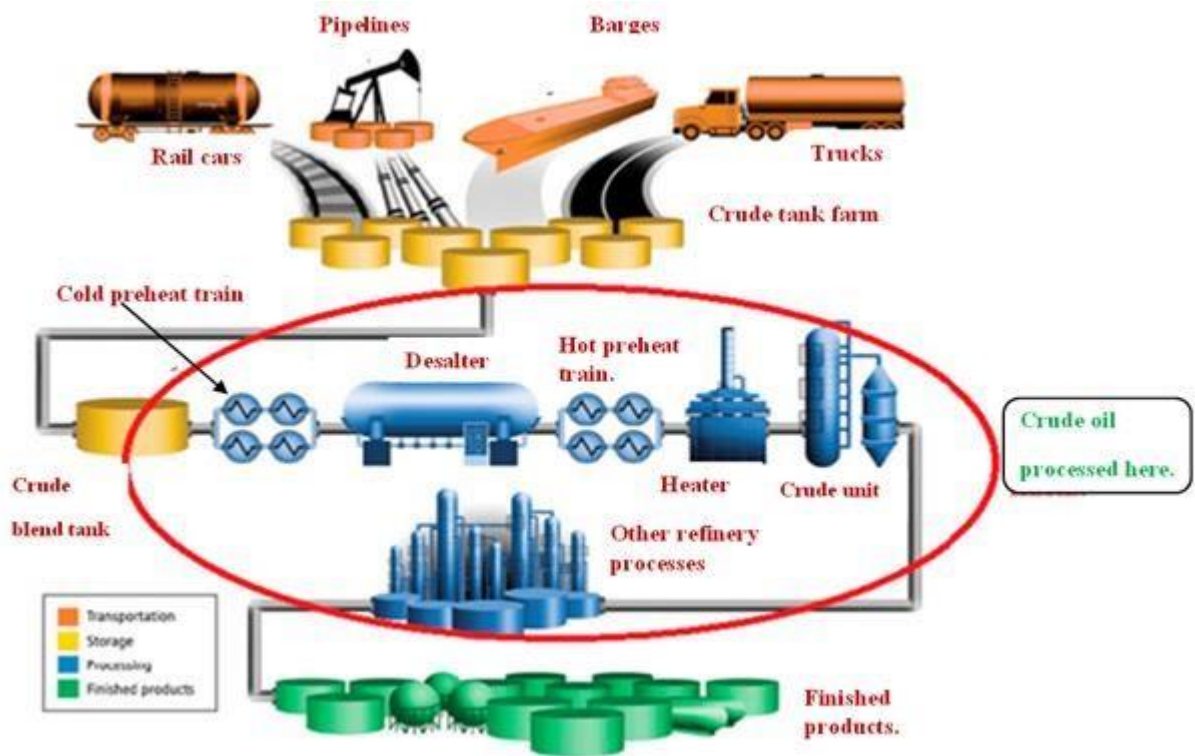


Figure 1. 5: Schematic representation for crude oil processing [28].

1.1.3 Mercury

As mentioned above, mercury is a trace contaminant of fossil fuels. This toxic contaminant exists naturally in these energy resources and cannot be controlled [34]. Mercury, also known as "quicksilver metal", is the most dangerous heavy metal, the negative effects of which have been widely investigated and reported [35]. This trace contaminant is known for being persistent in the environment and tends to accumulate in the internal organs of living organisms, just to mention a few health adverse effects [36]. This hazardous pollutant also has a negative impact on industrial machinery as well as the environment in general. Mercury forms amalgams with other metals, particularly aluminium, to generate mercury/aluminium amalgams, which typically deteriorate refinery equipment and lead to catalyst poisoning [37].

Furthermore, during the combustion of these energy sources, the amalgam mixture is released into the atmosphere, which threatens both animal and human health [38,39]. Mercury is typically released into the environment because of human and natural activities. **Figure 1.6** depicts the mercury cycle, illustrating how anthropogenic (such as refining

fossil fuels and burning their derivatives) and natural activities i.e. volcanic eruptions, release mercury into the environment. Mercury is first emitted into the environment as elemental mercury (Hg^0) or particulate mercury (Hg^p) while processing these energy resources. The latter is oxidized to form ionic mercury (Hg^{2+}) in the environment. Mercury in this form dissolves in water. Water bodies get the dissolved mercury species, which transforms into methyl mercury. Fish typically consume this type of mercury through contamination of their food sources, which is the most poisonous, and it bioaccumulates in their tissues [40]. Seafood is a major source of food consumption and revenue in many nations [41]. Consumption of these sea food products may have detrimental consequences on one's health because mercury is known to bio-magnify (**Fig. 1.7**) [35]. **Figure 1.8** illustrates the other routes of human exposure to mercury exposure.

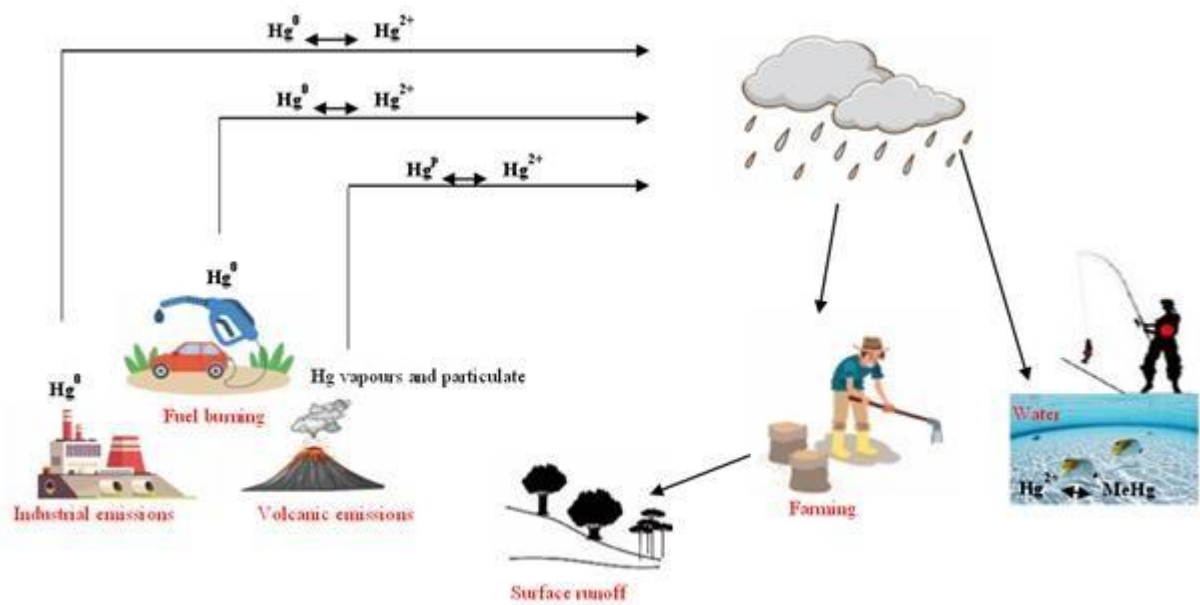


Figure 1. 6: General mercury life cycle [35].

Human mercury toxicity varies according to the chemical form of mercury, concentration levels, seafood diet, length of exposure, age, gender, and state of health of the individual. Every mercury species has detrimental effects on human health, particularly on the respiratory, digestive, liver, kidney, brain, heart, and reproductive systems (**Fig. 1.7**) [42].

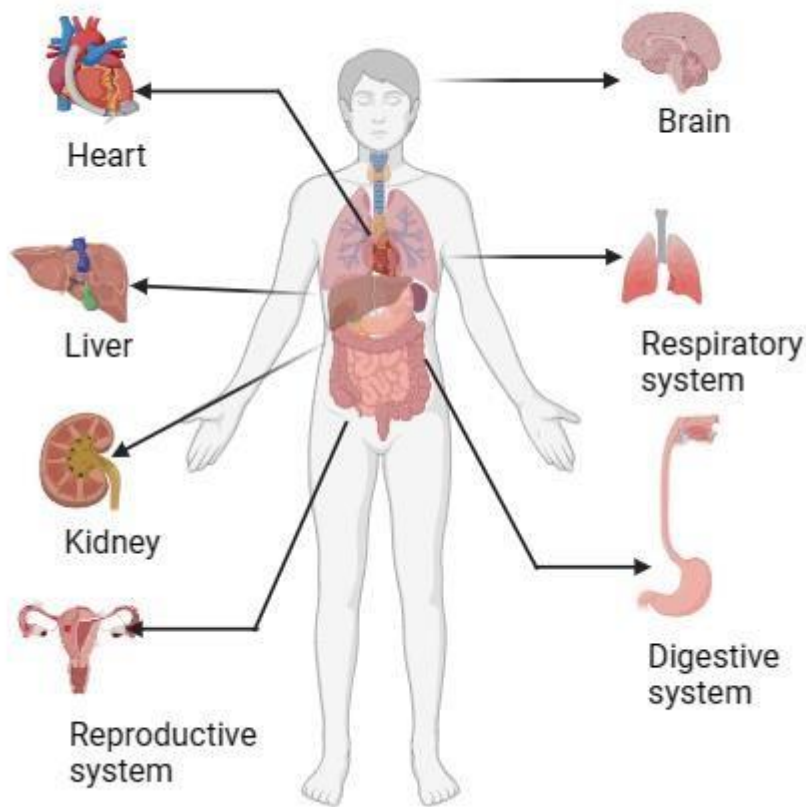


Figure 1. 7: Human organs which are affected by mercury.

Humans are exposed to mercury via different routes (if possible, name these various routes) (**Fig. 1.8**). The most common exposure route for through which humans can be exposed to mercury is oral, through the consumption of contaminated vegetables, fish, and water, among others [43,44]. Additionally, general exposure can be using contaminated cosmetics or damaged mercury-containing products [45]. Another route of mercury exposure can be occupational exposure. Under the latter, humans are exposed to mercury on the type of work they are doing such as, mining, manufacturing mercury-containing products or through waste [35,46].



Figure 1. 8: Types of human exposure to mercury [35].

1.2 Problem statement

The accurate determination of mercury remains a challenge in Analytical Chemistry. This is due to its loss mainly during sample preparation and analysis stages [47][48][49]. Furthermore, the sample preparation methods currently employed before mercury analysis are not environmentally friendly [50][51][52].

These sample preparation methods include microwave-acid digestion (MW-AD), combustion, solid phase extraction (SPE), liquid-liquid extraction (LLE), and solid phase extraction (SPE) [53][54][55]. However, there are some limitations to the mentioned sample preparation methods. MW-AD is not greener; it employs concentrated acids that generate toxic and environmentally unfriendly secondary wastes. For example, concentrated HNO_3 acid is known to produce carcinogenic nitrous oxides [56].

Furthermore, this method uses concentrated acids like hydrofluoric acid, which are reported to dissolve the glass optics of the analytical instrument [57]. In contrast, concentrated sulphuric acid and hydrochloric acid are known to cause ICP-OES spectral interferences due to the high concentration of the acids and undigested carbon [58]. Conversely, combustion is susceptible to analyte loss and cross-contamination, while SPE is known to be time-consuming due to the many steps that can lead to contamination [59].

Furthermore, the current adsorbents for SPE show poor selectivity for mercury and poor separation [60]. Lastly, LLE uses large volumes of toxic organic solvents [61]. Therefore, in this work, environmentally friendly micro-extraction sample preparation methods have been developed and applied to coal, crude oil, diesel oil, gasoline and kerosene to extract total mercury. The analysis was conducted using ICPOES.

1.3 AIMS AND OBJECTIVES

1.3.1 Aim

The primary goal of this research was to develop environmentally friendly microextraction sample preparation methods followed by inductively coupled plasma-optical emission spectroscopy to determine total mercury in fossil fuels and their derivatives which are gasoline, diesel oil and kerosene.

1.3.2 Specific objectives

The specific objectives of the proposed research project were:

- To optimize microwave-assisted hydrogen peroxide digestion using methionine as a trapping reagent, vortex-assisted deep eutectic solvent-based dispersive liquid-liquid microextraction, and ultrasound-assisted magnetic dispersive solid-phase microextraction for quantification of mercury in coal, crude oil, gasoline, diesel oil and kerosene.
- To validate microwave-assisted hydrogen peroxide digestion, vortex-assisted deep eutectic solvent based dispersive liquid-liquid microextraction and ultrasound-assisted magnetic dispersive solid-phase microextraction before mercury analysis.
- To apply the optimized and validated sample preparation methods using certified reference materials.
- To evaluate the environmental impact of each sample preparation method using AGREEprep software.
- To compare the analytical performance and environmental impact of the three sample preparation methods.

1.4 JUSTIFICATION

Sample preparation is an important stage in quantitative analysis. The primary aim of the latter is to separate and improve the analyte(s) concentration from the sample matrix [62]. Therefore, it is very vital to choose an appropriate sample preparation method before sample analysis [62]. It is also important to comply with Green Analytical Chemistry (GAC) procedures when applying sample pre-treatment protocols. It is well documented that classical sample preparation methods have a lot of shortcomings. It is reported that traditional separation methods involve the consumption of large volumes of hazardous solvents and generate waste, which is detrimental to the environment, and are not in line with the current Green Analytical Chemistry principles [62]. Therefore, this study aims to develop efficient sample preparation techniques that can reduce negative environmental impacts. Micro-extraction techniques have been posed to be a solution for many researchers as they are considered non-exhaustive and solvent-minimizing methods [63]. This study focused on various micro-extraction techniques for quantifying Hg in fuel matrices. These include microwave-assisted hydrogen peroxide digestion (MW-AHPD), ultrasound assisted magnetic dispersive solid phase extraction (UA-m-DSPME) and vortex assisted deep eutectic solvent-based dispersive liquid-liquid microextraction (VADES-LLME).

Microwave-assisted hydrogen peroxide digestion method makes use of dilute hydrogen peroxide instead of concentrated acids. The use of diluted hydrogen peroxide makes the procedure to be environmentally friendly because dilute hydrogen peroxide results in water as a product at high temperatures [64] [65]. The vortex-assisted-deep eutectic solvent-based dispersive liquid-liquid microextraction method showed several advantages, which include low vapor pressure, low flammability, cost-effective and zero loss of volatile analytes during sample preparation, less extraction time and analytes are in an aqueous form which eliminates the introduction of carbon compounds into the instruments [27]. Lastly, the ultrasound-assisted magnetic dispersive solid phase microextraction method showed several advantages such as (i) easy separation of the analyte without the use of centrifugation and filtration steps, (ii) minimum solvent used (μL), (iii) very fast compared to other SPE methods [66].

1.5 HYPOTHESIS

All the three proposed microextraction sample preparation methods (MWAHPD, VA-DES-LLME and UA-m-DSPME) followed by spectroscopic analysis are environmentally friendly and accurate for the determination total Hg in coal, crude oil, diesel oil, gasoline and kerosine samples.

1.6 RESEARCH QUESTIONS

The following research questions have been prepared to lead the proposed study through an in-depth analysis in this respect:

- What parameters can be optimized to extract mercury at lower levels in fossil fuels and their derivatives?
- Which microextraction technology is the most cost-effective, sensitive, reliable, and fast for determining Hg in fossil fuels?
- Are the analytical figures of merits (performances) of the microextraction strategies the same or better than those reported in the literature? What is the environmental impact of each sample preparation method?
- Are mercury concentration levels in South African coal, crude oil, gasoline, diesel oil and kerosene comparable with mercury concentrations in other nations?

1.7 DISSERTATION OUTLINE

There are six chapters in this dissertation, and each chapter is covered in the subsections that follow:

Chapter one: This chapter provides an overview on fossil fuels, including crude oil and coal. The origins, applications, varieties, and derivatives of various energy resources are also highlighted. Additionally, the chapter reiterates the difficulties brought on by the occurrence of mercury in crude oil, coal, and their derivatives. These issues are seen considering the harm they cause to both living things and inanimate

objects. In this chapter, the problem statement, hypothesis, rationale, aim, and objectives are all emphasized.

Chapter two: This chapter examines published research on quantifying the total concentration of mercury in non-aqueous matrices critically. Reviewing the various techniques for sample preparation to determine mercury levels is the main goal of this chapter. Wet digestion, combustion, and extraction (liquid-liquid, cloud point, and solid phase) were among the several sample preparation techniques that were documented. The chapter goes on to address the optimization techniques used to improve the processes for preparing the samples that were covered.

Chapter three: The outcomes of microwave-assisted hydrogen peroxide digestion (MW-AHPD) with dilute hydrogen peroxide application for Hg extraction and quantitative analysis are presented in this chapter. This chapter also covers the multivariate optimization stage for the five important extraction parameters (digestion temperature, duration, methionine concentration, hydrogen peroxide concentration, and sample mass). Furthermore, the instrument's working conditions for analysis (ICP-OES parameters) and digestion (microwave parameters) are covered in more detail in this chapter. Using the AGREEprep program, this chapter assesses the suggested method's greenness in the end.

Chapter four: The synthesis and characterization of the deep eutectic solvents (DESs) utilized in the vortex-assisted deep eutectic solvent-based-dispersive liquid-liquid microextraction (VA-DES-DLLME) method for mercury extraction are presented in this chapter. FT-IR, TGA, and ^{13}C NMR were the characterization techniques that were covered. More in-depth information about method optimization, validation, and application of the DES-based dispersive liquid-liquid microextraction which was assisted using a vortex (VA-DES-DLLME) is presented in this chapter. The multivariate optimization of the parameters influencing the suggested VA-DESDLLME is discussed in this section. Centrifugation time, pH, DES volume, extraction time, and dispenser solvent volume are among the optimized parameters. Following the multivariate optimization process, this chapter additionally presents and analyses the outcomes derived from the optimal parameters. The use of ICP-OES for target analyte analysis and results comparison with other literature

publications are also highlighted in this chapter. Finally, using the AGREEp prep program, the suggested method's greenness is evaluated and discussed.

Chapter five: This chapter describes the synthesis and characterization of magnetic nanoparticles used in an ultrasound-assisted magnetic dispersive solid phase microextraction (UA-m-DSPME) technique to recover mercury from fuel oils. Graphene oxide (GO), magnetic graphene oxide ($\text{Fe}_3\text{O}_4\text{-GO}$), and magnetic graphene oxide covered with gold ($\text{Fe}_3\text{O}_4\text{-GO-Au}$), were the synthesized nanocomposites. The techniques used for characterization were FT-IR, UV visible, TGA, SEM-EDS, TEM, BET, and P-XRD. The outcomes of (UA-m-DSPME) process are further discussed in this chapter. Multivariate optimization was used to investigate several factors that impacted the extraction process, including the amount of sorbent, the adsorption time, pH, eluent volume, and the desorption duration. The UA-mDSPME's results were presented and contrasted with those of other literature publications. The adsorbent was used to extract the amount of mercury in fuel samples overall. It is detailed how the suggested method's greenness is evaluated using the GREEp software.

Chapter six: This chapter presents all the study project's findings and contrasts the outcomes of the three sample preparation techniques. This chapter concludes by discussing the project's overall conclusion statements and providing recommendations for the future. It is important to note that each chapter ended with a reference list.

REFERENCES

- [1] N. Gaulin, P. Le Billon, *Climate Policy* 20 (2020) 888–901.
- [2] S.F. Lincoln, 34 (2016) 621–627.
- [3] N.R. Mashyanov, S.E. Pogarev, E.G. Panova, N. Panichev, V. Ryzhov, *Fuel* 203 (2017) 973–980.
- [4] D. Peatfield, *Journal of The South African Institute of Mining and Metallurgy* 103 (2003) 355–372.
- [5] O.C. Eneh, *Journal of Applied Sciences* 11 (2011) 2084–2091.
- [6] T. Major, (1996).
- [7] S.I. Arbuzov, I.Y. Chekryzhov, D.A. Spears, S.S. Ilenok, B.R. Soktoev, N.Y. Popov, *Ore Geol Rev* 139 (2021) 104537.
- [8] P. Mou, J. Pan, Q. Niu, Z. Wang, Y. Li, D. Song, *Energy and Fuels* 35 (2021) 7467–7484.
- [9] W.H. Orem, R.B. Finkelman, *Coal Formation and Geochemistry*, 2003.
- [10] S. Zhao, D. Pudasainee, Y. Duan, R. Gupta, M. Liu, J. Lu, *Prog Energy Combust Sci* 73 (2019) 26–64.
- [11] X. Zhao, F. Guo, Y. Zhang, J. Wu, *Colloids Surf A Physicochem Eng Asp* 625 (2021) 126935.
- [12] G. Liu, S. V. Vassilev, L. Gao, L. Zheng, Z. Peng, *Energy Convers Manag* 46 (2005) 2001–2009.
- [13] M. Teichmüller, *Int J Coal Geol* 12 (1989) 1–87.
- [14] P. Xu, B. Zhang, X. Zeng, Y. Xu, G. Luo, H. Yao, *Int J Coal Geol* 170 (2017) 14–18.
- [15] L. Li, D. Liu, Y. Cai, Y. Wang, Q. Jia, *Energy and Fuels* 35 (2021) 86–110.
- [16] H. Mahmoudi, M. Mahmoudi, O. Doustdar, H. Jahangiri, A. Tsolakis, S. Gu, M. LechWyszynski, *Biofuels Engineering* 2 (2018) 11–31.

- [17] A. De Klerk, I. Technology, (2008).
- [18] B.H. Bowen, M.W. Irwin, D. Canchi, (2007).
- [19] E. Mansoor-ul-hassan, 1 (2014) 43–61.
- [20] C. Chandia, M. Salamanca, A. Hernández, R. Urrutia, Mar Pollut Bull 178 (2022).
- [21] G.N. Balaji, N.V.H. Suriya, S. AnandVikash, R. Arun, S.A. Kumar, Imperial Journal of Interdisciplinary Research (IJIR) Vol 3 (2017) 664–669.
- [22] N.A.S. Khairi, N.A. Yusof, A.H. Abdullah, F. Mohammad, Int J Mol Sci 16 (2015) 10562–10577.
- [23] C. Duyck, N. Miekeley, C.L. Porto da Silveira, R.Q. Aucélio, R.C. Campos, P. Grinberg, G.P. Brandão, Spectrochim Acta Part B At Spectrosc 62 (2007) 939– 951.
- [24] A. De Jesus, R.E. Sturgeon, J. Liu, M.M. Silva, Microchemical Journal 117 (2014) 100–105.
- [25] P.D.O. Vicentino, D.M. Brum, R.J. Cassella, Talanta 132 (2015) 733–738.
- [26] L.M. Wu, C.H. Zhou, J. Keeling, D.S. Tong, W.H. Yu, Earth Sci Rev 115 (2012) 373–386.
- [27] N.S. Mdluli, P.N. Nomngongo, N. Mketi, Crit Rev Anal Chem 0 (2020) 1–18.
- [28] S.F. Wong, J.S. Lim, S.S. Dol, J Pet Sci Eng 135 (2015) 498–504.
- [29] C.F. Mabery, O.R. Palm, O.J. Sieplein, Proceedings of the American Academy of Arts and Sciences 40 (1904) 323.
- [30] A.K.T. Mohammad, A.T. Hameed, M.A. Alhamdany, K. Mohammad Al Azzam, G.A.A. Talk, Biomedical Chromatography 33 (2019) 1–23.
- [31] S.M. Wilhelm, L. Liang, D. Kirchgessner, Energy and Fuels 20 (2006) 180–186.
- [32] A. Al Ashraf, A. Al Aftab, (2012) 2–3.
- [33] G. Alfke, W.W. Irion, O.S. Neuwirth, Ullmann's Encyclopedia of Industrial Chemistry (2007).
- [34] P. De O Vicentino, D.M. Brum, R.J. Cassella, Talanta 132 (2015) 733–738.

- [35] K.G. Pavithra, P. SundarRajan, P.S. Kumar, G. Rangasamy, *Chemosphere* 312 (2023) 137314.
- [36] N. Khan, K. Su Kim, N. Khan, N. Jamila, J. Choi, E. Nho, I. Hwang, K. Kim, *World Appl Sci J* 34 (2016) 743–749.
- [37] G.P. Brandão, R.C. De Campos, A.S. Luna, *Spectrochim Acta Part B At Spectrosc* 60 (2005) 625–631.
- [38] A.R. Tu, 40 (2012) 523–530.
- [39] M. V Reboucas, G. Pereira, V.A. Lemos, L.S.G. Teixeira, (2006) 1327–1330.
- [40] Y. Gao, Z. Shi, Z. Long, P. Wu, C. Zheng, X. Hou, *Microchemical Journal* 103 (2012) 1–14.
- [41] S. Balshaw, J. Edwards, B. Daughtry, K. Ross, *Rev Environ Health* 22 (2007) 91–113.
- [42] S.T. Zulaikhah, J. Wahyuwibowo, A.A. Pratama, *Int J Publ Health Sci* 9 (2020) 103–114.
- [43] A. Miklavčič, A. Casetta, J. Snoj Tratnik, D. Mazej, M. Krsnik, M. Mariuz, K. Sofianou, Z. Špirić, F. Barbone, M. Horvat, *Environ Res* 120 (2013) 7–17.
- [44] N.E. Selin, E.M. Sunderland, C.D. Knightes, R.P. Mason, *Environ Health Perspect* 118 (2010) 137–143.
- [45] C.R.H. Ba, W. Boonchai, L. Wen, E. Nishijima, S. Dds, C. Chu, K. Hamann, C.P. Hamann, K. Sinniah, D.H. Ba, *Journal of American Dermatology* 70 (2013) 281287.e3.
- [46] S. Queipo Abad, P. Rodríguez-González, J.I. García Alonso, *Journal of Trace Elements in Medicine and Biology* 36 (2016) 16–21.
- [47] K.B.S. Perelonia, K.C.D. Benitez, R.J.S. Banicod, G.C. Tadifa, F.D. Cambia, U.M. Montojo, *Food Control* 130 (2021) 108363.
- [48] D.L.F. da Silva, M.A.P. da Costa, L.O.B. Silva, W.N.L. dos Santos, *Food Chem* 273 (2019) 24–30.

- [49] J.P. Souza, C. Cerveira, T.M. Miceli, D.P. Moraes, M.F. Mesko, J.S.F. Pereira, *Food Chem* 321 (2020) 126715.
- [50] H.B. Ulusoy, R. Gürkan, S. Ulusoy, *Talanta* 88 (2012) 516–523.
- [51] C. Mitani, A. Kotzamanidou, A.N. Anthemidis, (2014) 1491–1498.
- [52] M. Arjomandi, *Hamid Shirkhanloo, *Analytical Methods in Environmental Chemistry Journal* (2019) 97–126.
- [53] P.A. Mello, J.S.F. Pereira, M.F. Mesko, J.S. Barin, E.M.M. Flores, *Anal Chim Acta* 746 (2012) 15–36.
- [54] P.O. Vicentino, R.J. Cassella, *Talanta* 162 (2017) 249–255.
- [55] S.B. Adeloju, *Analyst* 114 (1989) 455–461.
- [56] D.G. Da Silva, L.A. Portugal, A.M. Serra, S.L.C. Ferreira, V. Cerdà, *Food Chem* 137 (2013) 159–163.
- [57] E.I. Muller, J.P. Souza, C.C. Muller, A.L.H. Muller, P.A. Mello, C.A. Bizzi, *Talanta* 156–157 (2016) 232–238.
- [58] N. Mketto, P.N. Nomngongo, J.C. Ngila, *RSC Adv* 5 (2015) 38931–38938.
- [59] L.S.F. Pereira, G.D. Iop, E.M.M. Flores, R.A. Burrow, P.A. Mello, F.A. Duarte, *Fuel* 163 (2016) 175–179.
- [60] N. Panichev, M.M. Kalumba, K.L. Mandiwana, *Anal Chim Acta* 813 (2014) 56–62.
- [61] Y.A. Abbasi, S. Shahida, A. Ali, M.H. Khan, *J Radioanal Nucl Chem* (2019).
- [62] M. Rutkowska, J. Płotka-Wasyłka, M. Sajid, V. Andruch, *Microchemical Journal* 149 (2019).
- [63] E.M. Martinis, P. Berton, R.G. Wuilloud, *TrAC - Trends in Analytical Chemistry* 60 (2014) 54–70.
- [64] N. Mketto, P.N. Nomngongo, J.C. Ngila, *Microchemical Journal* 124 (2016) 201–208.

- [65] G. Xin, X. Jia, C. Zheng, *Energy Sources, Part A: Recovery, Utilization and Environmental Effects* 34 (2012) 1516–1522.
- [66] J. Chen, Y. Wang, X. Wei, P. Xu, W. Xu, R. Ni, J. Meng, *Talanta* 188 (2018) 454–462.

CHAPTER II: LITERATURE REVIEW

PREAMBLE

This chapter begins by providing some background information on mercury, its presence in the environment, and its detrimental impacts on the ecosystem. Furthermore, this chapter evaluates and critically examines sample preparation techniques and optimization strategies for mercury extraction from non-aqueous matrices that have been reported in literature. Each strategy's advantages and disadvantages are also covered. The chapter goes into further detail on the characterization techniques that are utilized for the characterization of synthesized adsorbent materials that are used for the preconcentration of mercury in non-aqueous matrices. Furthermore, it details the spectrometric methods used in quantitative measurements of mercury. Finally, an analysis of the optimal strategy, analytical methodologies, and sample preparation methods that performed best in quantifying total mercury was conducted.

2.1 Background information

Mercury (Hg), also known as “quicksilver”, is a trace element that is found in the environment since the beginning of time. It is established that this metal is bio-toxic, volatile, persistent, and accumulates in organs and living things (humans and plants) [1]. This chemical element exists as a liquid at standard temperatures and pressures. It is usually found in ores such as cinnabar (mercuric sulfide), cordierite (mercuric sulfide chloride), and Livingstone (mercury antimony sulfosalt) [2]. Mercury is released into the environment through both anthropogenic and natural processes. Elemental, inorganic, and organic forms are the three forms in which the element exists in. Each form has distinct characteristics, toxicity, health risks, and precautions to avoid exposure [3]. Organic Hg compounds are considered the most poisonous species which can result in lung cancer, risks of brain cancer, and kidney cancer among others [4].

2.1.1 Physical and chemical properties of mercury

Mercury has unique physical properties, and they are summarized in **Table 2.1**. It can be highlighted that mercury has high density and surface tension, it is soluble with some metals like gold and silver giving amalgams. Furthermore, this element is soluble in water, has high specific gravity and it is a poor conductor of heat, but it contracts and expands evenly when the temperatures change[5].

Table 2.1: Physical properties of mercury[6].

Physical property	Quantity
Atomic number	80
Relative abundance	5×10^{-5}
Boiling point	357 °C
Density	13,546 g/cm ³ at 20 °C
Viscosity	1.685 at 0 °C
Heat capacity	0.0332 cal/g at 20 °C
Melting point	-38.87 °C
Surface tension (in air)	436 dyne/cm at 20 °C
Electrical conductivity	1.063×10^{-4} at 0 °C, mΩ ⁻¹ mm ⁻²
Thermal conductivity	1.063×10^{-4} at 0 °C, mΩ ⁻¹ mm ⁻²
Thermal expansion coefficient	1.86×10^{-4} at 0-100 °C
Crystal structure	Rhombohedral

The chemical properties of mercury are also unique. Mercury dissolves in concentrated sulfuric acid and nitric acid to give sulfate and nitrate salts. It also reacts with other metals except for iron, zinc, copper, manganese, and platinum to form amalgams and it can corrode aluminum [6].

2.1.2 Species of mercury

Mercury exists in three valence states (0, I and II) and is mostly found in three different forms. Each of these different forms have their unique properties, toxicity, implications for health and measures to prevent exposure. The three forms of mercury are, elemental mercury (Hg^0 , metallic mercuric and mercury vapor), inorganic mercury (Hg^+ and Hg^{2+}) and organic mercury (methyl and ethyl mercury)[7].

Elemental mercury has a peculiar behavior in that it exists as a monoatomic in the vapor phase and has a relatively high vapor pressure at 20 °C. It is known as a volatile species at room temperature and pressure. This species of mercury has a wide range of applications. It is used in chlorine-alkali manufacture, dental amalgams, electronic switches, and fluorescent lamps[8]. When Hg^0 is oxidized in the air, it forms inorganic mercury (Hg^+ and Hg^{2+}). Inorganic mercury is used in a range of medical and cosmetic products such as antiseptics, teething powders, and skin lightening creams. Inorganic compounds can either be mercury in monovalent (mercurous- Hg^+) or divalent (mercuric- Hg^{2+}). Lastly, the other form of mercury is organic mercury. The organic mercury compounds are mainly alkyl mercury and phenyl mercury. The phenyl mercury compounds are used in preservatives in medicine. The alkyl mercury compounds are mostly found in the environment [8].

2.1.3 Occurrence of mercury in non-aqueous matrices

All environmental media contain trace levels of this persistent contaminant. This comprises, among other things, food matrices, crude oil, diesel oil, gasoline, kerosene, biodiesel coal, sediments, plants, rice, soil, animal tissues, and rocks. In soil and sediments, mercury can be found as inorganic and organic-mercurial salts [9]. In coal, it exists naturally and is locked as mercury sulfide or organic mercury but released as gaseous mercury when coal is burnt above 90 °C [10]. Food matrices such as rice, cereals, fish, shellfish, and plant foods also contain this contaminant in trace amounts. Industrial discharge and atmospheric depositions are the main ways aquatic organisms are exposed to mercury. The use of tainted phosphate fertilizers in farming practices and stomatal respiration are two further ways that plant foods might absorb mercury [11] [12].

Additionally, oily matrices such as crude oil, gasoline, diesel oil, kerosene and edible oils have been reported to contain mercury. People regularly eat foods that are contaminated with Hg, such as edible oils. The food's flavor and texture can be enhanced by the presence of this trace element. Additionally, the consumption of these contaminated food products provides nutrition and energy to the human body [13][14]. These oils are found in plants like sunflower, rapeseed, and olives as well as in animals like fish. However, Hg contamination of food oils can be because of air, water, and soil pollution [14]. Mercury is added to biodiesel similarly to edible oils since it is an unpredictable element that occurs naturally in plants. Fuel called biodiesel is synthesized by chemically combining an alcohol such as methanol with vegetable or animal fat. Its primary usage is as a diesel engine substitute fuel [15]. Finally, mercury is naturally occurring in fossil fuels like crude oil [16]. Utilizing fractional distillation, the latter is separated to yield a range of hydrocarbons and serves as a source of energy. During refining, shipping, and storage, mercury can also contaminate the generated fractions of crude oil [17].

Most scholars have recently expressed interest in determining the amount of mercury in various non-aqueous matrices. This is due to the detrimental effects of large concentrations of these elements on plants, animals, and human tissues. The primary obstacle in quantifying mercury from these matrices is that most analytical instruments cannot quantify the samples directly. Hence sample preparation methods are required before instrumental analysis. The recent developments and paradigm changes in sample preparation techniques for the complete quantification of mercury in complex matrices will be thoroughly examined in this review. As a result, this will assist in identifying the gaps in sample preparation techniques for complex matrices and consequently offer appropriate suggestions for upcoming cleanup tactics.

2.2 Sample preparation methods for total determination of Hg in nonaqueous matrices

In chemical analysis total determination refers to quantifying the total amount of an analyte in a sample. Four main processes are taken in elemental research and other analytical studies. This covers sampling, sample preparation, and data interpretation. When quantifying mercury, the first three processes provide significant

challenges. This is due to the volatile nature and high memory effects of mercury during analysis. However, sample preparation is the most crucial and challenging step as it prepares the samples to be compatible with most analytical techniques. Sample preparation also preconcentrates the target analyte(s) if present in trace level concentration, improving the analytical techniques' detection limits. The sample preparation techniques include extraction (liquid-liquid extraction and solid phase extraction), thermal (combustion), or wet digestion employing concentrated acids.

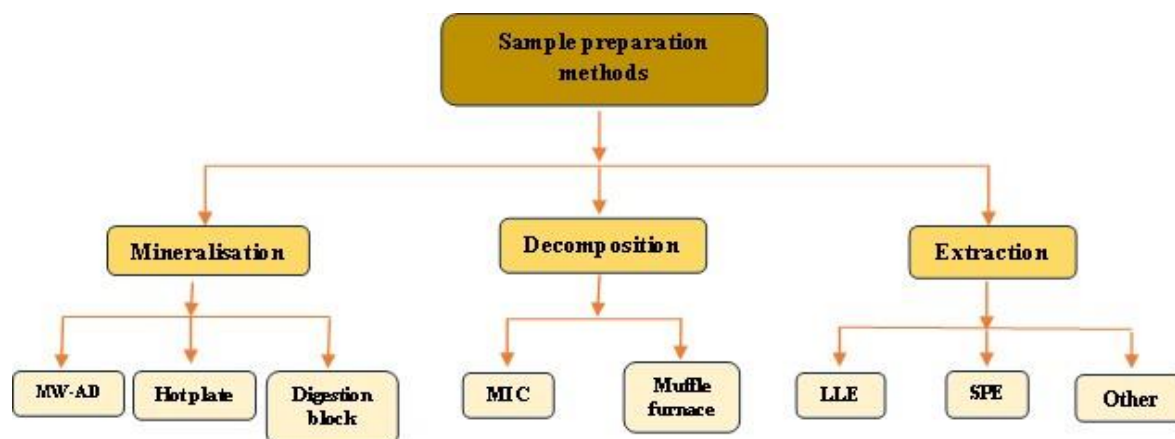


Figure 2. 1: Different sample preparation methods for the spectrometric determination of total mercury in non-aqueous matrices.

2.2.1 *Mineralization sample preparation methods*

The process of mineralization, also referred to as wet digestion, basically uses concentrated mineral acids' oxidizing and dehydrating qualities to break down sample matrices [18]. Sample matrices are mineralized in this process to produce aqueous solutions that work with analytical equipment. Strong oxidizing substances, either alone or in mixtures, including H_2O_2 , and mineral acids, such as HNO_3 , HF , HCl , and H_2SO_4 , are typically included in the digesting mixtures. It is commonly known that HNO_3 , out of all the oxidants used in wet digestion, is the most desired since it can be manufactured in high purity and may be used to oxidize nearly all organic molecules. The breakdown of silica-containing organic matrix, such as coal, is primarily accomplished by HF [19]. However, several of these oxidizing agents have some disadvantages, including spectrum interferences (HCl , $HClO_4$, and HF) during ICP-MS analysis, safety concerns (HF and $HClO_4$), detrimental effects on the spectrometric instruments' glass optics (HF and H_2SO_4), matrix effects (H_2SO_4 and H_3BO_3), and

other issues. Mineralization can occur in closed containers, such as microwave radiation or open vessels, such as hot plates and heating blocks (Fig. 2.2).

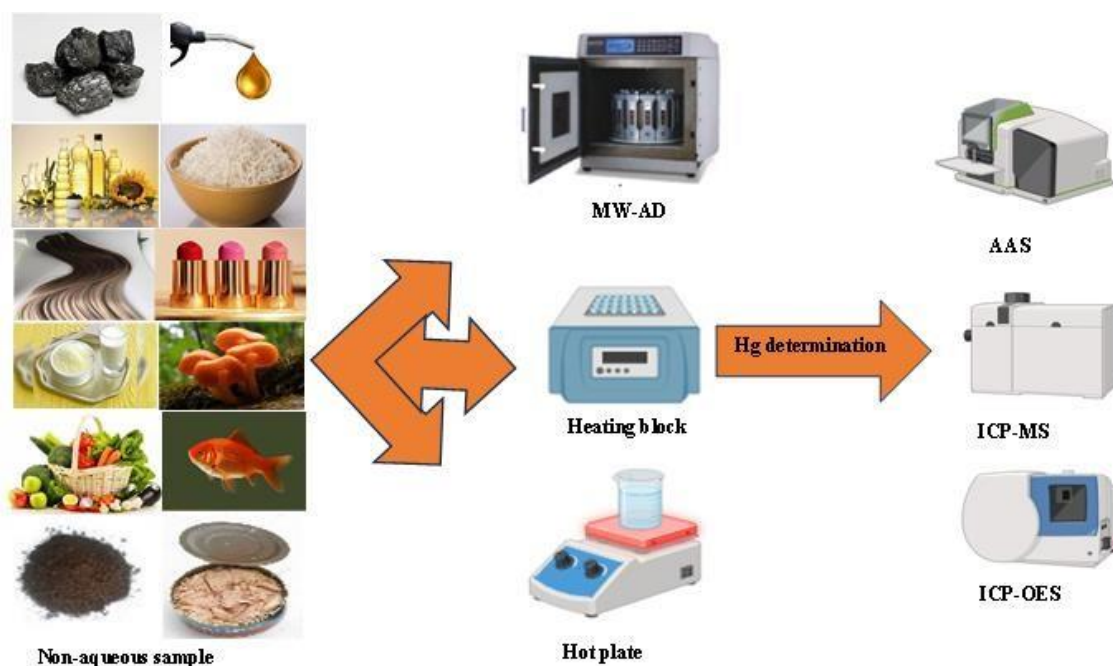


Figure 2. 2: Various techniques for the preparation of mineralization samples before spectrometric measurement of total mercury in non-aqueous matrices.

2.2.1.1 Microwave-assisted digestion (MW-AD)

Microwave-assisted digestion is the mostly utilized method under mineralization [20]. Molecules are moved by microwave energy by ion migration and dipole rotation. The efficient heating of materials using microwave dielectric heating effects is the foundation of microwave assisted processes. The ability of a material (such as a solvent or reagent) to absorb microwave radiation and convert it into heat determines the efficiency level. This method reduces the amount of acid needed, digestion time, cross-contamination, and loss of volatile species [21].

In contrast, these methods effectively decompose the organic matrix by using concentrated acids. It is commonly known that as the organic material is being destructively oxidized, concentrated acids such as HNO_3 release large amounts of carcinogenic nitrous gases. It was therefore advised to use diluted acids to address the issues that concentrated acids brought about. The former may lead to a large residual carbon content and poor recoveries due to partial breakdown of the organic

material. Furthermore, using ICP-based analytical techniques might cause both spectral and non-spectral interferences due to excessive residual carbon. The physical properties of the solution can be altered by the microwave digests' high acid percentage and residual carbon content. It can also alter the target analyte's transit to plasma and aerosol generation. This may result in a reduction in the emission (ICP-OES) or m/z (ICP-MS) signal, raising the background and detection limit. Therefore, it is strongly advised to utilize diluted hydrogen peroxide in this situation [22]. **Table 2.1** summarizes and delves into the discussion of all the work presented under MW-AD for the complete determination of mercury in non-aqueous matrices.

2.2.1.2 Heating block assisted digestion

Open vessel digesting techniques also make use of heating blocks. The former uses heater technology and is microprocessor-controlled. It's employed for heating samples in vials, flasks, and tubes. It's the perfect tool for reliable findings and exact temperature stability [23].

In 2013, Park and coworkers [24] developed a method for determining total mercury using heat block-assisted digestion. Common laboratory acids (HCl, HNO₃, H₂SO₄ and aqua regia) were used as oxidizing agents. Precision ranging from 1.71 – 6.55 % for soil and 0.97-12.11 % for coal, and recoveries ranging from 91.11 to 102.28 %, were archived. Another study on the use of a heating block was reported by Oreste and coworkers [25]. Their focus was on determining total mercury in biological samples using CV AAS. In their procedure, samples were digested with HNO₃ for 2 h in a heating block digester. The limit of detection (LOD) was 0.08 µg/L.

2.2.1.3 Hot plate assisted digestion

In open-vessel acid digestion processes, hot plates are used. In essence, an acid attack occurs in heated, exposed containers, like beakers or screw-top vials, during open vessel digestion. This technique is very useful for routine analysis since it can be used to control various digestion parameters like temperature, time, and the addition of reagents. However, the boiling point of the appropriate acid or acid mixture at ambient pressure sets a restriction on the maximum digestion temperatures. Open vessel digestion also has the drawback of possibly losing trace elements and needing

a lot of chemicals, which increases the possibility of contamination from laboratory air. Open vessel acid digestion has therefore not been thought of as a cutting-edge technique for producing trace and ultra-trace samples [23].

The data in **Table 2.1** provides an overview of the various mineralization techniques used to determine the total amount of mercury in non-aqueous matrices. According to this data, the most popular method under mineralization is microwave-assisted digestion.

Table 2. 1: Different wet digestion methods applied to non-aqueous matrices before quantification of Hg.

Matrix	Sample preparation	Reagent	Mass (g)	Temperature (°C)	Time (min)	Analytical technique	LOD (µg/kg)	R ²	Accuracy (%)	RSD (%)	Ref.
Plankton	MW-AD	HNO ₃	0.2	85	720	CV-AFS	0.0049		86.4-97.2	3.7-8.1	[26]
Fish	MW-AD	HNO ₃ /H ₂ O ₂ /HClO ₄	0.3	210	15	CV-AFS	0.118	0.9955	90.1-105.8	<3.0	[27]
Fish	MW-AD	HNO ₃ /H ₂ O ₂	N/R	190	10	CV-AAS	15	0.99	N/R	N/R	[28]
Fishery products	MW-AD	HNO ₃ /HCl/H ₂ O ₂	1	N/R	N/R	CV-AAS	20	N/R	N/R	N/R	[29]
Swordfish	MW-AD	HNO ₃ /H ₂ O ₂	0.75	190	10	CV-AAS	15	0.99	N/R	N/R	[30]
Canned fish	MW-AD	HNO ₃ /H ₂ O ₂	0.2	180	30	ICP-MS	2	0.9994	95.6	12.1	[31]
Fish	MW-AD	HNO ₃	1	200	10	AAS	N/R	N/R	101	N/R	[32]
Fish	MW-AD	HNO ₃ /HCl/H ₂ SO ₄	0.2	N/R	15	CV-AAS	8	0.9813	91	9	[33]
Fish	MW-AD	HNO ₃	0.4	180	15	ICP-MS	0.006	N/R	92	<10	[34]

Fish	MW-AD	HNO ₃ /H ₂ O 2/HCl	0.5	N/R	31	CV-AAS	0.3	N/R	95	<10	[35]
Fish	MW-AD	HNO ₃ /H ₂ O 2/HCl	0.1	180	30	ICP-MS	0.006	N/R	95.4	N/R	[36]
Fish tissues	MW-AD	HNO ₃	0.4	180	15	ICP-MS	0.006	N/A	92-98	10	[37]
Fish muscle	MW-AD	HNO ₃ /H ₂ O 2	0.2	N/R	N/R	CV-AAS	N/R	0.867	102.3	N/R	[38]
Fish	MW-AD	HNO ₃ /H ₂ O 2	0.5	185	14.5	ICP-MS	0.4	N/R	89-110	<15	[39]
Bauxite	MW-AD	HCl/HNO ₃	0.5	150	1440	FI-CV- AAS	0.023	0.999	95-111	1.5	[40]
Seafood	MW-AD	HNO ₃ /H ₂ O 2	0.9	180	40	ICP-OES	1.3	N/R	N/R	9	[41]
Medicinal plants	MW-AD	HNO ₃	1	165	30	ICP-MS	50	0.9995	N/R	8.32	[42]
Milk powder	MW-AD	HNO ₃	N/R	190	8.47	HG-AAS	0.2	0.998	92-108	<6.5	[43]
Meat	MW-AD	HNO ₃ /H ₂ O 2	0.2	90	20	ICP-MS	3	N/R	96-102	<10	[44]

Edible and non-edible tissues	MW-AD	HNO ₃ /H ₂ O ₂	0.5	200	20	CV-AAS	N/R	N/R	82.75-90.20	N/R	[45]
Plant tissue	MW-AD	HNO ₃	0.4	N/R	N/R	ICP-OES	N/R	0.999	90-99	N/R	[46]
Seafood	MW-AD	HNO ₃ /H ₂ O ₂ /HCl	0.2	180	15	ICP-MS	0.72	0.9991	97-103	3.5	[47]
Hair	MW-AD	HNO ₃	0.1	50	10	GF-AAS	0.1	0.995	90-110	N/R	[48]
Food	MW-AD	HNO ₃ /H ₂ O ₂	1	200	15	CV-AAS	0.050	0.9998	97.5	0.7-9.0	[49]
Dietary supplements	MW-AD	HNO ₃ /HCl	0.5	110	15	ICP-OES	1.0	0.999	92.12-102.08	10	[50]
Rice	MW-AD	HNO ₃	0.2	180	10	CV-AAS	0.95	N/R	N/R	1.98	[51]
Muscle tissue	MW-AD	HNO ₃	1	200	10	CV-AAS	7.0	0.9688	98.9	N/R	[52]
Leather and fur	MW-AD	HNO ₃ /H ₂ O ₂	0.2	220	20	ICP-AES	N/R	N/R	98.1-102.6	0.7-3.0	[53]
Yellowfin tuna	MW-AD	HNO ₃	N/R	200	10	CV-AAS	70	N/R	N/R	<10	[54]

Seafood	MW-AD	HNO ₃ /H ₂ O	1	190	20	ICP-MS	2	0.999	89.7	5.1	[55]
			2								
Muscle tissue	MW-AD	H ₂ O ₂ /HCl	0.25	N/R	N/R	ICP-MS	0.002	N/R	N/R	0.8	[56]
Hair	MW-AD	HNO ₃ /H ₂ O	0.2	25	10	CV-AAS	0.133	0,999	99.2-95.5	<10	[57]
			2								
Mushroom	MW-AD	HNO ₃	1	160	10	CV-AAS	9	N/R	N/R	N/R	[58]
Food	MW-AD	HNO ₃ /H ₂ O	1	190	15	ICP-MS	N/R	N/R	70-120	N/R	[59]
			2								
Feathers	MW-AD	HNO ₃ /H ₂ O	0.1	100	1440	CV-AAS	N/R	0.9996	88.6-99.2	<15	[60]
			2								
Vegetables	MW-AD	HNO ₃ /HF	1	95	30	ICP-MS	N/R	N/R	130	N/R	[61]
Food	MW-AD	HNO ₃ /H ₂ O	0.25	NR	N/R	ICP-OES	9	N/R	N/R	N/R	[62]
			2								
Coal	MW-AD	HNO ₃ /HF	0.05	240	60	ICP-MS	1.220	0.9999	95.7-106.28	0.34	[63]
Particulate matter	MW-AD	HNO ₃	N/R	180	10	GFAAS	1	N/R	N/R	N/R	[64]

Seaweeds	HB-AD	HNO ₃	0.5	95	120	CV-AFS	0.6	0.9999	95.6	4.2	[65]
Crude oil	HB-AD	HNO ₃	0.5	140	120	CV-AAS	8.6	0.9999	75-123	10	[66]
Fish tissue	HB-AD	HNO ₃	0.5	25	120	C-VAAS	NR	NR	91-97	NR	[67]
Soil and coal	HB-AD	HCl, HNO ₃ , H ₂ SO ₄ and aqua regia	N/R	30 and 90	120 and 70	CV-AAS	0.08	N/R	42.39-162.71	1.71-6.55 and 0.97-12.11	[24]
Biological samples	HB-AD	HNO ₃	N/R	120	90 and 120	CV-AAS	14	0.9998	N/R	5.3	[25]
Rice	HP-AD	HNO ₃ /HCl O ₄ /H ₂ SO ₄	0.1	230	30	CV-AAS	0.1	0.9994	80-118	N/R	[68]

Note: [N/R]- Not reported, [MW-AD]- Microwave-assisted acid digestion, [CV-AAS]- Cold vapor atomic absorption spectroscopy, [ICP-MS]Inductively coupled plasma mass spectrometry, [ICP-OES]- Inductively coupled plasma optical emission spectroscopy, [CV-AFS]- Cold vapor atomic fluorescence spectroscopy, [GFAAS]- Graphite furnace atomic absorption spectroscopy, [FI CV-AAS]- Flow injection cold vapor atomic absorption spectroscopy, [HG-AAS]- Hydride generation atomic absorption spectroscopy.

Hot plate-assisted digestion is the least popular technique for sample preparation at the same time. Fossil fuels are the least reported matrix, whereas fish samples are the most investigated matrix. Nitric acid appears to be the most popular oxidizing agent. This is because the acid works well with most analytical tools [27]. The reported mass of the sample varied from 0.1 g to 1 g. This sample preparation procedure used a temperature range of 20 to 230 °C and a time range of 10 to 1440 minutes. The analytical method most frequently used to determine the total amount of mercury in non-aqueous matrices was cold vapor atomic absorption.

Santos and coworkers [26] used a simple digesting process using CV AFS to measure the amount of mercury in plankton. Their optimum conditions were 85 °C for temperature, 3 mL w/w 65 % HNO₃ or 3 mL 50 % v/v HNO₃, and 12 h digestion time. Their precision ranged between 3.7 % to 8.1 %, and the recoveries were between 86.4 and 97.2 %. Yáñez-Jácome and coworkers [27] published a report on another fascinating investigation in 2020. by determining the total mercury in fish after an MW-mL HClO₄, an irradiation temperature of 210 °C, and 35 min of mineralization time resulted in accurate performance. The accuracy of their method ranged from 90.1 to 105.8 %, w AD followed by CV-AFS. Small volumes of reagents such as 1 mL HNO₃, 1 mL H₂O₂, and 1 mL with a precision ranging from 1.5 to 4.2 %. The MW-AD protocol was also reported in 2018 by Esposito and coworkers [28] to determine the total mercury in Swordfish. A mixture of HNO₃/H₂O₂ was used as an oxidizing agent and samples were digested under pressure for 10 minutes at 190. From the table, a lot of MW-AD work has been reported for mineralizing fish and fish-related samples from 2013 to 2023. It is worth noting that other samples such as hair, mushrooms, crude oil, Bauxite, plants, seaweed, herbs, feathers, particulate matter, canned vegetables, rice, and muscle tissue were also investigated under MW-AD.

A few studies have also been published on heating block-assisted digestion. For example, in 2015, A Karim and coworkers [65] reported the determination of mercury in seaweeds by CV-AFS. Their primary objective was to compare four methods for acid digestion of seaweed. All digestions were conducted using nitric acid. Recoveries of 95.6 % with a precision of 4.2 % were obtained. Pontes and coworkers [66] conducted

a study for the determination of total mercury in crude oil and related products. Recoveries obtained ranged from 75-123 %, and precision ≤ 14 was obtained. In 2017, E. Mohammed and coworkers [78] optimized an acid digestion procedure. The samples were digested at 25 °C for 120 minutes, nitric acid was also used as a digestion solvent. Recoveries ranging from 91 to 97 % were obtained. In 2013 C. Park and coworkers [67] reported a simple and accessible analytical method for determining mercury in soil and coal. Among all common laboratory acids, aqua regia was most effective for soil CRM, while coal HNO₃ was more effective. In this procedure, samples were treated with HNO₃ for two hours in a digester block at a temperature between 90 and 120 °C [26].

As mentioned, hot plate-assisted digestion procedures are the least reported mineralization protocols. This might be due to the method's limitations, the high risks of cross-contamination, and the loss of volatile species. As it is known, mercury is highly volatile; hence, many scholars do not utilize this procedure for the total determination of mercury [68].

2.2.2 Combustion sample preparation methods

Combustion is the process of thermally decomposing organic substances into simple organic matter. This exothermic reaction gives CO₂ and H₂O as the main product [18]. The reaction may be described as illustrated below for compounds containing only carbon, hydrogen, and oxygen (**Eq. 2.1**).



These processes consist of microwave-induced combustion (MIC) and ashing, both wet and dry (**Fig. 2.3**). Analytes that are not volatile after burning are typically present, and combustion products can be dissolved in an appropriate solution before analysis [19].

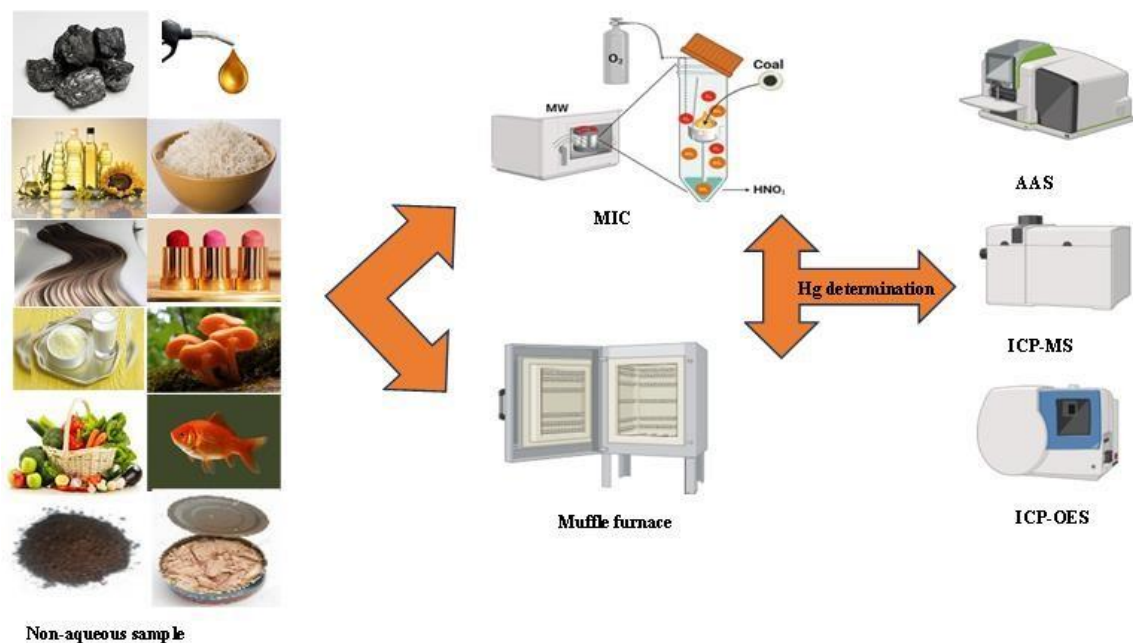


Figure 2. 3: Combustion techniques commonly applied in sample preparation and quantification of total mercury in non-aqueous matrices, determined spectroscopically.

2.2.2.1. Microwave-induced combustion

In this system, researchers combined the advantages of microwave-assisted wet digestion and traditional combustion. The general protocol for MIC digestion is to prepare the material into pellets of up to 0.5 g and place them on a filter paper disk. After that, the disk is placed into a quartz vessel holder with an absorbing solution. Usually, an ammonium nitrate solution is applied to the filter paper disc to ignite it. The vessel holder is then sealed and under oxygen pressure (up to 25 atm). Applying microwave radiation triggers the start of combustion. Refluxing stages can be added to aid in the target analyte's complete recovery. Dilute acids are used to absorb metals and metalloids [15]. Low detection limits are attainable for most necessities due to the sample mass. Due to the closed vessel used in this technique and the ability to digest organic matrices that are challenging to dissolve, there is little chance of sample contamination. Nevertheless, several drawbacks have been reported, such as a 250

mg sample size limitation, the need for pricey oxygen quartz jars, and a high concentration of chlorine [12].

Abdul Karim Talaq Mohammad and coworkers [84] reported using ICP-OES to determine the mercury content of crude oil following digestion through microwave-induced combustion. Mercury concentrations were found to be 0.4169 µg/g and 1.504 µg/g, respectively. The precision of the reported method was 2 %.

2.2.2.1. Muffle furnace-assisted ashing

The primary use of a muffle furnace is for dry or wet ashing. The external thermal energy is continuously provided by the comparatively basic structure of a traditional muffle furnace by the release of Joule heat, which occurs when an electric current passes through a conductor. Nichrome and alchrome are two common examples of high-temperature alloys, with maximum heating temperatures of 1100 and 1250 °C, respectively. Molybdenum disilicide and silicon carbide are two common silicon compounds that have maximal heating temperatures of 1300 and 1800 °C, respectively. High-temperature alloys are less brittle than silicon compounds, but they can corrode more easily, especially in gasses that contain sulfur [68].

For dry ashing a sample between 0.1 and 1 g is weighed in a crucible without any oxidizing agent added and then put inside the muffle furnace. The sample is heated to high temperatures usually between 450 and 550 °C within the muffle furnace. An acid such as nitric acid is added to the heated ash to dissolve the analytes; the dissolved material is then diluted with water for analysis. In wet ashing, like in dry ashing, the sample is heated in a muffle furnace and then acid is added until it dries.

Challenges associated with both dry and wet ashing sample preparation techniques include sample heating, airborne contamination, loss of volatile components from open systems, and longer preparation times. It can take up to twelve hours to heat a muffle furnace [68][69][70]. **Table 2.2** summarizes combustion sample preparation methods for quantitatively determining total mercury in non-aqueous matrices.

Table 2. 2: Determination of Mercury from different matrices using combustion method.

Matrix	Sample preparation method	Analytical technique	Absorbing solution	Mass (g)	Temperature (°C)	Time (min)	RSD (%)	Accuracy (%)	LOD (µg/kg)	Ref.
Cereals	MIC	AAS	HNO ₃	0.7	N/R	5	N/R	92-100	21	[71]
Soil	MIC	CV-AAS	HNO ₃	0.3	N/R	25	N/R	N/R	9	[72]
Coal (NIST 1632c and BCR 40)	MIC	ICP-OES/CV-AAS	HNO ₃	N/R	N/R	10	<15	>95	N/R	[73]
Graphite	MIC	CV-AAS	HNO ₃	0.1	N/R	10	N/R	N/R	0.012	[74]
Pharmaceutical	MIC	ICP-MS	HNO ₃	0.5	N/R	10	N/R	96	N/R	[75]
Graphite	MF-AA	CV-AAS	HNO ₃	1	1000	240	N/R	N/R	N/R	[76]
Plant	MF-AA	ICP-MS	HCl	4	500-600	120		<2	N/R	[77]

Note: [N/R]-Not reported, [MIC]-Microwave induced combustion.

In general, to the best of our knowledge, there are few studies reported under this protocol. This might be due to the susceptibility of the method to loss of volatile species, as it is well-known that mercury is volatile. When zooming in on the combustion procedure, microwave-induced combustion was the most favored technique.

For example, in 2020 Souza and coworkers [71] employed MIC to determine mercury in cereal. The sample mass was 700 mg, and HNO₃ was an absorbing solution. An accuracy of 100 % and the limit of detection of 21 µg/kg were achieved. In 2016 Enders and coworkers [73], developed a method based on MIC to determine total mercury in coal NIST 1632c. Nitric acid was also used as an absorbing solution. The procedure took 10 minutes, and recoveries of >95 % were obtained. To our best knowledge, only one study has been reported from 2013 to 2023 for the total determination of mercury in non-aqueous matrices. The study was reported by H.Muller and coworkers [76] as a comparative study for the total determination of mercury in plant samples. Poor recoveries of less than 2 % were obtained.

2.2.3 *Extraction sample preparation methods*

This is a separation process that involves the separation of a substance from a matrix. The first method eliminates organic content from the samples and raises the target analyte's detection limits. Cloud point extraction, ultrasound-assisted extraction, microwave-assisted extraction, and solid phase extraction (SPE) are a few of extracting methods (**Fig. 2.4**).

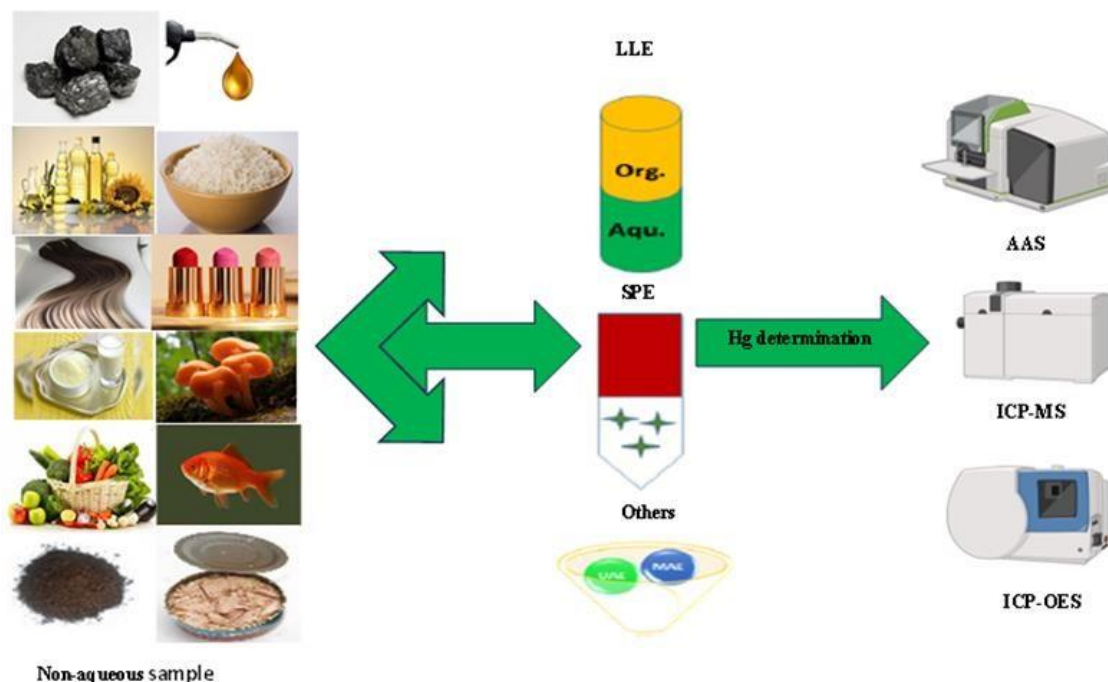


Figure 2. 4: Different extraction methods (such as SPE and LLE) used prior total mercury determination in non-aqueous matrices using analytical techniques

2.2.3.1 Liquid-liquid extraction

Liquid-liquid extraction (LLE) is a method that uses a solvent to separate one or more substances from a mixture. This process uses a variety of solvents, and selecting the right extracting solvent is paramount in achieving high efficiency [9]. Various extraction techniques for the measurement of total mercury are listed under this protocol. These include liquid-liquid microextraction (LLME), and extraction induced by emulsion breaking (EIEB) among others.

There are several types of LLME protocols which are reported in the literature. Under this extraction technique, we have dispersive liquid-liquid microextraction (DLLME), single-drop liquid-liquid microextraction (SD-LLME), and hollow fibre liquid-liquid microextraction (HF-LLME).

2.2.3.1.1 Dispersive liquid-liquid microextraction

In 2006, Mohammad Rezaee and coworkers [77] developed D-LLME (**Fig. 2.5**), a unique method for removing and preconcentrating organic molecules from water samples. The following are the fundamental ideas behind the D-LLME technique: a water-immiscible extraction solvent and a dispersive solution comprising the disperser solvent, which is miscible with both aqueous and extraction solvents, are rapidly injected into an aqueous sample containing target analytes. When the mixture is gently stirred, a cloudy solution forms in a test tube with droplets of the extraction solvent scattered throughout the sample solution. The aqueous phase and the extraction solvent provide a very large contact area, which allows analytes to be quickly removed into the extraction phase. Centrifugation is used to separate the extraction phase, and then analytical techniques are used to identify the enriched analytes in the sedimented phase, with or without further treatment. This protocol has recently gained popularity in the total determination of Hg in some solid and oil matrices [78].

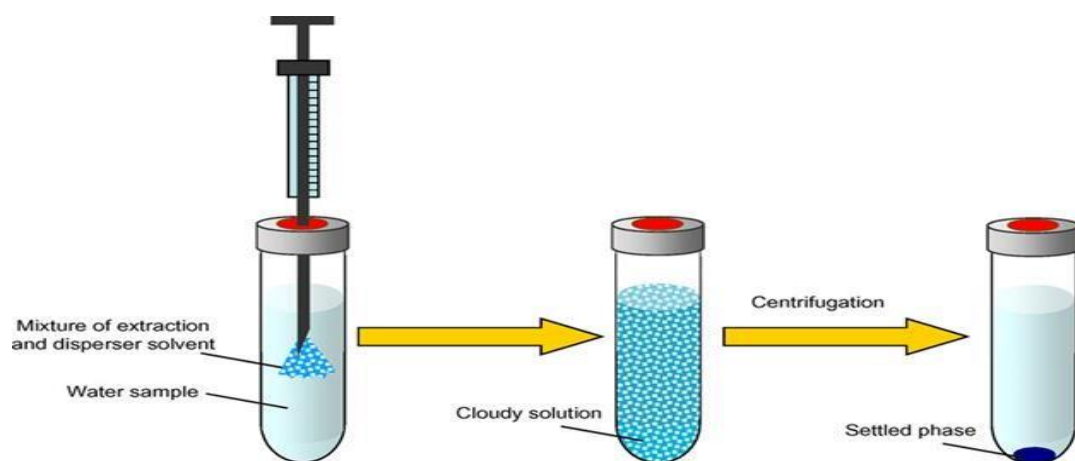


Figure 2. 5: Schematic representation of dispersive liquid-liquid microextraction [79].

In 2014, Mohadese Hossien-poor-Zaryabi and workers [80] reported the determination of Hg in pine leaves, river fish, and cigarettes using D-LLME. The enrichment factor, LOD and correlation coefficient of their method were 39, 0.15 $\mu\text{g/L}$, and 0.998, respectively. In 2018, Mohammad Hossein Habibollahi [81] reported a

study for the determination of mercury in soils and vegetables using DLLME. Analytical figures of their method were as follows: the enrichment factor was 114, the detection limit was 0.03 $\mu\text{g}/\text{kg}$, the linear range was 0.1-100 $\mu\text{g}/\text{kg}$, and the precision was 4.1 %. The DLLME method's benefits include high recovery, high enrichment, low cost, speed, and ease of operation [82].

2.2.3.1.2 Cloud point extraction

The cloud point extraction (CPE) method is another new and potentially green alternative preconcentration method to conventional liquid-liquid extraction. The former relies on the phase separation that non-ionic surfactant aqueous solutions show, which turns turbid and splits into two phases when heated above the cloud point temperature (**Fig. 2.6**). Usually, surfactants are absorbed at the interface between the phases where the polar head directs to aqueous part and hydrophobic tail towards lipophilic layer [83][84].

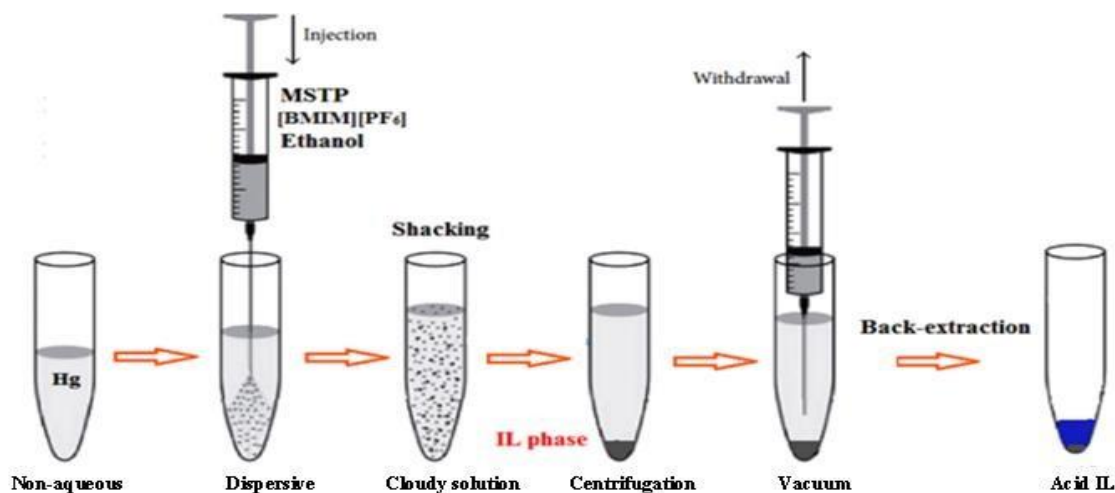


Figure 2. 6: Schematic presentation of CP-DLLME [85].

In 2021, Meiyi Xie and coworkers [86] well-documented the determination of trace levels of mercury in soil samples using the cloud point technique. They used a chelating agent sodium diethyldithiocarbamate and triton X-114 as a surfactant in their procedure. Recoveries in the range of 85.3-110 % were obtained. Li-ping Yu [87] also

reported the determination of mercury from fish samples using the cloud point extraction method. A surfactant of 0.08 % w/v triton and 0.04 % w/v ammonium pyrrolidine dithiocarbonate (APDC) chelating agent were used in their procedure. Low detection limits, which ranged from 2 to 9 ng/L were obtained.

A few other notable benefits of CPE are its affordability, ease of usage, and use of safe environmental solvents. However, it also has certain drawbacks, particularly concerning the surfactant-rich phase, which can affect the sample injection system and is quite dense at high concentrations [88].

2.2.3.1.3 Single drop microextraction

Single-drop microextraction (**Fig. 2.7**) was introduced in the mid-1990s by Liu and Dasgupta [89] as a method that involved using a single liquid drop to extract analytes. This technique consists of exposing a drop of organic solvent to the sample containing the target analytes for a predetermined amount of time. Then, before being collected and determined, the organic drop preconcentrates the relevant analytes [90]. SDME has several benefits that make it appealing, including simplicity (no need for specialized equipment), low cost, decreased solvent use and waste production, and absence of sample carryover. Solvent displacement in SD-LLME, however, is a serious drawback of this sample preparation method [90]. Two approaches are used for determining analytes under this protocol: direct immersion (DI-SDME) and head space (HS-SDME).

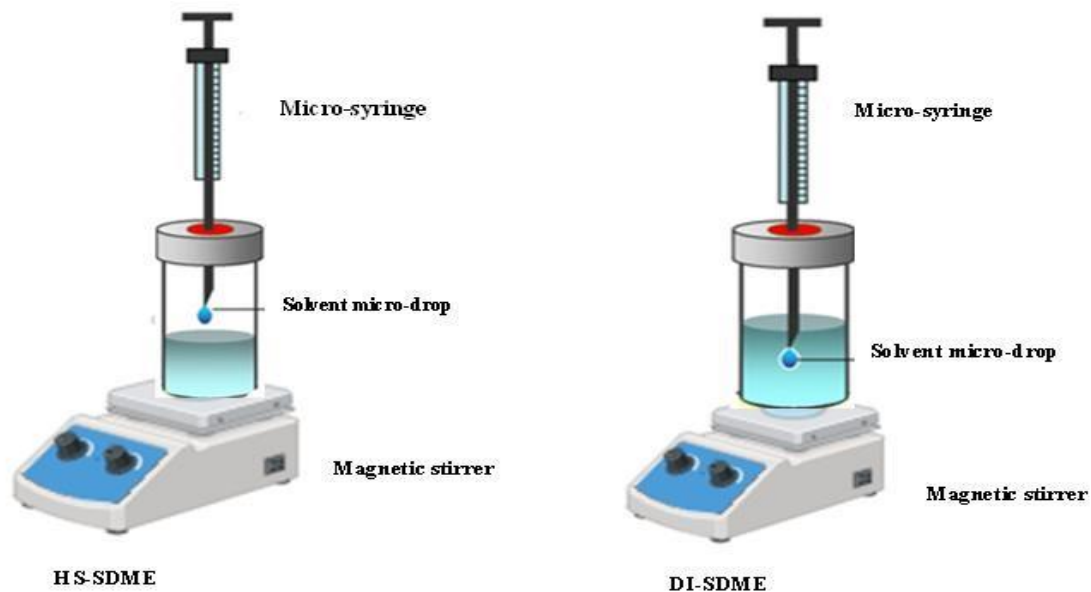


Figure 2. 7: Types of single drop microextraction.

Analytes in the gaseous phase of the HS-SDME method that are volatile or semi volatile in the liquid phase dissolve in the solvent drop at the end of the micro syringe needle that is placed over the surface of the sample. After the extraction, which takes a certain length of time, the micro drop is put back into the syringe needle. The analytes are injected into the chromatograph or detector to quantify them. The DI-SDME processes involve transferring the analytes from the sample to the extraction drop, where they remain in direct contact with each other until the extraction is stopped or a thermodynamic balance is established.

2.2.3.1.4 Hallow fiber-liquid phase microextraction

Another recently developed liquid phase microextraction is the hollow fiber-liquid phase extraction (HF-LPME) (**Fig. 2.8**). This method uses a hollow fibre, usually composed of polypropylene, to produce a semi-permeable membrane. An appropriate organic solvent is poured into the fibre's pores. Another option is to add a different immiscible solvent into the fiber lumen, which would establish two analyte equilibria between the water and solvent in the wall and the solvent and wall in the lumen, resulting in the three-phase system.

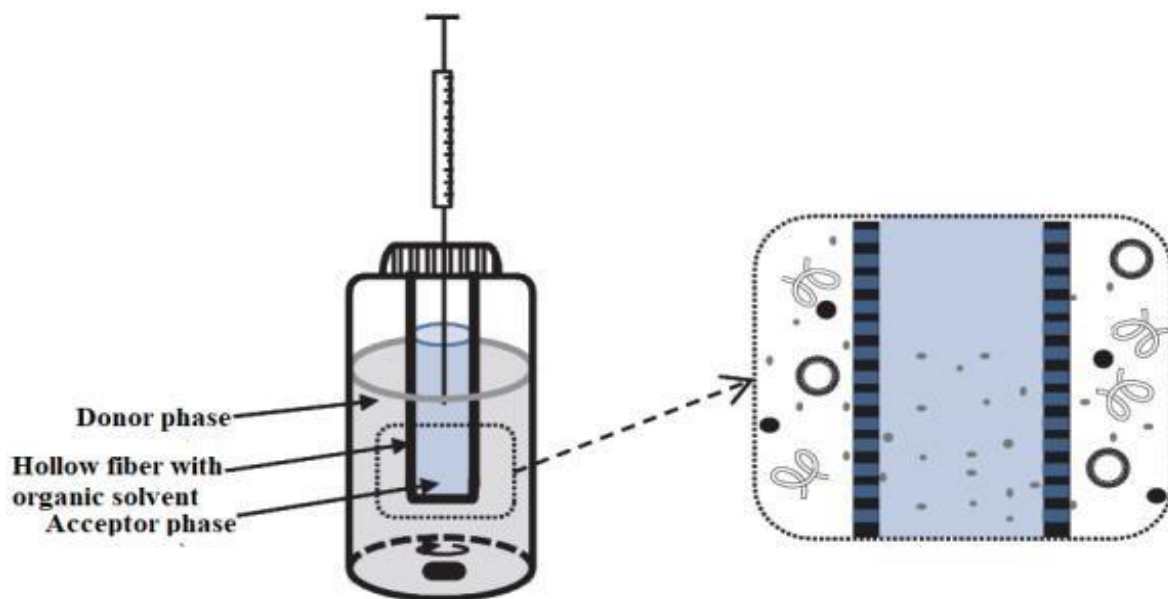


Figure 2. 8: Hollow fiber liquid-liquid microextraction [91].

Hongmei Jiang and coworkers [92] reported two methods based on hollow fiber liquid-liquid-liquid microextraction and hollow fiber liquid-liquid two-phase microextraction for the determination of Hg in human hair. The enrichment factor of the three phases was higher than that of the second phase. The limit of detection of the three phases was 0.1 $\mu\text{g/L}$ and that of the two phases was 0.4 $\mu\text{g/L}$. The precisions of the two methods were 13 % and 11 % for HF-LLLME and HFLLME, respectively. Recoveries were in the range 99-113 %. It was reported that the HFLLME was more economical because less reagent volume (μL) was used. However, as the analyte diffuses through the hollow fiber wall, creating dispersible hollow fibers, obstructing hollow fiber pores, and requiring lengthy procedures are some of the disadvantages associated with the production of this sample [93].

2.2.3.1.5 Extraction induced by emulsion breaking

Extraction induced by emulsion breaking, or EIEB, is another liquid-liquid extraction technique that has gained interest since 2010 (**Fig. 2.9**). This method creates and breaks an emulsion, which separates the organic component from the aqueous phase. Any suitable analytical technique can be used to remove and analyze

the aqueous phase using a micropipette. This method's main application is the measurement of mercury in oily matrices.

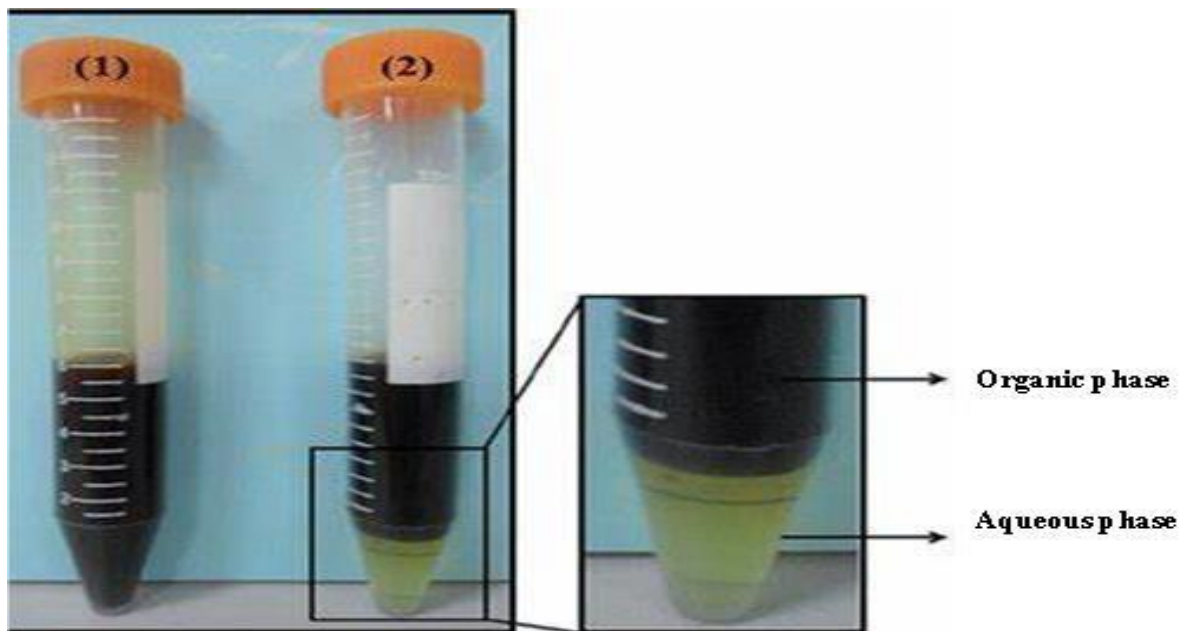


Figure 2. 9: Extraction induced by emulsion breaking [94].

Priscila O. Vicentino and Ricardo J. Cassella [95] proposed a novel approach for determining Hg in Brazilian gasoline samples. Their approach employed extraction induced by emulsion breaking. A microemulsion was formed by mixing the sample with n-propanol and HCl. Afterward, the emulsion was destabilized by adding water, and two phases were separated. Recoveries in the range of 88-109 % were obtained. The method's detection limit was 0.9 $\mu\text{g/L}$, and the limit of quantification was 2.9 $\mu\text{g/L}$.

The EIEB demonstrated several benefits, such as decreased risk of contamination, retention of volatile elements during sample preparation, shortened extraction times, and the presence of aqueous analytes, which prevent the introduction of carbon compounds into the analytical device and enable calibration with aqueous standards. Nevertheless, this approach has certain drawbacks, such as the need for multiple experimental steps for sample preparation and the occasionally carcinogenic use of organic solvents [9]. **Table 2.3** contains an overview of all the LLE methods that were used in nonaqueous matrices to determine mercury levels overall.

Table 2. 3: Liquid-liquid extraction methods for determining Hg from different non-aqueous samples.

Matrix	Type of LLE	Extractant	Time (min)	Dispenser solvent	Analytical method	EF	LOD ($\mu\text{g/L}$)	RSD (%)	%R	Ref.
Soil	LLE	Chloroform	0.5	N/R	CVAAS	N/R	0.018	N/R	92-104	[97]
Gasoline	EIEB	HCl	15	n-propanol	CV-AAS	N/R	0.9	4.8	88-109	[95]
Crude palm oil	EIEB	HCl	40	Triton-X-114	CV-AFS and VG-AFS	N/R	0.36	2.2	99-109	[98] [99]
Diesel oil, biodiesel, and mineral oil	EIEB	NH_3	20	Triton X-100	CV-AAS	5.1	0.6	3.5-5.6	80-103	[100]
Hair and fish	LLME	Deep eutectic solvents	10	Tetrahydrofuran	UV-vis	50	0.09	6.32	95-102	[101]
Fish	LLME	Natural deep eutectic solvents	7	Acetonitrile	UV-vis	95	0.25	1.9-5.5	92-98.7	[102]

Fish	D-LLME	Undecanol	N/R	Methanol	GF-AAS	68	0.04	6.2	83.8-102.3	[103]
Fish oils	DLLME	1-butyl-3-methylimidazolium hexafluorophosphate ([Bmim][PF6])	N/R	2.5	CV-AAS	54	0.045	1.2	104-112	[104]
Fish	D-LLME	1-octanol	5	Acetone	UV-vis	120	1.6	1.57	N/A	[105]
Fish	D-LLME	DESs	20	N/R	ETAAS	2400	0.34	3.68	>95	[106]
Human hair and fish	DLLME	1-octanol	N/R	N/R	UV-vis	120	4	1.57	101	[107]
Human hair	D-LLME	HNO ₃ -HClO ₄	4	1-octanol	UV-visible	120	1.6	1.82	97.4-102.1	[105]
Sea sand	D-LLME	Chloroform	1	ethanol	Spectrophotometer	39	0.15	2.6	95.1	[80]
Sand and clay stone	D-LLME	Supramolecular	10	undecanol	CV-AAS	N/R	0.006	<6	99.5-102	[108]

Soil and vegetables	D-LLME	deep eutectic solvent	4	1-undecanol	GFAAS	114-172	0.03	6.6	91-110	[81]
Wheat and rice	DLLME	CCl ₄	2	Methanol	GFAAS	N/R	0.019	3.4	92-106	[109]
Fish	CPE	N/R	10	N/R	CV-AAS	98	0.009	2.3	N/R	[87]
Snuff products	CPE	ammonium O, O-diethyldithiophosphate	40	Triton X-114	CV-AAS	84 and 97	0.004	2.6	98.7	[110]
Human hair, vegetables, and fruits	CPE	ionic liquid	10	Triton X-114	UV-visible spectrophotometer	N/R	0.4	1.0-2.4	97-101	[111]
Saline samples	SDME	Undecanol	N/R	N/R	UV-vis	N/R	1.9	8.5	100.9	[112]
Fish tissues	HS-SDME	tetradecyl(trihexyl)phosphonium chloride-	N/R	N/R	ETAAS	N/R	10	4.6	95-105	[113]

Dogfish muscles	HS- SDME	Pd (II)-HNO ₃	2	N/R	ETAAS	N/R	4	7	94+8	[114]
Fish	HF- LPME	Ionic liquids	10	N/R	UV-vis	120	0.2	5.4	94- 105	[115]
Human hair	HF- LPME	Toluene/thiourea	10	N/R	ICP-MS	N/R	0.4	11	99- 113	[93]

The most often used extraction technique for this kind of sample preparation is DLLME. Even with this protocol, the most researched matrix is Fish. M. Pirsahab and N. Fattahi created a DLLME-based technique in 2015 to determine the amount of mercury in fish samples. Methanol was utilized as a dispersing solvent in their process, while 1-decanol was used as an extraction solvent. The range of their enrichment factor was 68-93. The results showed a linearity range of 0.5-50 µg/kg and very low detection limits of 0.04 µg/kg [103]. In 2020, R. Menezes and coworkers [147] they have clarified another investigation regarding the entire analysis of fish oil samples with a DLLME process. They employed ammonium pyrrolidine dithiocarbonate (APDC) as a complexing agent and an ionic liquid as an extractant. A 54-enrichment factor was attained under optimal conditions, and the approach gives a limit of detection of 4.5×10^{-2} µg/L. In 2014, P. Liang and coworkers reported the determination of total mercury in food samples by DLLME coupled with GFAAS. A complexing agent, pyrrolidine dithiocarbonate (PDC), was used in their procedure. Additionally, they used methanol as their disperser solvent and carbon tetra chloride as their extracting solvent.

M. Hayati and coworkers [104] reported the determination of total mercury in fish and human hair samples. They optimized their DLLME with the aid of an experimental design. Their extracting solvent was 1-octanol, and they obtained recoveries at 101 %. E. Ragheb and coworkers [116] reported the determination of total mercury in fish using deep eutectic solvents based on DLLME. Good recoveries >95 % were obtained. Other matrices such as human hair, rice, wheat, sand, clay, vegetables, stones, and soil were also reported for the total determination of mercury after a DLLME procedure, as presented in **Table 2.3**.

2.2.3.2 Solid phase extraction

Solid phase extraction (SPE) is a pre-treatment technique that uses a sorbent through which target analytes are trapped and selectively extracted. This conventional technique was developed as a substitute for liquid-liquid extraction. This approach involves passing a liquid sample through a column or disposable cartridge packed with

the appropriate adsorbent until the liquid sample and solid phase reach equilibrium. Selecting the right adsorbent is crucial in SPE, affecting the method's accuracy and selectivity. Features include functionality, surface area, particle size and shape, pore size, and chemical inertness, all influencing the choice of adsorbent[117]. Numerous sorbents have been documented in the literature, including fullerenes, bonded silicas, carbon nanotubes, ion exchangers, nanoparticles, ion-imprinted polymers, and biosorbents [118]. In traditional SPE, there are four steps which are involved (**Fig. 2.10**), which are (i) Sorbent conditioning, (ii) Sample loading, (iii) Washing and (iv) Elution [117].

Sorbent conditioning: This is the initial stage, often known as wetting. To prepare for an effective interaction with the analyte, the sorbent is wetted with a solvent to activate its functional groups [118].

Sample loading: The cartridge is filled or run through with the sample, and the analyte is adsorbed in the sorbent bed along with certain interfering chemicals. A breakthrough volume is a crucial metric to consider avoiding analyte loss in this stage. When enough sample volume has been loaded, the analyte reaches a "breakthrough volume" stage when it is no longer absorbed because there is no active site to bind to [120].

Washing: a procedure wherein the sorbent is cleansed to extract contaminated species from it in a targeted manner [120].

Elution: a last stage that involves extracting the analytes kept in the active site using the right solvent [117] .

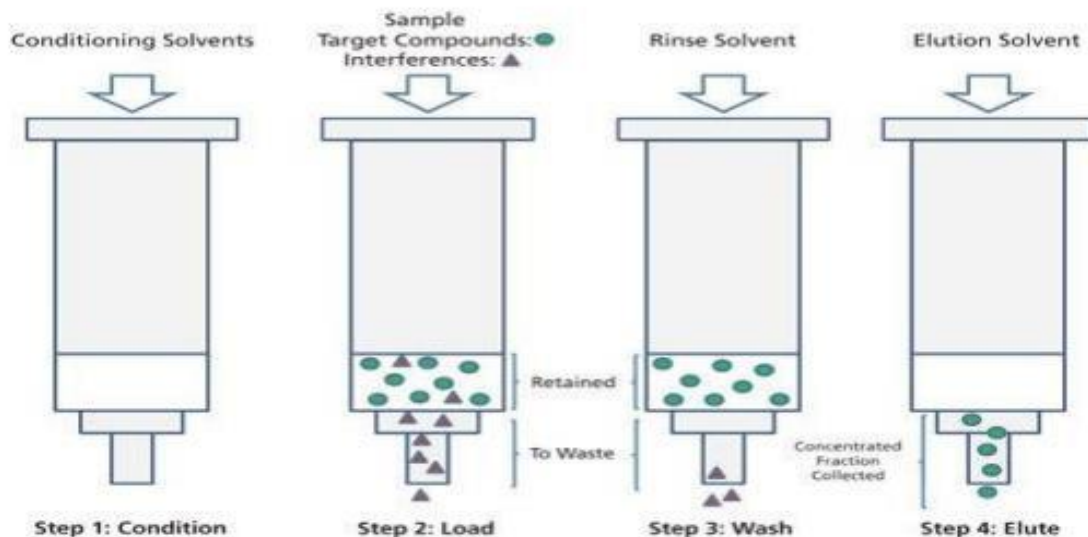


Figure 2. 10: Schematic diagram for solid phase extraction[121].

In 2009, N. Pourreza and coworkers [122] used a sulfur powder sorbent to determine Hg in fish and oyster samples. At a flow rate of 16 mL min^{-1} , the solid phase was placed on a mini-column, where the mercury ions were held in reserve. The calibration curve was linear in the range of $0.02\text{--}1.20 \text{ }\mu\text{g/L}$, with $r^2 = 0.9991$ ($n = 8$). With sample quantities of 250 and 1000 mL, respectively, the limit of detection (LOD) based on three times the blank's standard deviation was 0.012 and $0.003 \text{ }\mu\text{g/L}$. 3.9 and 1.2 % ($n = 8$) were the relative standard deviations for the measurements of 0.04 and $1.00 \text{ }\mu\text{g/L}$ of Hg (II), respectively. When compared to other conventional techniques, solid-phase extraction has numerous advantages.

Among these benefits are (i) speed and ease of use; a syringe and an SPE cartridge are all needed to complete the most basic SPE operation [118]. (ii) No emulsion formation [118]. (iii) reduced solvent usage (iv) low disposal costs, (v) Flexibility; there are limited choices in the mobile phase choices. (vi) high efficiency, (vii) ecologically safe, (viii) elimination of some of the glassware, (ix) isolation of analytes from large volumes of sample with minimal or zero evaporation losses, (x) reduced exposure of analysts to organic solvents (xi) more reproducible results [123].

Conversely, there are also some drawbacks to using this protocol. Primarily, solid phase extraction is considered an exhaustive traditional preparation technique. Furthermore, it is considered expensive and environmentally unfriendly [124]. Therefore, a significant effort has been made to develop new extraction methods with improved qualities than SPE. These methods include magnetic solid phase extraction, solid phase micro-extraction, and dispersive solid phase extraction.

2.2.3.2.1. Magnetic solid phase extraction

A novel kind of SPE called magnetic SPE (m-SPE) is created by combining nonmagnetic adsorbent with magnetic inorganic material. The target analytes are dissolved in a solution or suspension containing an adsorbent. An external magnetic field separates the adsorbent from the solution following the analytes' adsorption. Instead of centrifugation or filtration, the m-SPE's superior adsorption effectiveness enables quick separation from the sample matrix by applying an external magnetic field **(Fig. 2.11)** [125].

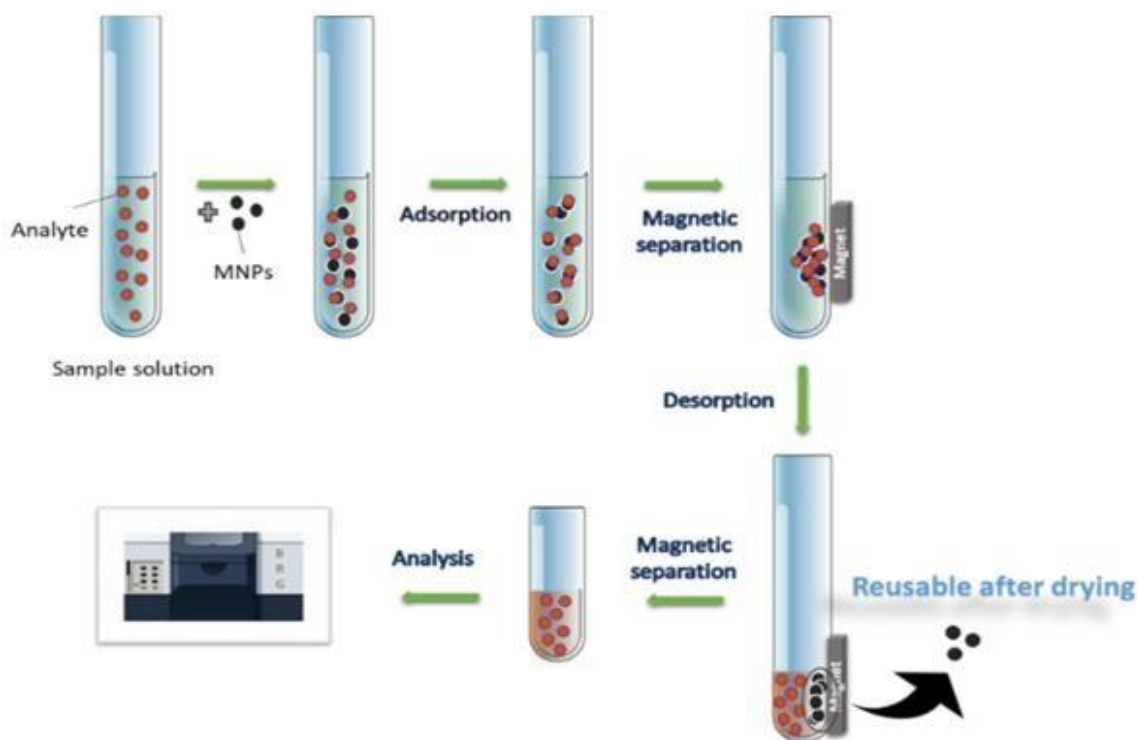


Figure 2. 11: Schematic representation of magnetic solid phase microextraction) [126].

A fascinating study that used a magnetic sorbent and UV-visible spectroscopy to measure mercury in fish samples was replicated in 2020 by Fateme Faryadras and coworkers [127]. After the optimization procedure, the computed limits of detection ($2.11 \mu\text{g L}^{-1}$), linearity of dynamic range ($7\text{--}100 \mu\text{g L}^{-1}$), relative standard deviation (2.59 %), and preconcentration factor (150) all showed that the sorbent was very dependable in preconcentrating mercury. Shahram Seidi and Mina Fotouhi [128] investigated a new magnetic sorbent for determining Hg from different fish and other marine species. A 21-minute extraction time, 20.0 mg of sorbent in 50 mL of the sample solution at pH 6.5, and 2.5 mL of HCl (1.7 mol/L) elution under a vigorous vortex for 2.0 minutes were found to be the optimal settings. In perfect conditions, an extraction recovery of 85 % and a preconcentration factor of 17 were attained.

It was discovered that the quantification and detection limits were, respectively, 1.0 ng/mL and 0.025 ng/mL . The correlation coefficient, intra, and inter-day precisions were 0.9997, 4.0 %, and 9.98 %, respectively.

2.2.3.2.1. Solid phase microextraction

An appropriate sorbent is coated on or inside a fibre during the SPME technique. While the vial top is securely closed, the fibre is placed either directly into the solution or in the headspace of a vial holding the sample solution (**Fig. 2.12**). To improve the analyte's mass transfer and speed up its absorption onto the fibre. The sample solution is agitated. The heated stirred solution is used in the headspace mode to accelerate the analyte's evaporation from the solution surface. Following the analyte extraction, the analyte is extracted from the adsorbed analyte on the fibre coating using either solvent or heat desorption techniques [124].

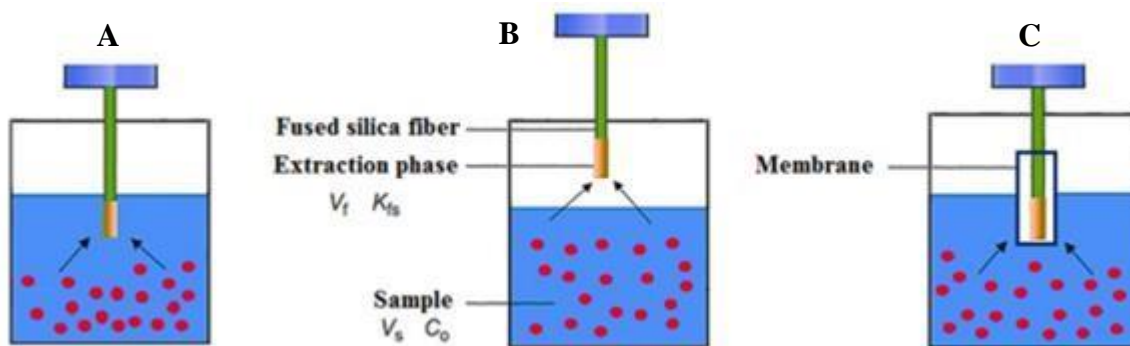


Figure 2.12: Modes of SPME. (a) DI-SPME, (b) HS-SPME and (c) Membrane-protected SPME[125].

Using SPME in conjunction with CV-AAS, Ewa Stanisiz and coworkers [130] examined the levels of mercury in soil samples in 2014. They used PTFE tubes coated with an ionic liquid specifically designed for the task of directly immersing microextraction of mercury. Under optimum conditions, the extraction phase of a PTFE tube coated with 32 μL of methyltrioctylammonium thiosalicylate produced good extraction efficiency for the extraction of 2 ng/mL mercury in 10.0 mL of solution. The Certified References were SRM2709 San Joaquin Soil, SRM 2711 Montana Soil, and SRM 2704 Buffalo River Sediment. Materials for evaluating the accuracy of the suggested approach. Recoveries of reference materials ranged from 97 % to 100 % of the total. The process was used to examine soil samples.

2.2.3.2.1. Dispersive solid phase microextraction

Dispersive solid phase microextraction (DSPME) is a non-fibre SPME technique that was created recently to get beyond the drawbacks of conventional SPME (**Fig. 2.13**). This process involves pouring the sorbent straight into the sample solution to extract the analyte rather than depositing it on the fibre core. Subsequently, the sorbent is disseminated to augment its surface area in contact with the sample solution or acceptor phase, thereby considerably diminishing desorption and extraction times [131].

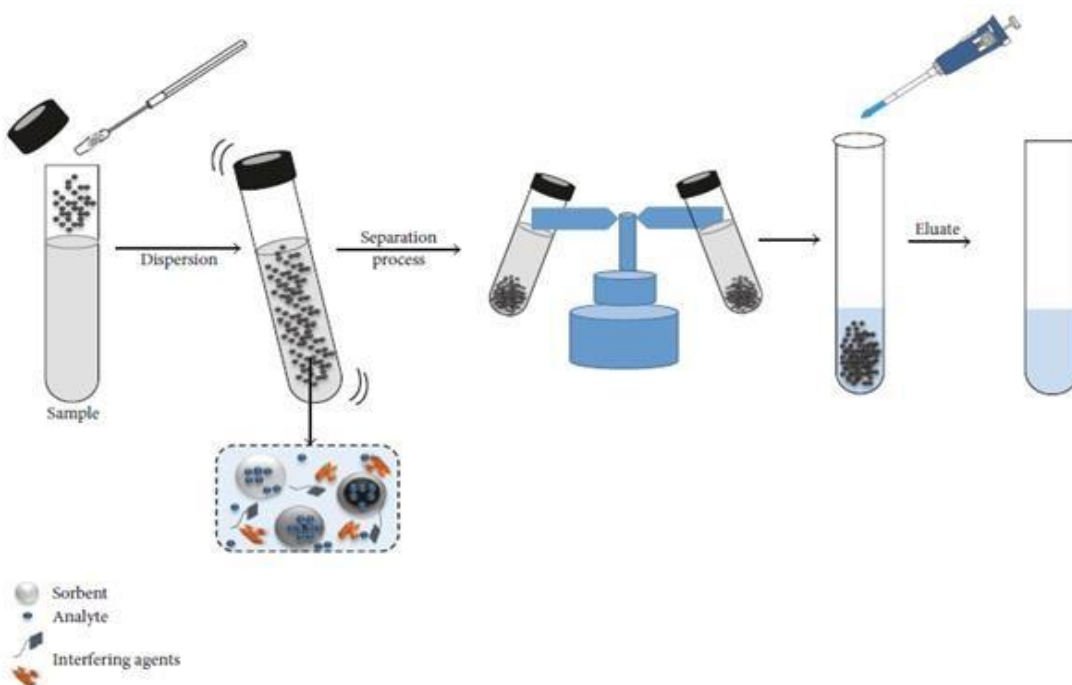


Figure 2. 13: Schematic representation of dispersive solid phase microextraction [132].

Atefeh nasrollahpour and coworkers [132] developed a new dispersive solid phase microextraction (DSPME) method for determining Hg from vegetables using ionic liquid-modified graphene oxide nanoparticles before measurement with CV-AAS. With a determination coefficient of 0.9995, a linear response in the concentration range of 0.08– 10 ng/mL was found at the optimum conditions. At a signal-to-noise ratio of 3,

the detection limit of the method was 0.01 ng/mL. Precisions within and between days were found to be 3.4 % and 4.5 %, respectively.

Fibre is not required for this process, removing the constraints and challenges associated with placing the sorbent on the fibre and shortening the extraction and desorption times. As a result, the approach is preferred over SPME. However, this process has certain drawbacks, namely the challenge of removing the sorbent from the sample solution and the restriction on method automation [132]. **Table 2.4** presents the information reported on SPE for the total determination of mercury in non-aqueous matrices

Table 2. 4: Solid phase extraction methods for the determination of Hg from different non-aqueous samples.

Matrix	Sorbent	Type of SPE	Detection technique	EF	LOD (µg/L)	RSD (%)	Accuracy (%)	Ref.
Aquatic plant	polytetrafluoroethylene	Column SPE	CV-AAS	35	0.02	2.1-3.4	94-110	[134]
Crude oil	Octadecyl silica membrane.	Column SPE	CV-AAS	240	0.25	1.9	88-109	[9]
Gasoline	Octadecyl silica membrane disk	Column SPE	CV-AAS	240	0.20	1.9	88-109	[9]
Fish	diethyl di thiophosphate (DDTP)	Column SPE	GFAAS	1540	0.009	4.8	98.1-100.	[135]
Fish	silica-based nanoparticles	Column SPE	HG-AAS	25	0.018	<3	98.3-100.	[136]
Fish	PCN-222/MOF-545 (Zr-MOF)	Column SPE	CV-AAS	120	0.02	1.3-5.6	74.3-98.7	[137]
Soil	Ionic liquid coated PTFE tube	SPME	CV-AAS	21	0.04	5	97-100	[130]
Food	Modified stainless	SPME	ICP-OES	50	0.82	2.89	70-97	[138]
Fish	Fe ₃ O ₄ @Ag@MESNa	m-SPME	ETAAS	200	0.01	N/R	95.8–103	[139]
Tea samples	Fe ₃ O ₄ @SiO ₂ /graphene	m-SPME	HG-AFS	23	0.004	4.27	90.0-97.3	[140]
Dogfish liver (CRM)	DPTH-MNPs	m-SPME	FI-MSPME-C -ETAAS	5.4	0.0074	1.7	103.8	[141]

Nails	Fe ₃ O ₄ @SiO ₂ -NH ₂ @HKUST-1	m-SPME	ETAAS	2400	0.34	3.8	>95	[106]
Vegetable samples	ionic liquid modified magnetic graphene oxide (IL-MrGO) nanoparticles	d-SPME	CV-AAS	200	0.01	3.4-4.5	97.8-100.	[132]
Lipstick	magnetic graphene oxide	m-SPME	CV-AAS	21	0.57	6.5	94-100	[142]
Fish and shrimp	magnetic graphene oxide	m-DSPE	FI-CV-AAS	17	0.025	4	85	[128]
Fish	Magnetic graphene oxide	m-DSPE	UV-Vis	250	2.11	2.59	N/R	[127]
Muscle Tissue SRM 2976	Fe ₃ O ₄ @graphene oxide nanoparticles	m-DSPE	FI-CV-GFAAS	250	0.00025	2.9	86-103	[143]
Fish	magnetite@MIL-53(Fe)-NH-CS	m-DSPE	CV-AAS	300	0.006	7.8	96.6	[144]
Fish, shrimp, tuna samples	(Fe ₃ O ₄ -2,5-dimercapto-1,3,4-thiodiazol)	m-DSPE	CV-AAS	N/A	0.01	5.5	83-106	[145]
Fish samples	magnetite (Fe ₃ O ₄)/chelating ethoxyphenyl)-3-(4-ethoxyphenyl)-functionalized multi-walled carbon nanotubes with silica shell	m-DSPE	CV-AAS	N/A	1.5±0.27	3.56-5.01	99.2-100.	[146]
Fish samples	magnetic graphene/ZnFe ₂ O ₄	m-DSPE	CV-AAS	30	0.001	2.7	91-17	[125]

Trout and shrimp	magnetic graphene oxide	m-DSPE	FI-CV-AAS	17	0.025, 0.015	5.3-6.6	90-103	[147]
Fish	magnetic graphene oxide	m-DSPE	UV-vis spectrophoto	143	2.11	2.59	107	[127]
Rice, fish and tea	Fe ₃ O ₄ @GO/2-PTSC	UA-DSPE	ICP-OES	193	0.0079	1.63	96.5	[148]

Note: [SPE]-Solid phase extraction; [m-DSPE]-Magnetic dispersive solid phase extraction; [SPME]-Solid phase microextraction; [d-SPME]-Dispersive solid phase microextraction; [m-SPME]-Magnetic solid phase microextraction; [UA-DSPE]-Ultrasound-assisted dispersive solid phase extraction

From the summary of publications, we observe that magnetic dispersive solid phase extraction (m-DSPE) was mostly reported. It seems like this procedure couples the merits of magnetic solid phase extraction with the merits of dispersive solid phase extraction (DSPE). For example, F. Faryadras and coworkers [127] developed a green magnetic sorbent in 2020 to determine the total amount of mercury in fish. In their procedure, they coupled magnetic solid phase microextraction with dispersive solid phase microextraction. High preconcentration factor of 150, LOD of 2.11 $\mu\text{g/L}$, and precision of 2.59 % were achieved. Another interesting study was reported by Shahram Seidi [128] and Mina Fotouhi in 2017 for the total determination of mercury in seafood followed by CV-AAS. Their sorbent consists of graphene oxide coated on the surface with thiophene. Their sample preparation method also combined the m-SPE and D-SPE. Their method gave a preconcentration factor of 17, lower than the above study, but their LOD of 0.025 $\mu\text{g/L}$ was lower than the other reported study. E. Yavuz and coworkers [129] developed a method based on m-DSPE to determine mercury in fish samples. Their magnetic sorbent was supported by graphene. A high preconcentration factor of 30 was achieved. Additionally, a LOD of 0.01 $\mu\text{g/L}$, with a precision of 2.7 % was obtained. In 2021, C. Garcia-Mesa and coworkers [125] reported a ferrofluid based on Fe_3O_4 @graphene oxide nanospheres together with an ionic liquid for the development of a magnetic dispersive solid-phase extraction (MDSPE) method for the extraction of mercury in biological and environmental samples. According to the optimal conditions, the detection limit, determination limit, and percentage RSD were 2.9 %, 0.25 ng/L, and 4.9 ng/L respectively. Additionally, a high preconcentration factor was attained.

It is also interesting to note that magnetic solid phase microextraction (m-SPME) was highly reported. For instance, in 2021 E. Ragheb and coworkers [143] prepared a novel magnetic biosorbent to preconcentrate total mercury in fish, hair, and nails. The procedure obtained a high enrichment factor 2400 with a low LOD of 0.34 $\mu\text{g/L}$. Lopez-Garcia [139] synthesized magnetic particles covered with functionalized silver nanoparticles, which they applied in a magnetic solid phase microextraction procedure (m-SPME) to preconcentrate mercury in edible fish oils. A preconcentration factor close to 200 and a LOD of 0.01 $\mu\text{g/L}$ were achieved. It is worth noting that the overall enrichment factor reported under SPE ranged from 5.4 to 2400, while the LODs and precision ranged from 0.00025 to 2.11 $\mu\text{g/L}$ and 1.3 to 7.8, respectively.

2.2.3.3 Other Extraction Methods

2.2.3.3.1 Ultrasound-assisted extraction

Another extraction technique that is frequently used for determining the total amount of mercury in solid and oily matrices is ultrasound-assisted extraction (UAE) (**Fig. 2.14**). A sound wave that has a frequency higher than 20 kHz is known as ultrasound [150]. Ultrasound and chemical species do not directly interact with one another under UAE. Rather, samples are combined with weaker acids. The latter facilitates the transfer of metal ions from the aqueous phase to the organic phase. To speed up the extraction process, the sample is submerged in an ultrasonic bath with temperature control. Centrifugation is then used to separate the aqueous and organic phases. The latter is then diluted to the known volume and ready for examination using the proper analytical tool [151].

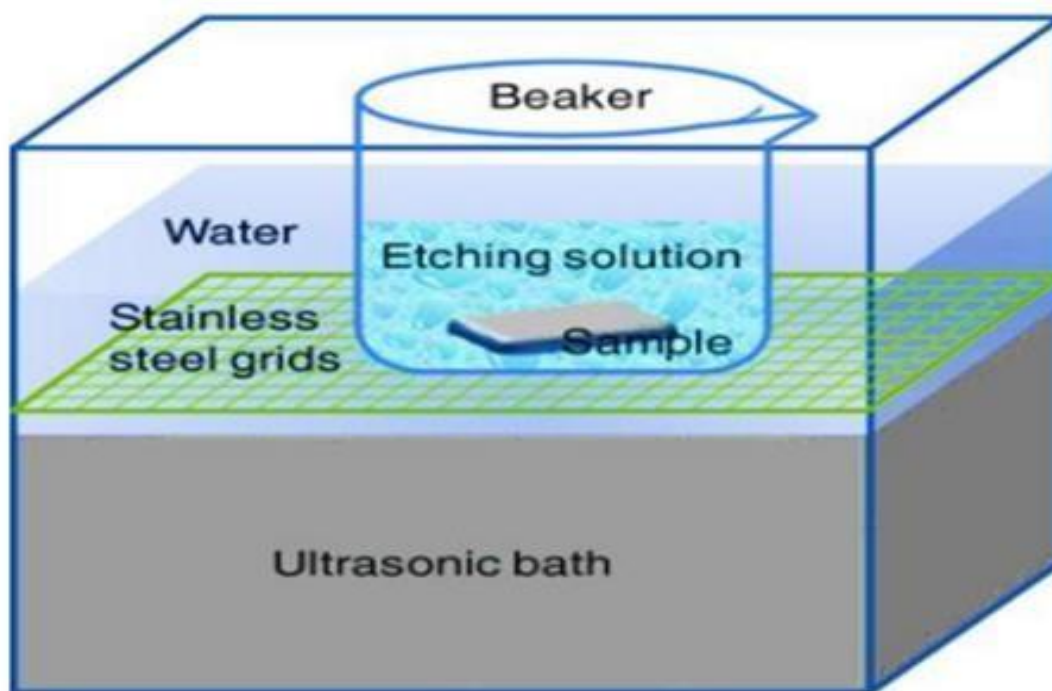


Figure 2.14: Ultrasound-assisted extraction [151].

In 2019, Altunay and coworkers [102] developed a method for determining total mercury in fish using natural deep eutectic solvents based in UAE. A preconcentration factor of 120, accuracy of 96.7 %, and precision of 3.6-4.3 % were obtained. Danilo J. Leao and coworkers [148] elucidated an interesting study on using UAE to determine mercury from sediments followed by CV-AAS. An external

calibration technique with a precision of 4.31 % was used for method validation. LOD and LOQ for the method were 1.04 and 3.46 ng/g.

The UAE demonstrated several benefits: quick extraction times, easy operations, little reagent usage, and cost-benefit. However, there were drawbacks to this sample preparation, such as low sample input and extremely low enrichment factors, which also harmed the limits of detection.

3.2.3.3.1 Microwave-assisted extraction

Finally, microwave-assisted extraction or MAE is a common technique for accurately quantifying mercury in various matrices. This process combines classic solvent extraction with microwave technology (**Fig. 2.15**) [19]. Less reagent consumption, reduced analyte loss risk, and aqueous standard calibration are benefits of this approach. This approach is also beneficial since it may be used successively, allowing for the addition of reagents during the extraction process, and it can effectively extract the target analyte during leaching cycles. However, there could be disadvantages to this method, like a strong matrix effect caused by a microwave-induced plasma operating at lower power (up to 1 kW) and the inability to extract multiple samples at once in a single cavity.

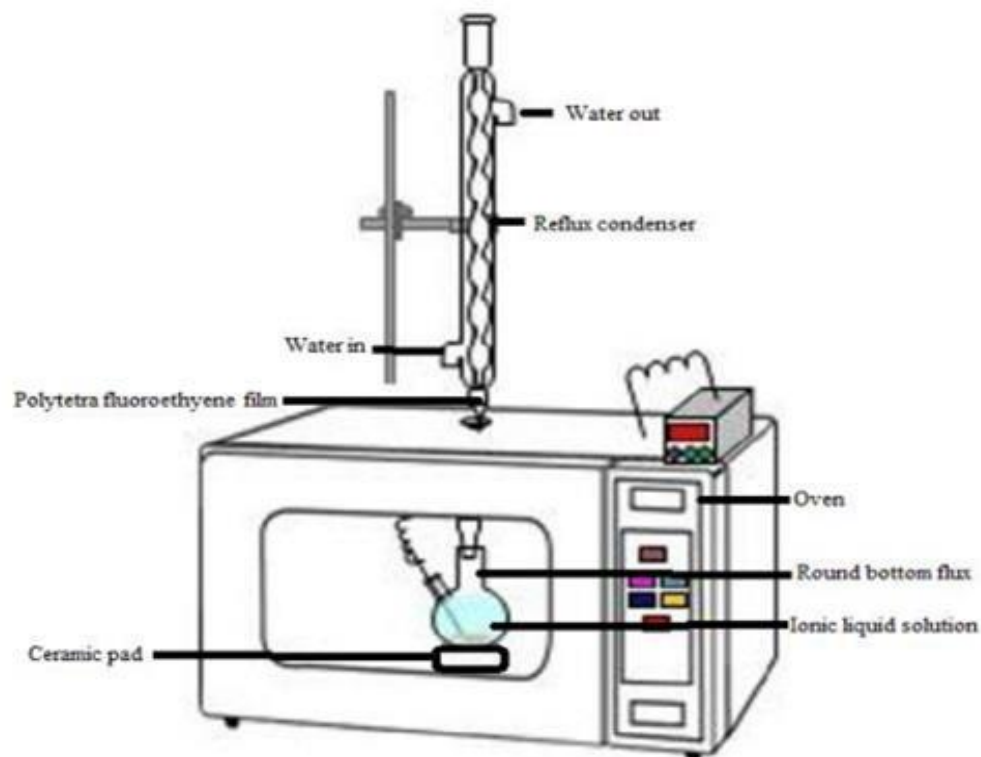


Figure 2. 15: Microwave-assisted extraction [153].

2.3 Optimization of sample preparation methods (Univariate or multivariate)

In analytical chemistry, optimization determines the ideal conditions for implementing a technique to yield the best possible result. In this field, two approaches are used to achieve it. The first strategy is univariate optimization, while the second is multivariate optimization.

2.3.1. Univariate optimization strategy

The univariate optimization strategy is regarded as the conventional optimization strategy. This method looks at one factor's impact on an experimental response at a time. The technique of this strategy is to alter one parameter but keep the other parameters constant. The main drawback is that the interacting effects between the variables under study are not considered. As a result, this method does not fully capture how the argument affects the response. An additional drawback of one-factor optimization is the rise in the number of experiments required to carry out

the study, which results in an increase in costs and time as well as an increase in material and reagent usage [144][145].

In 2015 Souza and coworkers [156] developed a method using the univariate approach for determining mercury in phosphate fertilizers using graphite furnace atomic absorption spectroscopy. Their method's accuracy, precision, and limit of detection were 103 %, 8.2 % and 4.8 ng/g, respectively. Another study that utilized univariate optimization in liquid-liquid microextraction procedures was reported in 2020 by Menezes and coworkers [104]. In their work, they were interested in determining mercury in food. Their method showed a preconcentration factor of 54 and a limit of detection of 0.04 µg/L. In 2021, Garcia-Mesa and coworkers [143] reported the determination of mercury in biological and environmental samples using m-SPME combined with flow-injection cold vapor graphite furnace spectrometry. Their sample preparation procedure was optimized using univariate strategies. A preconcentration factor of 250, a limit of detection of 0.25 and 4.9 ng/L and precision of 2.9 % were achieved, respectively.

2.3.2. *Multivariate optimization strategies*

This technique was introduced to overcome the limitations of univariate optimization. In this approach, more than one variable is optimized simultaneously, and chemometrics are mostly utilized. Four main steps are followed in this approach: (a) screening designs, (b) response modeling, (c) evaluation of the fitted model, and (d) determination of optimal conditions [157][158].

2.3.2.1. First order designs

First-order designs are utilized for screening. The latter has to do with the selection of significant parameters which affect the analytical response. It rules out variables that do not contribute significantly to the response. Experimental designs that are reported for screening include two-level full factorial design (FFD), two-level half factorial design (FrFD), and Plackett-Burman (P-B) design. Two-level and two-level half factorial designs are the most reported for quantifying total mercury in nonaqueous matrices; hence, they are discussed herein [159].

The general formula used for FFD is 2^k , with base 2 as the number of fixed levels for all variables and k as the number of variables. The implementation of FFD can be done easily when there are few variables to be examined. However, when the number of variables is high, the number of required experiments can significantly grow. FrFD can be used to decrease the number of experiments in this instance. They use the formula 2^{k-p} to reduce experiments by a number p. In the most typical scenario, the so-called half fraction is produced when p equals 1 [160].

2.3.2.2. Second order designs

Second-order designs are utilized for further optimization. The most utilized response modeling is the response surface methodology (RSM). The response surface methodology's primary goal is to identify a polynomial that accurately captures the response behavior with the levels of the variables under study. Under this approach, the simplest model that can be employed is based on a linear function. The acquired replies must fit the following equation **(Eq. 2.2)** [161]:

$$y = a_0 \sum_{n=1}^k (a_i x_i + \alpha) \text{Eq. 2. 2}$$

where k is the number of variables, a_0 is the constant term, and a_i represents the coefficients of the linear parameters, x_i represents the variables, and α is the residual associated to the experiments.

In the above case the response should not present any curvature. A second order model is employed to evaluate curvature. A second order model polynomial **(Eq. 2.3)** presents the following terms.

$$Y = a_0 + \sum_{i=1}^k a_i x_i + \sum_{1 \leq i < j}^k a_{ij} x_i x_j + \sum_{i=1}^k a_{ii} x_i^2 \text{Eq. 2. 3}$$

where k is the number of variables, Y is the response, x_i represents the variable levels and a_0 , a_i , a_{ii} and a_{ij} as the regression parameters of the independent term, the linear term, the quadratic term, and the interaction term, respectively [162].

It is important to note that under this RSM there are different experimental designs which are employed such as three-level factorial design (TLFD), central composite design (CCD), Box–Behnken design (BBD), Doehlert design (DD) and Taguchi designs. There are differences between these symmetrical designs in terms

of the number of runs and blocks, the number of levels for variables, and the choice of experimental sites [163]. However, only CCD, BBD, and DD are mostly utilized for the total determination of mercury in non-aqueous matrices, hence they are discussed herein.

Central composite design (CCD): This is the most reported matrix design for second-order polynomial adjustment. It combines two levels of factorial and other designs. This formula (Eq. 2.4) gives the number of experiments required for its implementation.

$$2^k + 2k + n_0 \quad \text{Eq. 2. 4}$$

where n_0 is the number of copies of the central point and k is the number of variables to be optimized. With regular CCD, all variables can be investigated in five levels ($-\alpha$, -1 , 0 , $+1$ e $+\alpha$). The formula $\alpha = 2^{(k-p)/4}$ can be used to determine the α values for axial points [163].

Box–Behnken design (BBD): In this mathematical modeling data points are located equidistant from the center point. (Eq. 2.5).

$$k^2 + k + n_0 \quad \text{Eq. 2. 5}$$

The main drawback of this modeling is the impossibility of conducting experiments in points located in the cube vertex [164].

Doehlert design (DD): Originally called uniform shell design, David H Doehlert developed it in the 1970s. This design is useful when the experimental points are distributed on a spherical shell. Thus, there is no orthogonality or rotatability nor is the variance of the predicted values in the experimental space uniform. In addition, all adjacent experimental points are placed at equal distances. Moreover, the number of experiments proposed by this design is calculated (Eq. 2.6) as

$$N = k^2 + k + c_0 \quad \text{Eq. 2. 6}$$

where k is the number of factors and c_0 is the number of central points. Unlike CCD, DD is efficient with few experimental runs [165].

2.3.2.3. Evaluation of the fitted model

It is paramount to evaluate the quality of the mathematical model after fitting the data. There are three ways to achieve the evaluation. The most reliable approach is through the analysis of variance (ANOVA). The central idea of the former is to contrast the variation brought on by the treatment with the variation brought on by random mistakes that are a natural part of measuring the generated responses. Considering the sources of experimental variance, this comparison allows one to assess the significance of the regression that was used to predict responses [166]. Another way of evaluating data quality is through the lack of fit. A model will be well fitted to the experimental data if it presents a significant regression and a nonsignificant lack of fit. Lastly, visual inspection of residual graphs also helps in the evaluation of a model. As a result, if the mathematical model fits well, the residuals graph it produces looks like a normal distribution [159] .

2.3.2.4. Determination of optimal conditions

For linear models, the generated surface can give direction in which the original design must be displaced to attain the best conditions. Otherwise, the optimum conditions can be obtained through inspection. On the other hand, for quadratic models, the critical point can be characterized as maximum, minimum or saddle. The coordinates of the critical point can be calculated through the first derivative of the mathematical function. The surface response plots can attain the visualization of the predicted model. Again, it is possible to find the optimum region through visual inspection of the surface plots [167].

A lot of studies have utilized multivariate optimization for the determination of mercury in non-aqueous matrices. Seidi and Fotouhi 2017 used a multivariate strategy based on a central composite design to optimize an m-SPE procedure for determining mercury in seafood. Accuracy, precision, detection limit, and quantification of 85 %, 4.0 %, 0.025 µg/L, and 1.0 µg/L, were achieved [128]. Ultra trace levels of mercury were obtained in green tea and vegetables after a preconcentration procedure optimized using a response surface based on a central composite design. A new functionalized magnetic material was developed and applied to determine mercury in that procedure. Accuracy, precision, limit of

detection, and preconcentration factor of the method were about 94.2 %, 10.1 %, 1.0 ng/mL, and 250 respectively [168]. In 2015 Karimi and coworkers [169] applied experimental design to mercury determination in hair samples. For their response surface methodology, they utilized Box–Behnken design. The recovery value in this method was 98.6 % with an RSD of 1.4 %, and the obtained LOD was 0.01 ng/mL. The preconcentration factor was calculated to be 179. In 2019, da Silva and coworkers [170] employed multivariate optimization based on the Doehlert design to quantify mercury in fish. A limit of detection equivalent to 0.33 ng/g and a precision of 4.59 % were obtained.

2.4 Characterization techniques

Characterization techniques are used to obtain information about the chemical, physical, mechanical, and electrical properties of materials. Characterization techniques include scanning electron microscopy, transmission electron microscopy, X-ray diffraction, Fourier transmission infrared spectroscopy, UV-visible spectroscopy, Brunauer-Emmett-Teller, nuclear magnetic resonance spectroscopy, and thermal gravimetric analysis.

2.4.1 Scanning electron microscopy

A scanning electron microscope uses a focused beam of electrons to create a magnified image of a sample. The electron beam is scanned in a regular pattern across the sample's surface, and the sample's electrons are used to create the image. This technique gives information about the structure and composition of a material. Materials are examined at the nano-to-micrometer scale. This method often yields semi-quantitative and qualitative results when combined with energy-dispersive X-ray spectroscopy (EDX) [171].

2.4.2 Transmission electron microscopy

Transmission electron microscopy is used to examine thin material through which electrons can travel, resulting in a projected picture [172]. The former is a strong approach for studying several aspects of materials, including morphology, size distribution, crystal structure, and chemical production, among others. Transmission

electrons flow through the thin material and are detected to create pictures, which is why the technique is known as transmission electron microscopy [173].

2.4.3 Fourier transform infrared spectroscopy

Fourier transform infrared spectroscopy is mostly used for identifying functional groups in a material. Infrared light interacts with the sample interface, causing some of it to be absorbed and the rest to be reflected. In FT-IR spectroscopy, measurements are taken throughout a broad spectrum rather than a limited range of frequencies [174].

2.4.4 UV-visible spectroscopy

UV visible spectroscopy is an analytical method that quantifies the number of distinct wavelengths of UV or visible light absorbed or transmitted by a sample in comparison to a reference or blank sample [175]. The former measures a chemical substance's ability to absorb light. It may be used to calculate concentrations, identify unknown compounds, and learn about the physical and electrical properties of organic and inorganic substances. The essential premise underlying this approach is the interaction of materials with radiation, which can result in many processes such as reflection, scattering, and absorption. When samples are examined to determine their UV visible spectrum, absorbance is calculated [176].

2.4.5 X-ray diffraction spectroscopy

This is a non-destructive technique for determining a material's crystallographic structure, chemical content, and physical characteristics. X-ray diffraction spectroscopy uses X-rays to determine the geometry or form of a molecular structure. The former relies on the constructive interference of monochromatic X-rays with a crystalline sample. A crystal diffracts X-rays because their wavelength corresponds to the inter-atomic gap in crystals [177].

2.4.6 Thermal gravimetric analysis

The principle of thermogravimetry is to measure the changes in the mass of a substance while it is constantly heated to elevated temperatures. This measurement reveals information about physical events such as heat breakdown, phase change,

adsorption, and desorption. In thermogravimetric analysis, the sample is heated at a regulated pace in a specified atmosphere (air, N₂, CO₂, He, Ar, etc.) [178].

2.4.7 Brunauer-Emmett-Teller

Brunauer-Emmett-Teller seeks to explain the physical adsorption of gas molecules onto a solid surface. It is an essential approach for determining the specific surface area of a substance [179]. Nitrogen is the most often utilized gaseous adsorbent for probing surfaces. To calculate surface area, the solid sample is cooled to cryogenic temperatures under a vacuum. Nitrogen gas is introduced into the sample in regulated increments. After each dosage of nitrogen gas, the relative pressure is allowed to equilibrate before the weight of nitrogen adsorbed is calculated. The slope and intercept of the BET plot are then used with the BET equation and the known molecular cross-sectional area of the nitrogen molecule to compute the sample's total surface area [190].

2.4.8 Nuclear Magnetic Resonance Spectroscopy

Nuclear magnetic resonance spectroscopy is a method commonly used to identify the molecular structure of a material. The operating concept is based on the spin of atomic nuclei. Nuclei having an odd mass or atomic number have nuclear spins. Because a nucleus is a charged particle in motion, it generates a magnetic field. When nuclei with non-zero spins are exposed to a strong magnetic field and supplied with suitable energy, they transition from a lower energy state to a higher energy state. The energy absorbed during the transition depends on the nucleus type and its chemical environment in the molecule [180].

2.5 Summary of Recently Published Work 2013-2023

This section discusses the quantity of publications for the three sample preparation techniques (extraction, combustion, and mineralization). The trend of publications for each method of sample preparation is displayed in **Figure 2.16**. On the one hand, until 2021, the annual number of publications for mineralization methods declined. However, since 2017, extraction techniques have been increasingly popular. Although the number of publications varied annually, in 2023

extraction procedures yielded the greatest number of articles compared to all other sample preparation techniques.

One reason for the observed decrease in the number of publications for mineralization methods might be due to the nature of the analyte. As mentioned earlier, mercury exists in trace amounts across all matrices, therefore, many researchers are developing more preconcentration methods to improve the detection limits of mercury. Another reason might be due to the environmental impact of the sample preparation methods. Most mineralization methods employ concentrated acids as oxidizing agents. These agents produce hazardous secondary wastes as compared to preconcentration methods. For instance, microextraction (LLME and SPME) techniques employ small volumes of toxic organic solvents (μL). This provides a rationale for the trend in the number of articles found for sample preparation techniques. In summary, the statistics also demonstrate that annually on average, there aren't many publications on combustion methods.

The volatile nature of this analyte makes decomposition techniques like ashing extremely vulnerable to cross-contamination and mercury loss. Furthermore, because they use pricey quartz jars, which are not readily available in most laboratories, other breakdown techniques like microwave-induced combustion are costly.

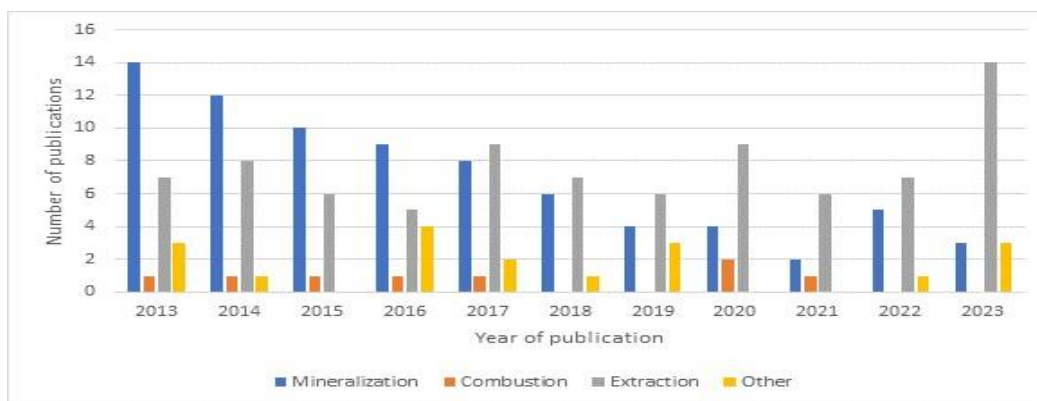


Figure 2. 16: The number of publications detailing various sample preparation techniques before spectrometric measurement of total mercury in non-aqueous matrices.

Additionally, we must scrutinize the most favored extraction methods (SPE, LLE, and others) for quantitatively determining total mercury in non-aqueous matrices. The number of publications fluctuated with almost all the procedures (**Fig.2.17**). Few extraction steps were recorded for LLE, which led to shorter extraction times in most LLE procedures, which made LLE more popular than SPE. Furthermore, the LLE process is more economical and ecologically beneficial due to the use of only a few reagents (diluted acid and dispenser solvent/surfactant). On the other hand, the synthesis of adsorbents under SPE and eluent solution requires many chemicals, which raises the expense of the analysis. Additionally, the synthesis of the sorbent and the adsorption and desorption processes can take longer with this approach, making it time-consuming. Throughout the ten years, SPE only displayed 28 publications, while LLE displayed 65. About 18 papers covering the other extraction techniques (MAE and UAE) were also reported between 2013 and 2023.



Figure 2. 17: Number of publications reported for different extraction methods for total determination of mercury in non-aqueous matrices.

It is also very crucial to investigate which matrix has been studied for the total determination of mercury in non-aqueous matrices. As we have mentioned earlier in our introduction, mercury enters the environment through natural and human activities, but the main route in which this toxic analyte enters living organisms is through food. Hence, **Fig. 2.18** reveals that food matrices were the most studied mercury matrices (57 publications). Food matrices are very different such as fish, seafood, chicken meat, canned vegetables, fishery products, canned fish, cereals, dietary supplements, etc. The largest number of papers in food matrices was

primarily contributed by fish. This hazardous analyte is mostly exposed to the latter through industrial discharge and atmospheric deposition. They acquire mercury in its most poisonous form, methyl mercury, which can bioaccumulate and biomagnifies up the food chain. This explains why food matrices have been the subject of most research over the years.

It is also vital to quantify the amount of mercury in our environment because it is regarded as a toxic, persistent, and bioaccumulate pollutant. Hence, environmental samples such as sediments, soil, particulate matter, sand, and clay were also investigated. A total of 25 publications were reported. Botanical samples such as leaves, vegetables, rice, and wheat were also reported in 15 publications. The category “other” in **Fig. 2.18** includes human hair, lipstick, nails, mushrooms, phosphate fertilizers, nuts, and pharmaceutical products. A total of 47 publications were reported. Lastly, **Fig. 2.18** shows that the least studied matrices are fossil fuels (11 publications). Coal, crude oil, and their derivatives (kerosene, diesel, and gasoline) are all classified as fossil fuels. This could be because using fossil fuels presents difficulties because of their high organic load. Therefore, there is still a great deal of study to be done on fossil fuels.

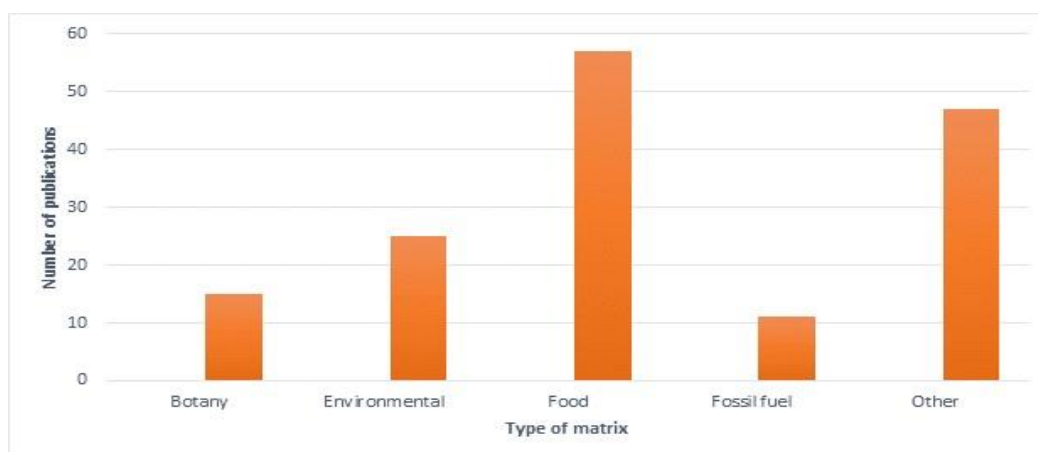


Figure 2. 18: Number of publications for different non-aqueous matrices.

There have been reports of various analytical methods for measuring mercury in non-aqueous matrices. Following sample preparation, **Fig. 2.19** illustrates the several spectrometric methods that have been used to measure mercury in nonaqueous matrices. The most used analytical technique for the quantification of

mercury is the CV-AAS. Mercury is known as a volatile analyte that exists in low abundance in most matrices, then CV-AAS is proven to have the required sensitivity for mercury quantification [181].

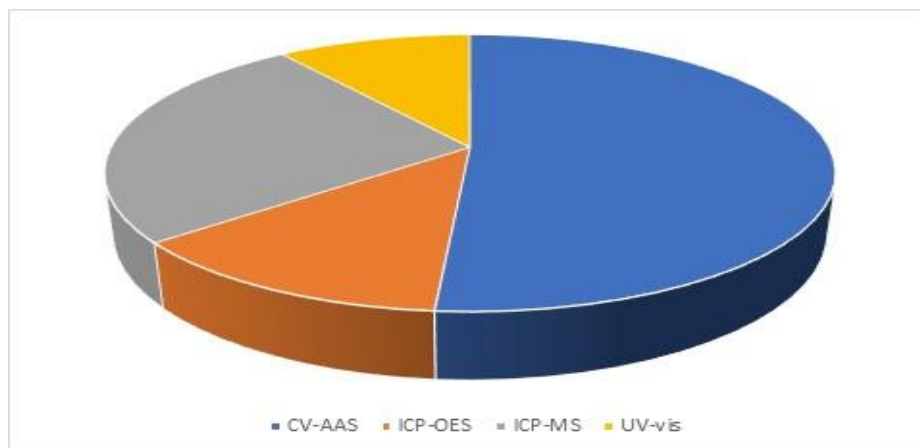


Figure 2. 19: Analytical techniques that have been reported for the spectrometric determination of total mercury in non-aqueous matrices.

Finally, it is paramount to ascertain which optimization strategy has been the most reported from 2013 to 2023 for the total determination of mercury in non-aqueous matrices. **Figure 2.20** presents the summary of each optimization strategy. From the figure, we observe that the multivariate optimization strategy has been the most utilized strategy for different sample preparation methods for quantifying mercury in nonaqueous matrices. This is because of the merits the strategy possesses. As mentioned earlier, a multivariate optimization strategy saves time and reagents. Above all, it considers the interaction of two or more factors, something that cannot be achieved with univariate optimization [181].

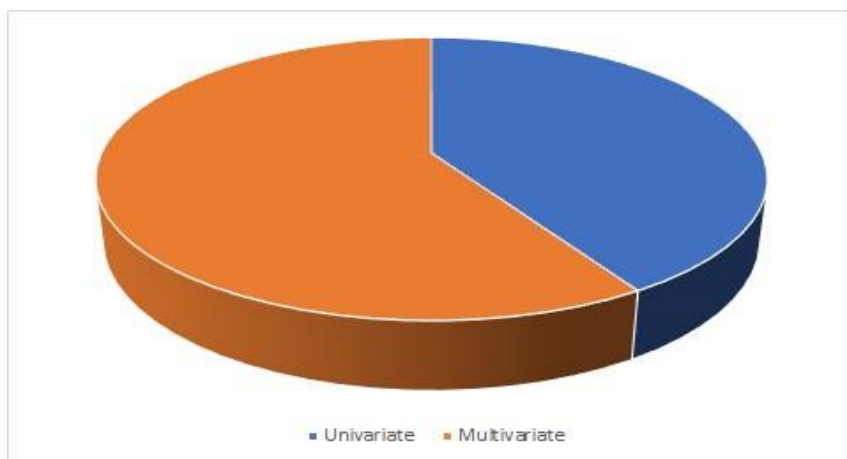


Figure 2. 20: Optimization strategies for sample preparation methods.

2.6 Conclusion

It can be summarized that the recent trends of the sample preparation methods before the spectrometric determination of mercury in nonaqueous matrices have been critically evaluated. Based on the number of publications reported from 2013 to 2023, the total determination of total mercury in fossil fuels and their derivatives such as gasoline, diesel, and kerosene has been poorly reported. Hence, the conceptualization of this study. It is important to note that the analysis of mercury in fossil fuels and their derivatives such as gasoline, diesel oil, and kerosene is paramount since these energy resources are being utilized daily. Under mineralization procedures, MW-AD is the most reported mineralization method. Concentrated HNO_3 has been widely used as a digestion agent. Hence this proposed work aims to use nitric acid with diluted H_2O_2 to mineralize fuel matrices. Using diluted H_2O_2 with HNO_3 minimizes the risks associated with the corrosive nature of HNO_3 and the production of carcinogenic nitrous oxides.

From the above investigation, it can be concluded that D-LLME has been widely reported for the total determination of mercury in non-aqueous matrices. This is due to the merits of the protocol, such as low costs, simplicity, and high enrichment factors, among others. To the best of our knowledge, deep eutectic solvents (DESs) have been poorly employed as extracting solvents to quantify mercury in fuel matrices. Deep eutectic solvents have low vapor pressure and low flammability, regarded as the green generation of ionic liquids. Hence, this current study aims to investigate the use of DESs as extractants for quantifying mercury in fuel matrices

based on a D-LLME procedure. Under SPE, the coupling of m-SPME and D-SPME has been widely reported for the quantification of mercury. To the best of our knowledge, no study has reported using magnetic graphene oxide coated with gold nanoparticles to quantify mercury in fuel matrices. Hence, this study aims to investigate using this adsorbent in an m-DSPME procedure. The use of ICP-OES has been poorly reported in the literature. This might be due to the low detection limits, poor sensitivity of the instrument towards mercury, and the memory effect. Lastly, multivariate optimization has gained much more attention than univariate strategies. Hence, the current study aims to utilize multivariate strategies to effectively develop our sample preparation methods for quantifying mercury in fuel matrices.

REFERENCES

- [1] Y. Peng, N. Shi, J. Wang, T. Wang, and W. P. Pan, *Total Environ.*, 787 (2021). 147597.
- [2] A. Gerard and S. Sa, 2013.
- [3] A. Saturday, *J. Environ. Heal. Sci.* 4 (2018) 37–43.
- [4] S. T. Zulaikhah, J. Wahyuwibowo, and A. A. Pratama, *Int. J. Public Heal. Sci.* 9 (2020) 103–114.
- [5] G. S. S. Nchez, (2013) 54–62.
- [6] J. A. Rodríguez Martín *Environ. Pollut.*, 283 (2021) 117397.
- [7] D. L. E. Uaciquete, K. Sakusabe, T. Kato, H. Okawa, K. Sugawara, and R. Nonaka, *Fuel*, 300 (2021) 120802.
- [8] C. Freire *Environ. Res.* 110 (2010) 96–104.
- [9] N. S. Mdluli, P. N. Nomngongo, and N. Mketi, *Crit. Rev. Anal. Chem.* (2020) 1–18.
- [10] H. Lin *Sensors Actuators, B Chem.*, 335 (2021) 129716.
- [11] J. Van Gerpen, *Fuel Process. Technol.*, 86 (2005) 1097–1107.
- [12] P. A. Mello, J. S. F. Pereira, M. F. Mesko, J. S. Barin, and E. M. M. Flores, *Anal. Chim. Acta*, 746 (2012) 15–36.
- [13] Jozef Stefan Institute, *UN Environ.* (2019).
- [14] V. S. Souza, L. S. G. Teixeira, M. G. A. Korn, U. M. F. M. Cerqueira, and M. A. Bezerra, *Fuel*, 242 (2018) 479–486.
- [15] N. Mketi, P. N. Nomngongo, and J. C. Ngila, *Trends Anal. Chem.* 85 (2016) 107–116.
- [16] J. S. Barin, P. A. Mello, M. F. Mesko, F. A. Duarte, and E. M. M. Flores, *Anal. Bioanal. Chem.* 408 (2016) 4547–4566.
- [17] W. Routray and V. Orsat, *Food Bioprocess Technol.*, 5 (2012) 409–424.
- [18] N. Mketi, P. N. Nomngongo, and J. C. Ngila, *Microchem. J.* 124 (2016) 201–208.
- [19] G. Islas, I. S. Ibarra, P. Hernandez, J. M. Miranda, and A. Cepeda, (2017).
- [20] C. H. Park, Y. Eom, L. J. E. Lee, and T. G. Lee, *Chemosphere*, 93 (2013) 9–13.
- [21] E. Q. Oreste, A. de Jesus, R. M. de Oliveira, M. M. da Silva, M. A. Vieira, and A. S. Ribeiro, *Microchem. J.* 109 (2012) 5–9.
- [22] J. P. Santos, L. Mehmeti, and V. I. Slaveykova, *Methods Protoc.* 5 (2022).
- [23] G. S. Yáñez-Jácome, D. Romero-Estévez, H. Navarrete, K. Simbaña-Farinango, and P. Y. Vélez-Terreros, *Methods Protoc.* 3 (2020) 1–12, 2020.
- [24] M. Esposito, A. De Roma, R. La Nucara, G. Picazio, and P. Gallo,

- Chemosphere,197 (2018) 14–19.
- [25] S. Zrelli *Biol. Trace Elem. Res.*199 (2021) 721–731.
- [26] N. J. Novakov, *Food Addit. Contam. Part B Surveill.*10 (2017) 208–215.
- [27] B. K. K. K. Jinadasa, E. M. R. K. B. Edirisinghe, and I. Wickramasinghe, *Food Addit. Contam. Part B Surveill.* 7 (2014) 309–314.
- [28] K. E. Kristian, S. Friedbauer, D. Kabashi, K. M. Ferencz, J. C. Barajas, and K. Obrien, *J. Chem. Educ.*,92 (2015) 698–702.
- [29] G. Kaya and S. Türkoğlu, *Environ. Sci. Pollut. Res.* 24 (2017) 9495–9505.
- [30] C. Vieira, S. Morais, S. Ramos, C. Delerue-Matos, and M. B. P. P. Oliveira, *Food Chem. Toxicol* 49 (2011). 923–932.
- [31] D. R. Nimmo, *Springerplus*, 5 (2016).
- [32] G. Kaya and S. Turkoglu, *Food Addit. Contam. Part B Surveill.*,11 (2018) 1–8.
- [33] C. Plessl *Sci. Total Environ.* 659 (2019) 1158–1167.
- [34] H. Jiang, D. Qin, Z. Chen, S. Tang, S. Bai, and Z. Mou, *Bull. Environ. Contam. Toxicol.* 97 (2016) 536–542.
- [35] N. Bansal, J. Vaughan, A. Boulemant, and T. Leong, *Microchem. J.*, 113 (2014) 36–41.
- [36] M. A. Morgano, L. C. Rabonato, R. F. Milani, L. Miyagusku, and K. D. Quintaes, *Food Control*, 36 (2014) 24–29.
- [37] V. M. Shchukin, E. S. Zhigilei, A. A. Erina, Y. N. Shvetsova, N. E. Kuz'mina, and A. I. Luttseva, *Pharm. Chem. J.*,54 (2020) 968–976.
- [38] E. Evgenakis, C. Christophoridis, and K. Fytianos, *Environ. Sci. Pollut. Res.*25 (2018) 26766–26779.
- [39] A. Maage, B. M. Nilsen, K. Julshamn, L. Frøyland, and S. Valdersnes, *Bull. Environ. Contam. Toxicol.*,99 (2017) 161–166.
- [40] S. Shabani, H. Ezzatpanah, M. M. A. Boojar, M. Seyedein Ardebili, and M. H. Givianrad, *Qual. Assur. Saf. Crop. Foods*, 7 (2015) 509–515.
- [41] V. Osuna-Vallejo, C. Sáenz-Romero, L. Escalera-Vázquez, E. de la Barrera, and R. Lindig-Cisneros, *Bull. Environ. Contam. Toxicol.*102 (2019) 19–24.
- [42] E. Vassileva, A. A. Krata, and S. Azemard, *Accredit. Qual. Assur.* 25,(2020) 221–231.
- [43] P. Jeevanaraj, Z. Hashim, S. Mohd, and A. Zaharin, *Int. J. Sci. Basic Appl. Res.*,24 (2015) 332–347.
- [44] T. Frentiu *Anal. Methods*,7 (2015) 747–752.
- [45] H. S. Canbay and M. Doğantürk, *Eurasian J. Anal. Chem.*,12 (2017) 45–53.
- [46] L. O. B. Silva, D. G. da Silva, D. J. Leao, G. D. Matos, and S. L. C. Ferreira, *Food Anal. Methods*, 5 (2012) 1289–1295.

- [47] B. K. K. K. Jinadasa, 2 (2015) 35–40.
- [48] Y. Zhao *Spectrochim. Acta - Part B At. Spectrosc.*, 112 (2015) 6–9.
- [49] B. K. K. K. Jinadasa, G. S. Chaturika, G. D. T. M. Jayasinghe, and C. D. Jayaweera, *Heliyon*, 5 (2019).
- [50] O. Miedico, M. Iammarino, C. Pompa, M. Tarallo, and A. E. Chiaravalle, *Food Addit. Contam. Part B Surveill.*, 8(2015) 85–92.
- [51] E. A. Renieri, *Food Chem. Toxicol.* 124 (2019) 439–449.
- [52] A. Q. Shah, T. G. Kazi, H. I. Afridi, and M. B. Arain, *Toxicol. Ind. Health*, 32 (2016) 1033–1041.
- [53] M. Slávik, T. Tóth, Árvay Július, L. Harangozo, and M. Kopernická, *Potravinárstvo*, 10 (2016) 232–236.
- [54] A. De Roma, M. Esposito, E. Chiaravalle, O. Miedico, S. P. De Filippis, and G. Brambilla, *J. Food Compos. Anal.*, 63(2017) 28–33.
- [55] M. Ahmadpour, L. Lan-Hai, M. Ahmadpour, S. H. Hoseini, A. Mashrofeh, and Ł. J. Binkowski, *Environ. Monit. Assess.*, 188 (2016).
- [56] Y. Fiamegos, *TrAC - Trends Anal. Chem.* 85 (2016) 57–66.
- [57] E. Covaci, *J. Anal. At. Spectrom.*, 33 (2018) 799–808.
- [58] S. Zhang and M. Zhou, *J. Anal. Methods Chem.*, (2020).
- [59] K. Deering, *Environ. Monit. Assess.*, 191 (2019).
- [60] R. Fernández-Martínez, I. Rucandio, I. Gómez-Pinilla, F. Borlaf, F. García, and M. T. Larrea, *J. Food Compos. Anal.*, 38 (2015) 7–12.
- [61] F. V. M. Pontes, *Fuel Process. Technol.* 106 (2013) 122–126.
- [62] E. Mohammed, T. Mohammed, and A. Mohammed, *MethodsX*, 4 (2017) 513–523.
- [63] D. B. Chu, H. T. Duong, M. T. Nguyet Luu, H. A. Vu-Thi, B. T. Ly, and V. D. Loi, *J. Anal. Methods Chem.* (2021).
- [64] H. Wuyke, T. Oropeza, and L. Feo, *Anal. Methods*, 9 (2017) 1152–1160.
- [65] A. Karim, T. Mohammad, and A. Thamer, (2020).
- [66] K. Shen, N. Zhang, X. Yang, Z. Li, Y. Zhang, and T. Zhou, *Appl. Spectrosc. Rev.* 50 (2015) 304–331.
- [67] L. Hu, X. Lu, and J. Ma, *BioResources*, 15 (2020) 2096–2110.
- [68] A. Szymczycha-Madeja, M. Welna, D. Jedryczko, and P. Pohl, *TrAC - Trends Anal. Chem.*, 55 (2014) 68–80.
- [69] J. P. Souza, C. Cerveira, T. M. Miceli, D. P. Moraes, M. F. Mesko, and J. S. F. Pereira, *Food Chem.*, 321(2019) 126715.
- [70] R. S. Picoloto, H. Wiltsche, G. Knapp, P. A. Mello, J. S. Barin, and E. M. M. Flores, *Spectrochim. Acta - Part B At. Spectrosc.*, 86 (2013) 123–130.

- [71] M. Stefani, *Microchem. J.*, 124 (2016) 321–325.
- [72] M. S. P. Enders, J. P. de Souza, P. Balestrin, P. de A. Mello, F. A. Duarte, and E. I. Muller, *Microchem. J.* 124 (2016) 321–325.
- [73] J. S. Barin, *J. Anal. At. Spectrom.*, 29 (2014) 352–358.
- [74] A. L. H. Muller, E. I. Muller, J. S. Barin, and E. M. M. Flores, *Anal. Methods* 7 (2015) 5218–5225.
- [75] M. Saraji and M. K. Boroujeni, 406 (2014).
- [76] M. M. Techniques, (2018)..
- [77] “Schematic-diagram-of-a-dispersive-liquid-liquid-microextraction-DLLME-procedure.” .
- [78] M. Hossien-poor-Zaryabi, M. Chamsaz, T. Heidari, M. H. A. Zavar, M. Behbahani, and M. Salarian, *Food Anal. Methods*, 7 (2014) 352–359.
- [79] “Extraction and determination of heavy metals in soil and vegetables irrigated with treated municipal wastewater using new mode of dispersive liquid – liquid microextraction based on the solidified deep eutectic solvent followed by GFAAS Mohammad Hossein H,” no. June, 2018, doi: 10.1002/jsfa.9230.
- [80] M. Rezaee, Y. Assadi, M. R. Milani Hosseini, E. Aghaee, F. Ahmadi, and S. Berijani, *J. Chromatogr.* 1116 (2006) 1–9.
- [81] I. M. Dittert, T. A. Maranhão, D. L. G. Borges, M. A. Vieira, B. Welz, and A. J. Curtius, *Talanta*, 72 (2007) 1786–1790.
- [82] A. Daneshfar and T. Khezeli, *J. Surfactants Deterg.* 17 (2014) 1259–1267.
- [83] A. Morni and S. M. Mostafavi, *Anal. Methods Environ. Chem. J.*, 3 (2020) 63–71.
- [84] M. Xie *J. Sep. Sci.*, 44 (2021) 2457–2464.
- [85] L. P. Yu, *J. Agric. Food Chem.*, 53 (2005) 9656–9662.
- [86] A. Thongsaw, R. Sananmuang, Y. Udnan, G. M. Ross, and W. C. Chaiyasith, *Spectrochim. Acta - Part B At. Spectrosc.*, 160 (2019) 105685.
- [87] S. Tang, *Trends Anal. Chem.* 108 (2018) 306–313.
- [88] N. S. Mdluli, P. N. Nomngongo, and N. Mketi, *Crit. Rev. Anal. Chem.* (2020). 1–18.
- [89] C. Mitani, A. Kotzamanidou, and A. N. Anthemidis, *J. Anal. At. Spectrom.*, 29 (2014) 1491–1498.
- [90] M. Ghambarian, Y. Yamini, and A. Esrafil, *Microchim. Acta*, 177 (2012) 3–4 271–294.
- [91] H. Jiang, B. Hu, B. Chen, and W. Zu, 63, (2008) 770–776.
- [92] Y. M. He, F. F. Zhao, Y. Zhou, F. Ahmad, and Z. X. Ling, *Anal. Methods*, 7(2015) 4493–4501.
- [93] P. O. Vicentino and R. J. Cassella, *Talanta*, 162(2017) 249–255.

- [94] “Automated liquid-liquid extraction procedure for the photometric determination of nanogram levels of Hg(II) in soil and sediment extracts - ScienceDirect.” .
- [95] G. Souza Valasques, *Food Chem.*,318 (2020). 126473.
- [96] G. Souza, *Food Chem.*,318 (2020) 126473.
- [97] P. D. O. Vicentino, D. M. Brum, and R. J. Cassella, *Talanta*,132 (2014) 733–738.
- [98] M. Khan and M. Soylak, *Anal. Lett.*,56 (2023) 1161–1173.
- [99] N. Altunay, A. Elik, and R. Gürkan, *Food Addit. Contam. - Part A Chem. Anal. Control. Expo. Risk Assess.*,36 (2019) 1079–1097.
- [100] M. Pirsahab and N. Fattahi, *Anal. Methods*, 7 (2015) 6266–6273.
- [101] R. M. Menezes, W. Nei, and L. Santos, (2020).
- [102] M. Hayati, M. Ramezani, and G. R. Bardajee, *Sep. Sci. Technol.*,(2021)1–10.
- [103] E. Ragheb, M. Shamsipur, F. Jalali, M. Sadeghi, and N. Babajani, *Microchem. J.*,166 (2021) 106209.
- [104] M. Hayati, M. Ramezani, G. Rezanejade Bardajee, and T. Momeni Isfahani, *Sep. Sci. Technol.*,57 (2022) 274–283.
- [105] J. Ali, M. Tuzen, and T. G. Kazi, *J. AOAC Int.*,100 (2017) 782–788.
- [106] P. Liang, J. Yu, E. Yang, and Y. Mo, (2015) 236–242.
- [107] A. Akhtar, T. G. Kazi, H. I. Afridi, J. A. Baig, S. G. Musharraf, and M. B. Arain, *Chem. Pap.*, 75 (2021) 3005–3015.
- [108] A. Gouda, R. elsheikh, W. Hassan, S. Ibrahim, and A. Youssef, *Bull. Fac. Sci. Zagazig Univ.* (2020) 12–22.
- [109] L. Pelit, I. Bağatir, F. O. Pelit, and F. N. Ertaş, *RSC Adv.*4 (2014) 32189–32196.
- [110] R. G. Wuilloud, (2010)1432–1439.
- [111] S. Gil, S. Fragueiro, I. Lavilla, and C. Bendicho, 60 (2005) 145–150.
- [112] C. Zeng, M. Li, Q. Xie, H. Yan, and X. Zhang, *Spectrosc. Lett.*, 48 (2015) 653–659.
- [113] E. Ragheb, M. Shamsipur, F. Jalali, M. Sadeghi, N. Babajani, and N. Mafakheri, *Microchem. J.*,166 (2020), 106209.
- [114] *A. Sci*, (2016).
- [115] I. Liška, J. Krupčík, and P. A. Leclercq, *J. High Resolut. Chromatogr.*12, (1989) 577–590.
- [116] M. E. I. Badawy, M. A. M. El, P. K. Kimani, L. W. Lim, and E. I. Rabea, 38 (2022).
- [117] P. N. Kunene (2019).
- [118] “Solid phase extraction of mercury on sulfur loaded with N-(2-chloro benzoyl)-N'-phenylthiourea as a new adsorbent and determination by cold vapor atomic absorption spectrometry - ScienceDirect_YDESIR.” .

- [119] A. R. Türker, *Sep. Purif. Rev.*,41 (2012) 169–206.
- [120] M. E. T. Padrón, C. Afonso-Olivares, Z. Sosa-Ferrera, and J. J. Santana-Rodríguez, *Molecules*,19 (2014) 10320–10349.
- [121] E. Yavuz, Ş. Tokal, and Ş. Patat, 142 (2018) 85–93.
- [122] E. Öztürk Er, G. Dalgıç Bozyiğit, Ç. Büyükpınar, and S. Bakırdere, *Crit. Rev. Anal. Chem.*,52 (2022) 231–249.
- [123] F. Faryadras, S. M. Yousefi, P. Jamshidi, and F. Shemirani, *Res. Chem. Intermed.*,46 (2020) 2055–2068.
- [124] S. Seidi and M. Fotouhi, *Anal. Methods*, 9 (2017) 803–813.
- [125] V. Jalili, A. Barkhordari, and A. Ghiasvand, *Microchem. J.* 152 (2020).
- [126] E. Stanisz, J. Werner, and H. Matusiewicz, *Microchem. J.*,114 (2014) 229–237.
- [127] H. Shirkhanloo, A. Khaligh, H. Zavvar, and A. Rashidi, *Microchem. J.*130 (2017) 245–254.
- [128] A. Nasrollahpour, S. M. J. Moradi, and S. E. Moradi, *J. Serbian Chem. Soc.*, 82 (2017) 551–565.
- [129] M. Ghorbani, M. Aghamohammadhassan, M. Chamsaz, H. Akhlaghi, and T. Pedramrad, *TrAC - Trends Anal. Chem.*,118 (2019) 793–809.
- [130] L. O. Dos Santos and V. A. Lemos, *Water. Air. Soil Pollut.*,225 (2014).
- [131] M. Sadeghi, *RSC Adv.*, 5 (2015) 100511–100521.
- [132] T. Ahmadi, S. Bahar, G. Mohammadi Ziarani, and A. Badiei, *Food Chem.* 300 (2019) 125180.
- [133] M. Reza, R. Kahkha, S. Daliran, and A. R. Oveisi,(2017) 2175–2184.
- [134] S. Goudarzi, B. Fahimirad, M. Rajabi, and O. Baigenzhenov, *Environ. Sci. Pollut. Res.* (2022).
- [135] I. López-García, Y. Vicente-Martínez, and M. Hernández-Córdoba, *J. Anal. At. Spectrom.*,30 (2015) 1980–1987.
- [136] Y. He, N. Li, and J. J. Ma, *J. Chem. Soc. Pakistan*, 36 (2015) 1162–1168.
- [137] E. Vereda, *Talanta*, 153 (2016) 228–239.
- [138] S. Jamshidi, M. K. Rofouei, S. Seidi, and Å. Emmer, *Sep. Sci. Technol.*,55 (2020) 1505–1514.
- [139] J. C. García-Mesa, P. Montoro-Leal, S. Maireles-Rivas, M. M. López Guerrero, and E. Vereda Alonso, *J. Anal. At. Spectrom.*,36 (2021) 892–899.
- [140] B. Veisi, B. Lorestani, S. S. Ardakani, M. Cheraghi, and L. Tayebi, *Appl. Organomet. Chem.*,35 (2021)1–11.
- [141] *J. Of*,38, no. 7, 2015.
- [142] Z. Es, G. R. Bardajee, and S. Azimi, *Microchem. J.*,127 (2016) 170–177.

- [143] S. Seidi and M. Fotouhi,(2017) 803–813.
- [144] A. Keramat and R. Zare-Dorabei, *Ultrason. Sonochem.*,38 (2017) 421–429.
- [145] E. Ragheb, M. Shamsipur, F. Jalali, M. Sadeghi, N. Babajani, and N. Mafakheri, *Microchem. J.*166 (2021).
- [146] B. Ambedkar, T. N. Chintala, R. Nagarajan, and S. Jayanti, *Chem. Eng. Process. Process Intensif.*,50 (2011) 236–246.
- [147] M. R. González-Centeno, F. Comas-Serra, A. Femenia, C. Rosselló, and S. Simal, *Ultrason. Sonochem.*,22 (2015) 506–514.
- [148] D. J. Leao, M. M. Silva Junior, J. B. Silva Junior, D. A. F. De Oliveira, A. F. S. Queiroz, and S. L. C. Ferreira, *Anal. Methods*,8 (2016) 6554–6559.
- [149] B. Kaufmann and P. Christen, *Phytochem. Anal.*,13 (2002) 105–113.
- [150] P. Kościelniak and M. Wieczorek, *Anal. Chim. Acta*, 944 (2016)14–28.
- [151] M. A. Bezerra, Q. O. dos Santos, A. G. Santos, C. G. Novaes, S. L. C. Ferreira, and V. S. de Souza, *Microchem. J.*124 (2016) 45–54.
- [152] S. De Oliveira Souza, L. L. François, A. R. Borges, M. G. R. Vale, and R. G. O. Araujo, *Spectrochim. Acta - Part B At. Spectrosc.*,114 (2015) 58–64.
- [153] R. F. Teófilo and M. M. C. Ferreira, *Quim. Nova*, 29 (2006) 338–350.
- [154] N. Kumar, A. Bansal, G. S. Sarma, and R. K. Rawal, *Talanta*, 123 (2014) 186–199.
- [155] M. P. Callao, *TrAC - Trends Anal. Chem.*,62 (2014) 86–92.
- [156] T. Næs, O. Tomic, K. Greiff, and K. Thyholt, *Food Qual. Prefer.*, 33 (2014) 64–73.
- [157] M. A. Bezerra, R. E. Santelli, E. P. Oliveira, L. S. Villar, and L. A. Escaleira, *Talanta*,76 (2008) 965–977.
- [158] R. G. Brereton, J. Jansen, J. Lopes, F. Marini, A. Pomerantsev, and O. Rodionova,(2018) 6691–6704.
- [159] J. Zolgharnein, A. Shahmoradi, and J. B. Ghasemi, *J. Chemom.*,27 (2013) 1–2.
- [160] V. Rajadurai, B. L. Anguraj, M. Inbasekaran, and H. Manivannan, *Chem. Pap.*,76 (2022) 2677–2690..
- [161] L. Mousavi, Z. Tamiji, and M. R. Khoshayand, *Talanta*,190 (2018) 335–356.
- [162] S. L. C. Ferreira, *Food Chem.*, 273 (2019) 3–8.
- [163] M. A. Bezerra, *Talanta* 194(2018) 941–959.
- [164] L. Adlnasab, H. Ebrahimzadeh, A. A. Asgharinezhad, M. N. Aghdam, A. Dehghani, and S. Esmaeilpour, *Food Anal. Methods*, 7 (2014) 628.
- [165] D. L. F. da Silva, M. A. P. da Costa, L. O. B. Silva, and W. N. L. dos Santos, *Food Chem.*,273 (2019) 24–30.
- [166] L. M. Khaskhanova, *J. Int. Dent. Med. Res.*, 15 (2022) 107–110.

- [167] A. Abdullah and A. Mohammed, Proc. 2018 Int. Conf. Hydraul. Pneum. - HERVEX, (2019) 77–85.
- [168] L. E. Franken, E. J. Boekema, and M. C. A. Stuart, Adv. Sci.,4 (2017) 1–9.
- [169] Z. L. Wang, Adv. Mater.,15 (2003) 1497–1514.
- [170] F. R. van de Voort, Food Res. Int.,25(1992) 397–403.
- [171] F. S. Rocha, A. J. Gomes, C. N. Lunardi, S. Kaliaguine, and G. S. Patience, Can. J. Chem. Eng.,96 (2018) 2512–2517.
- [172] M. Picollo, M. Aceto, and T. Vitorino, Phys. Sci. Rev., 4 (2019) 1–14.
- [173] A. Ali, Y. W. Chiang, and R. M. Santos, Minerals,12 (2022).
- [174] A. A. Bunaciu, E. gabriela Udriștioiu, and H. Y. Aboul-Enein, Crit. Rev. Anal. Chem.45 (2015) 289–299.
- [175] J. Yu, Mar. Pollut. Bull.,145 (2019) 153–160.
- [176] M. A. Khan and Y.-S. Ho, Environ. Eng. Manag. J.,14 (2018) 2163–2168.
- [177] P. Sinha, A. Datar, C. Jeong, X. Deng, Y. G. Chung, and L. C. Lin, J. Phys. Chem. C,123 (2019) 20195–20209.
- [178] J. H. F. Bothwell and J. L. Griffin, Biol. Rev.,86 (2011) 493–510.
- [179] A. J. Simpson, M. J. Simpson, and R. Soong, Environ. Sci. Technol., 46 (2012) 11488–11496.
- [180] W. Yang, Y. Gao, and J. F. Casey, Solut. Chem. Adv. Res. Appl. (2018) 159–205.
- [181] S. L. C. Food Chem.,273 (2017) 3–8.

Novel microwave assisted-hydrogen peroxide digestion of fuel oils using methionine as a capping reagent for the determination of mercury by inductively coupled plasma-optical emission spectrometry

ABSTRACT

Fossil fuels and their derivatives naturally contain impurities, such as mercury, due to the nature of their genesis. Accurately determining mercury remains a challenge in Analytical chemistry due to the volatile nature of mercury. A new analytical method was developed for routinely analyzing and quantifying total mercury in fuel oils using methionine as a capping reagent. For the development of the new method, parameters such as sample mass, methionine concentration, hydrogen peroxide concentration, time and temperature were optimized. Methionine was added to both fuel samples before microwave-assisted hydrogen peroxide digestion (MW-AHPD) and standard solutions as a preserving agent. It was also added to the inductively coupled plasma-optical emission spectrometry (ICP-OES) rinse solutions to eliminate the memory effect. To the best of our knowledge, it is the first-time methionine was used as a capping reagent for the total determination of mercury in fuel oils using ICP-OES with a pneumatic nebulizer. Multivariate optimization tools (two-level half factorial and central composite design) were used to investigate the most influential parameters of the MW-AHPD method. The optimum conditions obtained were 0.1 g, 5 M [H₂O₂], 5.95 M [methionine], 36 minutes extraction time at 200 °C with accepted accuracy which ranged from 93-107 % and good precision of 1.94 %. The developed MW-AHPD procedure culminated in linearity coefficient of 0.9989, limit of detection of 0.25 µg/L and limit of quantification of 0.8 µg/L, respectively. The developed MW-AHPD procedure was applied in real coal, crude oil, gasoline, diesel oil, and kerosene. The concentration obtained ranged from 0.876±0.023 - 0.975±0.025 µg/g in coal samples, 0.383±0.043 - 0.506±0.105 µg/g for crude oil samples, 0.306±0.010 - 0.390±0.035 µg/g for gasoline samples, 0.360±0.003 - 0.434±0.050 µg/g for diesel oil samples and all kerosene samples were below detection limit of the instrument, therefore no Hg were detected.

3.1. Introduction

Mercury is regarded as a toxic pollutant that has been widely studied for the past decades to its detrimental human health effects and environmental adverse effects. This toxic pollutant naturally exists in different forms in the environment, each with its own peculiar behavior and toxicity [1]. Mercury has existed within the environment for centuries and its concentration accumulates in environmental matrices and tissues of living organisms, and this has been observed as you move up the food chain, which makes it more detrimental to our ecosystem [2]. In human health, mercury is known for adverse effects in damaging the central nervous, digestive, respiratory, and kidneys [3]. This toxic element exists naturally in fossil fuels and cannot be controlled. Therefore, application of these fossil fuels and their derivatives are responsible for mobilization/ release of this toxic pollutant within the environment [4]. This has brought attention to several researchers to try and develop several analytical methods that can accurately quantify the amount of mercury in these energy resources, as this would help properly design and develop future clean up strategies of mercury from these matrices.

The main challenge with fuel oils analysis is that they cannot be introduced directly into the analytical instrument due to their high carbon content and they are not compatible with conventional detection techniques used for the quantification of Hg in oil samples. Hence, sample preparation is necessary to decompose the high organic load into an aqueous matrix compatible with the analytical instrument [5]. Various mineralization procedures for mineralizing organic matrices have been reported in the literature. This includes open vessel digestion, dry ashing microwave-assisted acid digestion (MWAD), and microwave-induced combustion (MIC) among others [6–8]. However, there are limitations that are reported in the application of the sample preparation techniques. Open vessel digestion and dry ashing procedures suffer from systematic errors due to cross-contamination risks and loss of volatile species [9]. MWAD makes use of concentrated acids like nitric acid (HNO₃), hydrofluoric acid (HF), perchloric acid (HClO₄) and hydrochloric acid (HCl), which all have negative health and environmental effects. Concentrated inorganic acids (HNO₃, H₂SO₄, HCl, HF, and HClO₄) are corrosive, take a long cooling time to open the vessels, emit carcinogenic gases and alter the physical look of the digests, which might result in interferences.

HCl and HF can also dissolve spectrometric glass optics [10,11]. On the other hand, MIC requires costly oxygen quartz vessels [12,13].

Conventionally, various analytical techniques have been employed to determine mercury in various matrices. This includes atomic-based techniques like cold vapor absorption spectrometry (CV-AAS) and cold vapor atomic fluorescence spectrometry (CV-AFS) and plasma-based techniques (inductively coupled plasma-optical emission spectroscopy (ICP-OES) and inductively coupled plasma-mass spectrometry (ICPMS) among others [14–16]. CV-AAS and CV-AFS are the most recommended techniques by the United States Environmental protection Agency (EPA) for Hg analysis. In 2023, Koesmawati and coworkers [17] conducted a study to determine mercury in fish using CV-AAS. Another interesting study was reported by Astolfi and coworkers [18] to determine mercury in hair using CV-AFS.

Inductively coupled plasma-optical emission spectroscopy elemental analysis is simple, fast, accurate, and tolerates high organic content. However, ICP-OES mercury measurements have been plagued by severe memory effects, sample instability and poor mercury detection limits. Hence, chemical vapor generation (CVG) and hydride generation (HG) are usually coupled to this technique for mercury analysis. In 2010 April and coworkers [19] reported the determination of mercury in wine by HG-ICP-OES. In 2022, a study was reported by El-Safty et al. [20] for the rapid determination of mercury in the dust using CV-ICP-OES. Alternatively, other researchers employ gold and hydrochloric acid as stabilizing agents and eliminate the memory effect for mercury analysis using ICP-OES. However, gold is expensive, and the chloride ions from HCl can lead to interferences [21]

Therefore, this study aimed to investigate using methionine as a preserving reagent for mercury when subjected to microwave radiation and eliminating the memory effect when solutions are introduced in ICP-OES using a pneumatic nebulizer. To our knowledge, it is the first time that methionine was investigated as a capping reagent for mercury under microwave-assisted hydrogen peroxide digestion (MWAHPD) followed by ICP-OES. The logic behind testing methionine as a capping reagent is that mercury is a soft acid with high affinity for soft bases such as sulfur containing compounds [22,23]. Multivariate optimization was employed to investigate

the most important extraction factors. The application of multivariate allows the simultaneous optimization of several extraction factors for an approach with limited experiments [24]. Therefore, it reduces analysis times and improves detection of analytes. Additionally, it identifies the variables that have the greatest effects and considers interactions between variables that influence the extraction and analytical response [25].

3.2. Experimental methods

3.2.1. *Samples, reagents, standard solutions, and glassware*

The suprapure HNO₃ (70% v/v) and H₂O₂ (30% v/v) were bought from Merck in South Africa. A water purification facility provided the Milli-Q water, which had a conductivity of 18.2 S/cm, which was used to prepare all the solutions. After scrubbing all the glassware with soap and water and soaking it in 5 % HNO₃, it was washed with deionized water. To make the mercury standards, a 1000 mg L⁻¹ mercury standard solution (Sigma-Aldrich, South Africa) was diluted to 100 mg L⁻¹. Methionine was bought from Merck, South Africa. Additionally, NIST SRM 2778 Hg in crude oil reference standard material was bought from Merck in South Africa. Samples of crude oil and coal were bought from Petro SA and labelled in accordance with **Table 3.1**.

Diesel oil, gasoline, and kerosene were purchased from three distinct filling stations around Johannesburg, South Africa and identified according to **Table 3.1**. Polyvinylidene Fluoride (PVDF) microfilters with a 0.45 µm pore diameter were purchased from Anatech Instrument South Africa. A mercury standard solution (1000 mg L⁻¹) was used to make five different mercury concentrations (0, 10, 20, 30, 50, and 100 µg L⁻¹), each spiked with 5 mol L⁻¹ methionine.

Table 3. 1: Real samples and their abbreviations.

Sample Type	Sample 1	Sample 2	Sample 3
Coal	CS 1	CS 2	CS 3
Crude oil	COS 1	COS 2	COS 3
Gasoline	GS 1	GS 2	GS 3
Diesel oil	DS 1	DS 2	DS 3
Kerosine	KS 1	KS 2	KS 3

3.2.2. Instrumentation

Fuel oil samples were digested using a Multiwave 5000 microwave digester (Anton Paar, Australia) The microwave has a rotor (20 SVT) that can accommodate 20 polytetrafluoroethylene-Teflon vessels (PTFE-TFM) simultaneously. A temperature program built into the microwave system managed the ramping and holding times. Using an axially oriented flame on a 700 Series ICP-OES (Agilent Technologies, USA), the produced digests were mercury analyzed. Additionally, sample uptake using a concentric nebulizer was performed using an Agilent Technologies SPS 3 autosampler, and sample introduction was performed using a cyclonic spray chamber.

Table 3.2 lists the ideal working conditions for analysis.

Table 3.2: Operating parameters of inductively coupled plasma optical emission spectroscopy (ICP-OES) for mercury analysis.

Agilent ICP-OES parameters	Instrumental conditions
RF power (W)	1200
Auxiliary gas Flow (L/min)	1.5
Plasma gas (Arg) flow (L/min)	15
Pump speed (rpm)	85
Peri-pump speed analysis (rpm)	15
Sample uptake delay (s)	15
Stabilization time (s)	15
Nebulizer (L/min)	0.75
Elemental wavelengths (nm)	Hg (184.887)

3.2.3. *Microwave-assisted hydrogen peroxide digestion (MW-AHPD)*

With minor modifications, the methodology was adopted from previous study described by Mketto and coworkers [26] was used in the current study. A mass of 0.1 g of the sample (coal, crude oil, diesel, gasoline, and kerosine), 9 mL of dilute H₂O₂ (5 mol L⁻¹), 1 mL of HNO₃, and 5.95 mol L⁻¹ of methionine were placed into 50 mL polytetrafluoroethylene-Teflon (PTFE-TFM) vessels (**Fig. 3.1**). The metal-carbon bond was subsequently broken by microwave radiation applied to the samples at temperatures as high as 200 °C for 36 minutes, which made it easier to extract the mercury from the fuel matrix. After the digests was complete, samples were to cool down at room temperature, they were transferred into a 10-mL volumetric flask and filled with Mill-Q water. Samples were prepared in triplicates, with the fourth serving as a blank. The digests from the 10 mL volumetric flask were filtered using PVDF with a 0.45 µm pore diameter size before being transferred to 15 mL centrifuge tubes for analysis. It is crucial to discuss how the temperature of MW digestion may affect the thermal stability of methionine and, consequently, the development of the Hg complex.

Firstly, an experiment using thermogravimetric analysis (TGA) was conducted to look at methionine's thermal stability.

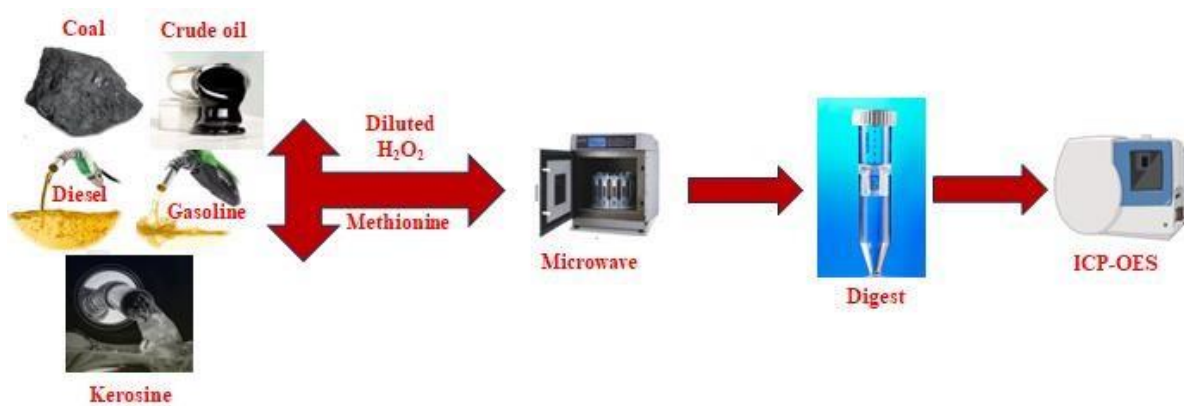


Figure 3.1: Key steps of a MW-AHPD procedure.

$$\%Recoveries = \frac{Spiked\ conc.-obtained\ conc.}{Spiked\ value} \times 100 \quad \text{Eq. 3. 1}$$

3.2.4. Multivariate optimization

The factors that were optimized using the multivariate approach were sample mass, hydrogen peroxide concentration [H₂O₂], methionine concentration [methionine], digestion time, and digestion temperature. The two-level half factorial design with 2⁵⁻¹ levels was used to optimize these values. The lowest (-), median (0), and maximum (+) levels of the factors under investigation are shown in **Table 3.3**. Seventeen tests from a first-order experimental design were subsequently displayed as Pareto charts. The response surface method (RSM) was then used to further optimize the significant parameters at the 95% confidence level, as indicated in **Table 3.4**. Minitab 2018 was used to generate central composite and two-level half factorial designs as well as designs for trials and data analysis.

Table 3.3: Variables that were investigated and their levels for half fractional design.

Factor optimized	Minimum level (-)	Central (0)	Maximum level (+)
Sample mass (g)	0.1	0.2	0.3
[H ₂ O ₂] (mgL ⁻¹)	3	4	5
[Methionine] (mgL ⁻¹)	1	5.5	10
Time (min)	30	45	60
Temperature (°C)	100	150	200

Table 3.4: Variables investigated and their levels in central composite design (sample mass was kept constant at 0.1g).

Factor optimized	Minimum level (-)	Central (0)	Maximum level (+)
[H ₂ O ₂] (mgL ⁻¹)	2	3.5	5
[Methionine] (mgL ⁻¹)	1	5.5	10
Time (minutes)	30	45	60
Temperature (°C)	140	170	200

3.3. Results and discussion

3.3.1. *Thermal stability of methionine*

As previously stated, it was crucial that we ascertain methionine's thermal stability initially. Methionine is thermally stable at the temperatures required for microwave digestion process, even though this thermal stability only pertains to the solid phase and not the solution phase. Methionine's TGA profile (**Fig. 3.2**) shows that the breakdown starts at 209 °C and ends at 270 °C, which is in line with several literature reports. At the optimal digestion temperature of 200 °C, approximately 0% of methionine weight is lost. Hence, this made it possible to use the methionine at such temperatures.

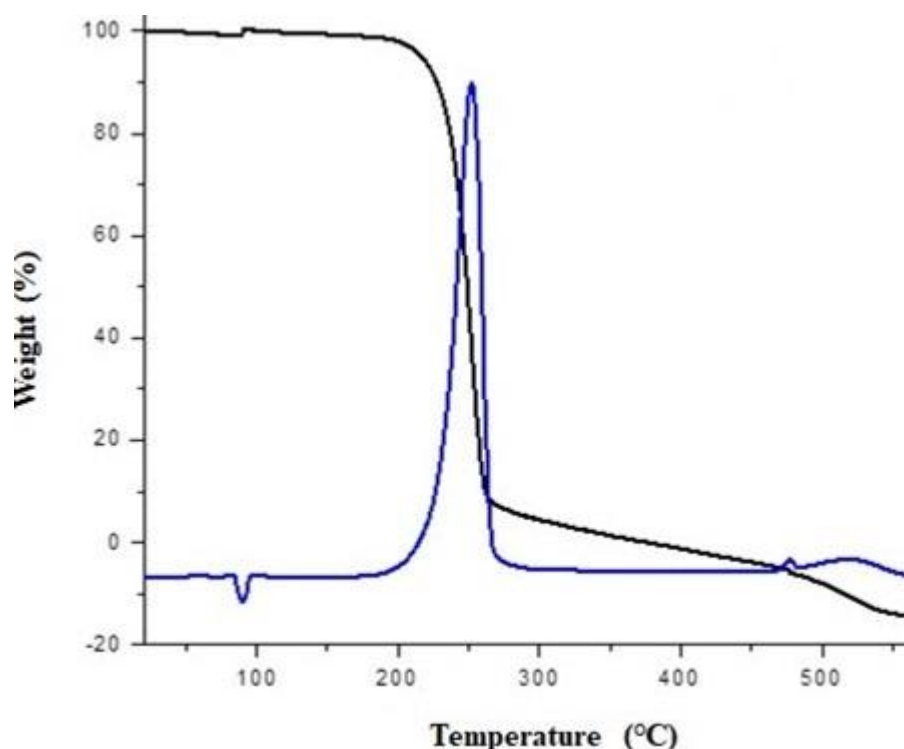


Figure 3. 2: Thermogram for methionine.

3.3.2. Two level half factorial design

A two-level half-factorial design (2^{5-1}) was utilized to evaluate the interactions between sample mass, hydrogen peroxide concentration, methionine concentration, time and temperature. These effects were influential in developing the microwave-assisted hydrogen peroxide digestion method. The experimental analysis of the two-level half factorial design is shown in **Appendix Table S1**. Analysis of variance (ANOVA) (**Appendix Table S2**) was used to examine the results at 95% confidence level. The ANOVA information was propagated as Pareto charts (**Fig. 3.3**). The vertical line represents the 95 % confidence level, and all the bars that crossed it were significant concerning the response for the extraction of Hg. According to the Pareto charts (**Fig. 3.3**) $[H_2O_2]$, [methionine], temperature and time were statistically significant, except for the sample mass at the 95 % confidence level. However, microwave temperature was significantly higher than the other effects. Additionally, the interaction of $[H_2O_2]$ and time (**Fig. 3.3**) was statistically significant. The results

indicated that these variables have a synergistic effect on percentage recovery. The central composite design (CCD) further refined the important variables.

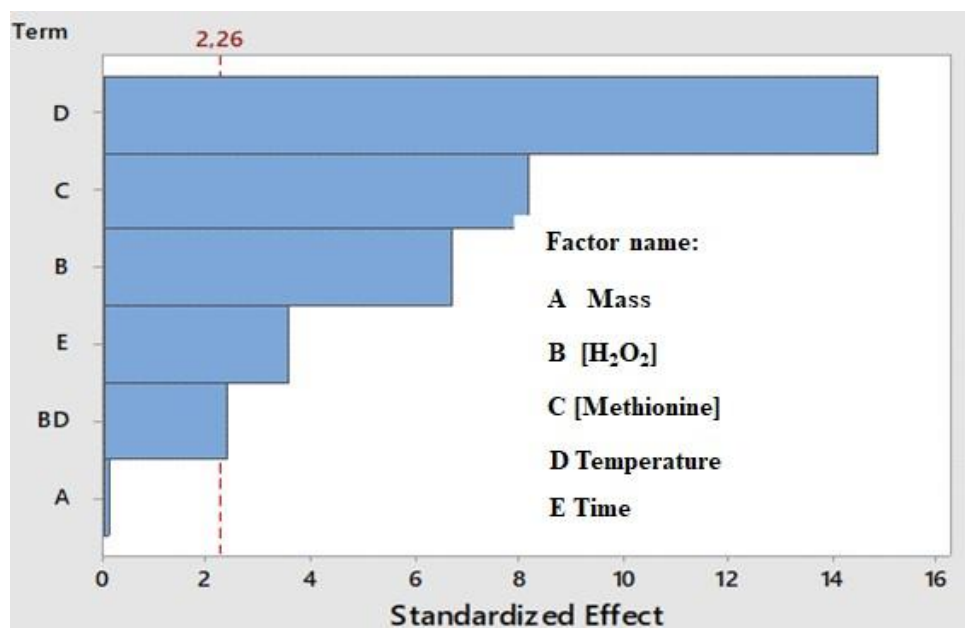


Figure 3.3: Pareto graphic for total Hg at 95% confidence level for two level half factorial design (2^{5-1}) for sample mass, time, temperature, [H₂O₂], and [Methionine] optimization (n=3).

3.3.3. Response surface methodology (RSM)

After screening the sample mass, hydrogen peroxide concentration, methionine concentration, time and temperature using half factorial design, central composite design was utilized to optimize further and identify optimum conditions. The results for the central composite design (CCD) are shown in **Appendix Table S3**. The matrix of the central composite design contained 31 experiments with responses (% recovery) correlating to each experimental run. The surface plots (**Fig.3.4 D**) reveal that increasing temperature beyond 200 °C resulted in the decrease in % recoveries. This might be due to the decomposition of methionine at higher temperatures. This is consistent with the thermal gravimetric analysis (TGA) of methionine (**Fig. 3.2**). It is also important to note that a decrease in (%) recoveries was seen when methionine concentrations were raised above 5.95 mol/L. This is because higher concentrations

of methionine resulted in high carbon deposits which result to decrease in instrument sensitivity. This observation is consistent with some literature reports [27].

The correlation between the analytical response and the assessed parameters ([H₂O₂] and [Methionine], temperature, and time) was interpreted using the ANOVA data obtained (**Appendix Table S4**) and the quadratic equation (**Eq. 3.2**) of the model. Using the quadratic equations (**Eq. 3.2**) and surface plots (**Fig. 3.4A–F**), the ideal parameters were determined to be 0.1g (sample mass), 5.95 mol L⁻¹ of [methionine], 200 °C for the digestion temperature, 36 minutes for mineralization, and 5 mol L⁻¹ of [H₂O₂]. When the obtained analytical responses were compared to the RSM model's projected values, there was no discernible variation at the 95 % confidence interval. To facilitate validation and application, the determined optimal criteria were employed.

$$\begin{aligned} \% \text{ Recoveries} = & 18.4A + 9.16B + 4.92C + 1.83D - 1.52A^2 - 0.448B^2 - 0.022C^2 - \\ & 0.00207D^2 + 0.018AB - 0.057AC - 0.0193AD - 0.0083BC - \\ & 0.0155BD - 0.01299CD - \\ & 280 \end{aligned}$$

Eq. 3. 2

Where A represents hydrogen peroxide concentration, B represents methionine concentration, C represents time and D represents temperature.

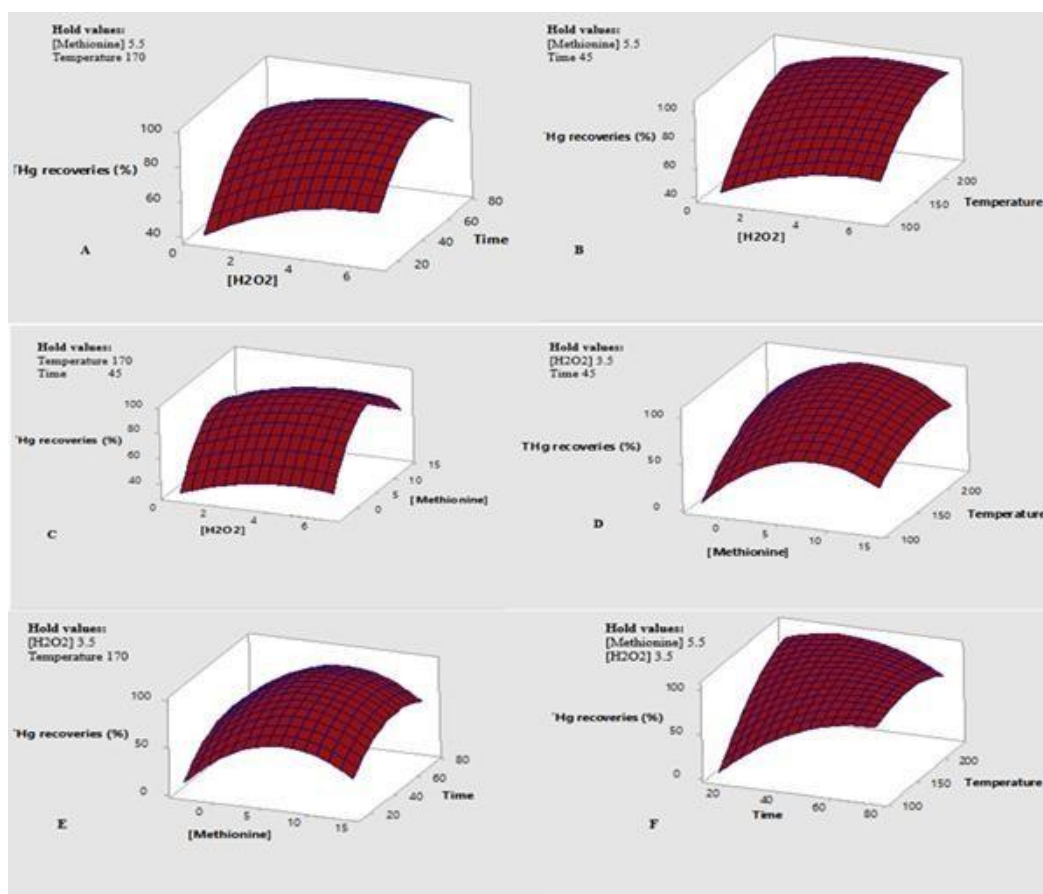


Figure 3.4: Total mercury response surfaces of total Hg vs [H₂O₂]. Time, [H₂O₂]. Temperature, [H₂O₂]. [Methionine], [Methionine]. Temperature, [Methionine]. Time and Time. Temperature measured with a CCD. 0.1 g of sample mass, 5 M [H₂O₂], 5.95 M [Methionine], and 200 °C were the experimental parameters.

3.3.4. Validation of the proposed MW-AHPD method

The accuracy of the proposed microwave-assisted hydrogen peroxide digestion procedure (MW-AHPD) was evaluated by applying the optimum conditions on NIST SRM 2778, with a certified mercury concentration of 38.98 µg/kg ±1.10 µg/kg in triplicates. The method showed excellent accuracy which ranged between 93-107 %. The proposed (MW-AHPD) procedure was further validated by comparing percentage recoveries with other two methods (a) no methionine and (b) standard method (**Fig. 3.5**). It is important to note that in method (a) we used the same procedure as the proposed method (MW-AHPD) but in the absence of methionine while standard

method (b) is a validated standard method for fuel samples found in Anton Paar Multiwave 5000 microwave manual. For the standard procedure, 10 mL of nitric acid was used for the digestion of 0.1 g NIST SRM 2778. On the other hand, 9 mL hydrogen peroxide and 1 mL of nitric acid were used for the proposed procedure with and without methionine. The results obtained (**Fig.3.5**) displayed in terms of total mercury recoveries, the proposed method showed higher recoveries (105 %) than the standard procedure (98 %). Nevertheless, there was no statistical difference between the two methods. Additionally, when comparing the recoveries achieved in the presence and absence of methionine, we observe that recoveries were improved in the presence of methionine (105 %) compared to the absence of methionine (92 %).

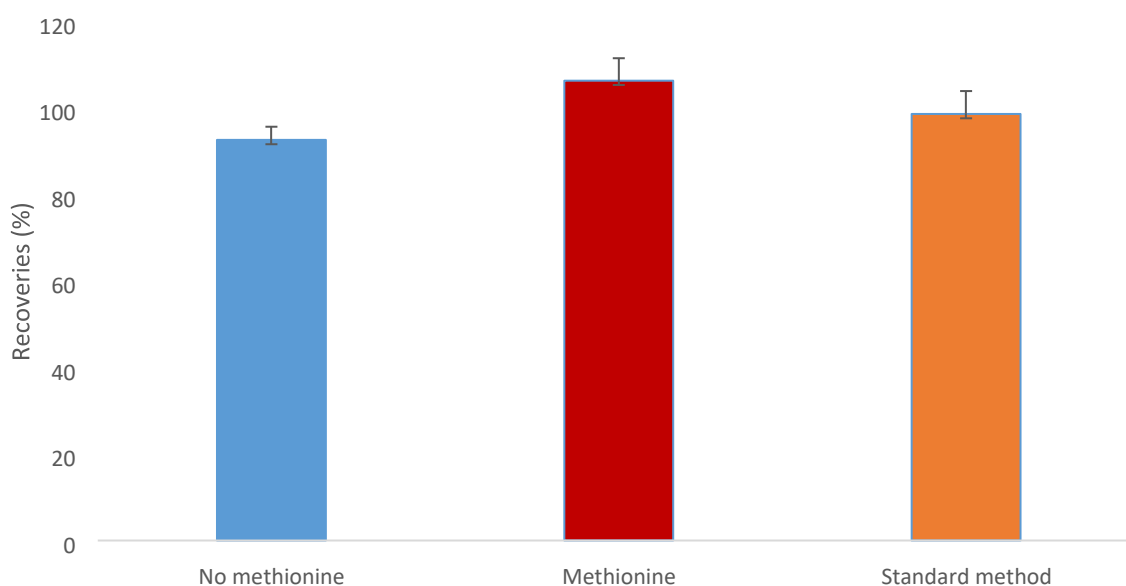


Figure 3.5: Comparison of percentage recoveries of total mercury under optimum conditions when digesting (a) no methionine, (b) methionine and (c) standard method.

With a few small adjustments, a method published by Mketo and coworkers [28] was used for the additional figures of merit, which included linearity, sensitivity, precision, limit of detection (LOD), limit of quantification (LOQ), and linearity. Using five different NIST SRM 2778 quantities (0.025, 0.05, 0.1, 0.15, and 0.2 g), a calibration with five points was built. The suggested MW-AHPD procedure's ideal conditions were applied to these five distinct amounts, and ICP-OES was used to analyze the resulting digests. The method's sensitivity was represented by a slope of 5,5845 cps L g⁻¹, and its correlation coefficient (R^2) was 0.9989. The gradient of the slope was used to

calculate the limit of detection (LOD) and limit of quantification (LOQ) (**Eqs. 3.3 and 3.4**).

The method limit of detection (MLOD) and method limit of quantification (MLOQ) were computed using **Eq. 3.5** and **Eq. 3.6**, respectively. All the results obtained for the figures of merits are presented in **Table 3.5**.

$$\text{LOD} = \frac{3 \times \text{SD}}{\text{Calibration slope}} \quad (\text{Eq. 3.3})$$

$$\text{LOQ} = \frac{10 \times \text{SD}}{\text{Calibration slope}} \quad (\text{Eq. 3.4})$$

$$\text{MLOD} = \frac{\text{LOD} \times \text{final volume}}{\text{Optimum mass}} \quad (\text{Eq. 3.5})$$

$$\text{MLOQ} = \frac{\text{LOQ} \times \text{final volume}}{\text{Optimum mass}} \quad (\text{Eq. 3.6})$$

Table 3. 5: Analytical performances of the newly developed MW-HPD.

Analytical features	Specifications
Sensitivity (cps L μg^{-1})	5,5845
Correlation coefficient (R^2)	0,9989
Limit of detection ($\mu\text{g L}^{-1}$)	0.25
Limit of quantification ($\mu\text{g L}^{-1}$)	0.8
Method detection limit ($\mu\text{g g}^{-1}$)	0.0025
Method quantification limit ($\mu\text{g g}^{-1}$)	0.0080
Accuracy (%)	93-107
Precision (%)	1.94

3.3.5. Greenness assessment of MW-AHPD method

AGREE prep was used to evaluate the suggested method's greenness. The latter is an analytical greenness meter that uses ten factors to assess if a suggested approach is green [29]. The tool consists of ten impact categories that are recalculated

using the 12 GAC principles, resulting in sub-scores on a scale from 0 to 1. A method that receives a total score of 1 has the best performance across all criteria, whereas a method that receives a total score of 0 performs worse across all criteria. Ten components surround the circle, each of which represents a performance criterion. Each part's color represents the performance in this criterion, while each part's length indicates the weight given to the corresponding assessment criterion.

The red-yellow-green color in the center shows how well the method performs in relation to each principle [30]. **Table 3.6** displays the ten criteria along with their default weights. A pictogram (**Fig.3.6**) was created to visualize the software's results. The many components of the pictogram make it possible to quickly compare various approaches and identify the method's strong and weak elements.

Table 3. 6: Default weights used in AGREEprep.

Criteria	Criteria description	Default weights
1	Favor <i>in situ</i> sample preparation placement	1
2	Use safer solvents and reagents	5
3	Target sustainable, reusable, and renewable materials	2
4	Minimise waste	4
5	Minimise sample, chemical and material amount	2
6	Maximise sample throughput	3
7	Integrate steps and promote automation	2
8	Minimise energy consumption	4
9	Choose the greenness possible post-sample preparation configuration for analysis	2
10	Ensure safe procedures for the operator	3

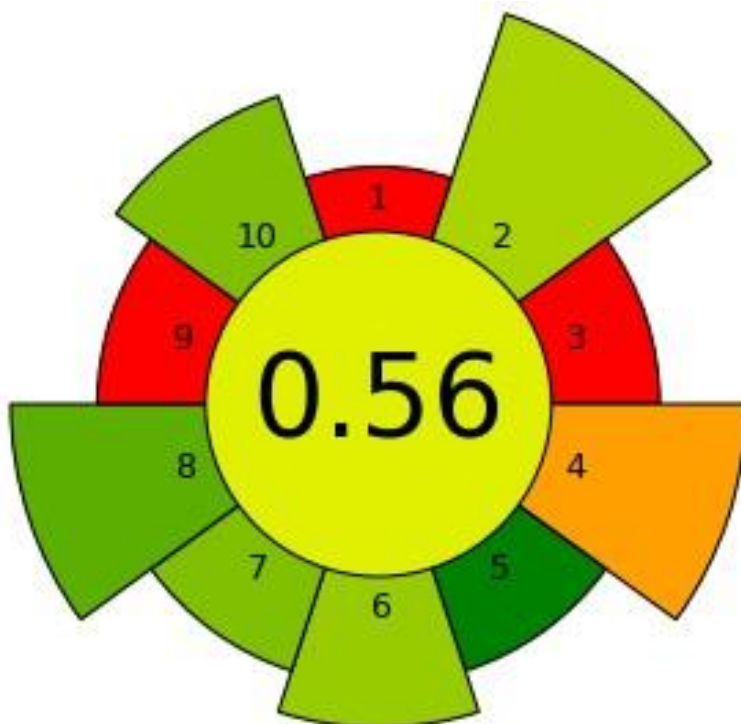


Figure 3.6: Pictogram visualising the greenness of the proposed procedure from AGREEprep. Software.

From the greenness pictogram (**Fig. 3.6**) we observe that the final score of the procedure was 0.56 which was a bit far from the ideal value. The color at the centre was light green indicating the method was green but far away from the ideal value. Criteria 1,3,4 and 9 contributed to the shift from the ideal value. The procedure was *ex-situ*, and the reagents used were not renewable (criteria 1 and 3). Furthermore, the amount of waste generated was suggested to be more than 5 mL as 1 mL of the final digests were taken and diluted to 10 mL (criterion 4). Finally, the detection technique was carried out using ICP-OES, which uses high energy and power, hence the red color in this criterion (criterion 9).

3.3.6. Comparison of the proposed MW-AHPD with other literature reports

Table 3.7 shows the comparison between the newly created MW-AHPD approach and previous literature reports. The figures demonstrate that the suggested strategy has outstanding accuracy (93–107 %), which is in line with other literature reports, when compared to most of the reported mineralization approaches. Furthermore, other published reports' figures of merit, like precision and method detection limit (MDL), were also quite like the proposed study. But perhaps most

significantly, in contrast to the previous literature findings that employed large volumes of pure HNO_3 , the suggested method used diluted H_2O_2 . While the latter produces toxic secondary pollutants, the conversion of dilute H_2O_2 to water and oxygen at increased temperatures is far more environmentally friendly.

Table 3.7: Comparing the newly established MW-AHPD's merit figures with those from other sources reports on MW-AD in fuel oils.

Matrix	Sample preparation method	Reagent	Trapping agent	Accuracy (%)	Precision (%)	Method limit of detection (ng/g)	Method limit of quantification (ng/g)	Detection technique	Ref
NIST SRM 2778	MW-AHPD	9 mL of 5molL ⁻¹ H ₂ O ₂ and 1 mL HNO ₃	Methionine	93-107	1.94	0.25	0.8	ICP-OES	This work
Crude oil	MW-AD	6 mL HNO ₃ , 2 mL HCl and 2 mL H ₂ O ₂	SnCl ₂	96-103	1.8	0.20	0.5	CV-AAS	[31]
Crude oil	MW-AD	8 mL conc. HNO ₃	NaBH ₄	92-105	5	0.16	NR	CV-ICP-MS	[32]
Coal	MW-AD	5 mL HNO ₃ and 2 mL HF	Gold	101.48-104.88	0.29	1.07	NR	ICP-MS	[32]
Crude oil	MW-AD	Conc.HNO ₃	SnCl ₂	75-125	NR	0.465	NR	CV-AFS	[33]
Crude oil	Closed pressurized system.	Conc.HNO ₃	SnCl ₂	75-123	13	1.3	4.0	CV-AAS	[34]

Note: **MW-AD:** microwave-assisted acid digestion; **MW-HPD:** microwave assisted-hydrogen peroxide digestion; **CV-AAS:** cold vapour atomic absorption spectrometry; **CV-ICP-MS:** cold vapour-inductively coupled plasma-mass spectrometry; **CV-AFS:** cold vapour atomic fluorescence spectrometry; **ICP-OES:** inductively coupled plasma-optical emission spectroscopy; **NR:** not reported; **SnCl₂:** Stannous chloride; **NaBH₄:** sodium boron tetra hydride; **HNO₃:** nitric acid; **HCl:** hydrochloric acid; **HF:** hydrofluoric acid; **H₂O₂:** hydrogen peroxide.

3.3.7. Application of MW-AHPD in real coal and fuel samples

Real fuel oils samples (crude oil, gasoline, diesel oil, and kerosene) as well as coal were subjected to the developed MW-AHPD procedure. Marked **CS 1**, **CS 2**, and **CS 3**, three distinct coal samples were taken from South African coal mines. Petro SA Chemical Company provided three distinct samples of crude oil, designated **COS 1**, **COS 2**, and **COS 3**. Three local filling stations provided coal and crude oil derivatives which were kerosene (**KS 1**, **KS 2**, and **KS 3**), diesel oil (**DS 1**, **DS 2**, and **DS 3**), and gasoline (**GS 1**, **GS 2**, and **GS 3**). All the samples were properly digested using the optimum conditions and quantified using ICP-OES. Additionally, each sample was properly digested without the use of a trapping agent before being ICP-OES analyzed. The concentration levels are presented in **Table 3.7**. From the table we observe that South African coal is the most contaminated energy source compared to the other energy sources. On the other hand, kerosene is the least contaminated with all the three different samples (**KS 1**, **KS 2**, and **KS 3**) reported below detection limits. This is good because kerosene is mostly utilized for domestic heating and for cooking more especially in rural areas. Lastly, there was no significant difference in mercury concentration levels between the other energy sources.

When compared to previous literature findings, the overall content of mercury in South African coal, crude oil, and crude oil derivatives was found to be within Hg content in other countries. For instance, Antes and coworkers [36] reported determining the mercury content of Brazilian coal by ICP-MS following MIC digestion. The obtained concentrations were 0.23 ± 0.01 , 0.066 ± 0.002 and $0.095 \pm 0.003 \mu\text{g g}^{-1}$ for Brazilian coals A, B, and C, respectively, without the application of a preservative. These total Hg concentrations were a bit lower than that of South African fuel oils. Another comparative investigation was echoed in 2013 by M. Pontes et al [35]. Three separate samples of crude oil were subjected to three different breakdown processes (closed pressured system, cold finger system, and pyrolysis), which were then analyzed using CVAAS. The concentration of total Hg ranged from 0.0046 ± 4 to $0.235 \pm 13 \mu\text{g g}^{-1}$ which is comparable to the Hg concentration in South African fuel oils.

Table 3.8: Total mercury concentration levels, reported in $\mu\text{g/g}$, were measured after digestion using MW-AHPD and ICP-OES in actual coal, crude oil, gasoline, diesel oil, and kerosine (1, 2, and 3).

Sample type	Concentration ($\mu\text{g/g}$)	
	Methionine	No methionine
CS 1	0.938 \pm 0.082	0.911 \pm 0.063
CS 2	0.975 \pm 0.025	0.945 \pm 0.080
CS 3	0.876 \pm 0.023	0.601 \pm 0.006
COS 1	0.383 \pm 0.043	0.321 \pm 0.004
COS 2	0.506 \pm 0.105	0.365 \pm 0.001
COS 3	0.470 \pm 0.090	0.427 \pm 0.006
GS 1	0.306 \pm 0.010	0.306 \pm 0.100
GS 2	0.376 \pm 0.075	0.398 \pm 0.009
GS 3	0.390 \pm 0.035	0.350 \pm 0.055
DS 1	0.434 \pm 0.050	0.398 \pm 0.001
DS 2	0.360 \pm 0.003	0.360 \pm 0.003
DS 3	0.431 \pm 0.001	0.410 \pm 0.085
KS 1	<DL	<DL
KS 2	<DL	<DL
KS 3	<DL	<DL

3.4. Conclusion

Methionine was successfully developed as a trapping agent in a novel, environmentally friendly microwave-assisted hydrogen peroxide digesting process for the determination of total mercury in South African coal and fuel samples using

ICPOES. Using a 2^{5-1} half factorial design and response surface methods, the most important parameters (sample size, $[H_2O_2]$, $[Methionine]$ duration, and temperature) were successfully optimized. MW-AHPD performed well under the following conditions: 0.1g, 5 M dilute $[H_2O_2]$, 6 mol L⁻¹ $[Methionine]$, 36 minutes, and 200 °C.

It can be concluded that temperature was the most influential parameter for MW-AHPD procedure. This is consistent with the decomposition of methionine and loss of mercury at elevated temperatures. It is necessary to conclude that the analytical performance of the newly developed method is within the performance of other literature reports. This is observed with the accuracy (93-107 %) of the method which is within other literature reports (**Table 3.7**). Currently, there is no legislation concerning the quantity of mercury permitted in fuel samples, but South African fuel samples contained mercury concentrations which are like other nations. Nevertheless, kerosene samples reported concentrations that were below detection limits, hence the necessity of preconcentration methods.

REFERENCES

- [1] A.B. Shabestari, B.A. Adergani, M. Shekarchi, S.M. Mostafavi, *Ekoloji* 27 (2018) 1935–1943.
- [2] P. Jeevanaraj, Z. Hashim, S. Mohd, A. Zaharin, *International Journal of Sciences: Basic and Applied Research (IJSBAR)* 24 (2015) 332–347.
- [3] C.H. Conaway, R.P. Mason, D.J. Steding, A.R. Flegal, *Atmospheric Environment* 39 (2005) 101–105.
- [4] D.P. Torres, I.M. Dittert, H. Höhn, V.L.A. Frescura, A.J. Curtius, *Microchemical Journal* 96 (2010) 32–36.
- [5] P. Zhang, L. Hu, R. Lu, W. Zhou, H. Gao, *Analytical Methods* 5 (2013) 5376– 5385.
- [6] Z. Hu, L. Qi, *Treatise on Geochemistry: Second Edition* 15 (2013) 87–109.
- [7] N.S. Mdluli, (2022).
- [8] R.S. Picoloto, H. Wiltsche, G. Knapp, J.S. Barin, E.M.M. Flores, *Analytical Methods* 4 (2012) 630–636.
- [9] M.C. Zuma, J. Lakkakula, N. Mketto, *Applied Spectroscopy Reviews* 0 (2020) 1–25.
- [10] K.K. Sodhi, M. Kumar, D.K. Singh, *Journal of Water Process Engineering* 39 (2021) 101858.
- [11] F. Ma, R. Wu, P. Li, L. Yu, (2016) 339–352.
- [12] N. Mketto, P.N. Nomngongo, J.C. Ngila, *Trends in Analytical Chemistry* 85 (2016) 107–116.
- [13] N.S. Mdluli, P.N. Nomngongo, N. Mketto, *Crit Rev Anal Chem* 52 (2022) 1–18.
- [14] C.H. Park, Y. Eom, L.J.E. Lee, T.G. Lee, *Chemosphere* 93 (2013) 9–13.
- [15] C.G. Yuan, K. Lin, A. Chang, *Microchimica Acta* 171 (2010) 313–319.
- [16] B. Liu, K. Tian, Y. He, W. Hu, B. Huang, X. Zhang, L. Zhao, *Ecotoxicol Environ Saf* 242 (2022) 113854.

- [17] T.A. Koesmawati, F. Febrianti, R. Halim, N. Fitria, S. Tanuwidjaja, O. Rohman, A. Syamsudin, IOP Conference Series: Earth and Environmental Science 1201 (2023) 1–8.
- [18] M.L. Astolfi, C. Protano, E. Marconi, D. Piamonti, L. Massimi, M. Brunori, M. Vitali, S. Canepari, Microchemical Journal 150 (2019) 104186.
- [19] M. April, P. Roy, V. Balaram, S. Sawant, K.S. V Subramanyam, M. Satyanarayan, K. Vani, K. Srivalli, L.J. Thompson, 31 (2010) 35–74.
- [20] S.M. El-Safty, M.A. Khorshed, M.M. Ghuniem, International Journal of Environmental Analytical Chemistry 102 (2022) 270–292.
- [21] G. Xin, X. Jia, C. Zheng, Energy Sources, Part A: Recovery, Utilization and Environmental Effects 34 (2012) 1516–1522.
- [22] M. Budanovic, M.E. Tessensohn, R.D. Webster, Environmental Pollution 252 (2019) 637–643.
- [23] J.P.K. Rooney, Toxicology 234 (2007) 145–156.
- [24] A. Akhtar, T.G. Kazi, H.I. Afridi, S.G. Musharraf, M.B. Arain, J.A. Baig, Analytical Letters 55 (2022) 2185–2198.
- [25] S.S.L. Da Costa, A.C. Lima Pereira, E. Andrade Passos, J.D.P. Hora Alves, C.A. Borges Garcia, R.G. Oliveira Araujo, Talanta 108 (2013) 157–164.
- [26] N. Mketto, P.N. Nomngongo, J.C. Ngila, Microchemical Journal 124 (2016) 201–208.
- [27] M. Budanović, B. Khezri, S.J.L. Lauw, M.E. Tessensohn, R.D. Webster, Analytica Chimica Acta 992 (2017) 24–33.
- [28] N. Mketto, P.N. Nomngongo, J.C. Ngila, RSC Adv 5 (2015) 38931–38938.
- [29] F. Pena-Pereira, M. Tobiszewski, W. Wojnowski, E. Psillakis, Advances in Sample Preparation 3 (2022) 100025.
- [30] W. Wojnowski, M. Tobiszewski, F. Pena-Pereira, E. Psillakis, TrAC – Trends in Analytical Chemistry 149 (2022) 116553.
- [31] M. Payehghadr, H. Shafiekhani, A.R. Sabouri, A.M. Attaran, M.K. Rofouei, Iranian Journal of Chemistry and Chemical Engineering 33 (2014) 1–10.

- [32] G.T. Druzian, M.S. Nascimento, R.S. Picoloto, M.F. Mesko, E.M.M. Flores, P.A. Mello, *Journal of Analytical Atomic Spectrometry* 37 (2022) 1799–1805.
- [33] G.T. Druzian, M.S. Nascimento, R.S. Picoloto, M.F. Mesko, E.M.M. Flores, P.A. Mello, *Journal of Analytical Atomic Spectrometry* 37 (2022) 1799–1805.
- [34] D.L. Cussen, C.E. Hensman, F. Geosciences, P.A. N, (2005).
- [35] F.V.M. Pontes, M.C. Carneiro, D.S. Vaitsman, M.I.C. Monteiro, A.A. Neto, M.L.B. Tristão, M.D.F. Guerrante, *Fuel Processing Technology* 106 (2013) 122– 126.
- [36] F.G. Antes, F.A. Duarte, M.F. Mesko, M.A.G. Nunes, V.A. Pereira, E.I. Müller, V.L. Dressler, E.M.M. Flores, *Talanta* 83 (2010) 364–369.

CHAPTER IV

Vortex-assisted deep eutectic solvent-based dispersive liquid-liquid microextraction (VA-DES-LLME) for spectroscopic determination of Hg in fossil fuels and their selected derivatives

ABSTRACT

Mercury is a toxic pollutant that is found naturally in fossil fuels due to the nature of their occurrence. The processing and combustion of these energy resources results in releasing this toxic pollutant into the environment. It is therefore crucial to accurately determine whether there are any mercury residues present within these energy sources. This work developed a green technique that uses inductively coupled plasma optical emission spectroscopy for the quantification mercury in fuel oils. Using a vortex-assisted dispersive liquid-liquid microextraction (VA-DLLME) technique, three distinct deep eutectic solvents (choline chloride + ethylene glycol, choline chloride + levulinic acid, and betaine + levulinic acid) were synthesized, characterized, and applied in Hg extraction in fuel oils prior to quantification using ICP-OES. The optimum conditions for the newly developed method were as follows 4.5 pH, 5 minutes extraction time, 164 μL volume and 665 μL disperser solvent. The values for the enrichment factor (EF), percentage RSD, and limit of detection (LOD) were 2.3 %, 234 %, and 0.25 $\mu\text{g/L}$, respectively. Higher recoveries of 99.9 % were achieved, and the method was validated by the analysis of NIST SRM 2778, which had a certified mercury value of 38.98 $\mu\text{g/kg}$ \pm 1.10 $\mu\text{g/kg}$. The newly developed method was applied in real crude oil, kerosene, diesel, and gasoline. The concentration obtained were 0.390 \pm 0.01-0.510 \pm 0.09 $\mu\text{g/g}$ for crude oil samples, 0.308 \pm 0.05-0.402 \pm 0.05 $\mu\text{g/g}$ for gasoline samples, 0.370 \pm 0.35-0.510 \pm 0.080 $\mu\text{g/g}$ for diesel oil samples and 0.09 \pm 0.09-0.098 \pm 0.02 $\mu\text{g/g}$ for kerosene samples.

4.1. Introduction

Hitherto, accurately determining total mercury in fuel oils remains a challenge in the analytical community. The reason it is a challenge to quantify mercury is due to its volatile nature. Mercury, in several of its chemical forms, such as Hg^0 , Hg^+ and Hg^{2+} is

a trace pollutant that exists naturally in these energy resources. The detrimental effects of the former are well documented in the literature, especially toxicity to human health and the environment [2]. The processing of these energy resources, such as crude oil and the burning of its derivatives (gasoline, diesel oil and kerosine), are responsible for the release of this toxic pollutant into the environment [3–6]. Therefore, accurately quantifying this pollutant in these energy resources is paramount.

Sample preparation is an important step in chemical analysis. Eliminating any species that could interfere and preconcentration of the analyte(s) was the main goal of the study. Furthermore, it enables the determination of analyte(s) at trace levels and the analysis of more complex matrix materials [7]. Analyte transfer from the starting phase into an acceptor phase that is better compatible with the analytical instrument is the basis of the former method [8]. Extraction techniques such as liquid-liquid extraction (LLE) and solid phase extraction (SPE) have been applied to extract mercury from various matrices. However, these traditional methods have some limitations. On the one hand, LLE makes use of large volumes of organic solvents, difficult automatization, high costs, high environmental pollution, low selectivity and low reproducibility. On the other hand SPE has low selectivity, makes use of large sample volumes, involves multiple stages of processing, it is laborious and time-consuming [9,10]. These days, smaller formats—known as microextraction techniques—are used to take advantage of the benefits of traditional extraction methods while eliminating the limits of conventional LLE and SPE techniques. such as minimum use of large volume of organic solvents and environmental pollution [11,12].

Techniques such as liquid liquid microextraction (LLME) have been developed to address the shortcomings of traditional LLE. Usually, LPME occurs in small amount of the acceptor phase (often in the μL range). Depending on how the extractant comes into contact analyte this new generation of extraction techniques can be split into three categories. Hollow-fiber liquid liquid microextraction (HF-LLME), dispersive liquid-liquid microextraction (DLLME), and single-drop microextraction (SDME) are a few examples of this [13]. Compared with published LLME procedures, dispersive liquid microextraction has become far more common. DLLME is widely used in the analytical community primarily due to its simplicity: it requires very little extraction solvent and produces high enrichment factors, rapid extraction, and phase separation. This method

involves injecting the sample solution with a syringe containing a suitable mixture of two solvents, one of which serves as an extractant and the other as a dispersive solvent. Finally, centrifugation occurs, which causes the extraction phase to congregate at the bottom of the extraction vessel. Following this, a hazy solution is produced in which the sample solution contains small, uniformly dispersed droplets of extraction solvent [14–17].

Deep eutectic solvents (DES) are liquid solvents that form at room temperature when two salts are added together namely a hydrogen bond donor, and a hydrogen acceptor bond are mixed together. In the former case, the eutectic mixture is characterized by having a melting point lower than the individual precursor constituents due to the phenomena of charge delocalization. DESs have excellent thermal stability, are non-volatile, non-toxic, and dissolve a wide range of inorganic and organic substances easily. Regarded as an environmentally friendly generation of ionic liquids. Furthermore, DESs have several advantages over ILs, including lower production costs, ease of synthesis, and superior biocompatibility when utilizing quaternary ammonium salts and have been used in various extraction methods [21–23].

Khan and Soylak [24] reported a green technique employing DESs to extract and measure mercury concentrations in fish, water, and hair samples. The method obtained reproducibility of 6.32 % and satisfactory recoveries ranging from 95 to 102 %. Their method obtained limit of quantification of 0.325 µg/L and detection limit of 0.09 µg/L. Altuny et al. [25] reported the use of natural DESs to quantify the total concentration of mercury in fish and ambient water.

Through statistical validation, the dependability (recovery of 92–98.7 % and RSD of 1.9–5.5 %) was confirmed through the examination of two standard reference materials (SRMs)—one with and one without spiking. The linearity range is 3–270 µg/g, with quantification and detection limits of 3.10 µg/g and 0.92, respectively, and preconcentration and sensitivity enhancement factors of 120 and 35.

To the best of our knowledge, no research has used DLLME based on DESs to report the total concentration of mercury found in crude oil. To measure mercury in crude oil and its derivatives, this work developed a dispersive liquid-liquid microextraction (DLLME) method that used DESs as extraction solvents for the first

time. Total mercury in crude oil and several of its derivatives can be measured accurately using natural DES based on ethylene glycol and choline chloride. Dithizone was originally used as a complexing agent to form the Hg-dithizone complex. The complex was then extracted using a small amount of the extractant (164 μ L). A vortex mixer was used to aid with the DLLME technique. Multivariate optimization was sometimes used instead of univariate optimization. The most important parameters were screened using a two-level half-factorial design, and response surface methodology based on Box-Behnken BBD was also used for additional optimization.

4.2. Materials and methods

4.2.1. Reagents and solutions

Choline chloride, ethylene glycol, lecithin acid and betaine were purchased from Sigma-Aldrich in South Africa. The choline chloride was vacuum-dried before use. Once received, the other compounds were used as is. In **Table 4.1**, the synthesized DESs and their abbreviations are shown. After being cleaned with soap and water, the glasswares were soaked in 5 % nitric acid and rinsed with deionized water before being dried and stored in lockers. A 1000 mg/L mercury standard solution (Sigma-Aldrich, South Africa) was diluted to create the mercury standards. 70 % suprapure HNO₃ and the mercury standard reference material (NIST SRM 2778) were acquired from Sigma-Aldrich in South Africa. The crude oil samples were purchased in triplicates from a South African crude oil refinery company. Crude oil derivatives such as gasoline, diesel, and kerosene were purchased from three local filling stations in the Johannesburg, South Africa. Nylon microfilters (0.45 μ m) were bought from Anatech Instrument, South Africa, and all the fuel samples that were obtained were labelled in accordance with **Table 4.2**.

Table 4. 1: The components of DESs, chemical structural information and their mole ratios.

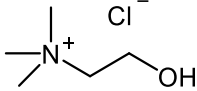
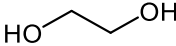
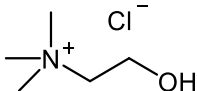
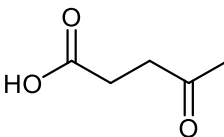
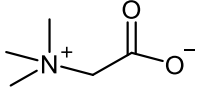
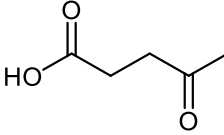
Abbreviation	Hydrogen bond acceptor (HBA)	Hydrogen bond donor (HBD)	Mole ratio (HBA:HBD)
DES 1	Choline chloride 	Ethylene glycol 	1:2
DES 2	Choline chloride 	Levulinic acid 	1:2
DES 3	Betaine 	Levulinic acid 	1:2

Table 4. 2: Different types of fuel samples and their derivatives.

Sample type	Sample 1	Sample 2	Sample 3
Crude oil	COS 1	COS 2	COS 3
Gasoline	GS 1	GS 2	GS 3
Diesel oil	DS 1	DS 2	DS 3
Kerosine	KS 1	KS 2	KS 3

4.2.2. Instrumentation

4.2.2.1. Inductively coupled plasma-optical emission spectroscopy

The sample oil and extractant solution were mixed in a VM-3000 MD vortex mixer for quantitative analysis. Using a pH meter equipped with an electrode made of glass, the pHs of the solutions were determined. Afterwards, to guarantee correct phase separation, a benchtop centrifuge was employed. Mercury analysis was performed on the generated digests using an axially oriented flame on an Agilent Technologies 720 Series ICP-OES. For all measurements, argon (99.9992 %, Carbueros Metalicos, Barcelona, Spain) was utilized. Additionally, an Agilent

Technologies SPS 3 autosampler was used for sample introduction using a cyclonic spray chamber and sample uptake utilizing a concentric nebulizer. All the instrument's sources and models are presented in **Table 4.3**. The ideal conditions of the Agilent Technologies 720 Series ICP-OES are presented in **Table 3.2**.

Table 4.3: Type of instrument, model and their sources.

Instrument	Model	Source
Vortex mixer	Medline Scientific	United Kingdom
pH meter	pH 2005, JP Selecta	Spain
Benchtop centrifuge	Universal-320, Hettich centrifuges	England
Inductively coupled plasma optical emission spectroscopy	Agilent technologies	Melbourne, Australia

4.2.3. Characterization techniques

4.2.2.1. Fourier Transform infra-red spectroscopy (FT-IR)

To determine the functional groups, present in the deep eutectic solvents and their precursor compounds, Fourier Transform infrared spectroscopy, or FT-IR, was utilized. The synthesized deep eutectic liquids' Fourier-transformed infrared (FTIR) spectra were measured using the KBr wafer technique on a Bruker Tensor 27 FTIR spectrophotometer (Bruker Optics, GmbH, Germany). While the liquid samples were supported on transparent KBr film, the solid samples were made in KBr pellets. During the analysis, the data was recorded in the 400–4000 cm^{-1} range.

4.2.2.2. Thermogravimetric analysis (TGA)

Thermogravimetric analyzer device model Q500 from TA Instruments-Waters LLC (TA Instrument firm, USA) was used to measure the thermal stability and thermal

decomposition temperatures of all the synthesized DES. Sample holders made of platinum were used to hold each sample individually, with a flow rate of 40 millilitres per minute of nitrogen atmosphere. Every sample underwent heating at a rate of 10 °C/min, rising to 600 °C.

4.2.2.3. ¹³C nuclear magnetic resonance (NMR)

Using a Bruker Advance II spectrometer (Massachusetts, United States) running at 100 MHz (¹³C), the nuclear magnetic resonance (NMR) data were collected at 289.2 K. CdCl₃ was used to prepare the samples, which were done in 5 mm tubes. The alteration in chemical composition was compared to that of CdCl₃. To analyze the spectra, MestreNova (version 9.1.0-14011) was employed.

4.2.4. ***Preparation of deep eutectic solvents***

Levulinic acid and ethylene glycol were the hydrogen bond donors (HBDs) in two of the three DESs that were synthesized, while choline chloride was the hydrogen bond acceptor (HBA) in the other two. Levulinic acid served as the HBD and betaine as the HBA in the preparation of the third one. The DESs were prepared in 50 g batches with a 1:2 molar ratio of HBA to HBD. An analytical balance was used to weigh the ingredients with an accuracy of ± 0.1 mg. After adding the liquid to 15 mL centrifuge tubes, a vortex mixer was used to fully vortex the mixture. After that, the mixture was put into a round-bottom flask and heated to a regulated temperature of 50 °C until a uniform, clear liquid was formed.

4.2.5. ***Vortex-assisted-natural deep eutectic solvent-based dispersive liquid-liquid microextraction (VA-DES-DLLME) procedure***

Five mL aliquots of working solutions which contained 100 µg/L of mercury (II) and 0.02 % m/v dithizone were adjusted to pH 4.5 and transferred into 15 mL centrifuge tubes. The sample solutions were then injected with 667 µL of disperser solvent (methanol) which was mixed with 164 µL of DES., The mixture was then vortexed for five minutes. The phases were then separated by centrifugation at 4000 rpm for five minutes. The enriched extract was then withdrawn using a syringe and transferred into 10 mL volumetric flasks before being diluted to the appropriate level.

Finally, the samples were transferred into 15 mL centrifuge tubes and later taken for ICP-OES analysis.

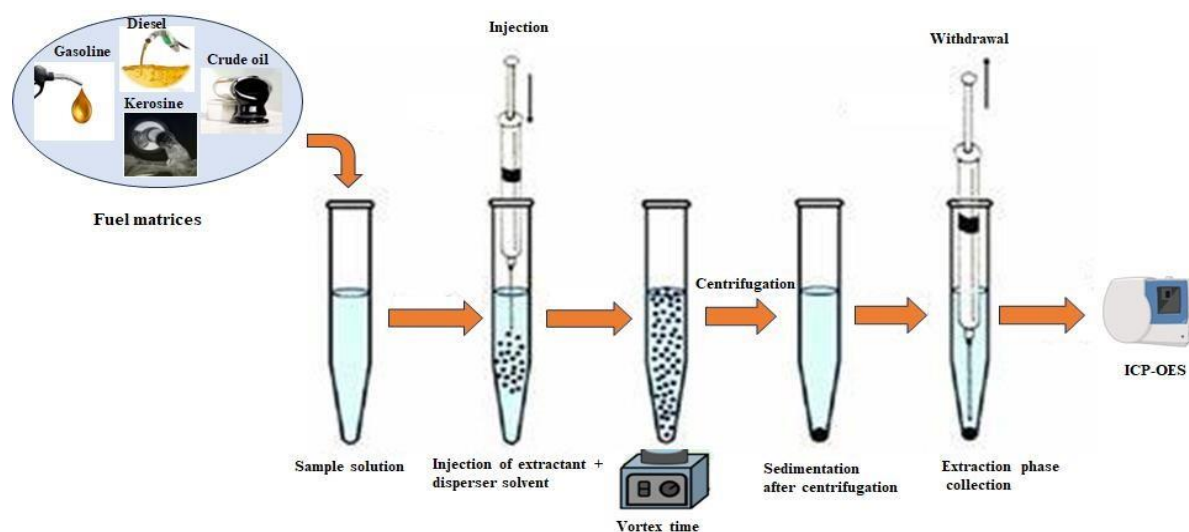


Figure 4. 1: Vortex assisted-natural deep eutectic solvents based dispersive liquid-liquid microextraction (VA-DES-DLLME) procedure.

4.2.6. Optimization of the VA-DES-DLLME procedure

The most influential parameters which affected the extraction process were first optimized. These variables included centrifugation time, pH, volume of extracting solvent, volume of disperser solvent, and extraction time. For this, a multivariate optimization strategy was used.

This approach is also useful in determining the most suitable model for the relationship between the components and the optimal experimental conditions [22]. The Box-Behnken (BBD) response surface methodology (RSM) was utilized to identify the optimal values for the relevant components following an initial screening using a two-level half factorial (2^{5-1}) design. Each factor was assigned three levels (minimum (-), middle (0), and maximum (+)), as shown in **Table 4.4**. A total of 17 experiments were conducted. To further optimize the relevant components, they were categorized into three tiers (**Table 4.5**), and a total of 27 trials were generated using Minitab software 2018.

Table 4. 4: Two-level half factorial (2^{5-1}) experimental design.

Factor	Min (-)	Central (0)	Max (+)
pH	1	7	13
Volume of dispersive solvent (mL)	0.25	0.625	1
Volume of extracting solvent (mL)	0.05	0.1	0.15
Extraction time (min)	10	15	20
Centrifugation time (min)	1	5.5	10

Table 4. 5: Response methodology based on BBD experiment design.

Factor	Min (-)	Central (0)	Max (+)
pH	2	6	10
Volume of disperser solvent (mL)	0.25	0.625	1.0
Volume of extracting solvent (mL)	0.05	0.275	0.5
Extraction time (min)	0.5	5.25	10

4.3. Results and discussion

4.3.1. *Characterization of synthesized deep eutectic solvents (DESs)*

4.3.1.1. Fourier Transform Infrared spectroscopy (FT-IR)

FT-IR (Fourier transform infrared spectroscopy) was used to confirm the functional groups in the synthesized DESs. **Figure 4.2 (A-C)** displays the FTIR spectra of the three synthesized DESs. The O-H stretching vibrations are represented by a large peak at 3220 cm^{-1} in the FT-IR spectra of pure choline chloride, as seen in **Fig. 4.2 A**. There was evidence of CH_2 aliphatic bending at 1480 cm^{-1} and a band at 955 cm^{-1} which was caused by C-N^+ stretching. C-O stretching vibrations and C-O-H bending vibrations are represented by the vibration bands at 1083 cm^{-1} and 1013 cm^{-1} , respectively [26]. Additionally, a C-H stretching at 3027 cm^{-1} and a CH_3 bending at 1346 cm^{-1} are noted [27]. A large peak at 3296 cm^{-1} was seen in the pure ethylene glycol spectra, and this peak corresponds to the O-H stretching vibrations. bands that matched the stretching vibrations of CH_2 at 2876 and 2934 cm^{-1} . Peaks for free C-OH and C-C are seen at 1089 and 879 cm^{-1} , respectively [28].

The primary mechanism for the creation of the deep eutectic solvent is the hydrogen bonding that occurs between the ethylene glycol and the chloride anion of

choline chloride. The FTIR spectra showed that most peaks in **DES 1** spectrum were from ethylene glycol. A vibrational band at 3296 cm^{-1} , which was associated to the O-H group was observed. Another peak at 955 cm^{-1} which was caused by choline chloride was also observed. The C-N⁺ stretching is the cause of this new band.

The C-H stretching vibrational bands are located at 2934 cm^{-1} and 2876 cm^{-1} , the CH₂ bending of an alkyl group is at 1480 cm^{-1} , and the functional groups—C-O stretching, C-C-O asymmetric stretching, and C-C-O symmetric stretching—are at 1083 cm^{-1} , 1036 cm^{-1} , and 861 cm^{-1} [29]. Hence, the synthesis of **DES 1** was successful.

The FTIR spectra of **DES 2**, levulinic acid, and choline chloride are displayed in **Fig. 4.2 B**. Choline chloride's spectrum is identical to the one shown in **Fig. 4.2 A** above. The presence of an aliphatic ketone is indicated by vibrational bands at 1399 cm^{-1} , 1363 cm^{-1} , 1206 cm^{-1} , 1159 cm^{-1} , and 1702 cm^{-1} in the FT-IR spectrum of levulinic acid. A large peak was seen at 3074 cm^{-1} which is the location of the carboxylic group found in levulinic acid's structure. Levulinic acid FTIR spectrum supports the categorization of the substance as a keto-acid. Ultimately, the synthesised **DES 2**'s spectrum was determined, and an alkyl group was identified by the vibrational bands at 2929 cm^{-1} and 1480 cm^{-1} . Furthermore, an aliphatic ketone group is indicated by vibrational bands at 1708 cm^{-1} , 1399 cm^{-1} , 1363 cm^{-1} , and 12001159 cm^{-1} . Finally, a fingerprint at 955 cm^{-1} was also detected, indicating that the CN⁺ group was derived from choline chloride [30].

The FTIR spectra of **DES 3**, betaine, and levulinic acid are displayed in **Fig. 4.2 C**. The stretching vibration frequency of a carbonyl group at 1702 cm^{-1} and a (COO-) group at 1621 cm^{-1} are seen in the betaine FT-IR spectra. There is also a peak at 937 cm^{-1} that corresponds to C-N⁺, and there are peaks at 1492 cm^{-1} and 1381 cm^{-1} that relate to CH₂ stretching. Levulinic acid's FT-IR spectra is identical to that of **Fig. 4.2 B** above. The creation of a hydrogen bond between the -COO- in betaine and the -OH in levulinic acid is what causes **DES 3** [31].

Due to the strong electronegativity of the O- in the -COO- group, a hydrogen bond is created when it encounters the positively charged H atom on the -OH. First, the hydrogen bonding between the HBD creating the DES and HBA caused the broad

band at 3074 cm^{-1} for -OH stretching vibrations to move 2922 cm^{-1} . The OH stretching vibration is lessened because of this molecule contact. Furthermore, betaine's -COO- stretching vibration shifted from 3016 cm^{-1} to 2922 cm^{-1} because of hydrogen bonding interaction [31]. This confirms the successful synthesis of DES 3.

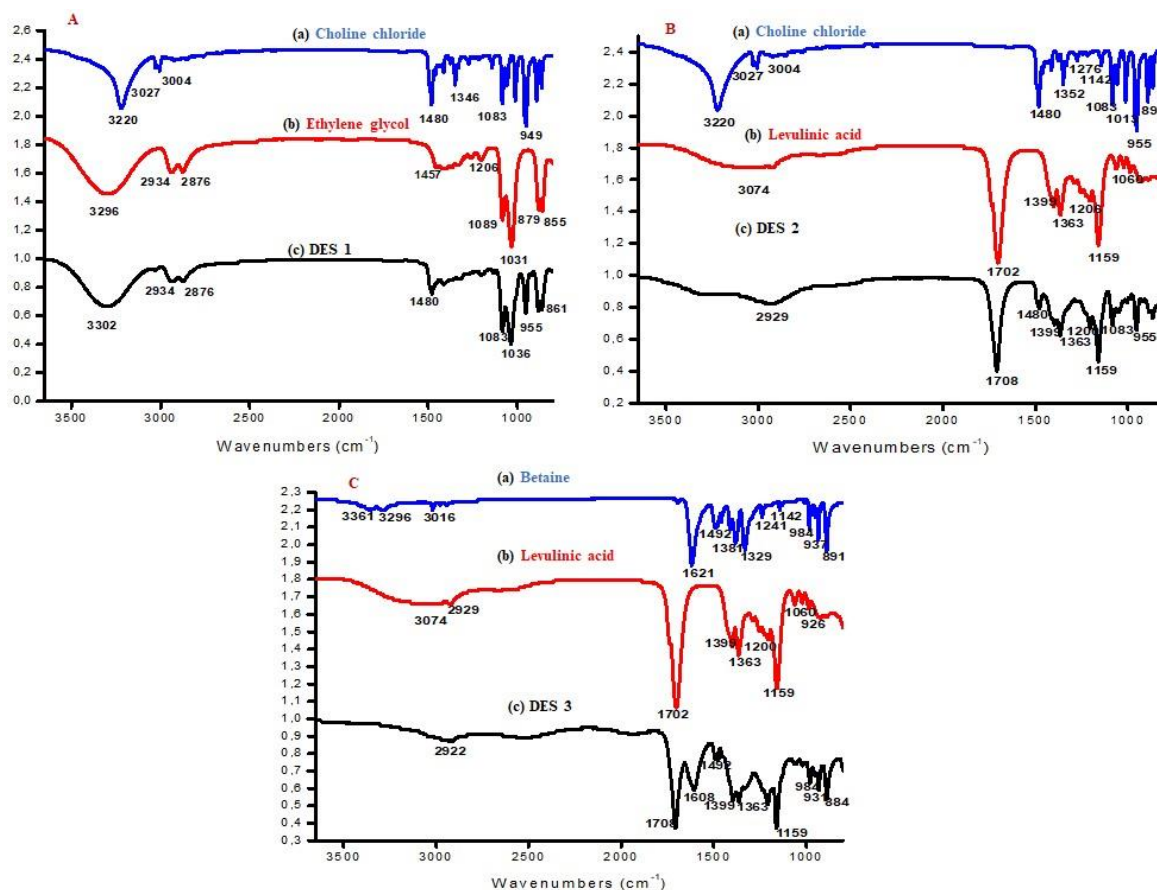


Figure 4. 2: FT-IR spectra for **A)** DES 1 and its pure compounds, **B)** DES 2 and its pure compounds and **C)** DES 3 and its pure compounds.

4.3.1.2. Thermogravimetric analysis (TGA)

To verify the thermal stabilities of the synthesized DESs and their pure constituents, thermogravimetric analysis (TGA) was employed. This technique's fundamental idea is to heat a sample at a regulated rate in a certain environment (air, Ar, or N_2). The substance's weight variation is noted in relation to temperature and/or time. Additionally, it offers details on the chemical analysis and the thermal stability forecast up to $1000\text{ }^\circ\text{C}$. TGA examination of DES will provide information about their

behaviour, particularly when used in industrial procedures like separation [32]. **Figure 4.3 (A-C)** shows the thermograms of the three synthesized DESs and their pure constituents.

The TGA curves for the three DESs and their precursors at a heating rate of 5 K.min⁻¹ are shown in **Fig. 4.3 (A-C)**. The three synthesized DESs generally exhibited decomposition at intermediate temperatures between their antecedents, supporting the interactions between the constituent parts. **DES 1**, a mixture of ethylene glycol and choline chloride, exhibits better thermal stability than ethylene glycol alone. There are three distinct phases of deterioration found. The initial phase of mass loss in **DES 1** from 58 to 213.2 °C is roughly 35.2 %, which is associated with ethylene glycol volatilization below its boiling point of 198 °C.

The second deterioration stage, which occurs between 213.2 °C and 262.4 °C and has a mass loss of 11.5 %, is associated with further ethylene glycol volatilization above its boiling point. The loss of choline chloride itself occurs at the final degradation stage, which is represented by a mass loss of 60 %. This pattern agrees with N. Gajardo-Parra's findings [33]. In contrast to **DES 1**, which displays numerous degradation steps, **DES 2** and **DES 3** only display one. In **DES 2** and **DES 3**, this suggests that the contacts between the hydrogen bond donor (HBD) and hydrogen bond acceptor (HBA) are stronger. As a result, their breakdown is compared to that of a pure substance. This analysis's most significant finding is that, at high temperatures, DESs first break down HBD and then HBA. These outcomes align with several findings from the literature [34,35].

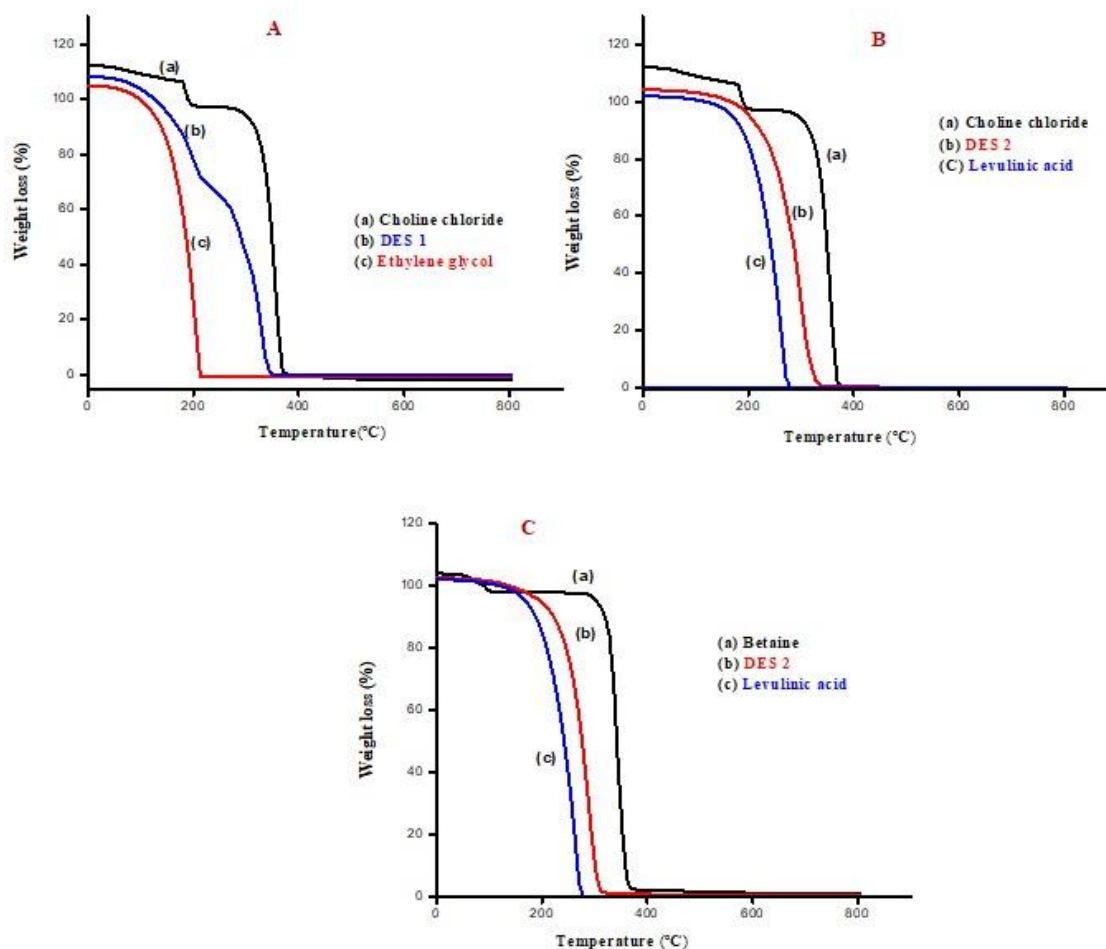


Figure 4. 3: Thermographs for **A)** DES 1 and its pure compounds, **B)** DES2 and its pure compounds and **C)** DES 3 and its pure compounds.

4.3.1.3. ¹³C nuclear magnetic resonance

Nuclear magnetic resonance (¹³C NMR) was used to further confirm the successful synthesis of the deep eutectic solvents, **Fig. (4.6, 4.7 & 4.8)** show the ¹³C NMR spectra for choline chloride, ethylene glycol, DES1, levulinic, DES2, betaine, and DES3. The ¹³C NMR data for each DES are shown in **Table 4.6, 4.7 & 4.8**. The signals in each table show excellent agreement with published values in the literature [36]. This confirms the successful synthesis of deep eutectic solvents.

Table 4. 6: ^{13}C NMR data for DES1.

Carbon level	Carbons	Integral	DES1 (ppm)
a	-N(C ₃)	3C	53.24
b	α -CH ₂	1C	55.35
c	β -CH ₂	1C	67.27
d	CH ₂	2C	63.12

Table 4. 7: ^{13}C NMR data for DES2.

Carbon level	Carbons	Integral	DES2 (ppm)
a	-N(C ₃)	3C	53.56
b	α -CH ₂	1C	67.37
c	β -CH ₂	1C	55.74
d	CH ₃	1C	27.85
e	CO	1C	207.69
f	CH ₂	1C	39.03
g	CH ₂	1C	29.85
h	COO	1C	174.14

Table 4. 8: ^{13}C NMR data for DES3.

Carbon level	Carbons	Integral	DES3 (ppm)
a	$\text{N}(\text{CH}_3)_3$	3	53.94
b	CH_2	1	65.92
c	C	1	77.56
d	C	1	167.11
e	CH_2	1	29.96
f	CH_2	1	37.98
g	C	1	174.89
h	CH_2	1	28.18

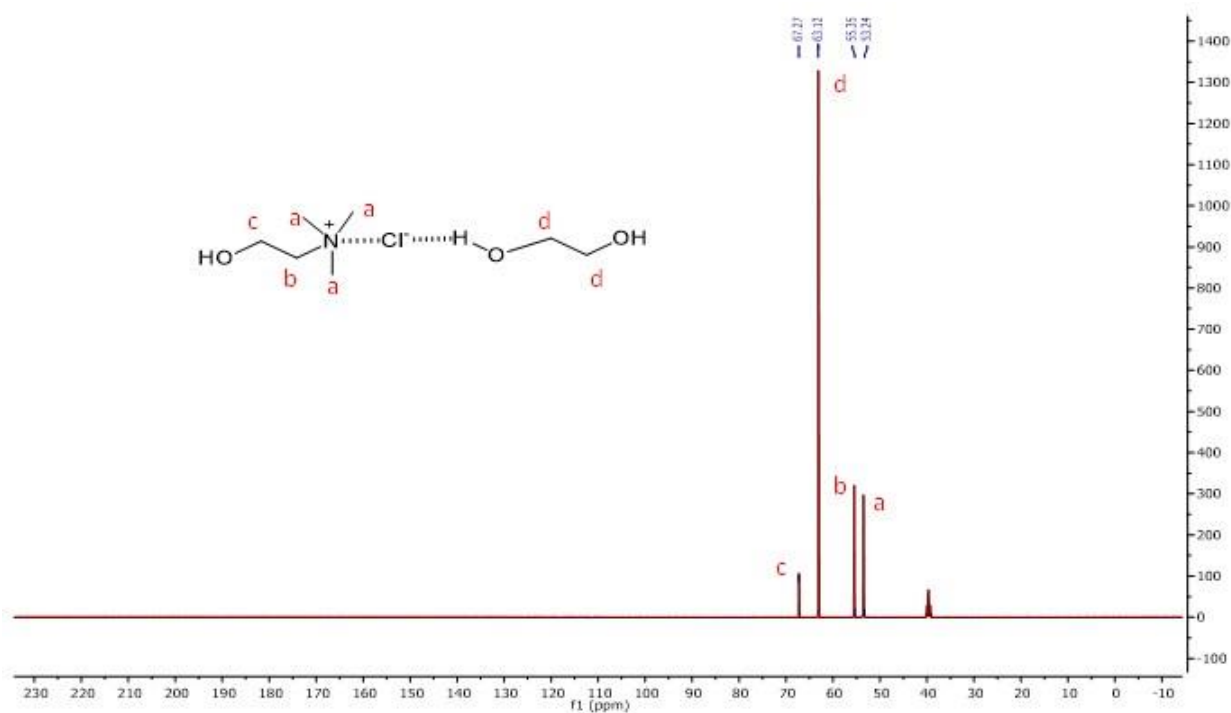


Figure 4. 4: ^{13}C NMR for DES 1.

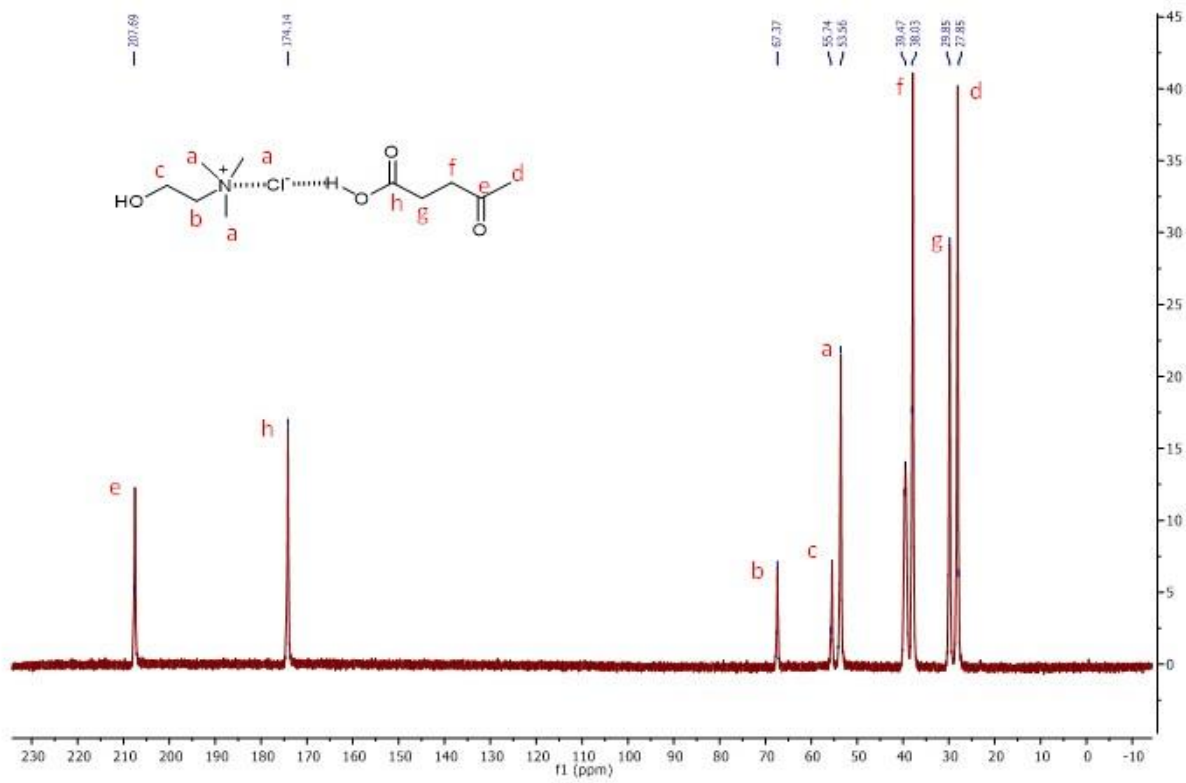


Figure 4. 5: ^{13}C NMR for DES 2.

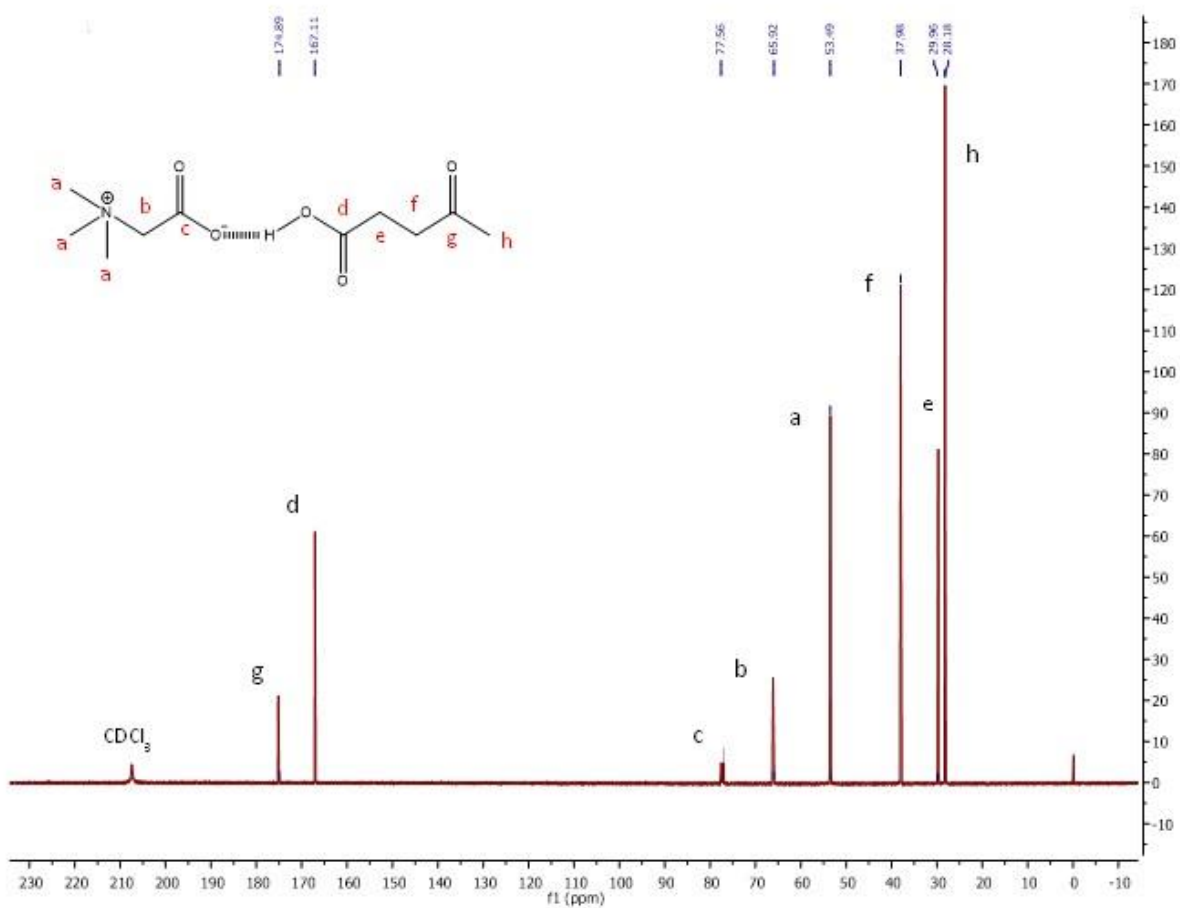


Figure 4. 6: ^{13}C NMR for DES 3.

4.3.2. Selection of deep eutectic solvents (DESs)

The type of extracting solvent used in dispersive liquid-liquid microextraction is of great importance for efficient extraction. In most cases, the ideal extraction solvent has two properties: hydrophobicity and higher solubility for the analytes compared with water. Three different deep eutectic solvents were compared for the extraction of mercury from fuel matrices. Choline chloride: ethylene glycol (**DES 1**), choline chloride: levulinic acid (**DES 2**), and betaine: levulinic acid (**DES 3**) was studied as extracting solvents. Mercury complex was formed by 0.02 % m/v of dithizone which was then extracted with 100 μL of each deep eutectic solvent using 0.75 mL of methanol as a dispersive solvent. According to the results (**Fig. 4.7**), all the DESs showed good recoveries above 80 % with **DES 1** showing the highest recoveries. The good extraction performance for **DES 1**, and **DES 2** can likely be attributed to the

coordination of mercury by chloride anion. However, it seems like the electron cloud was richer around the chloride anion for **DES 1** than **DES 2**, hence higher recoveries for **DES 1**. For the zwitterionic **DES 3**, coordination by the carboxylate group may provide a favorable environment for mercury [37].

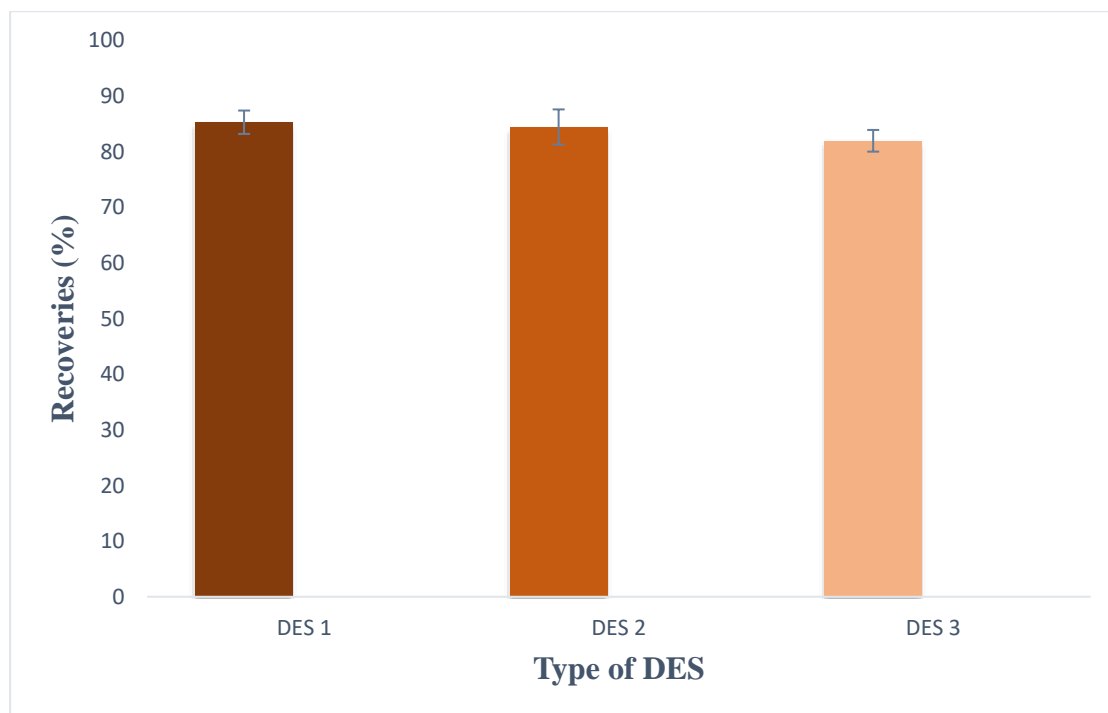


Figure 4. 7: Recoveries for DES1, DES2 & DES3 after a DES-DLLME procedure

4.3.3. Multivariate optimization of deep eutectic solvent based dispersive liquid-liquid microextraction parameters

4.3.1.1. Two-level half factorial design

It was critical that we first identify the key variables influencing the VA-DESDLLME process. The parameters that were investigated included pH, extraction time, centrifugation time, volume of extracting solvent, and volume of disperser solvent. This was accomplished by using a two-level half factorial design (2^{5-1}). The two-level half factorial design parameters, number of experiments, experimental

conditions, and results are shown in **Appendix Table S5**, and the analysis of variance (**Appendix Table S6**) was propagated as a pareto chart (**Fig. 4.8**). The bars show the estimated effect's absolute value, while the red vertical line denotes the 95 % confidence level. The graph indicates that, with a 95 % confidence level, pH was the most important parameter.

The extraction efficiency and chelate formation are both impacted by sample pH [24]. The volume of the disperser solvent, the volume of the extracting solvent, and the extraction duration were additional significant factors at the 95 % confidence level. There was a considerable interaction between the disperser solvent volume and both the centrifugation and extraction times. The two stages were simple to differentiate because the centrifugation duration was the only factor that did not matter. These important variables were selected for additional optimization through the application of the Box-Behnken design-based response surface methodology.

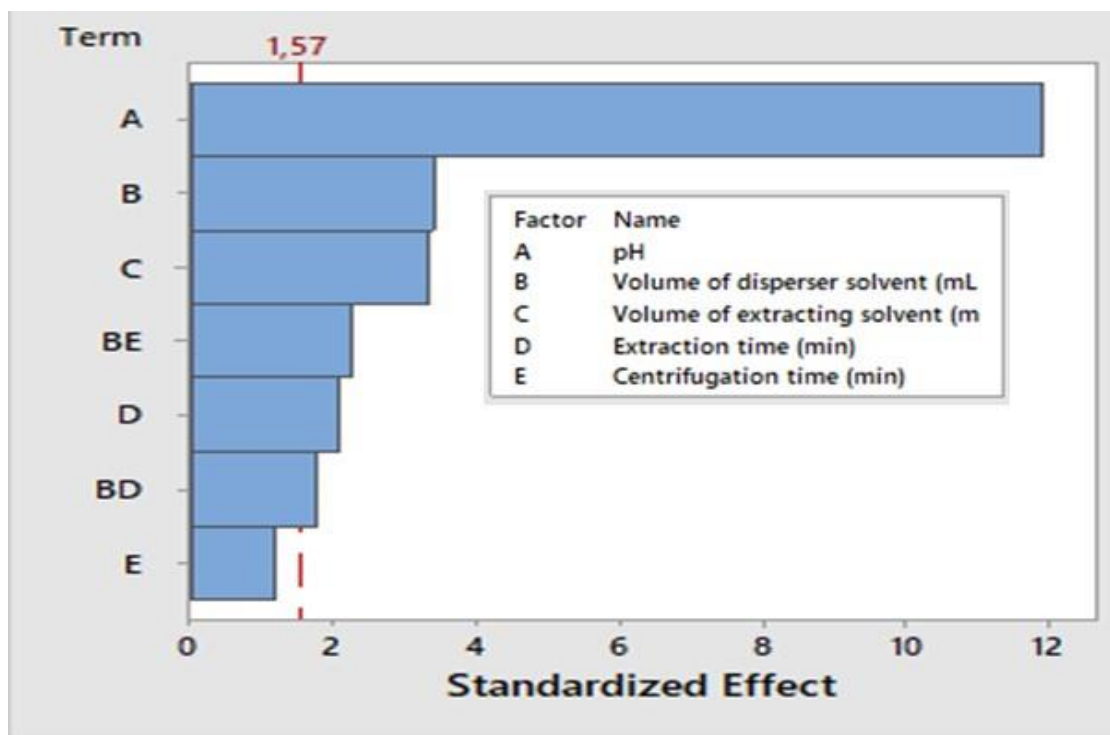


Figure 4. 8: Pareto chart showing the overall mercury content of fuel oils using a two-level two-level half factorial design (2^{5-1}).

4.3.1.2. Box Behnken design

After screening the most significant variables at 95 % confidence level, Response surface methodology (RSM) based on Box Behnken (BBD) was utilized for further optimization. The reason behind choosing BBD over CCD (both are mostly reported in the literature) is that CCD gave us some negative values and more experiments on our experimental design than BBD. The latter enabled us to obtain optimum values for the significant parameters, and we were able to examine the interaction between two variables and their analytical response. **Appendix Table S7** presents the factors, number of experiments, experimental conditions, and outcomes of the two-level half factorial design. **Appendix Table S8** employs analysis of variance (ANOVA) to assess the caliber of the findings. The model's adjusted R^2 value of 0.9338 and determination coefficient (R^2) of 0.9542 indicated that it was appropriate for optimizing the preconcentration process. This indicates that the model was able to accommodate more than 93 % of the data.

According to **Fig. 4.9 (A, B and C)**, mercury recoveries increase with the increase in pH but start to decrease beyond pH 4.5. This is consistent with some literature reports. On one hand, low pH values lead to severe acidity effects and instability of the Hg-DTz complex. On the other hand, higher pH values lead to the hydrolysis of Hg^{2+} , which leads to the subsequent decomposition of Hg-DTz complex [38]. Zhongben Gao and Xiaoguo Ma [39] state that most possible coexisting metal ions are not chelated with dithizone at this acidity, approximately at pH 4.5. The extraction efficiency rises when the volume of DES increases from 50 to 164 μ L, as seen in **Fig. 4.9 (A & D)**. However, when the DES volume exceeded 164 μ L, the extraction efficiency dropped. It appears that the superabundant extractant in 665 μ L of methanol is not dispersed sufficiently to produce fine droplets, which leads to a decrease in extraction efficiency. It was discovered that the extraction efficiency rose when the methanol volume was increased to 665 μ L and then fell when the methanol volume was increased even higher (**Fig. 4.9 B & D**).

The following explanation can be given for this phenomenon: A reduced volume of methanol did not adequately distribute DES, resulting in a poorer extraction efficiency. Conversely, employing more methanol would make the analyte-DZ

combination more soluble, which would reduce extraction efficiency [39]. Finally, improving the vortex time resulted in better recoveries up to five minutes; after that, the recoveries were unchanged. Therefore, the ideal vortex time was determined to be five minutes.

By utilizing surface plots and the quadratic equation (Eq. 4.1), the ideal parameters were determined to be pH 4.5, vortex time of 5 minutes, extractant volume of 164 μL , and disperser solvent volume of 665 μL . It is crucial to emphasize that the optimal concentration of the chelating agent (dithizone) was acquired from the literature rather than being optimized for this investigation [39].

$$\begin{aligned} \% \text{ Recoveries} = & 11.86 - 2.0746 A^2 - 0.1474 B^2 - 32.93 C^2 - 58.6 D^2 - 0.0776 \\ & AB - 1.800 AC - 0.64 AD - 1.333 BC - 3.478 BD - \\ & 10.7 CD \end{aligned} \quad \text{Eq. 4.1}$$

Where A represents sample pH, B represents vortex time, C represents disperser solvent volume, D represents extractant volume.

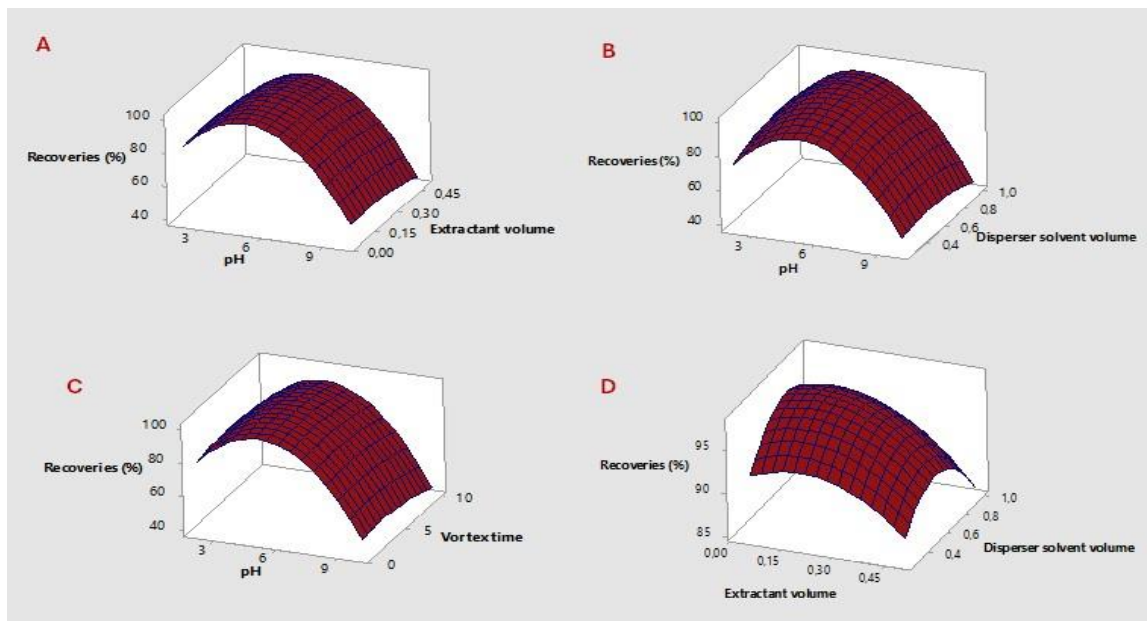


Figure 4. 9: Response surfaces vs (A) pH. Extractant volume, (B) pH. Disperser solvent volume, (C) pH. Vortex time, (D) extractant volume. disperser solvent volume obtained from Box Behnken design. Experimental conditions: 5 mL sample mass, 4.5 pH, 164 μL extractant volume and 665 μL disperser solvent volume.

4.3.4. Validation studies

The analytical performance of the developed method was investigated using optimum conditions. A procedure developed by Rastegarifard et al 2017 [21] was followed with some minor modifications. Briefly, crude oil samples were spiked with varying concentrations of Hg to generate a calibration plot. The calibration curve is linear in the range 10-100 µg/L with a correlation coefficient of $R^2 = 0.9974$. The limit of detection (LOD) and limit of quantification (LOQ) were defined by $3S_b/m$, and $10S_b/m$ (where S_b is the standard deviation of 10 blank samples and m is the calibration slope), respectively. The LOD and LOQ were 0.025 and 0.083 µg/L, respectively. The enrichment factor (EF) was determined by dividing the slope of the analyte's calibration curve, as obtained with organic standards following the preconcentration procedure, by the slope of the same calibration curve, as obtained with organic standards without preconcentration [40]. The enrichment factor was obtained to be 234.

Considering the analytical merits achieved, the validity of the method was tested before its application to real samples. To achieve that, the accuracy, repeatability, and reproducibility of the developed method was evaluated. For accuracy, a NIST SRM 2778, was analyzed using the ideal conditions of the developed method. Recoveries obtained were 99.9 % showing that the proposed method was acceptable. The intra and inter-day precision of the proposed method were also assessed. The precision (as % RSD) for the repeatability was calculated by performing seven replicates spiked at 10 µg/L Hg (II) in the same day. The % RSD obtained was 2.3 % with recoveries ranging from 95.5–97.5 %. Moreover, the reproducibility was calculated by extractions on three consecutive days for seven replicates spiked at 50 µg/L Hg (II), and the % RSD obtained was 4.5 % with recoveries in the range 92.5-95.6 %.

4.3.5. Greenness assement of VA-DLLME procedure

The environmental impact of the vortex-assisted deep eutectic solvent-based dispersive liquid-liquid microextraction procedure was evaluated using AGREEprep greenness metric. The former is a qualitative and quantitative tool which only focuses on the greenness of the sample preparation method, hence the name AGREEprep [41]. In addition to evaluating greenness, AGREEprep assessment can assist in

detecting the strengths and weaknesses of methods, thereby facilitating the greening of sample preparation procedures.

Ten effect categories serve as the foundation for this metric tool, which is recalculated into sub-scores on a 0–1 scale. A pictogram's sections are each a distinct color, ranging from red to green. The following are the AGREEprep categories: In situ sample preparation (a), safer solvent and reagent use (b), the use of sustainable, reusable, and renewable materials (c), waste reduction (d), the reduction of sample, chemical, and material amounts (e), maximizing sample throughput (f), step integration and automation (g), energy consumption reduction (h), selecting the most environmentally friendly post-sample preparation configuration for analysis (i), and operator safety (j).ensure operator's safety [42]. The outcome of the assessment of this study is presented in the form of a pictogram (**Fig. 4.10**).

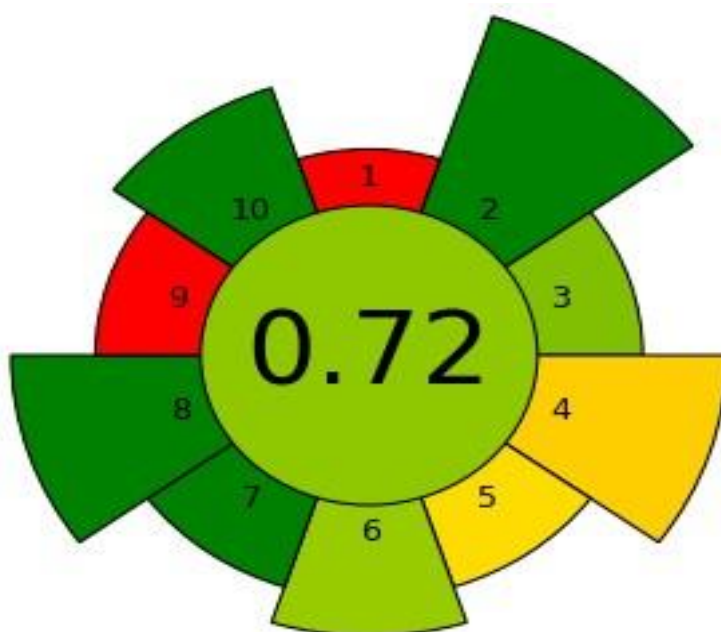


Figure 4. 10: Pictogram for AGREEprep for VA-DES-DLLME method.

The pictogram (**Fig. 4.10**) indicates that the VA-DES-DLLME technique was more environmentally friendly because it shows a total score of 0.72, which is near to the ideal value of 1. Furthermore, certain literature studies [43] state that a method is deemed greener if it achieves a score of at least 0.6, which validates the suggested VA-DLLME procedure's greenness. This discovery aligns with a research study published in 2022 by Hay et al. [44]. Criteria 1, 4, 5, and 9 all had low scores. Because

the extraction was done in a lab setting (ex-situ), the score for criteria 1 was low. Criterion 4 received a low score from the approach due to the quantity of garbage it generated. Because the sample size was 5 mL, which was a tad high, Criterion 5 was likewise subpar. Criteria 9, on the other hand, was subpar since the ICP-OES, a powerful and energy-hungry analytical equipment, was used for the analysis. Therefore, by choosing more environmentally friendly options for criteria 1, 4,5, and 9, this approach can be made greener.

4.3.6. Comparison of the proposed method with other literature reports

The analytical performance of the proposed VA-DES-DLLME was compared with other literature-reported LLE procedures, as shown in **Table 4.9**. The analytical features that were compared include, correlation coefficient (R^2), limit of detection (LOD), limit of quantification (LOQ), accuracy and precision, which are mostly reported in the literature. From **Table 4.9** it is clear that the figures of merits of the proposed method are comparable with the others reported methods. However, the proposed VADES-DLLME method showed very low detection limits, limit of quantification, high accuracy, and low %RSD compared to most of the reported LLE methods. There are only two studies that reported better limits of quantification (0.12 and 0.47 $\mu\text{g/L}$) but with poor precision (3.7 and 5 %) and accuracy (95.3 and 98 %) [42][43]. Therefore, the data tabulated in **Table 4.9** confirms that DESs are excellent alternatives to toxic organic solvents for mercury quantification in fuel oils.

Table 4. 9: Comparing the suggested method's figures of merit with other LLE figures of merit that have been published.

Sample	Sample preparation method	Extractant	Correlation coefficient (R ²)	LOD (µg/L)	LOQ (µg/L)	Precision (%)	Accuracy (%)	Analytical technique	REF
Crude palm oil	EIEB	HCl	N/A	0.036	0.12	3.7	95.3	CV-AFS	[42]
Gasoline	LLE	Propan-1-ol and HNO ₃	0.9999	0.14	0.47	5	98-101	CV-AAS	[43]
Diesel oil, biodiesel oil and mineral oil	EIEB	HNO ₃	0.9985	0.6	1.9	3.5	80-103	CV-AAS	[44]
Gasoline	EIEB	HCl	0.9935	0.9	2.9	4.8	88-109	CV-AAS	[45]
Gasoline	LLE	Propan-2-ol	0.9990	0.1	NR	7-8	90-94	PVG-GF AAS	[46]
Naphtha and petroleum condensate	LLE	Propan-1-ol	0.9971-0.0075	0.5-0.6	1.8-2.1	4	92-113	CV-AAS	[47]
NIST SRM 2778	VA-NADES-DLLME	DESs	0.9974	0.25	0.83	2.3	99.9	ICP-OES	This work

4.3.7. Application of VA-DES-DLLME in real fuel samples

After optimizing the most influential parameters and validation of VA-DESDLLME, the method was applied on real crude oil, gasoline, diesel oil and kerosene. The real samples were labelled according to **Table 4.2**. The obtained mercury concentrations were presented in **Table 4.10**. According to the table crude oil was the most contaminated energy resource (0.390-0.510 $\mu\text{g/g}$) compared to its derivatives. This might be since crude oil is susceptible to mercury contamination due to the nature of its genesis. Kerosene was the least contaminated energy source (0.090-0.098 $\mu\text{g/g}$). This is good because kerosene is mostly used for domestic heating and cooking in households. The contamination of gasoline and diesel oil samples might be associated with contamination during storage and transportation.

Comparing South African crude oil, gasoline, diesel oil and kerosene with other countries, the same are within mercury concentrations in other countries. For instance, in 2010 Torres et al [52] reported a preconcentrating method for the determination of mercury in gasoline. Mercury values ranging from 0.40 to 0.87 $\mu\text{g/L}$ were obtained by the researchers using their approach on five gasoline samples. Lia and coworkers [53] investigation of the picograms of mercury in US gasoline was another intriguing study. The study found that the quantities of mercury in gasoline, kerosene, and diesel oil varied from 0.22 to 1.43 ng/g , 0.04 ng/g , and 0.40 ng/g , respectively. The determination of total mercury in crude oil and related products was the subject of a comparative study published in 2013 by Pontes and colleagues. It was discovered that the range of the total mercury concentration in crude oil was 46 to 204 ng/g [54]. This indicates that South African crude oil and its byproducts are not significantly mercury polluted.

Table 4.10: Total mercury concentration levels ($\mu\text{g/g}$) in real crude oil, gasoline, diesel oil and kerosine.

Sample type	Concentration ($\mu\text{g/g}$)
COS 1	0.390 \pm 0.01
COS 2	0.510 \pm 0.09
COS 3	0.475 \pm 0.08
GS 1	0.308 \pm 0.05
GS 2	0.379 \pm 0.02
GS 3	0.402 \pm 0.05
DS 1	0.438 \pm 0.20
DS 2	0.370 \pm 0.35
DS 3	0.510 \pm 0.08
KS 1	0.095 \pm 0.01
KS 2	0.098 \pm 0.02
KS 3	0.090 \pm 0.09

4.4. Conclusion

The proposed vortex-assisted deep eutectic solvent based dispersive liquid-liquid microextraction (VA-DES-DLLME) was successfully developed and applied for the determination of total mercury in crude oil and its derivatives which are gasoline, diesel oil, and kerosene. The limit of detection and quantification obtained for the VA-DES-DLLME were 0.025 $\mu\text{g/L}$ and 0.083 $\mu\text{g/L}$, respectively. Recoveries and enrichment factor obtained from this method were 99.9% and 234, respectively. The mercury concentrations obtained in real crude oil were between 0.390 \pm 0.01 - 0.510 \pm 0.09 $\mu\text{g/g}$ which was in line with mercury concentrations from other countries. Mercury concentrations in crude oil derivatives ranged between 0.308 \pm 0.05 - 0.402 \pm 0.05 $\mu\text{g/g}$, 0.370 \pm 0.35 - 0.510 \pm 0.08 $\mu\text{g/g}$ and 0.090 \pm 0.09 - 0.098 \pm 0.02 $\mu\text{g/g}$ for gasoline, diesel oil and kerosene, respectively. AGRREEprep was successfully applied

for the assessment of environmental friendliness of the newly developed method. The score obtained in this method was 0.72 which is near the optimum value of 1. Hence, it can be summarized that the newly developed VA-DES-DLLME procedure was environmentally friendly.

REFERENCES

- [1] S.M. Wilhelm, L. Liang, D. Kirchgessner, *Energy and Fuels* 20 (2006) 180– 186.
- [2] A.A. Krata, E. Vassileva, *Talanta* 217 (2020) 121113.
- [3] R. Hernández-martínez, I. Navarro-blasco, *Food Control* 30 (2013) 423–432.
- [4] R. Azevedo, E. Rodriguez, *J Bot* 2012 (2012) 1–6.
- [5] Z. Izakian, (2021).
- [6] M. Beldowska, D. Saniewska, K. Gębka, U. Kwasigroch, E. Korejwo, J. Kobos, *Talanta* 182 (2018) 340–347.
- [7] M. Rutkowska, J. Płotka-Wasyłka, M. Sajid, V. Andruch, *Microchemical Journal* 149 (2019).
- [8] C. Hellmann, R.D. Costa, O.J. Schmitz, *Chromatographia* 82 (2019) 125–141.
- [9] M. Pirsaeheb, N. Fattahi, *Analytical Methods* 7 (2015) 6266–6273.
- [10] J.C. García-Mesa, P. Montoro-Leal, S. Maireles-Rivas, M.M. López Guerrero, E. Vereda Alonso, *J Anal At Spectrom* 36 (2021) 892–899.
- [11] S. Pedersen-Bjergaard, K.E. Rasmussen, *J Chromatogr A* 1184 (2008) 132– 142.
- [12] Y. Yamini, M. Rezazadeh, S. Seidi, *TrAC - Trends in Analytical Chemistry* 112 (2019) 264–272.
- [13] A.N. Anthemidis, K.I.G. Ioannou, *Talanta* 80 (2009) 413–421.
- [14] N. Campillo, P. Viñas, J. Šandrejová, V. Andruch, 4928 (2017).
- [15] M.Z. Corazza, C.R.T. Tarley, *Microchemical Journal* 127 (2016) 145–151.
- [16] S.L.C. Ferreira, V.A. Lemos, L.O.B. Silva, A.F.S. Queiroz, A.S. Souza, E.G.P. da Silva, W.N.L. dos Santos, C.F. das Virgens, *Microchemical Journal* 121 (2015) 227–236.
- [17] S. Motahar, M. Saber-Tehrani, P. Aberoomand Azar, Faribatadayon, *Journal of the Chilean Chemical Society* 63 (2018) 4190–4194.
- [18] B.M. Soares, E.R. Pereira, J. V Maciel, A.A. Vieira, F.A. Duarte, (2013) 3411– 3418.

- [19] V. Andruch, I.S. Balogh, L. Kocúrová, J. Šandrejová, *J Anal At Spectrom* 28 (2013) 19–32.
- [20] (n.d.).
- [21] F. Rastegarifard, K. Ghanemi, M. Fallah-Mehrjardi, *Analytical Methods* 9 (2017) 5741–5748.
- [22] F.C. Pinheiro, M.Á. Aguirre, J.A. Nóbrega, N. González-Gallardo, D.J. Ramón, A. Canals, *Anal Chim Acta* 1185 (2021).
- [23] A. Thongsaw, Y. Udnan, G.M. Ross, W.C. Chaiyasith, *Talanta* 197 (2019) 310–318.
- [24] M. Khan, M. Soylak, *Analytical Letters* 56 (2023) 1161–1173.
- [25] N. Altunay, A. Elik, R. Gürkan, *Food Additives and Contaminants - Part A Chemistry, Analysis, Control, Exposure and Risk Assessment* 36 (2019) 1079– 1097.
- [26] T. Jurić, D. Uka, B.B. Holló, B. Jović, B. Kordić, B.M. Popović, *Journal of Molecular Liquids* 343 (2021).
- [27] R.K. Ibrahim, M. Hayyan, M.A. AlSaadi, S. Ibrahim, A. Hayyan, M.A. Hashim, *Journal of Molecular Liquids* 276 (2019) 794–800.
- [28] M. Ștefănescu, M. Stoia, O. Ștefănescu, C. Davidescu, G. Vlase, P. Sfirloagă, *Revue Roumaine de Chimie* 55 (2010) 17–23.
- [29] N. Delgado-Mellado, M. Larriba, P. Navarro, V. Rigual, M. Ayuso, J. García, F. Rodríguez, *Journal of Molecular Liquids* 260 (2018) 37–43.
- [30] R. Ullah, M. Atilhan, B. Anaya, M. Khraisheh, G. García, A. Elkhattat, M. Tariq, S. Aparicio, *Physical Chemistry Chemical Physics* 17 (2015) 20941–20960.
- [31] G. Li, Q. Xie, Q. Liu, J. Liu, C. Wan, D. Liang, H. Zhang, *Asia-Pacific Journal of Chemical Engineering* 15 (2020) 1–10.
- [32] M.F. Majid, H.F. Mohd Zaid, C.F. Kait, N.A. Ghani, K. Jumbri, *Journal of Molecular Liquids* 294 (2019) 111588.
- [33] N.F. Gajardo-Parra, M.J. Lubben, J.M. Winnert, Á. Leiva, J.F. Brennecke, R.I. Canales, *Journal of Chemical Thermodynamics* 133 (2019) 272–284.

- [34] P.B. Sánchez, B. González, J. Salgado, J. José Parajó, Á. Domínguez, *Journal of Chemical Thermodynamics* 131 (2019) 517–523.
- [35] W. Chen, Z. Xue, J. Wang, J. Jiang, X. Zhao, T. Mu, *Wuli Huaxue Xuebao/ Acta Physico - Chimica Sinica* 34 (2018) 904–911.
- [36] I. Alfurayj, R. Pandian, S. Springer, C. Burda, *Journal of Molecular Liquids* 386 (2023) 122454.
- [37] S.E.E. Warrag, E.O. Fetisov, D.J.G.P. Van Osch, D.B. Harwood, M.C. Kroon, J.I. Siepmann, C.J. Peters, *Industrial and Engineering Chemistry Research* 57 (2018) 9222–9230.
- [38] M. Hossien-poor-Zaryabi, M. Chamsaz, T. Heidari, M.H.A. Zavar, M. Behbahani, M. Salarian, *Food Analytical Methods* 7 (2014) 352–359.
- [39] Z. Gao, X. Ma, *Analytica Chimica Acta* 702 (2011) 50–55.
- [40] L. Pelit, I. Bağatir, F.O. Pelit, F.N. Ertaş, *RSC Adv* 4 (2014) 32189–32196.
- [41] L.P. Kowtharapu, N.K. Katari, S.K. Muchakayala, V.M. Mariseti, *TrAC - Trends in Analytical Chemistry* 166 (2023) 117196.
- [42] M.S. Imam, M.M. Abdelrahman, *Trends in Environmental Analytical Chemistry* 38 (2023) e00202.
- [43] D. Moema, T. Makwakwa, H.N. Nyambaka, S. Dube, M. Nindi, *Food Analytical Methods* (2024).
- [44] A.O. Hay, F.A. Hansen, E. Psillakis, S. Pedersen-Bjergaard, *Green Analytical Chemistry* 3 (2022) 100028.
- [45] G. Souza Valasques, A. Maria Pinto dos Santos, D. Levi França da Silva, U. Mozart Ferreira da Mata Cerqueira, S. Luis Costa Ferreira, W. Nei Lopes dos Santos, M. Almeida Bezerra, *Food Chem* 318 (2020) 126473.
- [46] G.P. Brandão, R.C. De Campos, A.S. Luna, *Spectrochim Acta Part B At Spectrosc* 60 (2005) 625–631.
- [47] P. De O Vicentino, D.M. Brum, R.J. Cassella, *Talanta* 132 (2015) 733–738.
- [48] P.O. Vicentino, R.J. Cassella, *Talanta* 162 (2017) 249–255.

- [49] A. De Jesus, R.E. Sturgeon, J. Liu, M.M. Silva, *Microchemical Journal* 117 (2014) 100–105.
- [50] A. de Jesus, A.V. Zmozinski, M.A. Vieira, A.S. Ribeiro, M.M. da Silva, *Microchemical Journal* 110 (2013) 227–232.
- [51] G.P. Brandão, R.C. De Campos, A.S. Luna, *Spectrochimica Acta - Part B Atomic Spectroscopy* 60 (2005) 625–631.
- [52] D.P. Torres, I.M. Dittert, H. Höhn, V.L.A. Frescura, A.J. Curtius, *Microchemical Journal* 96 (2010) 32–36.
- [53] L. Liang, M. Horvat, P. Danilchikb, 9697 (1996) 0–7.
- [54] F. Veronesi, M. Pontes, M.C. Carneiro, D.S. Vaitsman, M. Inês, C. Monteiro, A.A. Neto, M. Luíza, B. Tristão, M.D.F. Guerrante, *Fuel Processing Technology* 106 (2013) 122–126.

Ultrasound-assisted magnetic dispersive solid phase microextraction based on Fe₃O₄-GO-Au for the preconcentration of mercury in fuel oils followed by ICP-OES determination

ABSTRACT

For the extraction of metal ions, graphene oxide (GO) is a highly effective adsorbent. GO surface functional moieties, however, are not metal ion specific. As a result, in this work, GO was chemically functionalized using gold to increase its mercury selectivity. To make the adsorbent's separation easier, the GO was first magnetized using the coprecipitation technique. The synthesized adsorbent was characterized using a variety of microscopic and spectroscopic methods. Trace amounts of mercury were extracted from crude oil and its byproducts, such as gasoline, diesel, and kerosene, using the sorbent. To analyze the extract, inductively coupled plasma optical emission spectroscopy (ICP-OES) was utilized. To find the optimal conditions for the extraction parameters, multivariate optimization techniques were used. The optimal parameters were determined to be a 20-minute extraction period, 30 mg of sorbent mass, pH 7, and 1.75 mol/L of HCl. Better recoveries were seen when 0.2 mol/L of thiourea was added to the eluent (HCl) as a mercury trapping agent. Preconcentration factor was 255 and extraction recoveries were 105 % under optimal conditions. The limits of quantification and detection were 1.19 µg/L and 0.35 µg/L, respectively. For intraday, the relative standard deviation was 3.5 %. Real crude oil, diesel oil, gasoline, and kerosene samples were successfully treated using the synthesized adsorbent. It was discovered that there is not a significant mercury contamination in South African gasoline oils.

5.1 Introduction

Mercury in fuel matrices, which is recognized as a key source of energy, has drawn more attention in recent years [1]. Since crude oil has been in contact with many earthly layers for millions of years, the presence of mercury in these energy resources is unmanageable. The primary obstacle in quantifying total mercury is its presence in extremely low concentrations (trace levels), which are typically beyond the limits of

most analytical instruments' detection [2]. Preconcentration is therefore required prior to spectroscopic determination. Many preconcentration techniques, like liquid-liquid extraction (LLE) and solid phase extraction (SPE), are often used in analytical chemistry [3–5].

Solid phase extraction is a preconcentration technique that separates and preconcentrates target analytes from a complex matrix by using a sorbent. The conventional SPE, from which all other new SPE techniques are derived from, is the one covered by this extraction methods. Four steps characterize the typical SPE: Sample loading, sorbent conditioning, washing, and elution [6]. Nevertheless, due to difficulties with separation and the need for significant amounts of organic solvents, classical SPE demonstrated certain drawbacks, including being labor-intensive and time-consuming. To eliminate these restrictions, several additional SPE were later developed. These consist of batch, column-based, dispersive, magnetic, and solid phase micro-extraction (m-SPME) as well as batch and micro-extraction (SPME) techniques. Out of all the newly listed SPE techniques, m-SPME has drawn the most attention because they require small amount of organic solvent to extract and preconcentrate analytes [7,8].

The primary characteristic of the m-SPME is the easy separation achieved by mixing a magnetic sorbent with a non-magnetic adsorbent for ease of separation. As a result, the protocol is more practical than other ones. Many researchers combine the advantages of m-SPME with DSPME, such as its high adsorption efficiency and ease of operation [9]. In this case, the sample solution is mixed with the magnetic adsorbent and then ultrasonically dispersed. The magnetic sorbent containing the target analyte is extracted from the solution using an external magnet. The target analyte is finally separated from the adsorbent using an eluent before being collected for analysis. Numerous adsorbents have been documented in the literature to extract target analytes from various matrices. These include functionalized ZrO₂ nanoparticles, magnetic iron oxide nanoparticles (Fe₃O₄), graphene oxide (GO), molybdenum disulfide nanosheets (MoS₂), metal-organic frameworks (MOF), carbon nanotubes (CNTs), activated carbon, and cellulose nanoparticles, all of which have been extensively explored in SPE and possess intrinsic characteristics such huge surface

areas, ease of surface functionalization, and great mechanical strength, which have demonstrated significant potential [10].

Among these nanomaterials, GO is a good sorbent for SPE because of its two-dimensional geometrical structure and the availability of hydroxyl, epoxy, and carboxyl groups on its surface. By exchanging a single pair of electrons with those at their basal plane and edges, these oxygen-containing functional groups can attach to heavy metal ions efficiently [11,12]. GO's adsorption efficacy for Hg (II) is, however, negligible, or non-existent. Therefore, GO structures containing groups that have a strong affinity for mercury must be modified.

The initial goal of this effort was to magnetize GO through functionalization, which combines its benefits of GO with magnetic particles for simpler separation [13]. Finally, gold (Au) coating was applied to the synthesized nanocomposite to improve selectivity towards total Hg. Additionally, the addition of GO to the nanocomposite improves its support, which prevents the nanocomposite from clumping [13,14]. According to our best knowledge, for the first-time magnetic graphene oxide coated with gold ($\text{Fe}_3\text{O}_4\text{-GO-Au}$) was tested for the preconcentration of total Hg in fuel matrices. Using a solution of hydrochloric acid and thiourea as an eluent, inductively coupled plasma optical emission spectroscopy (ICP-OES) was utilized to analyze the final extracts. To maximize the most important parameters (pH, sorbent mass, sonication time, elution time, and eluent concentration), a multivariate optimization technique was used.

5.2 Experimental section

5.2.1 Chemicals and reagents

Glassware (volumetric flask and beakers) washed with soap and water, soaked in 5 % nitric acid, and then rinsed with deionized water. Then, the glassware was dried overnight at 100 °C in an oven. Using the proper dilution of a 1000 mg/L mercury standard solution (Sigma-Aldrich, South Africa), mercury standards were created. NIST SRM 2778, the standard reference material, contains certified mercury concentrations of 38.98 $\mu\text{g}/\text{kg}$ \pm 1.10 $\mu\text{g}/\text{kg}$ in fuel, 70 % ultra-pure HNO_3 , iron (II) chloride tetrahydrate ($\text{FeCl}_2 \cdot 4\text{H}_2\text{O}$), iron (III) chloride hexahydrate ($\text{FeCl}_3 \cdot 6\text{H}_2\text{O}$), graphite, thiourea, tetra chloroauric (III) acid (HAuCl_4), sodium hydroxide (NaOH),

potassium permanganate (KMnO₄), hydrochloric acid, hydrogen peroxide, sulfuric acid, phosphoric acid, and ammonia were obtained from Sigma-Aldrich, South Africa. A South African petrochemical company provided the crude oil samples, while actual gasoline, kerosene, and diesel samples were obtained from nearby filling stations in the Johannesburg area.

Sigma-Aldrich, South Africa, supplied the 99 % xylene used to lower the viscosity of the crude oil sample and the neodymium-iron-boron alloy magnet used to eliminate magnetic nanoparticles. Every fuel sample that was purchased was labelled in accordance with **Table 5.1**. Nylon microfilters (0.45 µm) were purchased from Anatech Instruments in South Africa. **Table 5.2** lists the synthesized nanocomposites along with their acronyms.

Table 5. 1: Different types of fuel oils and their abbreviations.

Sample type	Sample 1	Sample 2	Sample 3
Crude oil	COS 1	COS 2	COS 3
Gasoline	GS 1	GS 2	GS 3
Diesel oil	DS 1	DS 2	DS 3
Kerosine	KS 1	KS 2	KS 3

Table 5. 2: Synthesized nanocomposites and their abbreviations.

Abbreviation	Full name
GO	Graphene oxide
MGO	Magnetic graphene oxide
MGO-Au	Magnetic graphene oxide coated with gold

5.2.2. Instrumentation

The ICP-OES proved advantageous for determining trace elements in m-SPE extracts due to its multielement analysis capacity and sensitivity. The operating conditions of the ICP-OES are reported in **Table 3.2**. Using an axial torch orientation, Agilent Technologies 700 Series ICP-OES was used to analyze the extracted results for mercury. For sample uptake, an Agilent Technologies SPS 3 autosampler was also utilized.

5.2.3. *Characterization techniques*

The synthesized nanoparticles (GO, MGO, and MGO-Au) were confirmed using the following characterization techniques.

5.2.3.1. Fourier Transform infra-red spectroscopy (FT-IR)

To determine which functional groups are present in a molecule, FT-IR is utilized. The synthesized nanoparticles' (GO, MGO, and MGO-Au) Fourier transformed infrared (FTIR) spectra were measured using the KBr wafer technique on a Bruker Tensor 27 (Bruker Optics, GmbH, Germany) FTIR spectrophotometer. The synthesized samples were compacted into a pellet after being combined with KBr. The data was recorded between 400 and 4000 cm^{-1} for the analysis.

5.2.3.2. Ultraviolet visible spectroscopy (UV-vis)

To verify the UV spectra of the synthesized nanoparticles (GO, MGO, and MGO-Au), a 150 W Xenon lamp linked to a Shimadzu UV1800 spectrophotometer (RF-5301PC, Shimadzu) was utilized.

5.2.3.3. Powder-X-ray diffraction (P-XRD)

The PANalytical X'Pert Pro powder diffractometer (P-XRD, PANalytical, Almelo, the Netherlands) was used to verify the crystalline size and diffraction pattern of the synthesized nanoparticles (GO, MGO, and MGO-Au). This instrument was fitted with 1D X'Celerator detector, 10 mm programmable divergence slit and sample spinner (Spinner PW3064) with a rotation time of 1 s. Operating at 40 kV and 40 mA, the Cu $K\alpha$ ($\lambda = 0.15405$ nm) tube served as the source of X-ray radiation. It is important to note that a monochromator was added to the detector to reduce the strong background brought on by the sample's fluorescence because of the presence of iron. Under the Gonio scan axis, the measurement was performed using a continuous scan type, step size, scan step time, and a 2h range of 5 to 90°, 0.0170°, 87 s, and 2h, respectively. After being pulverized with a pestle and mortar, the P-XRD samples were placed on the low background silicon sample holder. Following the X-ray measurements, the ICDD PDF-4+ 2019 database and High Score (Plus) software was used to evaluate the raw data. Scherer's equation (**Eq.5.1**) determines the size of the crystallite:

$$D = \frac{0.9\lambda}{\beta \cos\theta}$$

Eq. 5.1

where λ is X-ray wavelength (1.5406 Å), and β is the full width of the half maximum (FWHM) [15].

5.2.3.4. Transmission electron microscopy (TEM)

Using a Jeol JEM-2100F transmission electron microscope apparatus (TEM, JOEL Ltd., Tokyo, Japan), transmission electron microscopy (TEM) was used to confirm the particle size, shape, and structure of the synthesized nanoparticles (GO, MGO, and MGO-Au). The latter had a LaB6 source and a charge-coupled device (CCD) digital camera, and it ran at 200 kV. Before TEM examination, a tiny layer of lacy carbon material was applied to the Cu-grid, a TEM grid of 200 mesh size, and a little amount of iron oxide material was scattered across it.

5.2.3.5. Scanning electron microscopy-energy dispersive spectroscopy (SEMEDS)

Scanning electron microscopy-energy dispersive spectroscopy (SEM/EDS, Tescan, Brno, Czech Republic) was used to verify the shape, particle size, and elemental composition of the synthesized nanoparticles (GO, MGO, and MGO-Au). A Tescan Vega 3 LMH operating at 20 kV accelerating voltage was used for the scanning electron microscope (SEM) observations. Energy dispersive spectroscopy (EDS) and a secondary electron detector (SED) were employed. Prior to measurement, the samples' conductivity was increased by applying an Agar Turbo Carbon coater to them.

5.2.3.6. Brunauer-Emmett teller (BET)

A Micromeritics ASAP 2460 was used to conduct a Brunauer-Emmett-Teller (BET) study, which looked at the synthesized nanocomposites' surface area, porosity, pore size, and pore volume. During the analysis, the synthesized materials were degassed with nitrogen gas at 150 °C for ten hours. The pore sizes and volumes were computed using adsorption curves and the BJ H model, and the experiments were carried out at 195.8 °C.

5.2.3.7. Thermogravimetric analysis (TGA)

The thermal stability and thermal decomposition temperatures of all the synthesized nanoparticles were investigated using a thermogravimetric analyzer instrument model Q500 from TA Instruments-Waters LLC. Sample holders made of platinum pans were used to hold each sample individually, with a nitrogen atmosphere flow rate of 40 milliliters per minute (40 mL/min). With a heating rate increase of 10 °C /minute, all samples were heated from 10 to 600 °C.

5.2.4. ***Synthesis of nanoparticles***

5.2.4.1. Preparation of Graphene oxide (GO)

Hammer's method was adopted, albeit slightly modified, for synthesis of graphene oxide (GO). Briefly, 50 g of NaCl was ground for 10 minutes with 4 g of natural graphite powder. Next, NaCl was eliminated by filtering after dissolving in ultrapure water. Graphite powder (3 g) that was initially treated with NaCl was gradually added to the mixture of H₂SO₄ and H₃PO₄ (9:1) while stirring continuously. After that, the combination above was gradually mixed with 18 g of KMnO₄ while it was submerged in an ice bath. After mixing the final product in a flask, it was stored at 50 °C for a whole day [16,17]. To the reaction mixture, 50 ml of distilled water was added. For two more hours, the temperature was raised and stirring was done. Next, 10 mL of H₂O₂ and 20 mL of deionized water were added to stop the reaction. The final mixture was then centrifuged, and the brown precipitate was washed three times using deionized water and 5 % HCl [18]. To remove any last traces of salts and acids, the brown precipitate was subjected to dialysis. For later use, GO sheets were created by drying the final suspensions [19].

5.2.4.2. Preparation of magnetic graphene oxide (MGO) nanocomposite

Approximately 1 g of GO powder was first sonicated for an hour in 250 mL of deionized water [20]. Next, the reaction mixture was placed on a heater that was surrounded by nitrogen. Dropwise additions of 2 mmol of FeCl₃.6H₂O and 1 mmol of FeCl₂.4H₂O (dissolved in 25 mL of deionized water) were made to the graphene oxide solution after the initial addition of 5 mL of ammonia. The reaction was stirred for five

hours at 80 °C, after which the resultant product (MGO) was centrifuged, cleaned with deionized water, and dried for the night at 60 °C [21].

5.2.4.3. Preparation of magnetic graphene oxide coated with gold (MGO-Au) nanocomposite

Initially, 50 mg of MGO powder were sonicated for an hour at room temperature in 20 mL of deionized water. The dispersion was separated using an external magnet and then re-dispersed in 10 millilitres of deionized water. About 2 mL of sodium citrate solution (0.5% w/v) was mixed with 120 mL of NaOH solution (2 M), and 3 mL of H₂AuCl₄ solution (20 mM). The redispersed sample from the previous stage was then added to the mixture [22]. After being mixed for an hour at room temperature, the finished product, MGO-Au, was separated using an external magnet, rinsed several times with deionized water, and dried at 60 °C.

5.2.5. *Ultrasound assisted magnetic dispersive solid phase microextraction (UA-m-DSPME) procedure*

With a few minor modifications, the ultrasonic assisted magnetic dispersive solid phase microextraction (UA-m-DSPME) method was executed in accordance with the method published by Biata et al. [23] (**Fig. 5.1**). In summary, 5 mL of crude oil was tampered with using 100 µg/L of mercury standard. After the sample's pH was brought down to 6.5 with a buffer solution, it was put into a glass vial with 30 mg of MGO-Au adsorbent. The analyte was preconcentrated for 20 minutes at room temperature (25 °C) in an ultrasonic bath. An alloy magnet made of neodymium, iron, and boron was then used to separate the adsorbent from the sample. The adsorbent containing the target analyte was then left behind when the fuel oil was decanted. 0.2 mol/L thiourea plus 1.75 mol/L HCl in 500 µL were used to elute the analyte(s) that were retained. It's crucial to remember that, for six minutes, ultrasonication also helped with elution. Ultimately, the eluent was gathered, filtered, and ICP-OES analyzed. Both real samples and blanks underwent the same process.

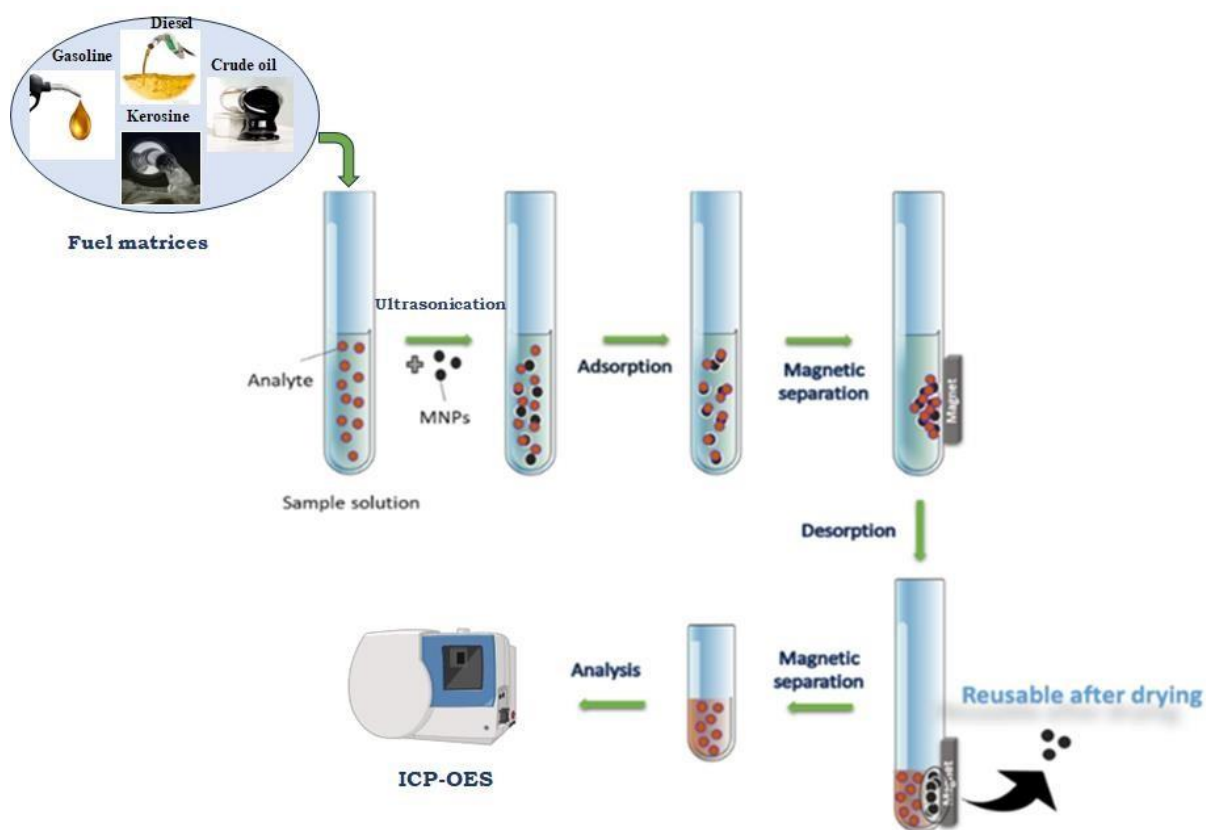


Figure 5.1: Crucial steps for ultrasound assisted-dispersive magnetic solid phase microextraction procedure (UA-m-DSPME).

5.2.6. Optimization of UA-D-m-SPME procedure

A multivariate technique was used to carry out the UA-m-DSPME procedure's optimization process. The latter approach was utilized to minimize laboratory experiments and enable the assessment of interactions between the factors [24]. The Min tab 2018 program was used for this. The most important parameters were screened using a two-level half fractional design (2^{5-1}). Eluent concentration, elution time, sorbent mass, pH, and sonication time were the most important extraction parameters that were optimized. 17 experiments in all were produced, with the factors and levels (minimum, middle, and maximum) of the experimental designs used for the optimization process shown in **Table 5.3**. Response surface methodology (RSM) was utilized to optimize the significant parameters at a 95 % confidence level. This study employed BBD to optimize the most significant variables further. These factors were assigned three levels (minimum, central, and maximum), using literature reports as our guide. These levels are shown in **Table 5.4** and 27 experiments were generated.

From these experiments results, we could deduce optimum conditions for each variable.

Table 5.3: Two-level half factorial (2^{5-1}) experimental design.

Factor	Minimum (-)	Central (0)	Maximum (+)
Sorbent mass (mg)	10	30	50
Sonication time (min)	10	35	60
pH	3	6	9
Eluent concentration (mol/L)	0.1	0.55	1.0
Elution time (min)	3	4	5

Table 5.4: Response methodology based on BBD experiment design.

Factor	Minimum (-)	Central (0)	Maximum (+)
Sorbent mass (mg)	10	30	50
pH	2	5	8
Sonication time (min)	10	20	30
Eluent concentration (mol/L)	1.0	1.75	2.5

5.2.7. *Application of the MGO-Au nanocomposite to real fuel samples*

The study examined the adsorption of mercury onto the synthesized MGO-Au nanocomposite derived from genuine fuel samples, including kerosine, gasoline, diesel, and crude oil, at the optimal circumstances previously mentioned.

5.2.8. *Reusability studies*

The adsorption and desorption experiments were repeated to evaluate the adsorbent's reusability. First, under ideal circumstances, several experiments (10) were carried out to determine whether the magnetic nanoparticles could be reused. Every experiment was followed by a 90-minute oven drying of the MGO-Au at 60 °C.

5.3 Results and discussion

5.3.1. Characterization methods for the prepared nanoparticles

5.3.1.1. Fourier Transform Infra-red spectroscopy (FT-IR)

Figure 5.2 a-c shows the Fourier transformed infrared (FT-IR) spectra of the GO, MGO, and MGO-Au core-shell nanocomposite. Stretching vibrations of O-H led to the exploration of the GO peak at 3419 cm^{-1} . The stretching vibrations of the C=O and C=C groups were attributed to the less pronounced intensity peaks at 1746 cm^{-1} and 1619 cm^{-1} , respectively, as depicted in **Fig. 5.2 a**. The vibrations of alkoxy C–O stretching and O–H bending was identified as the cause of the peaks at 1061 cm^{-1} and 665 cm^{-1} [22]. This validates that GO was successfully synthesized. **Figure 5.2 b** shows an MGO spectrum. In the former, the asymmetric stretching vibration of C=O and the aromatic C=C vibrations of graphene give rise to a minor intensity peak at 1644 cm^{-1} and a band at 1544 cm^{-1} , respectively. Like findings reported in the literature, the broad band at 3400 cm^{-1} was attributed to the O-H group, and a sharp peak at 540 cm^{-1} was related to the stretching vibrations caused by the interactions of Fe–O–Fe in Fe_3O_4 NPs [25]. **Figure 5.2 c** shows a spectrum that attests to the effective synthesis of MGO-Au. After Au NPs were deposited, the MGO-Au core-shell nanocomposite showed less intense peaks at 582 cm^{-1} , and the band at 1544 cm^{-1} became stronger [26]. These outcomes validate that the nanocomposite was successfully synthesized.

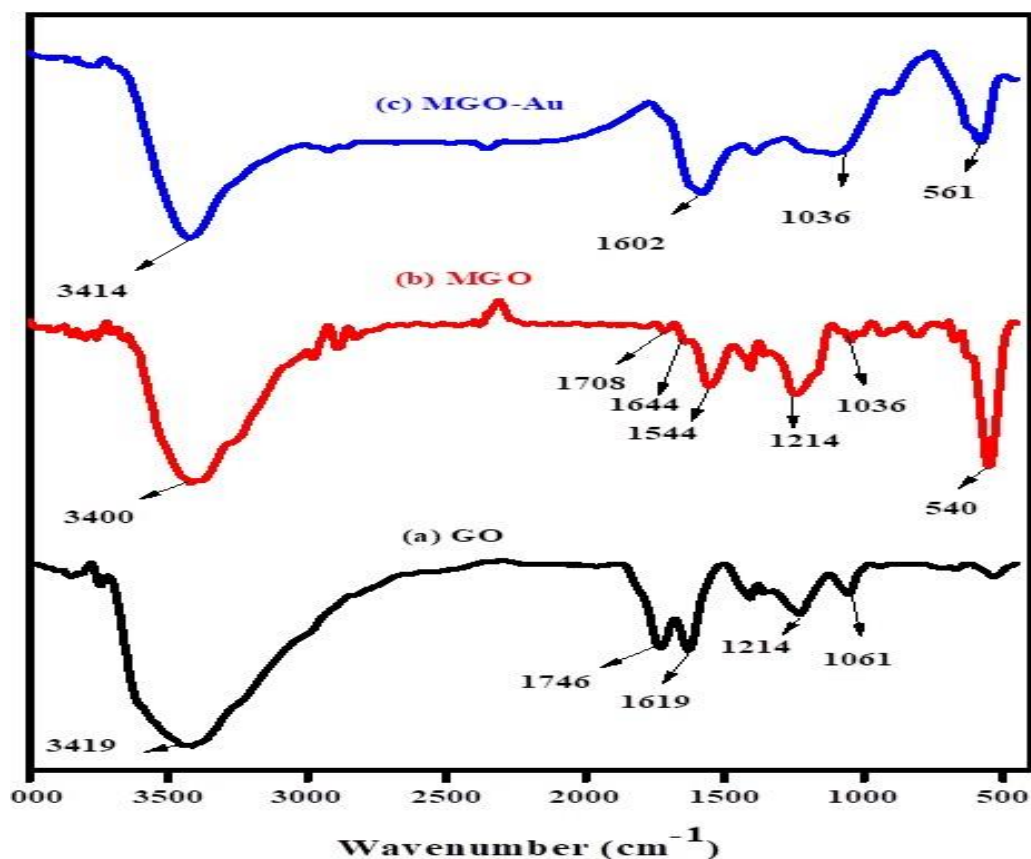


Figure 5.2: FT-IR spectra for (a) GO, (b) MGO and (c) MGO-Au.

5.3.1.2. UV-visible absorbance spectra analysis

An additional method of verifying the synthesized nanocomposites was ultraviolet-visible spectrophotometry (UV-visible). To determine the transitions from the ground state to the excited states, the UV absorption spectra of GO, MGO, and MGO-Au were recorded (**Fig.5.3 a-c**). The latter displays the GO spectrum, which is attributed to the π - π^* transition of C=C bonds and has a strong peak at 222 nm. The n - π^* transitions of the epoxide (C-O-C) and peroxide (O-O) links, which are present in the GO structure, correlate to another large peak between 275 and 300 nm [27]. The effective synthesis of GO is confirmed by the presence of these functional groups, which are compatible with FT-IR data. The UV absorption peaks of GO and Fe₃O₄ in the MGO nanocomposite are compared to the absorption peaks for MGO (**Fig.5.3 b**) at 270 and 396 nm [25]. The peaks for magnetic GO are visible at 225 nm in the UV spectra of MGO-Au (**Fig. 5.3 c**), and there is a broad peak from 265–301 nm.

Additionally, a new peak that represents the absorption of gold nanoparticles can be seen in this spectrum between 500 and 530 nm. Several reports from the literature support this trend [28]. This attests to the three nanomaterials' effective synthesis.

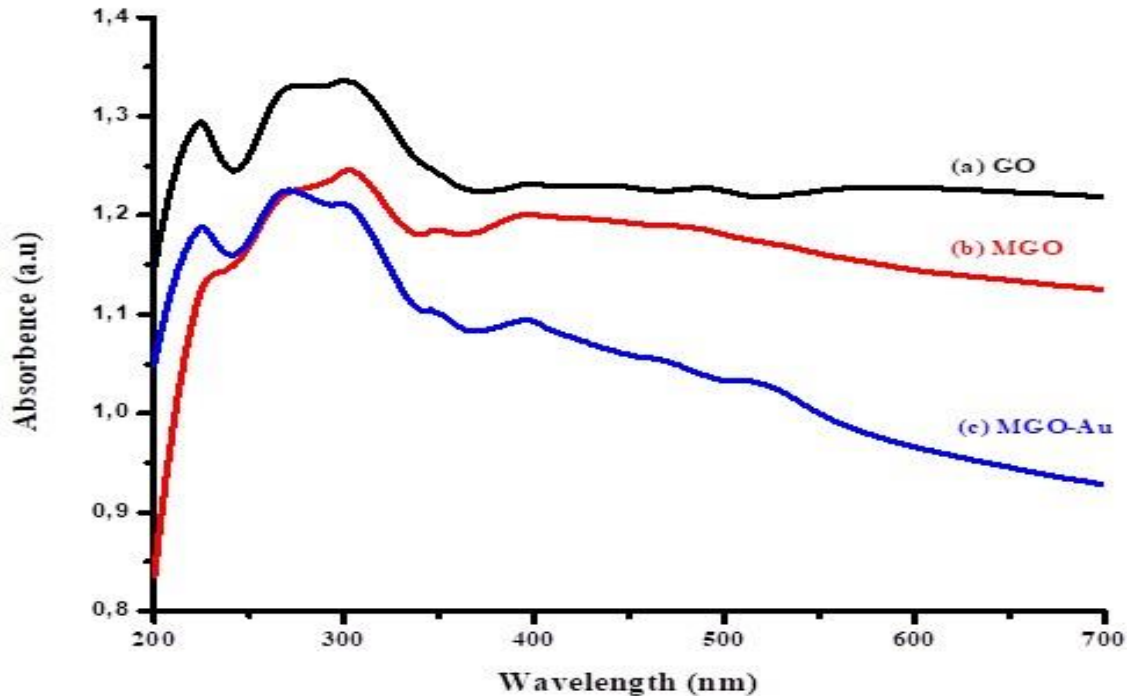


Figure 5.3: UV-vis spectra for (a) GO, (b) MGO, and (c) MGO-Au.

5.3.1.3. Powder-X-ray diffraction (P-XRD)

Using powder XRD, the crystalline structures and crystalline sizes of GO, MGO, and MGO-Au nanocomposites were examined; **Fig.5.4(a-c)** shows exemplary diffraction patterns. Sharp and intense diffraction peaks in 12.7° (001)'s 2θ are indicative of graphene oxide. The peak was ascribed to the amorphous nature of GO and its oxygenated functional groups, as illustrated in **Fig. 5.4 a** [29]. The GO reacts with the iron oxide nanoparticles, destroying the GO sheets, which is why the peak vanishes (**Fig.5.4 b**). The Fe_3O_4 cubic lattice's (220), (311), (400), (422), (511), and (440) crystal planes are responsible for the diffraction peaks at 2θ values of 30.4° , 35.6° , 43.2° , 53.8° , 57.7° , and 62.9° , respectively [30]. These results are in line with reports from the literature and validate the successful synthesis of MGO. Gold nanoparticles (**Fig. 5.4 c**) are visible at 2θ : 38.0° , 44.2° , 64.5° , 77.5° , and 81.5° , which correspond to the (111), (200), (220), (311), and (222) planes, in that order. Still visible,

though, are the iron oxide diffraction peaks [22]. These results verify that the MGO-Au nanocomposite was appropriately synthesized. Using the Sherrer equation (**Eq. 5.1**), the average crystallite size was determined to be 13.34 nm.

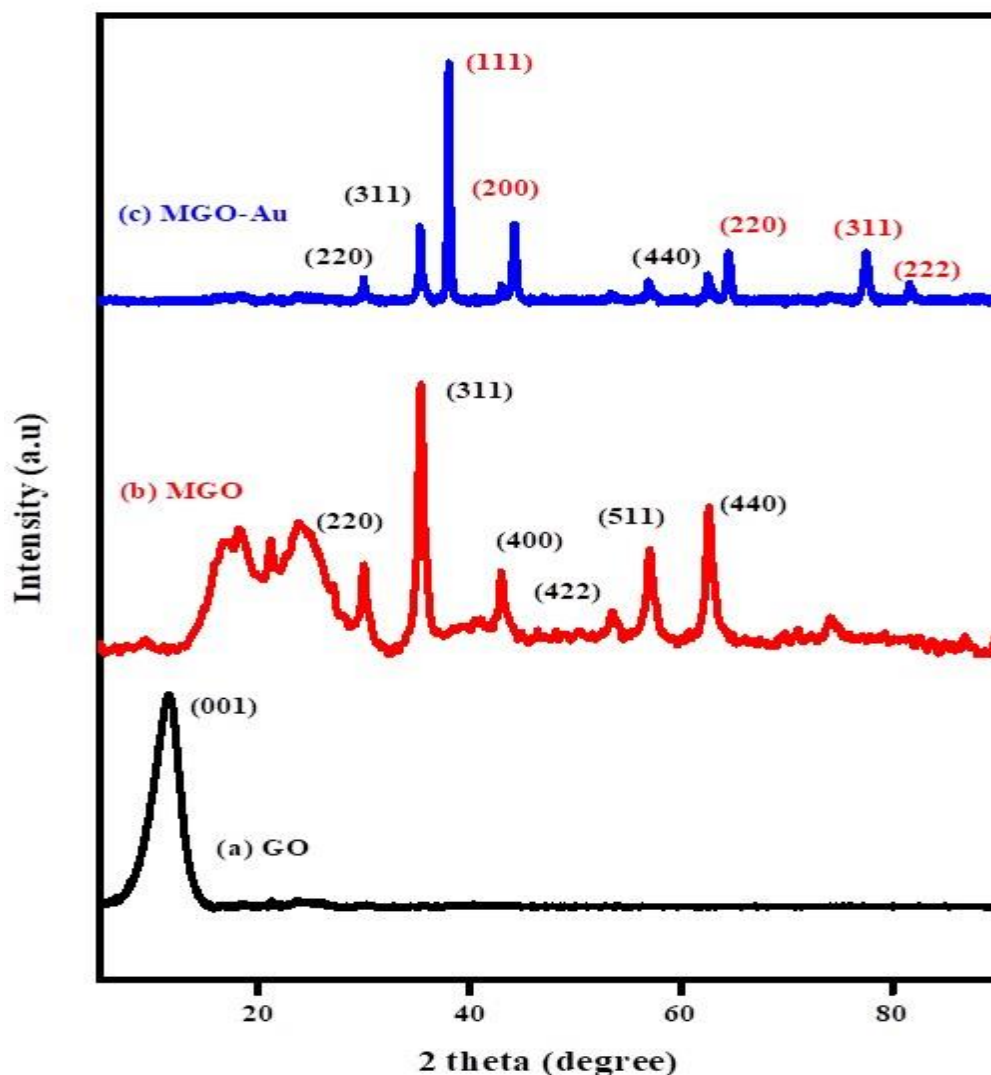


Figure 5. 4: Powder X-ray diffraction patterns for (a) GO, (b) MGO, and (c) MGO-Au.

5.3.1.4 Thermogravimetric Analysis (TGA)

Figure 5.5 a-c shows the comparison of the thermogravimetric curves for GO, MGO, and MGO-Au. For GO, three unique phases of weight loss were identified (**Fig. 5.5 a**). The vaporization of the adsorbed water molecules during the first stage caused a small mass loss below 100 °C. During the second stage, certain functional GO groups that contain oxygen break down into water vapor, which is responsible for the mass loss that occurs between 100 and 180 °C. Large mass loss happened over 180 °C because of GO's carbon backbone breaking down [29]. **Figure 5.5 b** shows how MGO breaks down thermally. The MGO and MGO (**Fig.5.5b&c**) thermal breakdowns

were comparable. Below 100 °C, a small weight loss occurred due to thermal desorption of water. While the second loss is related to GO's slow breakdown [18].

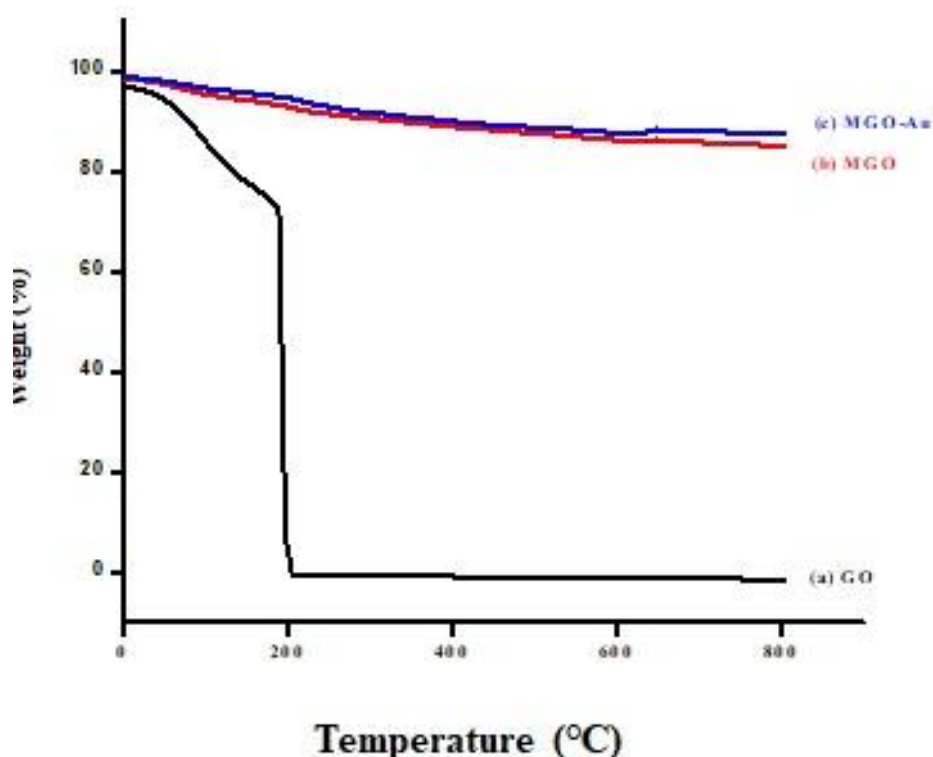


Figure 5. 5: Thermographs for (a) GO, (b) MGO, and (c) MGO-Au.

5.3.1.5. Scanning electron microscopy-energy dispersive spectroscopy (SEM-EDS)

A scanning electron microscope (SEM) in conjunction with energy dispersive spectroscopy (EDS) was used to further examine the morphology and elemental content of the synthesized materials (GO, MGO, and MGO-Au core-shell nanocomposite), as shown in **Fig. 5.6 (A-C)**. According to the results, GO sheets were formed, as seen in **Fig. 5.6 A**. The interplay of functional groups containing oxygen results in layered structures being seen [31]. Adding Fe_3O_4 nanoparticles to GO caused it to appear as brilliant spots evenly distributed across its surface, in contrast to GO's smooth surface (**Fig. 5.6 B**). According to some literature publications, these outcomes are equivalent [29]. The MGO-Au formation is shown in **Fig. 5.6 C**. On the surface of the GO nanosheet, the Au and Fe_3O_4 nanoparticles are exhibited as spherical formations with an average size of 14 nm. Furthermore, EDS (**Fig. 5.6 D**)

confirmed the successful synthesis of MGO-Au due to the presence of Fe, C, O, and Au. The synthesis of the MGO-Au nanocomposite was successfully confirmed by this.

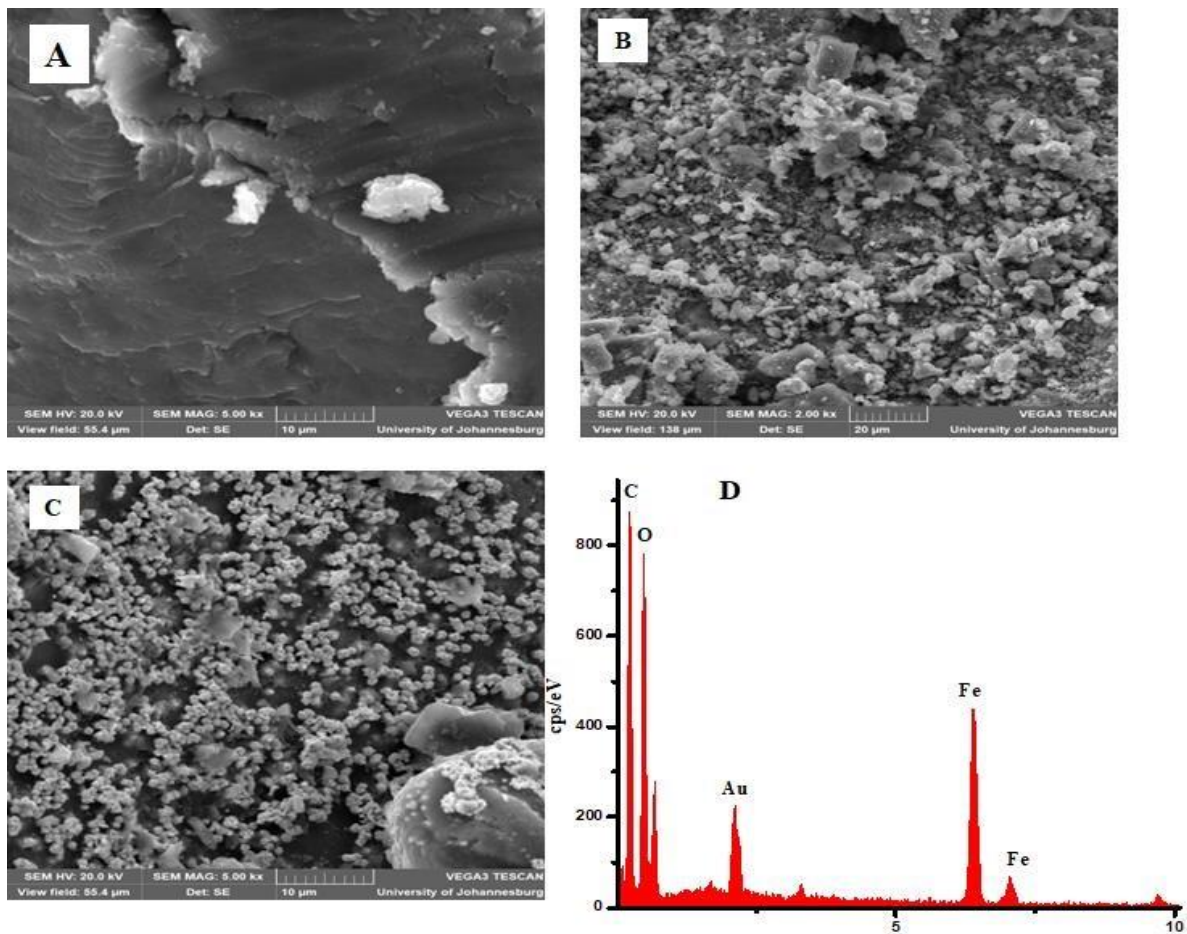


Figure 5. 6: Scanning electron microscopy for (a) GO, (b) MGO, (c) MGO-Au. And (d) EDS for MGO-Au.

5.3. 1.6. Transmission electron microscopy (TEM)

Figure. (5.7 A-D). presents Transmission Electron Microscopy results. The thin, layered structure of graphene oxide sheets is characterized by folded wrinkles, and their vast surface area makes them particularly advantageous for loading nanoparticles (NPs) (**Fig. 5.7 A**). The Fe_3O_4 NPs anchored on GO sheets and created a huge number of Fe_3O_4 NPs with various sizes, as seen in **Fig. 5.7 B**. By adding Fe_3O_4 NPs to the GO sheets, a stacked graphitic structure cannot form, and the

composites have magnetic characteristics that make them easily recyclable [32]. The typical shape of the synthesized nanocomposite is depicted in the TEM image (**Fig. 5.7 C**). The produced nanoparticles are visible as they are distributed across the GO surface, displaying lighter iron oxide particles and darker gold nanoparticles. The electron density of gold nanoparticles gives them a deeper color [22]. Image J software was used to calculate the particle size distribution of the synthesized MGO-Au, as shown in **Fig. 5.7 D**. Corresponding to the XRD and SEM data, an average particle size of 14 nm was obtained.

Figure 5.7 A, B, and C display insets of GO, MGO, and MGO-Au selected area electron diffraction (SAED) patterns. **Figure 5.7 A** SAED patterns insert show that GO has an amorphous pattern, but **Fig. 5.7 B** shows that the MGO nanoparticles were extremely crystalline and could be accurately indexed to the cubic structure of pure Fe_3O_4 [29]. A polycrystalline pattern for MGO-Au nanocomposite is also shown in the inset in **Fig. 5.7 C**. The SAED data correlates very well with the P-XRD patterns.

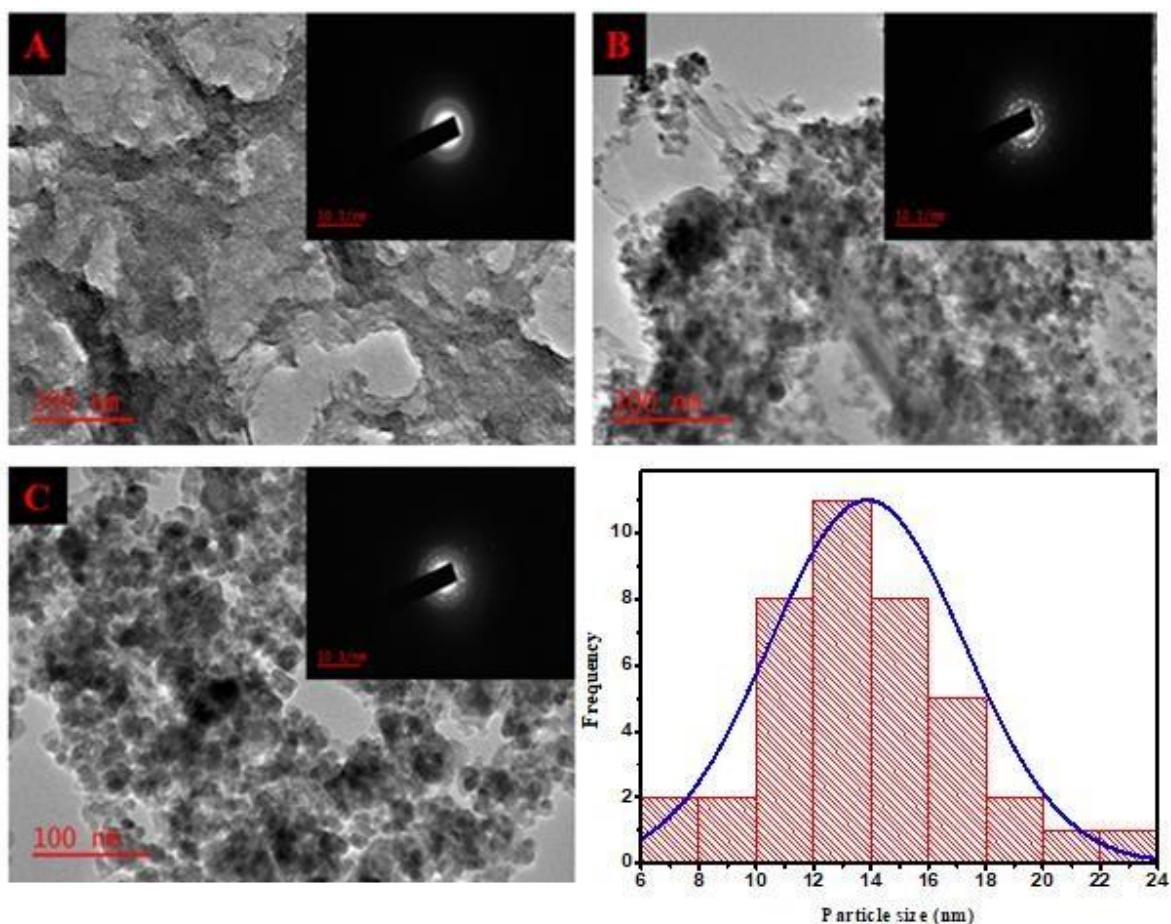


Figure 5. 7: Transmission electron microscopy for (a) GO, (b) MGO, and (c) MGOAu.

5.3.1.7. Brunauer-Emmett-Teller (BET)

The parameters that typically influence the adsorption property include the specific surface area, surface functional group, and pore size distribution. We performed Brunauer Emmett Teller (BET) measurements. The porosity was determined using the nitrogen adsorption isotherm, and the pore size distribution was determined using the Barrett-Joyner-Halenda (BJH) method (**Figs. 5. 8 & 9**). The surface areas of GO, MGO nanocomposite, and MGO-Au core-shell nanocomposite was 42.222, 32.187, and 57.92 m² g⁻¹, respectively, according to **Table 5.5**. The isotherm (**Fig. 5.8**) displays characteristics of an H3 hysteresis loop in the range of 0.4-0.9 (P/P₀), or a type IV isotherm [33]. Moreover, **Fig. 5.9** illustrates the MGO-Au core-shell nanocomposite's average pore size distribution at around 17–47 nm,

indicating that the material was mesoporous as well. This observation is also consistent with some literature reports [34,35].

Table 5. 5: The BET results of the GO, MGO and MGO-Au core shell nanocomposite.

Sample	Surface area (m ² /g)
GO	42.222
MGO	32.187
MGO-Au	57.962

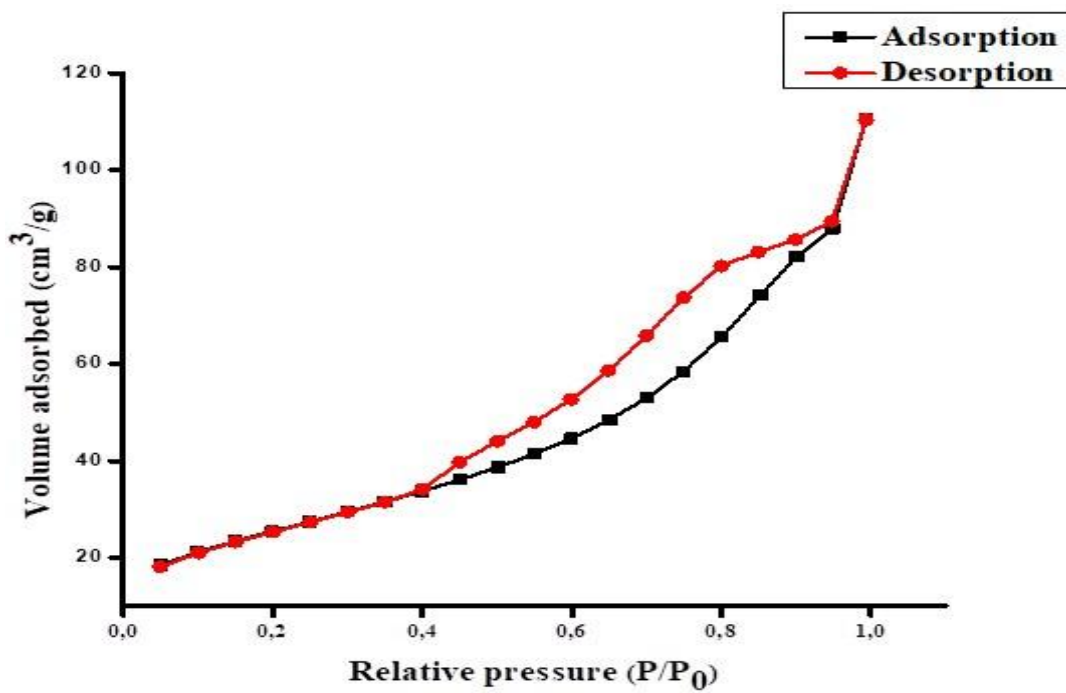


Figure 5. 8: The nitrogen adsorption isotherm curve of MGO-Au core shell nanocomposite.

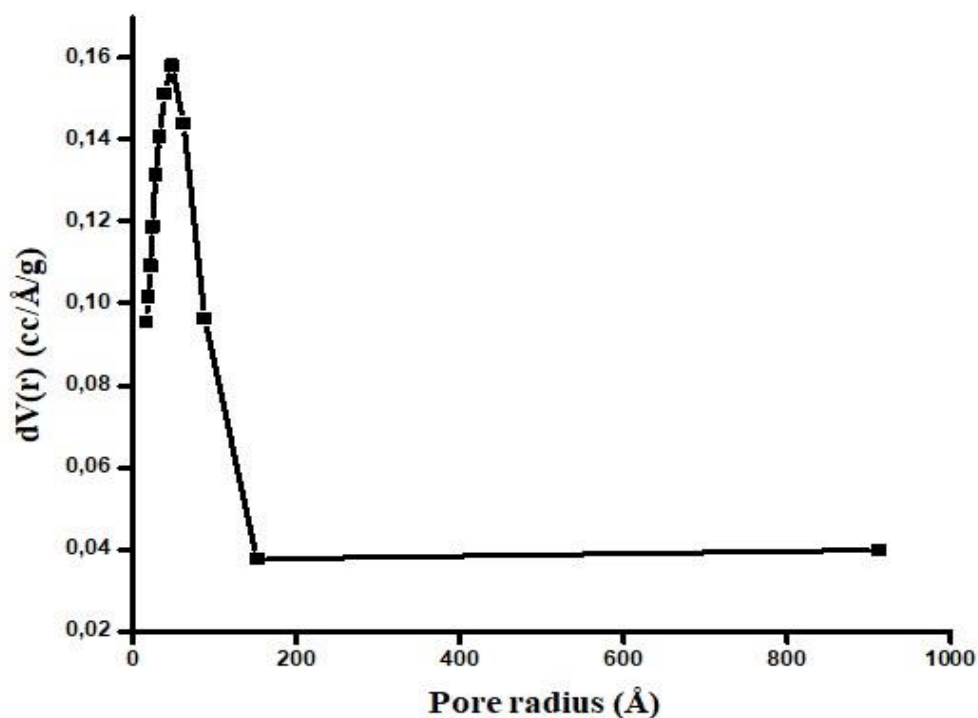


Figure 5. 9: The pore size distribution of MGO-Au core shell nanocomposite.

5.3.2. Choice of eluent

For the desorption of mercury from different nanomaterials, HCl is typically recommended as an eluent of choice in the literature studies. Comparing the results was necessary since screening was done in this experiment to see how adding various trapping agents to the eluent would affect it. This was accomplished by analyzing a NIST SRM 2778 under the following experimental conditions, which resulted in a certified mercury concentration of $38.98 \mu\text{g}/\text{kg} \pm 1.10 \mu\text{g}/\text{kg}$: Sample mass: 30 mg; pH: 6; sonication period: 30 minutes; elution period: 6 minutes. The following three eluent combinations were examined: 10 % HCl, HCl+Au, and 0.05 mol/L thiourea + 10 % HCl. **Figure 5.10** displays the findings. This figure shows that increasing the thiourea concentration as a trapping agent in HCl results in higher recoveries (101 %). The thiourea concentration was maintained at 0.2 mol/L while the HCl content was further optimized.

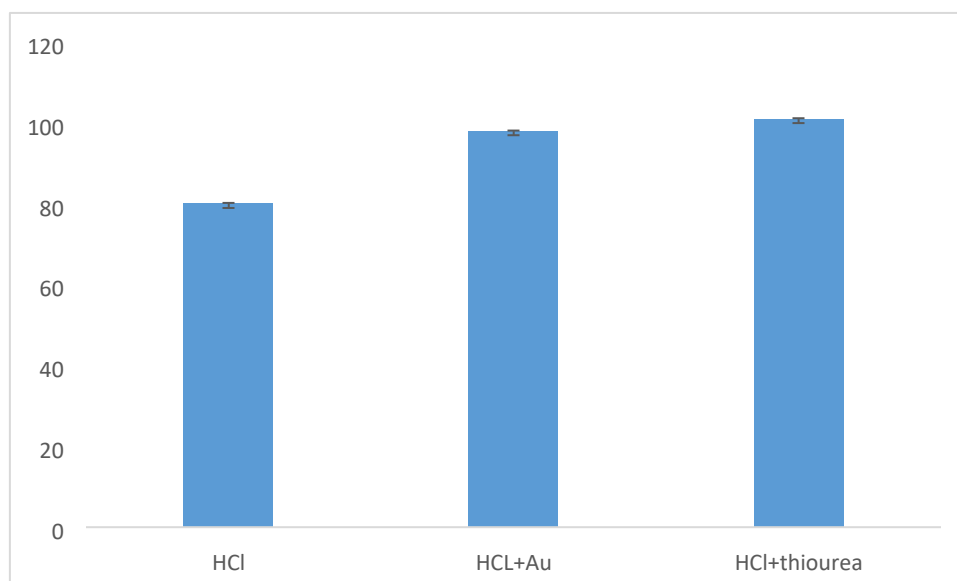


Figure 5. 10: Recoveries (%) for (a) HCl, (b) HCl+ Au, and (c) HCl+ thiourea.

5.3.3. Multivariate optimization

5.3.3.1. Two-level half factorial design

The effects of several experimental parameters, including adsorbent mass, pH, adsorption time, eluent concentration, and elution time, were examined using a two level half-factorial design. **Appendix Table S9** presents the parameters, number of experiments, experimental conditions, and outcomes of the two-level half factorial design. The primary effects and their interactions were assessed using the analysis of variance (ANOVA) (**Appendix Table S10**), which was displayed as Pareto charts (**Fig. 5.11**). The bar length relates to the absolute value of the estimated impacts, while the vertical line shows the 95 % confidence level. Comparing the proportional importance of the impact is made easier by the bar length. According to the ANOVA results, the eluent concentration, pH, adsorbent mass, and adsorption period were all significant at the 95 % confidence level (bar length is greater than the reference line). The Box Behnken design further optimized the critical factors.

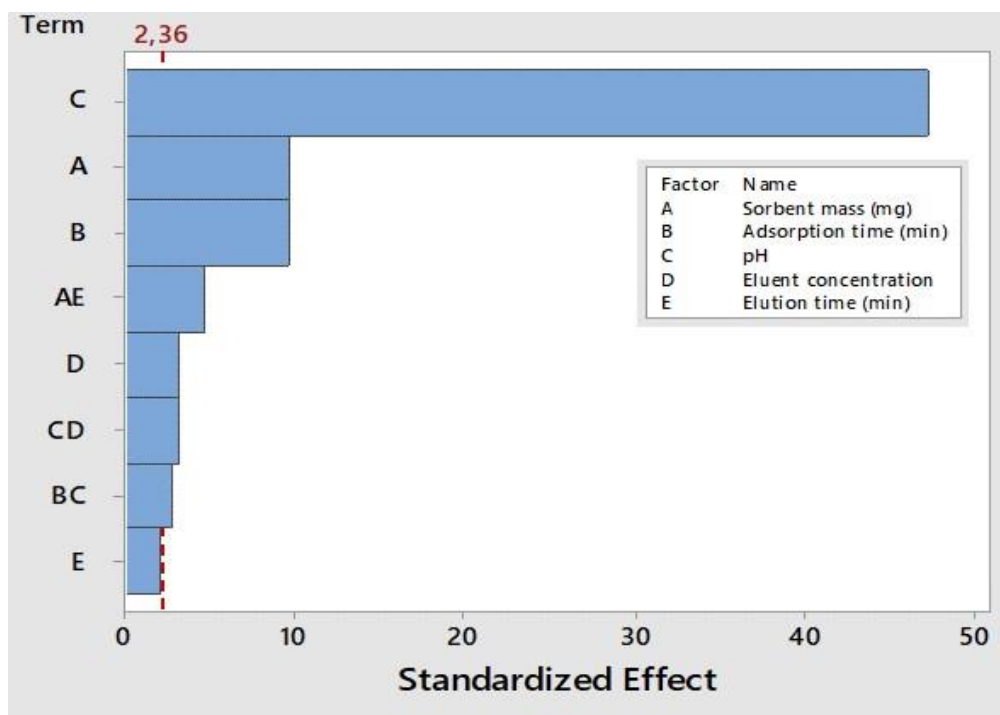


Figure 5. 11: Two-level half factorial design.

5.3.3.2. Further optimization using response surface methodology

Response surface methodology based on Box-Bohnken design was used to determine the ideal conditions of the relevant factors. **Appendix Table S11** displays the Box-Bohnken design matrix along with the analytical response values. For all the tests, the Hg (II) concentration was maintained at 100 µg/L and the statistically insignificant factor elution duration was kept constant at 6 minutes. This is how the model was described:

The design model led to coefficient of determination (R^2) and adjusted R^2 values of 0.9035 and 0.8191, respectively, indicating that it was appropriate for optimizing the preconcentration, according to the ANOVA data (**Appendix Table 12**). It is not significant in relation to pure error, as indicated by the F-value of 35.8 for the lack of fit.

Figure 5.12 (A-D) illustrates how the two factors interact to provide the highest adsorption capacity. The analytical response rises as pH rises, but it falls at higher pH levels ($\text{pH} > 7$), as seen in **Fig. 5.12 A**. Mercury creates a variety of species at pH values

higher than 7, including stable mercuric hydroxide, which prevents the production of Au-Hg complexes, which explains this phenomenon [36]. Nehar Thakur et al. 2014 [37] also noted and commented on the similar pattern. The surface plots, as presented in **Fig. 5.12 B&D**, demonstrate that the analytical response both rises and falls with increasing sorbent mass. One could argue that insufficient sorbent causes an incomplete extraction. However, high concentrations cause the sorbent to become saturated, necessitating a considerable volume of eluent to fully desorb the analyte from the adsorbent's surface [38]. The duration of sonication was examined within the range of 10 to 30 minutes. Shorter sonication intervals result in lower recoveries because of inadequate adsorption, as **Fig. 5.12 B** illustrates, but longer times do not clearly boost stability. The same pattern was noted by Mina Fotouhi and Shahram Seidi [38].

Response surface plots and the quadratic equation showed that sample pH of 6.5, sorbent mass of 30 mg, sonication time of 20 minutes, and eluent concentration of 1.75 mol/L are the values that yield the best response.

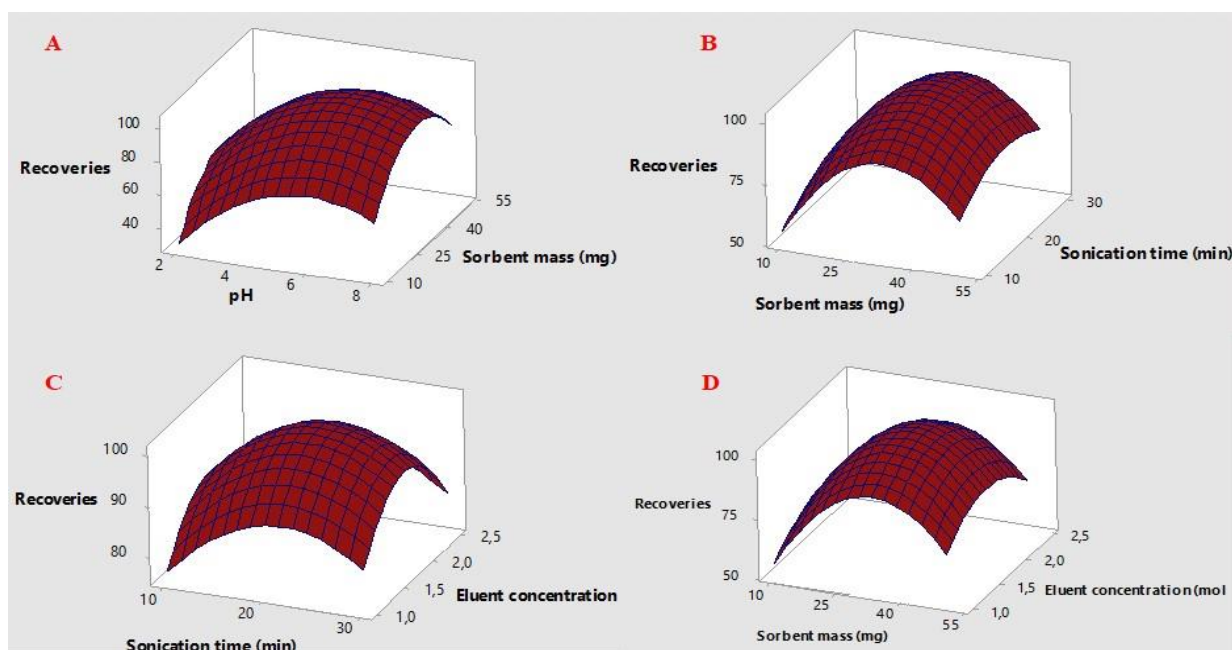


Figure 5. 12: Surface responses total Hg versus (A) pH. Sorbent mass, (B) sorbent mass. (C) Sonication time, sonication time. Eluent concentration and (D) sorbent mass. Eluent concentration.

5.3.4. Validation of the proposed method

Using NIST SRM 2778 under ideal conditions and a certified mercury content of $38.98 \mu\text{g}/\text{kg} \pm 1.10 \mu\text{g}/\text{kg}$, the accuracy of the proposed UA-m-SPE method was assessed. **Figure 5.13** compares the precision of the three nanomaterials: GO, MGO, and MGO-Au. With percentage recoveries of 35 %, 40 %, and 105%, respectively, the obtained values were $13,64 \mu\text{g}/\text{kg}$ for GO, $15,59 \mu\text{g}/\text{kg}$ for MGO, and $40,929 \mu\text{g}/\text{kg}$ for MGO-Au.

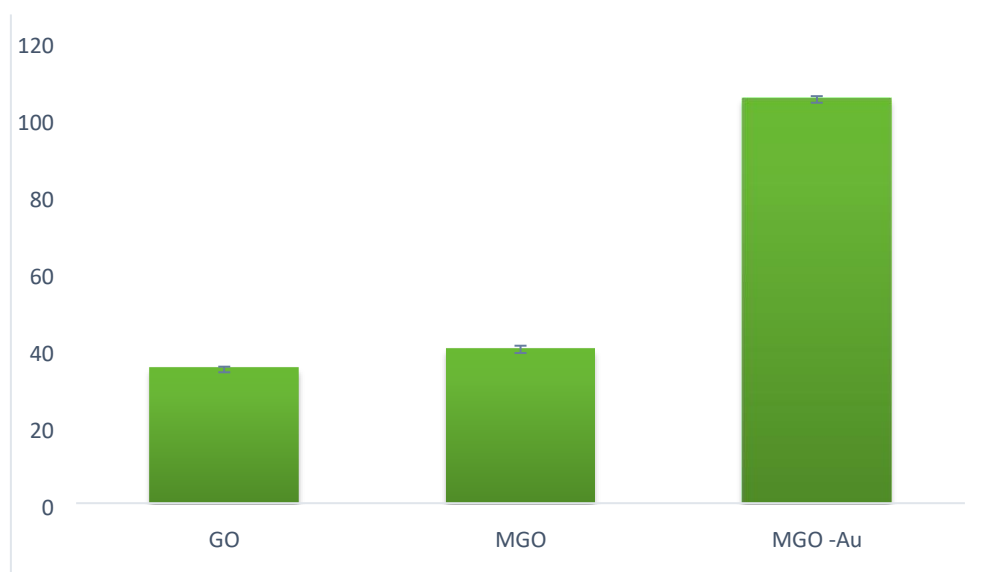


Figure 5. 13: Comparative analysis of the adsorbents GO, MGO, and MGO-Au for the total mercury measurement in fuel oils.

By utilizing the ideal conditions, the sensitivity, limit of detection, limit of quantification, and precision of the proposed method were further assessed to assess its analytical performance. By applying the m-SPME method to analyze seven standard solutions (0-100 ppb), the calibration curve was obtained. A correlation coefficient (R^2) of 0.9996 indicated the presence of linearity between 10 and $65 \mu\text{g}/\text{L}$. Preconcentration factor, which is the ratio of the calibration curve before and after preconcentration, is 255 for the m-SPME.

The UA-m-SPME's limits of detection and quantification were $0.035 \mu\text{g}/\text{L}$ and $0.119 \mu\text{g}/\text{L}$, respectively. These limits were specified as $3\text{SD}/m$ and $10 \text{SD}/m$, where SD is the standard deviation of ten replicate measurements of blank samples and m is the calibration slope. Through the processing of a series of standard solutions

containing 50 µg/L of mercury ions, the precision of the suggested procedure was examined. The intraday was 3.5 %, and the findings were presented as relative standard deviations (RSD).

5.3.5. Comparison of the developed method with other literature reports

Table 5.6 presents the comparison of the analytical qualities of the proposed technique with those reported in the literature to assess the superiority of the developed m-SPME based on the MGO-Au method on the preconcentration of mercury in fuel samples. Based on the available data, the recently established m-SPME technique appears to be a promising protocol for the preconcentration of total mercury in fuel oils. Based on the comparable analytical numbers of the suggested procedure, this is done. A good accuracy of 105 % was achieved which is comparable with studies reported in literature as can be seen on **Table 5.6**.

With most of the reported produced methods, this newly developed method demonstrated good precision, albeit showing a high limit of detection (LODs). The use of ICP-OES, which is widely known for having low sensitivity towards the target analyte, is to blame for these high LODs [39]. Additionally, compared to other published methods, the new method had greater preconcentration factors (PF), which made it a favorable substitute for the preconcentration of total mercury.

Table 5. 6: Comparison of the figures of merits between newly developed m-SPE with other SPE report on fuel matrices.

Sample preparation	Adsorbent	Adsorbent mass (mg)	Contact time (min)	Analytical technique	LOD ($\mu\text{g/L}$)	LDR ($\mu\text{g/L}$)	PF	Greenness assessment	Accuracy (%)	Reusability	RSD (%)	REF
m-SPME	MGO-Au	30	20	ICP-OES	0.035	0-100	255	0.64	105	7	3.5	This work
m-SPE	DT-Fe ₃ O ₄	80	5	CV-AAS	0.05	2-70	250	N/R	94.2	N/R	10.1	[40]
UAS-D-IL μ SPE	NG-COOH	10	3	FI-CV-AAS	0.01	N/R	22	N/R	97-103	N/R	4	[41]
m-SPE	Fe ₃ O ₄ @UiO-66-SH	20	15	ICP-MS	0.0026	20-1000	45.7	N/R	84.5-96.8	10	5.7	[42]
m-SPE	Fe ₃ O ₄ @SiO ₂ @AMPTs	10	15	DMA	0.0017	N/R	100	N/R	94.9-107	N/R	2.37	[43]
m-SPE	DPTH@MGO	4	3	ICP-OES	0.05	0.2-1000	3	N/R	93-105	N/R	1.6	[44]
m-DSPE	Fe ₃ O ₄ @GO@ ILs	N/R	1	FI-CV-GFAAS	0.00025	0.002-0.2	250	N/R	86-103	N/R	2.9	[12]

m-SPE	G/ZnFe ₂ O ₄	100	3	CV-AAS	0.001	0.25-10	N/R	N/R	91-107	50	2.7	[45]
SPE	GO-SH	30	N/R	ICP-OES	0.04	1-1000	200	N/R	N/R	55	4.20	[46]

Note: N/R: Note reported; **MGO-Au:** Magnetic graphene oxide coated with gold; **m-SPE:** Magnetic solid phase extraction; **UAS-D-IL- μ SPE:** Ultrasound assisted dispersive ionic liquid based solid phase microextraction; **UAS-DM-SPE:** Ultrasound assisted dispersive magnetic solid phase extraction; **DT-Fe₃O₄:** Magnetic nanoparticles functionalised with dithizone; **GO-SH:** Graphene oxide thioglycolic acid; **NG-COOH:** carboxyl-functionalised nanoporous graphene; **Fe₃O₄ @UiO-66-SH:** Magnetic nanospheres with sulfur-functionalised UiO-66; **Fe₃O₄@SiO₂@AMPTs:** Magnetic silica N-(2-acetylaminoethyl)-N'-(3triethoxysilylpropyl)thiourea; **DPTH@MGO:** Silica functionalised magnetic graphene oxide; **Fe₃O₄@GO@ ILs:** Magnetic graphene oxide coated with ionic liquid; **GO/ZnFe₂O₄:** graphene/ZnFe₂O₄ nanocomposite adsorbent

5.3.6. Greenness assessment of the newly developed m-SPME procedure

Analytical chemistry relies heavily on this assessment section since it assesses the environmental impact of every established process. For these reasons, several metric instruments with differing degrees of comprehensiveness have been created. They are predicated on the inclusion of additional criteria, and the assessment's generic response varies greatly in terms of both complexity and appearance [47]. When evaluating the greenness of any analytical procedure, the analytical greenness approach (AGREEp) has received a lot of attention. Ten factors make up this statistic, which is used to evaluate how environmentally friendly a sample preparation technique is [48]. Every criterion has a default weight of its own (Table 3.6). A pictogram representing the results is displayed (Fig. 5.14).



Figure 5. 14: Pictogram for UA-m-SPME procedure.

The pictogram (Fig.5.14) displays a total score of 0.64, exceeding the minimum requirement of 0.6 for a method to be classified as environmentally friendly [49]. This implies that the recently created m-SPME is more environmentally friendly. For the analytical approach to get the desired result of 1, a few steps still need to be improved. There is room for improvement in stages 1, 4, 5, 7, and 9. Because the extraction was done in a lab setting, criteria 1 received a low score. Criteria 4 did not meet

expectations due to the method's high waste output. Moreover, the sample size of 5 mL was a little excessive, making Criterion 5 subpar. ICP-OES, an energy-intensive post-sample preparation approach, was used instead of the recently developed method, which did not encourage automation. Consequently, criteria 7 and 9 were likewise poor. Therefore, this recently established technology can be lot greener if the inadequate criteria can be modified.

5.3.7. Interference studies

To examine the selectivity of the suggested UA-m-SPME approach, standard solutions containing 10µg/L Hg (II) and other metal cations that are typically found in fuel oils (200 µg/L) were prepared and analyzed using the established method. Among the metallic cations are Ni (II), Fe (II), Cd (II), Pb (II), Co (II), Cu (II), and Mn (II). The highest concentration of interfering ions that results in a recovery of less than 95% of Hg (II) was designated as the tolerance limit in this investigation. The recoveries varied from 95 % to 99 % (**Table 5.7**), indicating that the current method's selectivity is comparatively good. The same process was also used to examine the selectivity of GO and magnetic GO. Nevertheless, recoveries below 95 % indicate that the two materials' selectivity was poor.

Table 5. 7: Effect of various interfering cations on the preconcentration and determination of total Hg using online UA-m-DSPME method: Concentration of interfering ion = 100 µg L⁻¹.

Cation	Recovery (%)
Ag (I)	97±0.1
Cd (II)	95.9±0.01
Co (II)	98.5±0.3
Fe (II)	99±0.2
Pb (II)	95±0.03
Zn (II)	98.9±0.09

5.3.8. Reusability studies

When considering industrial applications, the adsorbent's reusability is essential. **Fig. 5.15** displays the MGO-Au adsorbent's reusability investigations. According to the figure, the adsorbent can be used up to seven times, with a 93–100 % mercury recovery rate. As a result, it can be said that the adsorbent was reasonably

reusable for a long time when it came to mercury. In 2014, Jing Hu and colleagues [26] recorded an equivalent quantity of cycles with the same material but their focus was on the reduction of 4-nitrophenol.

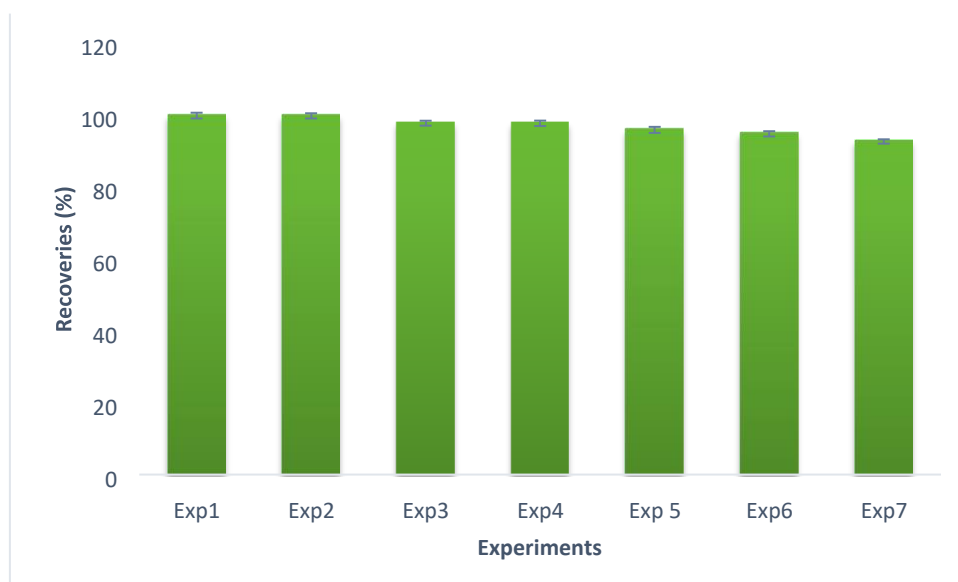


Figure 5. 15: Reusability of the MGO-Au core-shell nano-composite for adsorption of Hg in fuel matrices.

5.3.2. Application of UA-m-DSPME procedure in real samples

Real crude oil, gasoline, diesel oil, and kerosine samples were subjected to the recently developed ultrasonic assisted-magnetic dispersive solid phase microextraction (UA-m-DSPME). **Table 5.1** was followed in labelling the actual fuel samples. **Table 5.8** displayed the obtained total concentrations of mercury. Regarding the mercury contamination of the fuel samples, the table shows a pattern. Samples of crude oil had the highest level of contamination, followed by those of diesel, gasoline, and kerosene. This is consistent with some literature reports. This indicates that the recently developed preconcentration process is reliable and a good substitute for existing techniques.

When compared to fuel oils from other nations, South African fuel oils don't have a significant mercury contamination. In diesel oil, Wu and colleagues' investigation yielded a total mercury content of 0.83 $\mu\text{g/g}$ [50]. Uddin and associates repeated an intriguing study about the extraction of total mercury from crude oil. They

found that Arabian crude oil had a total mercury concentration of 0.18 $\mu\text{g}/\text{kg}$ using their method [51]. In 2018, Mohammad et al. [52] measured concentrations in Basrah crude oil of 0.4169350 ppm and Khanaken crude oil of 1.5043600 ppm, respectively. This demonstrates that South African fuel oils contain mercury at levels comparable to those of other nations.

Table 5. 8: Total mercury concentration levels ($\mu\text{g}/\text{g}$) in real crude oil, gasoline, diesel oil and kerosene.

Sample type	Concentration ($\mu\text{g}/\text{g}$)
COS 1	0.410 \pm 0.03
COS 2	0.560 \pm 0.09
COS 3	0.490 \pm 0.15
GS 1	0.310 \pm 0.07
GS 2	0.425 \pm 0.08
GS 3	0.480 \pm 0.01
DS 1	0.500 \pm 0.05
DS 2	0.431 \pm 0.04
DS 3	0.550 \pm 0.01
KS 1	0.089 \pm 0.30
KS 2	0.090 \pm 0.50
KS 3	0.081 \pm 0.004

5.4 Conclusion

This work effectively synthesized and characterized a magnetic graphene oxide coated with gold nanocomposite utilizing FT-IR, P-XRD, UV-vis, SEM-EDS, TEM, TGA, and BET. The synthesized adsorbent was effectively used to preconcentrate the total amount of mercury presents in kerosine, diesel, gasoline, and crude. Under ideal circumstances, NIST SRM 2778 was used to precisely analyze the figures of merits of the analytical method, with a certified mercury concentration of 38.98 $\mu\text{g}/\text{kg}$ \pm 1.10 $\mu\text{g}/\text{kg}$. The validity of the newly designed UA-m-DSPME process was demonstrated by the analytical performance of the newly developed approach being similar with reported literature reports.

For the preconcentration of total mercury in fuel oils, the synthesized adsorbent may be reused seven times. The AGREEprep metric tool was also utilized to assess

the sample preparation method's environmental impact. Thus, the method is more environmentally friendly, but it still must be refined to get to the desired value of 1. With real crude oil, gasoline, diesel oil, and kerosine, the recently synthesized nanocomposite was effectively used to determine the overall concentration of mercury present. While samples of kerosene were below the limit of detection, crude oil was the energy source that was most contaminated. Currently, there is no legislation concerning the quantity of mercury permitted in gasoline samples, but South African gasoline oils contained mercury concentrations which are like others.

REFERENCES

- [1] M. Enrico, A. Mere, H. Zhou, M. Loriau, E. Tessier, B. Bouyssiére, *Energy and Fuels* 34 (2020) 13307–13320.
- [2] M. Payehghadr, H. Shafiekhani, A.R. Sabouri, A.M. Attaran, M.K. Rofouei, *Iranian Journal of Chemistry and Chemical Engineering* 33 (2014) 1–10.
- [3] M.A. Gab-Allah, E.S. Goda, A.B. Shehata, H. Gamal, *Crit Rev Anal Chem* 50 (2020) 161–178.
- [4] E. Öztürk Er, G. Dalgıç Bozyiğit, Ç. Büyükpınar, S. Bakırdere, *Crit Rev Anal Chem* 52 (2022) 231–249.
- [5] R.G. Wuilloud, (2010) 1432–1439.
- [6] P.N. Kunene, (2019).
- [7] N.S. Mdluli, P.N. Nomngongo, N. Mketi, *Crit Rev Anal Chem* 52 (2022) 1–18.
- [8] N.S. Mdluli, (2022).
- [9] T. Xia, X. Yang, R. Zhang, A. Huang, K. Hu, F. Hao, Y. Liu, Q. Deng, S. Yang, X. Wen, *Talanta* 256 (2023) 124316.
- [10] H. Ahmad, R. Ahmad Khan, B. Heun Koo, A. Alsalmé, *Journal of Physics and Chemistry of Solids* 168 (2022).
- [11] A. Keramat, R. Zare-Dorabei, *Ultrason Sonochem* 38 (2017) 421–429.
- [12] T. Note, (2021) 892–899.
- [13] W.A. Khan, M.B. Arain, M. Soylak, *Food and Chemical Toxicology* 145 (2020) 111704.
- [14] S. Mpelane, N. Mketi, M. Mlambo, N. Bingwa, P.N. Nomngongo, *ACS Omega* 7 (2022) 23302–23314.
- [15] Y. Wang, Y. Wang, H. Xia, G. Wang, Z. Zhang, (2016) 17451–17457.
- [16] S. Seidi, M. Fotouhi, *Analytical Methods* 9 (2017) 803–813.
- [17] H. Zhang, D. Hines, D.L. Akins, *Dalton Transactions* 43 (2014) 2670–2675.
- [18] J. Chen, Y. Wang, X. Wei, P. Xu, W. Xu, R. Ni, J. Meng, *Talanta* 188 (2018) 454–462.
- [19] L. Cui, X. Guo, Q. Wei, Y. Wang, L. Gao, L. Yan, T. Yan, B. Du, *Journal of Colloid and Interface Science* 439 (2015) 112–120.
- [20] M. Ahmadi, M.Á. Aguirre, T. Madrakian, A. Afkhami, A. Canals, *Fuel* 210 (2017) 507–513.
- [21] J. Sun, Q. Liang, Q. Han, X. Zhang, M. Ding, *Talanta* 132 (2015) 557–563.

- [22] A.S. Sazezi, M. Kermanian, A. Ramazani, S. Sadighian, *Journal of Inorganic and Organometallic Polymers and Materials* 32 (2022) 1541–1550.
- [23] N.R. Biata, K.M. Dimpe, J. Ramontja, N. Mketi, P.N. Nomngongo, *Microchemical Journal* 137 (2018) 214–222.
- [24] P.N. Nomngongo, J.C. Ngila, *Fuel* 139 (2015) 285–291.
- [25] L.L. Cao, S.M. Yin, Y.B. Liang, J.M. Zhu, C. Fang, Z.C. Chen, *Materials Research Innovations* 19 (2015) S1364–S1368.
- [26] J. Hu, Y. lei Dong, X. jiao Chen, H. juan Zhang, J. min Zheng, Q. Wang, X. guo Chen, *Chemical Engineering Journal* 236 (2014) 1–8.
- [27] S. Tanwar, D. Mathur, *Materials Today: Proceedings* 30 (2020) 17–22.
- [28] J.R.G. Sanchez, P.R.S. Joson, M.M. Vega, *Journal of Environmental Science and Health - Part A Toxic/Hazardous Substances and Environmental Engineering* 55 (2020) 216–223.
- [29] M.Z. Kassaee, E. Motamedi, M. Majdi, *Chemical Engineering Journal* 172 (2011) 540–549.
- [30] M. Kermanian, S. Sadighian, A. Ramazani, M. Naghibi, 1 (2021) 284–291.
- [31] A. Keramat, R. Zare-Dorabei, *Ultrasonics Sonochemistry* 38 (2017) 421–429.
- [32] J. Hu, Y. lei Dong, X. jiao Chen, H. juan Zhang, J. min Zheng, Q. Wang, X. guo Chen, *Chemical Engineering Journal* 236 (2014) 1–8.
- [33] S. Fu, W. Han, (2021) 80–100.
- [34] F. Ambroz, T.J. Macdonald, V. Martis, I.P. Parkin, 1800173 (2018) 1–17.
- [35] A. Dubey, N. Bhavsar, V. Pachchigar, M. Saini, M. Ranjan, C.L. Dube, *Ceram Int* 48 (2022) 4821–4828.
- [36] K.C. Hsu, C.F. Lee, W.C. Tseng, Y.Y. Chao, Y.L. Huang, *Talanta* 128 (2014) 408–413.
- [37] N. Thakur, S.A. Kumar, A.K. Pandey, S.D. Kumar, A.V.R. Reddy, *Analytical Methods* 6 (2014) 7823–7830.
- [38] S. Seidi, M. Fotouhi, *Analytical Methods* 9 (2017) 803–813.
- [39] H.B. Zengin, R. Gürkan, *Biological Trace Element Research* 191 (2019) 254–268.
- [40] L. Adlnasab, H. Ebrahimzadeh, A.A. Asgharinezhad, M.N. Aghdam, A. Dehghani, S. Esmailpour, *Food Anal Methods* 7 (2014) 616–628.
- [41] H. Shirkhanloo, A. Khaligh, H. Zavvar, A. Rashidi, *Microchemical Journal* 130 (2017) 245–254.
- [42] D.B. Zhou, Y.B. Xiao, F. Han, Y.N. Lv, L. Ding, W. Song, Y.X. Liu, P. Zheng, D.

- Chen, *Journal of Chromatography A* 1654 (2021) 462465.
- [43] Y. Cui, S. Liu, K. Wei, Y. Liu, (2015) 1337–1344.
- [44] J.C. García-Mesa, P. Montoro Leal, M.M. López Guerrero, E.I. Vereda Alonso, *Microchemical Journal* 150 (2019) 104141.
- [45] E. Yavuz, Ş. Tokal, Ş. Patat, 142 (2018) 85–93.
- [46] A. Alsalmé, H. Ahmad, R.A. Khan, B.H. Koo, G.M. Alharbi, S.I. Alhadlaq, *Water (Switzerland)* 15 (2023) 1–13.
- [47] F. Pena-Pereira, M. Tobiszewski, W. Wojnowski, E. Psillakis, *Advances in Sample Preparation* 3 (2022) 100025.
- [48] W. Wojnowski, M. Tobiszewski, F. Pena-Pereira, E. Psillakis, *TrAC - Trends in Analytical Chemistry* 149 (2022) 116553.
- [49] D. Moema, T. Makwakwa, H.N. Nyambaka, S. Dube, M. Nindi, *Food Anal Methods* (2024).
- [50] C.H. Wu, S.J. Jiang, A.C. Sahayam, *Spectrochimica Acta - Part B Atomic Spectroscopy* 147 (2018) 115–120.
- [51] R. Uddin, M.A. Al-Fahad, A.K. Al-Rashwan, M.A. Al-Qarni, *Environmental Monitoring and Assessment* 185 (2013) 3681–3685.
- [52] A.K.T. Mohammad, A.T. Hameed, M.A. Alhamdany, K. Mohammad Al Azzam, G.A.A. Talk, *Biomedical Chromatography* 33 (2019) 1–23.

CHAPTER VI (OVERALL CONCLUSION & FUTURE RECOMMENDATIONS)

PREAMBLE

This chapter finally makes an overall conclusion of the study. It further compares the three developed sample preparation methods in terms of greenness and analytical performances. In addition to that chapter gives proper future recommendations.

6.1 Overall conclusion

The proposed microwave-assisted hydrogen peroxide digestion method (MW-HPD), vortex-assisted deep eutectic solvent based dispersive liquid-liquid microextraction (VA-DES-DLLME) and ultrasound assisted magnetic dispersive solid phase microextraction (UA-m-DSPME) were successfully developed and were found to be appropriate for the determination of total mercury in coal, crude oil and their derivatives which are gasoline, diesel oil and kerosene. Basically, the microwave-assisted hydrogen peroxide digestion method was used to screen the presence of mercury in coal, crude oil, gasoline, diesel oil and kerosene. The limit of detection and quantification for the MW-HPD method were 0.25 µg/L and 0.8 µg/L. For VA-DES-DLLME, the limit of detection and quantification were 0.025 µg/L and 0.083 µg/L. For UA-m-DSPME method, the limit of detection and quantification were 0.035 µg/L and 0.119 µg/L. It can be concluded that VA-DES-DLLME showed low limit of detection and quantification compared to MW-HPD and UA-m-DSPME, respectively. The analytical figures of the newly developed sample preparation methods are comparable with other literature reports.

The mercury concentrations obtained from MW-HPD method ranged between 0.876±0.023-0.975±0.025 µg/g in coal samples, 0.383±0.043-0.506±0.105 µg/g for crude oil samples, 0.306±0.010-0.390±0.035 µg/g for gasoline samples, 0.360±0.003-0.434±0.050 µg/g for diesel oil samples and all kerosene samples were below detection. For VA-DES-DLLME procedure, mercury concentrations ranged between 0.390±0.01-0.510±0.09 µg/g for crude oil, 0.308±0.05-0.402±0.05 µg/g for gasoline, 0.370±0.35-0.510±0.08 µg/g for diesel samples and 0.090±0.09-0.098±0.02 µg/g for

kerosene. For UA-m-DSPME method, mercury concentrations were 0.410 ± 0.03 - 0.560 ± 0.09 $\mu\text{g/g}$ for crude oil, 0.310 ± 0.07 - 0.480 ± 0.01 $\mu\text{g/g}$ for gasoline, 0.431 ± 0.04 - 0.550 ± 0.01 $\mu\text{g/g}$ for diesel oil and 0.081 ± 0.004 - 0.090 ± 0.50 $\mu\text{g/g}$ for kerosene. The two preconcentration methods (VA-DES-DLLME and UA-m-DSPME) successfully enriched mercury concentration in fuel oils. This was observed with mercury concentrations in kerosene samples. Under the two preconcentration methods, trace levels of mercury were detected, but with the MW-AHPD method, mercury concentrations in kerosene samples were below detection limits. It can also conclude that mercury concentrations in South African fossil fuels and their derivatives are comparable with mercury concentrations from other nations.

The environmental impact of each sample preparation method was evaluated using AGREEprep software. The VA-DES-DLLME procedure, proved to be greener (0.72) than UA-m-DSPME (0.64) and MW-AHPD (0.56) based on the results obtained from AGREEprep. The greenness of the former can be attributed to the use of DESs which don't require any toxic solvent to synthesized, and the application process made use of a vortex mixer which used less power. On the other hand, for UA-m-DSPME, the synthesis of the adsorbent made use of large volumes of toxic solvents and the application process made use of an ultrasound which used more power. Microwave assisted hydrogen peroxide digestion made use of microwave energy which uses a lot of power, and this resulted in a lower score in AGREEprep. Additionally, this protocol made use of non-renewable reagents (dilute hydrogen peroxide) and it resulted in large volume of wastes which further decreased the scores.

It can be summed up that VA-DES-DLLME was the most cost-effective, fast, sensitive, and environmentally friendly sample preparation method. The cost effectiveness of this protocol can be based on the use of deep eutectic solvents (DESs) which are cheap and very easy to synthesize. On the other hand, UA-m-DSPME needed a lot of reagents which are a bit costly than the DESs for the synthesis of the magnetic nano-adsorbent. The VA-DES-DLLME was fast, as it took only 5 minutes while the UA-m-DSPME took 20 minutes for adsorption. Additionally, the synthesize of the DESs was a single step process which took a very short time (30

minutes), while the synthesis of the magnetic adsorbent took a long time with many steps. For MWAHPD, was the most time consuming as it took almost 36 minutes.

For VA-DES-DLLME, the proposed deep eutectic solvents were successfully developed, characterized and applied for the preconcentration of total Hg in fuel oils. Additionally, the magnetic graphene oxide gold nanocomposite (MGO-Au) was also successfully synthesized, characterized and applied in UA-m-DSPME procedure for the preconcentration of total mercury in fuel oils.

Under MW-AHPD, the most influential factor was temperature. This influence can be based on the volatile nature of Hg and decomposition of methionine. At higher temperatures there are high risks of degradation of the trapping agent (methionine) and hence high Hg loss. Based on the pareto charts for the two preconcentration procedures, it can be concluded that pH was the most influential factor in the adsorption of total mercury in these energy resources. The length of the bar in the pareto charts gives information on the significance of each factor. For the pH of both preconcentration methods the bars were long compared to the other factors, hence signifying that pH was the most influential. The logic behind the high effect of pH can be based on the formation of different mercury complexes at different pH values. For instance, for VADES-DLLME, lower pH values led to severe acidity and instability of the Hg-DTz complex which reduced recoveries, whereas higher pH values led to the decomposition of the complex. Almost the same phenomenon was observed under UA-m-DSPME. At higher pH values, a formation of stable mercury complexes, which prevented the formation of Hg-Au complex were observed.

It can be summed up that VA-DES-DLLME was the most cost-effective, fast, sensitive, and environmentally friendly sample preparation method. The cost effectiveness of this protocol can be based on the use deep eutectic solvents (DESs) which are cheap and very easy to synthesize. On the other hand, UA-m-DSPME needed a lot of reagents which are a bit costly than the DESs for the synthesis of the magnetic nano-adsorbent. The VA-DES-DLLME was fast, as it took only 5 minutes while the UA-m-DSPME took 20 minutes for adsorption. Additionally, the synthesize of the DESs was a single step process which took a very short time (30 minutes), while

the synthesis of the magnetic adsorbent took a long time with many steps. For MWAHPD, was the most time consuming as it took almost 36 minutes.

6.2 Future recommendations

The validation of the MW-AHPD procedure still needs to be improved by employing a standard technique (hydride or CV-AAS) for analysis. Additionally, the characterization of the DESs needs to be improved by confirming the water content density and dynamic viscosity. The reproducibility and selectivity studies of DESs still need to be evaluated for the preconcentration of total mercury in fuel oils. Adsorbents coated with organ sulphur compounds still need to be utilized as substitute for gold as there are cost effective compared to gold. Proper removal strategies need to be developed for the removal of mercury in crude oil, gasoline, diesel oil and kerosene.

APPENDIX

PREAMBLE

This section displays all the tables for experimental design and ANOVA for chapter 3, chapter 4, and chapter 5.

Table S1: The effect of varying sample mass, hydrogen peroxide concentration, methionine concentration, digestion time and temperature on the digestion of real crude oil sample to achieve high percentage recoveries of total Hg. Replicates (n=3).

Std Order	Run Order	Center Pt	Blocks	Mass (g)	[H ₂ O ₂] (mol/L)	[Methionine] (mol/L)	Time (min)	Temperature (°C)	Recoveries (%)
1	1	1	1	0.1	3	1.0	30	200	49.08
2	2	1	1	0.3	3	1.0	30	100	35.62
3	3	1	1	0.1	5	1.0	30	100	61.63
4	4	1	1	0.3	5	1.0	30	200	65.81
5	5	1	1	0.1	3	10.0	30	100	61.12
6	6	1	1	0.3	3	10.0	30	200	69.76
7	7	1	1	0.1	5	10.0	30	200	79.74
8	8	1	1	0.1	5	10.0	30	100	79.98
9	9	1	1	0.3	3	1.0	60	100	76.18
10	10	1	1	0.1	3	1.0	60	200	84.84
11	11	1	1	0.3	5	1.0	60	200	94.45
12	12	1	1	0.1	5	1.0	60	100	88.33
13	13	1	1	0.3	3	10.0	60	200	99.36
14	14	1	1	0.1	3	10.0	60	100	91.57
15	15	1	1	0.3	5	10.0	60	100	97.96
16	16	1	1	0.1	5	10.0	60	200	105.12
17	17	1	1	0.2	4	5.5	45	150	93.20

Table S2: Analysis of variance (ANOVA) for two-level half factorial design for MWAHPD.

Source	DF	Adj. SS	Adj. MS	F-Value	P-Value
Model	7	5698.08	814.01	52.36	0.002
Linear	5	5378.41	1075.68	69.19	0.001
Mass	1	0.14	0.14	0.01	0.926
[H ₂ O ₂]	1	695.51	695.51	44.74	0.004
[Methionine]	1	1034.75	1034.75	66.56	0.001
Time	1	3453.62	3453.62	222.16	0.000
Temperature	1	194.39	194.39	12.50	0.005
2-Way interactions	1	88.69	88.69	5.70	0.041
[H ₂ O ₂] *Time	1	88.69	88.69	5.70	0.041
Curvature	1	230.98	230.98	14.86	0.004
Error	1	139.91	15.55		
Total	9	16	5837.99		

Table S3: The effect of varying digestion time, temperature, [H₂O₂], [Methionine] while keeping sample mass constant in further optimization using on the digestion of central composite design. Experimental conditions: 0.1g (n =3).

Std Order	Run Order	Pt Type	Blocks	[H ₂ O ₂] (mol/L)	[Methionine] (mol/L)	Time (min)	Temperature (°C)	Recoveries (%)
1	1	1	1	2.0	1.0	30	140	23.60
2	2	1	1	5.0	1.0	30	140	37.95
3	3	1	1	2.0	10.0	30	140	37.48
4	4	1	1	5.0	10.0	30	140	50.05
5	5	1	1	2.0	1.0	60	140	62.79
6	6	1	1	5.0	1.0	60	140	68.46
7	7	1	1	2.0	10.0	60	140	73.07
8	8	1	1	5.0	10.0	60	140	74.37
9	9	1	1	2.0	1.0	30	140	77.68
10	10	1	1	5.0	1.0	30	200	79.10
11	11	1	1	2.0	10.0	30	200	75.88
12	12	1	1	5.0	10.0	30	200	84.78
13	13	1	1	2.0	1.0	60	200	84.93
14	14	1	1	5.0	1.0	60	200	99.46
15	15	1	1	2.0	10.0	60	200	96.96
16	16	1	1	5.0	10.0	60	200	92.14
17	17	-1	1	0.5	5.5	45	170	90.30
18	18	-1	1	6.5	5.5	45	170	99.37
19	19	-1	1	3.5	0.0	45	170	50.12
20	20	-1	1	3.5	14.5	45	170	94.35
21	21	-1	1	3.5	5.5	15	170	89.11
22	22	-1	1	3.5	5.5	75	170	87.59
23	23	-1	1	3.5	5.5	45	110	91.06
24	24	-1	1	3.5	5.5	45	230	74.01
25	25	0	1	3.5	5.5	45	170	96.78

26	26	0	1	3.5	5.5	45	170	93.23
27	27	0	1	3.5	5.5	45	170	94.52
28	28	0	1	3.5	5.5	45	170	92.94
29	29	0	1	3.5	5.5	45	170	98.63
30	30	0	1	3.5	5.5	45	170	93.50
31	31	0	1	3.5	5.5	45	170	94.38

Table S5: The effect of varying sample pH, volume of disperser solvent, volume of extracting solvent, extraction time and centrifugation time, on the VA-DESDLLME of real crude oil sample to achieve high percentage recoveries of total Hg. Replicates (n=3).

Std Order	Run Order	Center Pt	Blocks	pH	Volume of disperser solvent (mL)	Volume of extracting solvent (mL)	Extraction time (min)	Centrifugation time (min)	Recoveries (%)
1	1	1	1	1	0.250	0.05	10	10.0	70.22
2	2	1	1	13	0.250	0.05	10	1.0	35.89
3	3	1	1	1	1.000	0.05	10	1.0	88.90
4	4	1	1	13	1.000	0.05	10	10.0	50.00
5	5	1	1	1	0.250	0.15	10	1.0	72.00
6	6	1	1	13	0.250	0.15	10	10.0	50.00
7	7	1	1	1	1.000	0.15	10	10.0	90.05
8	8	1	1	13	1.000	0.15	10	1.0	52.00
9	9	1	1	1	0.250	0.05	20	1.0	67.00
10	10	1	1	13	0.250	0.05	20	10.0	52.99
11	11	1	1	1	1.000	0.05	20	10.0	78.00
12	12	1	1	13	1.000	0.05	20	1.0	53.08
13	13	1	1	1	0.250	0.15	20	10.0	92.00
14	14	1	1	13	0.250	0.15	20	1.0	55.00
15	15	1	1	1	1.000	0.15	20	1.0	94.09
16	16	1	1	13	1.000	0.15	20	10.0	59.00
17	17	0	1	7	0.625	0.10	15	5.5	60.09

Table S6: Analysis of variance for two-level half factorial design for VA-DESDLLME.

Source	DF	Adj. SS	Adj.MS	F-value	P-value
Model	7	4687.46	669.64	25.67	0.002
Linear	5	4473.77	894.75	34.30	0.003
pH	1	3730.16	3730.16	143.00	0.021
Volume of disperser solvent (mL)	1	306.43	306.43	11.75	0.001
Volume of extracting solvent (mL)	1	289.51	289.51	11.10	0.005
Extraction time (min)	1	110.78	110.78	4.25	0.004
Centrifugation time (min)	1	36.91	36.91	1.41	
2-way interactions	2	213.69	106.84	4.10	
Volume of disperser solvent (mL)*Extraction time(min)	1	79.48	79.48	3.05	
Volume of disperser solvent (mL)*Centrifugation time (min)	1	134.21	134.21	5.15	
Error	9	234.77	26.09		
Curvature	1	35.87	35.87	1.44	
Lack of fit	8	198.89	24.86		
Total	16	4922.23			

Table S7: The effect of varying pH, vortex time, disperser solvent, extractant volume, while keeping centrifugation time constant in further optimization using BBD. Experimental conditions: 5 minutes centrifugation time (n =3).

Std Order	Run Order	Pt Type	Blocks	pH	Vortex time (min)	Disperser solvent volume(mL)	Extractant volume (mL)	Recoveries (%)
1	1	2	1	2	0.50	0.625	0.275	78.90
2	2	2	1	10	0.50	0.625	0.275	48.90
3	3	2	1	2	10.00	0.625	0.275	78.00
4	4	2	1	10	10.00	0.625	0.275	42.10
5	5	2	1	6	5.25	0.250	0.050	95.00
6	6	2	1	6	5.25	1.000	0.050	93.60
7	7	2	1	6	5.25	0.250	0.500	90.00
8	8	2	1	6	5.25	1.000	0.500	85.00
9	9	2	1	2	5.25	0.625	0.275	78.90
10	10	2	1	10	5.25	0.625	0.275	45.00
11	11	2	1	2	5.25	0.625	0.275	76.00
12	12	2	1	10	5.25	0.625	0.275	39.80
13	13	2	1	6	0.50	0.250	0.275	87.00
14	14	2	1	6	10.00	0.250	0.275	89.00
15	15	2	1	6	0.50	1.000	0.275	92.00
16	16	2	1	6	10.00	1.000	0.275	84.50
17	17	2	1	2	5.25	0.250	0.275	73.00
18	18	2	1	10	5.25	0.250	0.275	43.00
19	19	2	1	2	5.25	1.000	0.275	79.90
20	20	2	1	10	5.25	1.000	0.275	4.00
21	21	2	1	6	0.50	0.625	0.050	94.00
22	22	2	1	6	10.00	0.625	0.050	95.00
23	23	2	1	6	0.50	0.625	0.500	93.90
24	24	2	1	6	10.00	0.625	0.500	80.03
25	25	0	1	6	5.25	0.625	0.275	97.80
26	26	0	1	6	5.25	0.625	0.275	96.60
27	27	0	1	6	5.25	0.625	0.275	97.20

Table S8: Analysis of variance for CCD for VA-DES-DLLME.

Source	DF	Adj. SS	Adj. MS	F-value	P-value
Model	14	9041.5	645.82	7.65	0.001
Linear	4	2747.5	686.88	8.14	0.002
pH	1	2274.3	2274.25	26.94	0.001
Vortex time (min)	1	0.1	0.1	0.00	0.003
Disperser solvent volume (mL)	1	450.2	450.19	5.33	0.040
Extractant volume (mL)	1	23.0	22.96	0.27	0.004
Square	4	5409.9	1352.48	16.02	0.002
pH*pH	1	4591.6	4591.64	54.39	0.001
Vortex time*vortex time	1	320.7	320.68	3.80	0.075
Disperser solvent volume*Disperser solvent volume	1	10.4	10.39	0.12	0.732
Extractant volume*Extractant volume	1	86.0	86.05	1.02	0.333
2-way interactions	6	884.1	147.35	1.75	0.194
pH*Vortex time	1	0.0	0.01	0.00	0.991
pH*Disperser solvent volume	1	818.0	817.96	9.69	0.009
pH*Extractant volume	1	1.4	1.44	0.02	0.898
Vortex time*Disperser solvent volume	1	38.4	38.44	0.46	0.513
Vortex time*Extractant volume	1	0.7	0.72	0.01	0.928
Disperser solvent volume*Extractant volume	1	25.5	25.50	0.30	0.593
Error	12	1013.0	84.42		
Lack of fit	10	1012.4	101.24	313.10	0.003
Pure error	2	0.6	0.32		
Total	26	10054.5			

Table S9: The effect of varying sorbent mass, sample pH, sonication, eluent concentration, and elution time and centrifugation time, on the UA-mDSPME of real crude oil sample to achieve high percentage recoveries of total Hg. Replicates (n=3).

Std Order	Run Order	Center Pt	Blocks	Sorbent mass (mg)	Sonication time (min)	pH	Eluent concentration (mol/L)	Elution time (min)	Recoveries (%)
1	1	1	1	10	10	3	0.1	5	38.0
2	2	1	1	50	10	3	0.1	3	49.0
3	3	1	1	10	60	3	0.1	3	48.0
4	4	1	1	50	60	3	0.1	5	58.0
5	5	1	1	10	10	9	0.1	5	87.7
6	6	1	1	50	10	9	0.1	3	90.0
7	7	1	1	10	60	9	0.1	3	89.9
8	8	1	1	50	60	9	0.1	5	99.9
9	9	1	1	10	10	3	1.0	5	50.0
10	10	1	1	50	10	3	1.0	3	55.0
11	11	1	1	10	60	3	1.0	3	49.9
12	12	1	1	50	60	3	1.0	5	60.0
13	13	1	1	10	10	9	1.0	5	79.9
14	14	1	1	50	10	9	1.0	3	89.0
15	15	1	1	10	60	9	1.0	3	95.0
16	16	1	1	50	60	9	1.0	5	104.0
17	17	0	1	10	35	6	0.55	4	89.0

Table S 10: Analysis of variance of half factorial design for UA-m-DSPME.

Source	DF	Adj. SS	Adj. MS	F-value	P-value
Model	7	7175.4	1025.1	5.79	0.009
Linear	5	5354.3	1070.9	6.05	0.10
Sorbent mass	1	175.6	175.1	0.99	0.345
Ultrasonication time1 (min)		2002.6	2002.6	11.32	0.008
pH	1	1580.1	1580.1	8.93	0.015
Eluent concentration (mol/L)	1	798.1	798.1	4.51	0.063

Elution time (min)	1	798.1	798.1	4.51	0.063
2-way interactions	2	1821.1	910.6	5.15	0.032
Sorbent mass (mg)*Eluent concentration (mol/L)	1	1105.6	1105.6	6.25	0.034
Sonication time (min)*Elution time (min)	1	715.6	715.6	4.04	0.075
Error	9	1592.7	177.0		
Curvature	1	220.7	220.7	1.29	0.289
Lack of fit	8	1372.0	171.5		
Total	16	8768.1			

Table S 11: Analysis of variance of BBD for UA-m-DSPME.

Source	DF	Adj. SS	Adj. MS	F-value	P-value
Model	14	9051.7	646.55	10.70	0.001
Linear	4	5758.8	1439.70	23.84	0.015
Sonication time (min)	1	928.0	927.95	15.36	0.004
pH	1	3627.9	3627.90	60.06	0.003
Eluent concentration (mol/L)	1	442.3	442.34	7.32	0.004
Elution time (min)	1	760.6	760.60	12.59	0.150
Square	4	3109.0	77.24	12.87	0.030
Sonication time (min)*Sonication time (min)	1	1361.0	1361.03	22.53	0.050
Eluent concentration (mol/L) * Eluent concentration (mol/L)	1	1458.8	1458.84	24.15	0.040

pH*pH	1	756.4	756.38	12.52	0.050
Elution time (min)*Elution time (min)	1	7.1	7.12	0.12	0.060
2-Way interaction	6	183.9	30.65	0.51	0.010
Sonication time (min)*pH	1	39.7	39.74	0.66	0.050
Sonication time (min)*Eluent concentration (mol/L)	1	9.2	9.22	0.15	0.005
Sonication time (mol/L) *Elution time (min)	1	22.4	22.37	0.37	0.010
pH*Eluent concentration (mol/L)	1	105.1	105.09	1.74	0.060
Error	16	5.0	5.04	0.08	
Lack of fit	10	827.8	82.78	0.34	
Pure error	6	138.6	23.09	3.58	
Total	30	10018.1			

Spectra



wavelength Hg
184.950.pdf



wavelength Hg
184.950 b.pdf

Publications



Book with Chapters
from Mxolisi Kiwani